BUILDING ENVELOPE CONTAINING PHASE CHANGE MATERIALS FOR ENERGY-EFFICIENT BUILDINGS

A Dissertation
Submitted to the Graduate Faculty
of the
North Dakota State University
of Agriculture and Applied Science

By

Mingli Li

In Partial Fulfillment of the Requirements
for the Degree of
DOCTOR OF PHILOSOPHY

Major Department:
Civil and Environmental Engineering

July 2021

Fargo, North Dakota

North Dakota State University
Graduate School

Title

BUIDING ENVELOPE CONTAINING PHASE CHANGE MATERIALS FOR ENERGY-EFFICIENT BUILDINGS

By

Mingli Li

The Supervisory Committee certifies that this ***disquisition*** complies with North Dakota State University's regulations and meets the accepted standards for the degree of

DOCTOR OF PHILOSOPHY

SUPERVISORY COMMITTEE:

Zhibin Lin
Chair

Fardad Azarmi

Mijia Yang

Long Jiang

Xiaoning Qi

Approved:

July 9, 2021
Date

Xuefeng Chu
Department Chair

ABSTRACT

Energy consumption in the building sector has increased dramatically over the past two decades. The incorporation of phase change materials (PCMs) into building envelopes is considered as effective thermal energy storage to improve building thermal performance and reduce space heating/cooling load. Despite significant efforts in PCMs technologies and their application to buildings, how to select proper PCMs for buildings and maximize the activation of their latent heat to effectively improve building energy efficiency still post great challenges. The lack of systematic and comprehensive studies in these gaps hinders their broad applications in the building sector.

This study aims to develop a holistic framework through experimental and numerical studies to gain a deep understanding of the thermal property of PCM and the heat transfer mechanism of the exterior wall integrated with PCM. A novel shape-stabilized paraffin/expanded graphite(EG) composite is prepared and its thermal behavior is investigated through thermal energy storage and heat transfer test. The impact of critical design parameters including the location, thickness, latent heat, melting point, and thermal conductivity of PCM on the thermal performance of a multilayer wall is explored using COMSOL Multiphysics® software.

The thermal storage and heat transfer test show that EG can significantly enhance the heat transfer rate of paraffin. In addition, the paraffin/EG composite possesses favorable thermal energy storage ability to decrease the indoor temperature fluctuation and shift the peak load. Among the aforementioned design parameters, melting point of PCM is critical to significantly influence the building thermal performance. To effectively account for melting point of PCM and enhance the service efficiency of PCM, a new wall configuration containing PCM with hybrid melting points is proposed. The proposed wall assembly is found to benefit the indoor

thermal comfort and the activation of the latent heat of PCM when the ambient temperature covers cold, mild, and hot loading conditions for the long term. Moreover, coupling vacuum insulation panels (VIP) with extremely low thermal conductivity and PCMs with a large amount of latent heat in the building envelope is another solution to further enhance building thermal performance due to the increased thermal insulation and thermal inertia.

ACKNOWLEDGEMENTS

First and foremost, I would like to thank my advisor, Dr. Zhibin Lin for his constant and patient guidance throughout my doctoral work. Dr.Lin led me to become a researcher with a deeper understanding and more effective communication through visual and written means. I could always get support and encouragement from him whenever I came across academic problems and cannot move forward on my research. He inspired me to reach toward greater self-awareness and solve problems in scientific ways from a different point of view. I consider these lessons provided by Dr.Lin to be of utmost importance to both my personal and professional development.

My sincere appreciation dedicates to the members of my dissertation committee, Professor Fardad Azarmi, Mijia Yang, Longjiang, and Xiaoning Qi, for their continuous attention and input regarding this work. The advice you provided on my research topic and academic writing benefit me a lot and encourage me to explore more insightful research, which has always been and will continue to be invaluable to me. I am particularly grateful to Dr. Fardad Azarmi, Dr. Long Jiang, and Dr. Xiaoning Qi for their great help in my experimental study in this dissertation.

Great thanks to my colleagues at North Dakota State University: Fei Yan, Xingyu Wang, Hong Pan, Zi Zhang, and Matthew Pearson. Thank you for your contributions and help with the experimental study.

Special thanks to my family. I am incredibly grateful for your steadfast support, love, and encouragement throughout this journey.

DEDICATION

To my parents and sister.

TABLE OF CONTENTS

ABSTRACT iii

ACKNOWLEDGEMENTS v

DEDICATION vi

LIST OF TABLES xiii

LIST OF FIGURES xiv

1. INTRODUCTION 1

1.1. Building Energy Consumption-Overview 1

1.2. Applications of PCM in Buildings 3

1.3. Problem Statement 5

1.4. Research Objectives 7

1.5. Research Significance 8

1.6. Organization of the Dissertation 9

1.7. References 11

2. LITERATURE REVIEW 16

2.1. Introduction 16

2.2. Thermal Energy Storage 17

2.2.1. Sensible Heat Storage 17

2.2.2. Chemical Heat Storage 18

2.2.3. Latent Heat Storage 19

2.3. Phase Change Material Classifications and Applications 21

2.3.1. Classification of PCMs 21

2.3.2. Current Applications of PCMs 23

2.4. Review of Previous Studies of PCMs in Building Applications 24

2.4.1. Selection Criteria of PCMs for Building Applications 24

2.4.2. Critical Thermophysical Properties of PCM Used in Buildings 26
2.4.3. Integration of PCMs into Building Elements 45
2.4.4. Inclusion of PCMs into Building Elements 48
2.5. Numerical Simulation of Buildings with PCMs 51
2.5.1. Dynamic Simulation of PCM-based Buildings 51
2.5.2. Simulation Tools 52
2.6. Summary 53
2.7. References 54
3. EXPERIMENTAL STUDY ON THE THERMAL PERFORMANCE OF PCM INTEGRATED INTO LABORATORY-SCALE PROTOTYPES 70
3.1. Introduction 70
3.2. Experimental Description 72
3.2.1. Materials 72
3.2.2. Preparation of EG 72
3.2.3. Preparation of Paraffin/EG Composite PCMs 73
3.2.4. Characterization of Paraffin/EG Composites 74
3.2.5. Thermal Energy Storage Test 74
3.2.6. Thermal Performance Test of Prototypes 75
3.3. Results and Discussions 77
3.3.1. Paraffin Absorption into EG Samples 77
3.3.2. The Phase-change Temperature and the Latent Heat of Phase-change 82
3.3.3. Thermal Storage and Heat Transfer of Paraffin/EG Composite 83
3.3.4. Thermal Performance of Prototypes 86
3.4. Summary 88
3.5. References 89

4. NUMERICAL THERMAL CHARACTERIZATION AND PERFORMACE METRICS OF BUILDING ENVELOPES CONTAINING PHASE CHANGE MATERIALS FOR ENERGY-EFFICIENT BUILDINGS[1] 92

4.1. Introduction 92

4.2. PCMs for Building Envelopes and Building Systems 95

4.2.1. Critical Factors Affecting the Thermodynamics and Energy Efficiency of PCM-Enabled Building Envelopes 95

4.2.2. Performance Metrics for Assessing Energy Efficiency of the Building System 96

4.3. Simulation of Thermodynamics of Building Envelopes Using Exterior Walls Reinforced by PCMs 98

4.3.1. Modeling the Thermodynamics of Building Envelopes in COMSOL 98

4.3.2. Validation of the Model 100

4.3.3. Characterization of Thermodynamics of the Wall Assembly 103

4.4. Results and Discussions 107

4.4.1. Thermodynamics of Building Walls under Instantaneous Loading Conditions 107

4.4.2. Effect of the Location of the PCM Layer within the Wall Assembly on the Thermal Performance 109

4.4.3. Effect of the Melting Point of PCM on the Thermal Performance 112

4.4.4. Effect of the Thickness of PCM Layer on the Thermal Performance 114

4.4.5. Effect of the Latent Heat of PCM on the Thermal Performance 116

4.4.6. Effect of the Thermal Conductivity of PCM on the Thermal Performance 118

4.5. Summary 119

4.6. References 120

5. EFFECT OF MELTING POINT ON THERMODYNAMICS OF THIN PCM REINFORCED RESIDENTIAL FRAM WALLS IN DIFFERENT CLIMATE ZONES[2] 124

5.1. Introduction 124

5.2. Numerically Modeling of PCM-based Building Wall System 128

5.2.1. Wall Types as Thermal Enclosure Commonly Used for the Residential Buildings 128

5.2.2. Description of the Multilayer Frame Walls 131

5.2.3. Numerical Procedure for the PCM-based Multilayer Wall System 132

5.3. Validation of the Numerical Model 136

5.3.1. A Multilayer Wall Building in the Literature 136

5.3.2. Loading Conditions Associated with the Weather 137

5.3.3. Model Calibration and Discussion 138

5.4. Parametric Studies Using the Model 139

5.4.1. Prototype of the Frame Wall 139

5.4.2. Design of Test Cases for the Parametric Study 139

5.4.3. Performance Indexes for Assessing Thermal Performance of the Multilayer Wall System 145

5.5. Results and Discussion 147

5.5.1. Effects of the PCM Location on the Selection of the PCM Melting Point 147

5.5.2. Effects of the PCM Thickness on the Selection of PCM Melting Point 152

5.5.3. Effects of the Loading Conditions Associated with Climate Zones on the Selection of the PCM Melting Point 155

5.5.4. Effects of the Loading Conditions Associated with Different Months on the Selection of the PCM Melting Point 162

5.6. Summary 169

5.7. References 171

6. A NOVEL RESIDENTIAL FRAME WALL CONTAINING PCM WITH HYBRID MELTING POINTS FOR ENERGY-EFFICIENT BUILDINGS 179

6.1. Introduction 179

6.2. Problem Description 182

6.2.1. Description of the Multilayer Frame Walls 182

6.2.2. Case One—Multilayer Wall Including Composite PCM with Hybrid Melting Points 183

6.2.3. Case Two—PCM Blocks with Different Melting Points 184

6.3. Methodology 185

6.3.1. Mathematical Model 185

6.3.2. Boundary Conditions 187

6.3.3. Grid Sensitivity Check and Model Calibration 188

6.3.4. Performance Indexes for Assessing Thermal Performance of the Multilayer Wall System 188

6.4. Results and Discussion 189

6.4.1. Case One—Multilayer Wall Including Composite PCM with Hybrid Melting Points 189

6.4.2. Case Two—Thermal Performance of PCM Blocks 194

6.5. Summary 199

6.6. References 200

7. NUMERICAL INVESTIGATION OF THE THERMAL PERFORMANCE OF BUILDING ENVELOPES COUPLING THERMAL INSULATION AND STORAGE STRATEGIES[3] 204

7.1. Introduction 204

7.2. Numerically Modeling of VIP-PCM-based Building Wall System 208

7.2.1. Description of the Multilayer Frame Walls 208

7.2.2. Thermal Behavior of VIPs 208

7.2.3. PCMs 210

7.2.4. Computational Simulation 211

7.2.5. Mesh Generation and Grid Check 213

7.2.6. Temperature Profiles 214

7.3. Validation of the Numerical Model 217

7.3.1. A Multilayer Wall Building in the Literature 217
7.3.2. Model Calibration and Discussion 219
7.4. Results and Discussion 220
7.4.1. Comparison of Exterior Wall Thermal Performance with VIP and EPS 220
7.4.2. Coupling Effect of VIP and PCM 225
7.5. Summary 237
7.6. References 239
8. CONCLUSIONS AND FUTURE WORK 244
8.1. Conclusions 244
8.2. Future Work 248

LIST OF TABLES

Table		Page
2.1.	Comparison of storage densities of different TES methods (adapted from [15]).	20
2.2.	Application of PCMs in buildings for thermal energy efficiency enhancement.	36
2.3.	Overview of advantages and drawbacks of different incorporation methods.	51
3.1.	The maximum sorption capacity of different EG samples.	78
4.1.	Thermal and physical properties of materials [13].	101
4.2.	Thermal and physical properties of materials used in the building envelope assembly.	104
4.3.	Test matrix of the building envelope under varying design parameters.	105
5.1.	Grid sensitivity check for the numerical model.	135
5.2.	Thermal properties of materials [49].	136
5.3.	Test matrix of the building envelope under varying design parameters.	143
5.4.	The climate characteristics of typical cities in different climate zones.	144
6.1.	Thermal properties of materials [14].	186
6.2.	*ITD* value of RW1, RW2, and the proposed wall.	193
7.1.	Thermal and physical properties of materials [23, 31].	212
7.2.	Thermal properties of materials [23].	218
7.3.	Comparison of VIP and EPS thickness.	221
7.4.	Maximum heat flux oscillation and time delay of each model under various temperature profiles.	232

LIST OF FIGURES

Figure — Page

1.1. Global share of buildings and construction final energy uses and greenhouse gas emissions (2017) [5]. 2

1.2. Energy consumption by end-use in the U.S. (a) Commercial buildings in 2012 and (b) residential buildings in 2015 (modified from EIA data) [8, 9]. 3

1.3. Schematic of building wall including PCM showing the working principle of PCM (adapted from [26]). 5

2.1. TES classifications [9, 10]. 17

2.2. Methods of thermal energy storage (a) Sensible heat, (b) thermochemical reaction, and (c) latent heat (replotted from [12]). 18

2.3. Subcooling effect of a salt hydrate [26]. 22

2.4. Distribution of PCM in building applications (summarized from Table 2.2). 26

2.5. Melting enthalpy versus melting temperature for various materials used as PCMs, modified from [42][43]. 27

2.6. Thermal conductivity of PCMs in building applications (summarized from Table 2.2). 28

2.7. The techniques of thermal conductivity enhancement (adapted from [47]). 29

2.8. History of interior wall surface temperature over time [56]. 31

2.9. Melting temperature of PCMs in building applications (summarized from Table 2.2). 33

2.10. DSC measurement curve of (a) Paraffin [61] and (b) $CaCl_2 \cdot 6H_2O$[62] under different heating/cooling cycles. 34

2.11. Building element that including PCM for thermal management (summarized from Table 2.2). 46

2.12. Integrating location of PCM in building elements (summarized from Table 2.2). 48

3.1. Scanning electron microscopy (SEM) images of (a) flaky expandable graphite and (b) worm-like expanded graphite [14]. 73

3.2. The fabrication process of paraffin/EG composite. 74

3.3. Thermal energy storage test. 75

3.4. Test prototypes and schematic representation of wall configurations. 1: oriented strand board (OSB), 2: PCM composite, and 3: insulating layer. 76

3.5. FTIR spectra of the EG prepared under different heating temperatures and NEG. 79

3.6. Pore size distribution of EG. 80

3.7. SEM images of (a) EG and (b) paraffin/EG composite. 81

3.8. DSC curves of the pure paraffin and paraffin/EG composites. 83

3.9. Thermal storage and heat transfer of paraffin/EG composite. 84

3.10. Thermal behavior of paraffin/EG composites with different paraffin contents. 86

3.11. Instantaneous temperature of the chamber and the inside of the prototypes as a function of time. 87

4.1. ITD_{over} and *FTC*: graphic definition (replotted from [18]). 97

4.2. Loading conditions of Austin, Texas (a) External dry air temperature and (b) radiation on the external surface of the wall. 100

4.3. The wall assembly used for the calibration. 101

4.4. Input loading condition for validation (a) External dry air temperature and (b) radiation on the external surface of the wall (replotted from [13]). 102

4.5. Temperature profile through the wall thickness at 20 h. 103

4.6. A schematic diagram showing the wall assemblies of a typical external wall (unit: mm). 104

4.7. Figure Different schematic diagrams showing the investigated wall configurations. 106

4.8. Thermodynamics of the (a) heating and (b) cooling processes through the temperature profile over the wall thickness. 108

4.9. Thermal contour over the wall thickness under different test periods: (a) 30 h and (b) 10 h. 108

4.10. History of interior wall surface temperature over time: (a) transient temperature and (b) peak temperature. 110

4.11. Performance metrics ITD_{over} and *FTC* under different placements of the PCM layer..... 111

4.12. Transient temperatures of the interior wall surface over time. 113

4.13. ITD_{over} under different melting points of the PCM layer. 114

4.14. History of interior wall surface temperatures over time: (a) transient temperatures and (b) *FTC* results. 115

4.15. ITD_{over} under different thicknesses of the PCM layer..... 116

4.16. Time history of interior wall surface temperature with under different melting points of the PCM layer: (a) 24 °C and (b) 28 °C..... 117

4.17. Performance metrics of the models with different heat of fusions of the PCM: (a) ITD_{over} and (b) *FTC*..... 118

4.18. History of interior wall surface temperatures over time: (a) transient temperature and (b) peak temperature. 118

5.1. Methods of thermal energy storage (a) Sensible heat, (b) latent heat, and (c) thermochemical reaction (replotted from [6]) 124

5.2. Typical configurations of exterior walls (a) Masonry wall, (b) steel frame wall, and (c) wood frame wall (replotted from [43]). 130

5.3. Schematics of residential wall systems strengthened by thin PCM layer. 132

5.4. COMSOL heat transfer model (a) geometry, mesh and boundary conditions and (b) mesh sensitivity study. 135

5.5. The multilayer wall (a) dynamic wall simulator in the laboratory test [49] and (b) schematic diagram showing the wall assembly. 137

5.6. The boundary conditions of the multilayer wall. 137

5.7. Comparison of test results and proposed study (a) transient temperature result (b) heat flux result..... 138

5.8. A schematic diagram showing (a) the assembly of the investigated external wall (unit: mm) and (b) boundary conditions. 139

5.9. Evolution of the temperature at the first week of July in Chicago. 141

5.10. Schematic of wall systems with different PCM layer locations. For the numbers in the schematics, 1: gypsum board, 2: PCM layer, 3: insulating layer, 4: OSB. 142

5.11. Map of different climate zones. 143
5.12. Weather conditions of (a) Minneapolis and (b) Austin. 145
5.13. Graphic definition of (a) ITD_{up} and (b) ITD_{down} (adapted from [60]). 145
5.14. Transient temperature of the interior wall surface over time. 149
5.15. *ITD* values of (a) L0-D5 and (b) L4-D5. 150
5.16. ITD_{up} contour of (a) whole test period and (b) 4-days test period. 151
5.17. ITD_{down} contour of (a) whole test period and (b) 4-days test period. 152
5.18. Temperature changes over thickness. 153
5.19. *ITD* contour showing the effectiveness of PCM layer thickness. 154
5.20. ITD_{up} contour of different test period (a) 1 day, (b) 4 days, and (c) 7 days. 155
5.21. ITD_{down} contour of the different test periods (a) 1 day, (b) 4 days, and (c) 7 days. 155
5.22. The equivalent sol-air temperature of five typical U.S. cities. 156
5.23. Indoor transient temperature of the wall located in different cities over time. 159
5.24. *ITD* contour of different cities. 161
5.25. Indoor transient temperature over the first week of different months in Austin. 164
5.26. Optimal PCM melting point for different months in Austin. 165
5.27. Monthly ITD_{up} and ITD_{down} value of the PCM-based and reference wall. 166
5.28. Transient temperature of the interior wall surface over time in Minneapolis. 167
5.29. Optimal PCM melting point for different months in Minneapolis. 168
5.30. Monthly ITD_{up} and ITD_{down} value of the PCM-based and reference wall. 169
6.1. Schematics of reference wall systems. 183
6.2. Schematics of wall systems including PCMs with hybrid melting points. 184
6.3. Schematics of PCM blocks with (a) hybrid melting point and (b) single melting point. 184
6.4. Solar-air temperature applied on the wall exterior surface. 188

6.5. Instantaneous indoor temperature of RW1, RW2, and the proposed wall..... 190

6.6. (a) Maximum and (b) minimum peak of the instantaneous temperature of each wall..... 191

6.7. Instantaneous indoor temperature of the proposed wall incorporating PCMs with 180 J/g and 360 J/g, respectively. 194

6.8. Instantaneous temperature of the PCM blocks with various melting points and latent heat capacities. 195

6.9. Temperature contour of PCM blocks at different center temperatures..... 196

7.1. Typical VIP structure showing (a) the main components [7], and (b) a comparison of equivalent thermal resistance thickness between traditional thermal insulation and VIP [8]..... 205

7.2. Schematic diagram of the original residential wall configuration. 208

7.3. COMSOL heat transfer model (a) geometry, mesh, and boundary conditions and (b) mesh sensitivity study. 214

7.4. Sinusoidal function temperature profiles as input loading conditions..... 215

7.5. Solar-air temperature profiles of Minneapolis and Austin for (a) January and (b) July..... 216

7.6. The multilayer wall (a) dynamic wall simulator in the laboratory test [23] and (b) schematic diagram showing the wall assembly. 217

7.7. The boundary conditions of the multilayer wall. 218

7.8. Comparison of test results and proposed study (a) transient temperature result (b) heat flux result..... 219

7.9. Schematic of the wall investigated. 1: gypsum board, 2: insulation layer, 3: OSB, 4: PCM layer. 220

7.10. Heat flux changes through walls with different insulation layers..... 222

7.11. Comparison of the thermal performance of walls with VIP and EPS. 223

7.12. Schematic of wall assemblies with various VIP thicknesses..... 226

7.13. Instantaneous heat flux through walls under sinusoidal temperature profiles with different amplitudes. 227

7.14. Maximum heat flux oscillation of the wall with different VIP thicknesses and subjected to temperature profile with different amplitudes. 228

7.15. Schematic of wall assemblies with various PCM thicknesses. 229

7.16. Instantaneous heat flux through walls under sinusoidal temperature profiles with different amplitudes. 231

7.17. Instantaneous heat flux through walls under real temperature profiles of Austin and Minneapolis with various VIP thicknesses. 234

7.18. Instantaneous heat flux through walls under real temperature profiles of Austin and Minneapolis with various PCM thicknesses. 236

1. INTRODUCTION

1.1. Building Energy Consumption-Overview

The fast economic and population growth all over the world relies on the rapid increase in energy consumption, which leads to accelerated depletion of the conventional energy resources (fossil fuels) and the associated environmental impact such as greenhouse gas emissions [1, 2]. Furthermore, global energy consumption is expected to grow by nearly 50% in 2050, and energy-related carbon dioxide (CO_2) emissions rise at a rate of 0.6% per year between 2018 and 2050 [3]. Currently, the worldwide concern for energy exhaustion and environmental contamination significantly boosts the demand to improve energy efficiency and develop more environmentally benign energy use.

Among different energy end-uses, the buildings sector is the largest energy demand sector, consuming over one-third of total global energy [4]. In 2017, building constructions and operations are responsible for 36% of the global final energy use and 39% of energy-related CO_2 emissions (see Figure 1.1) [5]. More specifically, residential and commercial buildings account for approximately 40% of the total U.S. energy consumption, greater than that for either industry (32%) or transportation (29%) according to the U.S. DOE report 2019 [5]. Similar statistics hold for Europe. In 2015, the Building-related sector produces a demand of 422 million tons of oil equivalent, corresponding to 39% of the total final energy demand of the European Union member [6][7]. Therefore, moving towards more energy-efficient buildings has gained increasing attention to save energy.

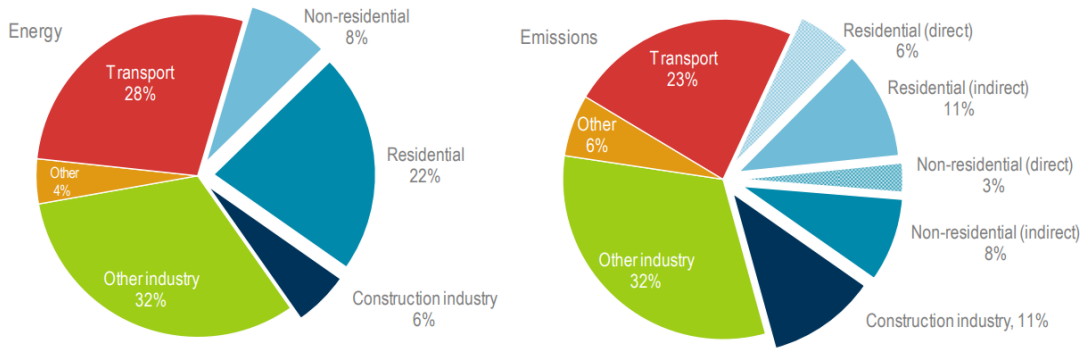

Figure 1.1. Global share of buildings and construction final energy uses and greenhouse gas emissions (2017) [5].

Looking at the energy end-uses, space heating and cooling make up a large proportion of the total energy consumption in buildings. Figure 1.2(a) and 1.2(b) show the relative energy consumption by end-use for commercial buildings in 2012 and residential buildings in 2015 in the U.S., respectively. One can see that space heating and cooling account for approximately 17% of the primary energy consumption by commercial buildings in 2012 [8]. For residential buildings, this number even reaches 51% in 2015[9]. According to the latest data published by Eurostat [10], about 64% of the European household's annual energy supply was consumed by the heating, ventilation, and air conditioning (HVAC) system in 2018.

Given the considerable energy consumed by space heating and cooling all over the world, reducing the energy required by HVAC systems becomes a primary backbone of enhancing building energy efficiency. On the other hand, enhancing the use of renewable energy sources is decisive concerning the reduction of buildings' dependency on traditional energy resources. According to the work programme of European Commission in "Secure, Clean and Efficient Energy" Horizon2020, the requirements of increasing energy efficiency can be fulfilled by utilizing thermal energy storage (TES) system [11]. TES system is a temporary energy storage medium that allows the renewable energy generated from solar radiation or night-time cold and

stored in building elements for later use. This technology exhibits benefit in various aspects, such as maintaining indoor thermal comfort for a longer time [12], shifting the electrical load from peak to off-peak operation period [4], and thus improving the overall building energy efficiency [13, 14].

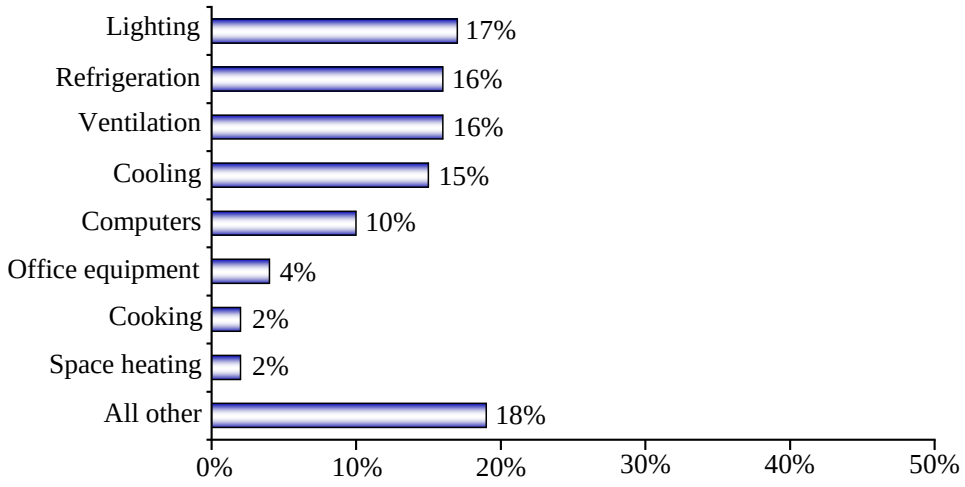

(a)

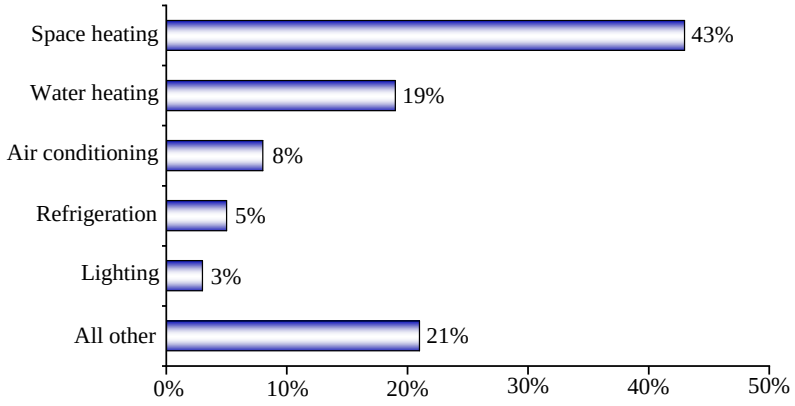

(b)

Figure 1.2. Energy consumption by end-use in the U.S. (a) Commercial buildings in 2012 and (b) residential buildings in 2015 (modified from EIA data) [8, 9].

1.2. Applications of PCM in Buildings

Thermal energy storage can be accomplished by using sensible heat, latent heat, and chemical heat according to Abhat [15] and Khadrian et al. [16]. Among them, latent heat storage

in the form of phase change material (PCM) shows its superiority in enhancing energy efficiency due to its higher thermal energy storage capacity than sensible heat and more stable operating process than chemical reaction method [17]. PCMs undergo a phase transition from solid to liquid state when subjected to temperatures exceeding their melting point, during which a large amount of heat can be absorbed and stored. Reversibly, they can release the stored thermal energy when the ambient temperature falls below their freezing point. During these phase transition processes, the temperature of PCMs keeps in a small interval, rendering them promising isothermal nature and the feasibility of better thermal management.

During the last decades, PCMs have been widely used as passive or active TES strategies in different fields to bridge the gap between the increasing energy consumption demand and the full utilization of renewable energy sources. With proper physical and thermal properties, they can be used against heat and cold and smooth the temperature swing in a variety of applications. For instance, PCMs integrated in the solar energy system can produce an increase in solar fraction and heat accumulation compared with the traditional water-based solar thermal system [18]. They also attract tremendous attention in the application field of electronic cooling [19], industrial heat recovery [20], spacecraft thermal system[21], textiles [22], thermal protection of food [23], medical transport [24], etc.

In this dissertation, the application of PCMs in buildings is emphatically discussed. When being integrated into building elements, they show desirable qualities like increasing the thermal inertia of building elements, smoothing the indoor temperature fluctuations, and delaying the peak temperature occurrence, thus enhancing the use of off-peak power. Owing to PCMs' isothermal nature, the indoor temperature of a building can be leveled in the vicinity of their melting and freezing temperature (see Figure 1.3). With high heat of fusion and proper phase

transition temperature interval, they are capable of enhancing the thermal comfort of the occupants and the overall building energy efficiency [25].

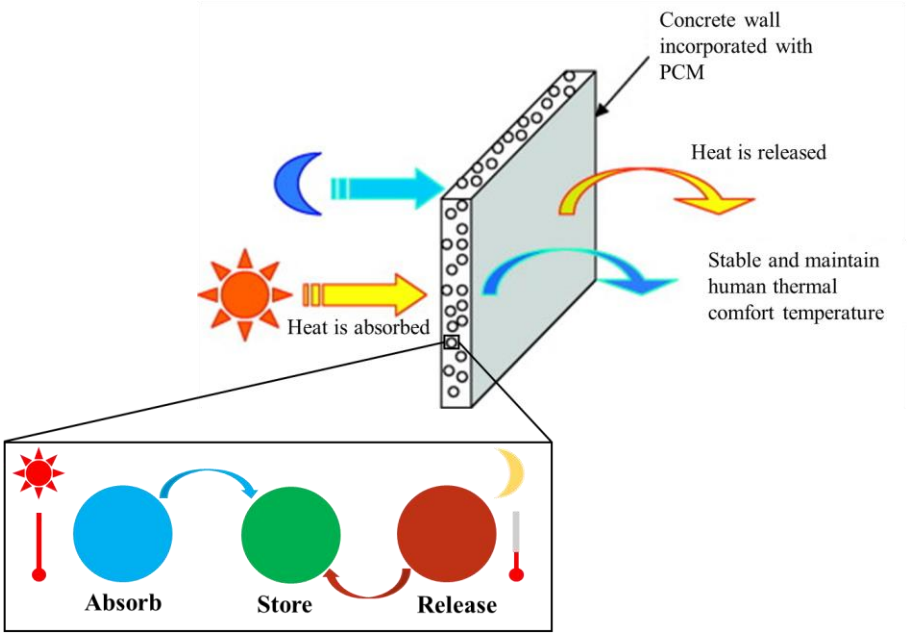

Figure 1.3. Schematic of building wall including PCM showing the working principle of PCM (adapted from [26]).

In recent years, the feasibility of applying PCMs in building envelopes and construction materials for energy saving has received considerable attention. The field of research has covered various aspects, such as the selection criteria of PCMs for building use [26], the impact of incorporating location of PCM layer [27, 28], thermal conductivity enhancement technology for improving PCMs' heat transfer rate [29], and different enclosing methods for preventing PCMs leakage[30], which will be detailly reviewed in Chapter 2.

1.3. Problem Statement

Despite the aforementioned superiorities of PCMs as a thermal management strategy, widespread use of PCMs in buildings still faces several challenges, and the currently existing problems are yet to be clarified and solved.

During the last decade, researchers have made great efforts in the integration of PCM in building envelopes, however, how to select proper PCMs for various building envelopes under different temperature loading conditions still poses high challenges. Several attempts have been conducted through the determination of proper PCM melting temperature, to improve the efficiency of the latent heat energy absorbed and released by PCMs. Tyagi and Buddhi [17] recommended that PCMs with melting temperatures between 20°C and 32°C can be used for thermal energy storage in terms of heating and cooling in buildings. Zhou et al. [31] indicated that PCMs with phase change temperatures ranging from 18°C to 30°C were preferred to meet the need for thermal comfort in the building applications since they covered the thermal comfort range of human beings. Clearly, there were high variances among these studies and more importantly, these investigations limited their applications to specific cases, in which few attempted to address the impacts of wide ranges of climate zones. Therefore, more research is needed to comprehensively address the factors affecting the selection of PCMs for a building envelope.

Considering that the utilization efficiency of the latent heat capacity of PCMs could be affected by multiple critical factors, including the integrating location of PCM layer, melting points of PCM, PCM heat of fusion, the volume of the integrated PCM, and thermal conductivity of PCM. The existing studies that often discussed one or two variables fell short to systematically explore the thermal dynamics of a structure element, especially under specific and realistic temperature profiles for various U.S. cities. Moreover, limited resources are available to demonstrate the strategy to further improve the energy efficiency of PCM-based building envelopes based on the crucial factors that may influence their thermal performance.

1.4. Research Objectives

In this dissertation, to address the challenges mentioned above, the major objectives of this research are:

- To develop new understandings and technologies that form the basis for a fundamental understanding of the working mechanism of PCMs applied in buildings for better thermal management, using both experimental and numerical methods.
- To investigate the influence of different factors including the integrating location, melting point, latent heat capacity, total volume, and thermal conductivity of PCM on the thermal performance of the PCM-based building envelopes.
- To analyze the thermal dynamics of PCM-based building envelopes subjected to different weather conditions, including the sinusoidal function temperature profile and the real-time temperature profiles of different U.S. cities.
- To provide design suggestions for better utilization of the PCM-based building envelope in different climate regions.
- To comprehensively evaluate the thermal performance of the wall using various performance indexes.
- To develop a strategy that integrating PCM with hybrid melting points into buildings to further enhance the energy efficiency of the PCM-based building envelope according to the fundamental understanding of PCM's working principle.
- To evaluate the feasibility of an energy-saving building wall by coupling PCMs with vacuum insulation panels (VIPs) as a compact unit that could significantly reduce heat flux through the building wall.

1.5. Research Significance

PCMs generally demonstrate great potential as a building thermal management strategy in the implementation of free cooling and heating. Their high heat of fusion, isothermal nature, and ability to employ renewable natural resources bring them greater prospects than the traditional indoor temperature control method using the HVAC system. Although the utilization of PCMs in building applications has gained great achievements by various investigations, more comprehensive analysis is still needed to provide a fundamental understanding of PCMs' working mechanisms, thus leading to new strategies to further improve the energy efficiency of buildings reinforced by PCMs.

More extensive acceptance and application of PCMs in building applications requires: (1) fully understanding of the thermal dynamics of building envelopes associated with the integrating location, melting point, heat of fusion, total integrated volume, and thermal conductivity of PCM; (2) an estimate on the long-term thermal performance of PCM-based building envelope under real-time temperature loading conditions of cities located in different climate zones; (3) strategy that can further improve the energy efficiency of PCM-based buildings.

Previous tests have provided various short-term data mainly from the point of the whole building; however, those test results generally exhibit large discrepancies, without detailly showing the thermal dynamics of building components with PCM. Meanwhile, long-term monitoring statistics for the thermal performance in field conditions are time-consuming whereas the building energy efficiency at present needs urgent enhancement. Moreover, the short-term data lacks general applicability when environmental condition changes, such as the temperature changes during different months all the year round or cities located in different climate zones.

Despite significant efforts in PCMs technologies and their applications to buildings, how to effectively improve the energy efficiency of latent heat generated from PCMs for building application and how to select proper PCMs for buildings under different loading conditions still post great challenges. The lack of systematic and comprehensive studies in these gaps hinders their broad applications in the building sector. Therefore, this dissertation aims to present both experimental and numerical analysis, providing a fundamental understanding of the thermal dynamics of the PCM-based building envelopes which will aid in designing strategies for enhancing the long-term energy efficiency of the building subjected to different loading conditions. The proposed improvement strategy can help to enhance the building's energy efficiency, thus downsizing the use of HVAC systems.

1.6. Organization of the Dissertation

This dissertation is constructed with eight chapters:

Chapter 1 introduces the background and currently existing problems of the application of PCM in buildings, and then presents the research significance and objectives, as well as the organization of this dissertation.

Chapter 2 presents a comprehensive literature review on the thermal performance of buildings reinforced by PCMs. The critical criteria that govern the selection of PCM for buildings and the current selection tendency are studied based on the statistical analysis, providing a sound basis for the subsequent experimental and numerical study.

Chapter 3 presents an experimental investigation on the thermal performance of a novel shape-stabilized PCM. Both microscopic and macroscopic experiments are conducted to explore its potential to be used for building thermal management.

Chapter 4 presents the thermodynamics of PCM-enabled building envelopes using numerical investigation. A comprehensive and systematic study is conducted on external wall assemblies reinforced by a PCM layer as a representative under summer weather loading conditions. A parametric study focuses on identified critical variables, including the integrating location, melting temperature, latent heat, total integrating thickness, and thermal conductivity of PCMs. Four metrics including the temperature swings, the peak temperature reduction, the intensity of thermal discomfort for overheating, and frequency of thermal comfort are utilized to assess the building thermal performance.

Chapter 5 presents the study that numerically investigates the optimal PCM melting temperature when being used to improve the thermal performance of multi-layered residential walls. Real temperature profiles extracted from Typical Meteorological Year databases of various U.S. cities located in different climate zones are applied to the wall external surface as the boundary condition. The developed model is used to explore the influence of PCM location, thickness, and loading conditions associated with different climate zones and months on the selection of PCM melting points for building thermal management.

Chapter 6 presents a numerical study that explores the potential thermal comfort benefits of integrating PCM with hybrid melting points into an external wall of the residential building subjected to changeable loading conditions covering cold, mild, and hot scenarios. The impact of latent heat capacity of the PCM on the thermal performance of the investigated domain is also investigated.

Chapter 7 investigates the thermal performance of a multilayered frame wall coupling PCM and VIP layer on the wall interior side. The examined combinations of the multilayer assemblies can find direct application in frame wall construction due to their exceptionally good

thermal insulation properties, relatively low thickness and weight, as well as high thermal storage capacity.

Chapter 8 summarizes the primary conclusions and addresses future research directions.

1.7. References

[1] S. Ramakrishnan, X. Wang, J. Sanjayan, J. Wilson, Thermal performance of buildings integrated with phase change materials to reduce heat stress risks during extreme heatwave events, Applied Energy 194 (2017) 410-421.

[2] D. David, F. Kuznik, J.-J. Roux, Numerical study of the influence of the convective heat transfer on the dynamical behavior of a phase change material wall, Applied Thermal Engineering 31(16) (2011) 3117-3124.

[3] USDOE., 2019. Office of Energy Efficiency and Renewable Energy (EERE) [WWW Document]. URL https://eere-exchange.energy.gov/FileContent.aspx?FileID=47a67630-e409-4a5e-bb3f-951bee69d864 (accessed 3.19.2020)

[4] P. Devaux M.M. Farid, Benefits of PCM underfloor heating with PCM wallboards for space heating in winter, Applied Energy 191 (2017) 593-602.

[5] IEA, 2018. Global Status Report: Towards a zero-emission, efficient and resilient buildings and construction sector, Internatl Energy Agency and UN Environ Progr.

[6] Olivieri, L., Tenorio, J.A., Revuelta, D., Navarro, L. and Cabeza, L.F., 2018. Developing a PCM-enhanced mortar for thermally active precast walls. Construction and Building Materials, 181, pp.638-649.

[7] Eurostat, Energy Balance Sheets. 2015 Data (2017 ed.) (2017) [WWW Document]. URL https://ec.europa.eu/eurostat/web/products-statistical-books/-/KS-EN-17-001 (accessed 5.18.2018)

[8] EIA, 2012, Energy use in commercial buildings [WWW Document]. URL https://www.eia.gov/energyexplained/use-of-energy/commercial-buildings.php (accessed 12.10.2018)

[9] EIA, 2015, Energy use in homes[WWW Document]. URL https://www.eia.gov/energyexplained/use-of-energy/homes.php (accessed 12.10.2018)

[10] Eurostat, Energy consumption in households. (2018) [WWW Document]. URL https://ec.europa.eu/eurostat/statistics-explained/pdfscache/58200.pdf (accessed 10.12.2018)

[11] European Commission. Secure, Clean and Efficient Energy. (2020) [WWW Document]. URL http://ec.europa.eu/programmes/horizon2020/en/h2020-section/secure-clean-and-efficient-energy (accessed on 7.16.2020).

[12] G. Evola, L. Marletta, F. Sicurella, Simulation of a ventilated cavity to enhance the effectiveness of PCM wallboards for summer thermal comfort in buildings, Energy and Buildings 70 (2014) 480-489.

[13] K.H. Khan, M.G. Rasul, M.M.K. Khan, Energy conservation in buildings: cogeneration and cogeneration coupled with thermal energy storage, Applied Energy 77(1) (2004) 15-34.

[14] R. Parameshwaran, S. Harikrishnan, S. Kalaiselvam, Energy efficient PCM-based variable air volume air conditioning system for modern buildings, Energy and Buildings 42(8) (2010) 1353-1360.

[15] A. Abhat, Low temperature latent heat thermal energy storage: Heat storage materials, Solar Energy 30(4) (1983) 313-332.

[16] T. Khadiran, M.Z. Hussein, Z. Zainal, R. Rusli, Advanced energy storage materials for building applications and their thermal performance characterization: A review, Renewable and Sustainable Energy Reviews 57 (2016) 916-928.

[17] V.V. Tyagi D. Buddhi, PCM thermal storage in buildings: A state of art, Renewable and Sustainable Energy Reviews 11(6) (2007) 1146-1166.

[18] M. Kenisarin K. Mahkamov, Solar energy storage using phase change materials, Renewable and Sustainable Energy Reviews 11(9) (2007) 1913-1965.

[19] M. Li, N. Gong, J. Wang, Z. Lin, Phase Change Material for Thermal Management in 3D Integrated Circuits Packaging. In International Symposium on Microelectronics (2015) 000649-000653.

[20] J. Jia W.L. Lee, Applying storage-enhanced heat recovery room air-conditioner (SEHRAC) for domestic water heating in residential buildings in Hong Kong, Energy and Buildings 78 (2014) 132-142.

[21] W.F. Wu, N. Liu, W.L. Cheng, Y. Liu, Study on the effect of shape-stabilized phase change materials on spacecraft thermal control in extreme thermal environment, Energy Conversion and Management 69 (2013) 174-180.

[22] A. Shaid, L. Wang, S. Islam, J.Y. Cai, R. Padhye, Preparation of aerogel-eicosane microparticles for thermoregulatory coating on textile, Applied Thermal Engineering 107 (2016) 602-611.

[23] H.M. Hoang, D. Leducq, R. Pérez-Masia, J.M. Lagaron, E. Gogou, P. Taoukis, G. Alvarez, Heat transfer study of submicro-encapsulated PCM plate for food packaging application, International Journal of Refrigeration 52 (2015) 151-160.

[24] Y.J. Kim, B. Kim, J.W. Kim, G. Nam, H.S. Jang, S.W. Kang, U. Jeong, Combination of nanoparticles with photothermal effects and phase-change material enhances the non-invasive transdermal delivery of drugs, Colloids Surf B Biointerfaces 135 (2015) 324-331.

[25] F. Agyenim N. Hewitt, The development of a finned phase change material (PCM) storage system to take advantage of off-peak electricity tariff for improvement in cost of heat pump operation, Energy and Buildings 42(9) (2010) 1552-1560.

[26] Ningbo Thermal New Energy Technology co.,ltd. <https://www.phasechange-material.com/sale-13479253-lhs-non-corrosive-non-toxic-pcm-building-materials.html>.

[27] H. Akeiber, P. Nejat, M.Z.A. Majid, M.A. Wahid, F. Jomehzadeh, I. Zeynali Famileh, J.K. Calautit, B.R. Hughes, S.A. Zaki, A review on phase change material (PCM) for sustainable passive cooling in building envelopes, Renewable and Sustainable Energy Reviews 60 (2016) 1470-1497.

[28] K.O. Lee, M.A. Medina, E. Raith, X. Sun, Assessing the integration of a thin phase change material (PCM) layer in a residential building wall for heat transfer reduction and management, Applied Energy 137 (2015) 699-706.

[29] X. Jin, M.A. Medina, X. Zhang, On the importance of the location of PCMs in building walls for enhanced thermal performance, Applied Energy 106 (2013) 72-78.

[30] Y. Lin, Y. Jia, G. Alva, G. Fang, Review on thermal conductivity enhancement, thermal properties and applications of phase change materials in thermal energy storage, Renewable and Sustainable Energy Reviews 82 (2018) 2730-2742.

[31] S. Ramakrishnan, J. Sanjayan, X. Wang, M. Alam, J. Wilson, A novel paraffin/expanded perlite composite phase change material for prevention of PCM leakage in cementitious composites, Applied Energy 157 (2015) 85-94.

[32] D. Zhou, C.Y. Zhao, Y. Tian, Review on thermal energy storage with phase change materials (PCMs) in building applications, Applied Energy 92 (2012) 593-605.

2. LITERATURE REVIEW

2.1. Introduction

Thermal energy storage (TES) system is a temporary energy storage medium that can be used to store the renewable energy generated from solar radiation or night-time cold for later use. During the last few decades, a large number of researches have focused on the integration of this system in buildings for energy saving [1, 2]. It turns out to be a promising technology to reduce the energy consumption in buildings [3], to increase building energy efficiency [4], to shift the electrical energy peak load [5], and to maintain indoor thermal comfort for a longer time [6]. TES can be implemented by sensible heat, chemical heat, and latent heat. When being used for thermal management of buildings, latent heat storage based on PCMs is gaining increasing interest due to its advantages such as high energy storage capacity, isothermal nature during the phase change process, and high potential to increase the thermal inertia of the building envelope. PCM is firstly considered to be used as TES media for building thermal management before 1980 [7]. Telkes [8] conducts the first experimental application of PCMs for solar energy storage in buildings in 1974. Since then, a considerable amount of research work has been accomplished. In recent years, both experimental and numerical investigations on the utilization of PCMs in buildings have been carried out to explore the selection criteria of PCMs for building applications, the development of high-performance PCMs, methods of incorporation into building envelopes, crucial design parameters influencing building energy efficiency, and the thermal performance of PCM-based buildings subjected to various loading conditions.

Despite numerous investigations on PCMs in different applications, only a few have addressed the relationship between the overall using tendency of PCMs and the corresponding building thermal performance. This review mainly focuses on the application of PCM in building

components with section 2.2 about the classification of TES system, Section 2.3 about the categories of PCMs and their application in different fields, Section 2.4 about the main criteria that govern the selection of PCM for buildings and the selection tendency based on current existing investigations, as well as Section 2.5 about the numerical simulation of buildings reinforced by PCMs. This study may help to provide guidelines for a building thermal management design and point to future research possibilities on PCM-based building envelopes subjected to different climatic conditions.

2.2. Thermal Energy Storage

Thermal energy can be stored in the material in three main forms including sensible heat, latent heat, and chemical heat based on the summary of Khadrian et al. [9] and Abhat [10]. Figure 2.1 shows the TES classifications and insight on their substances.

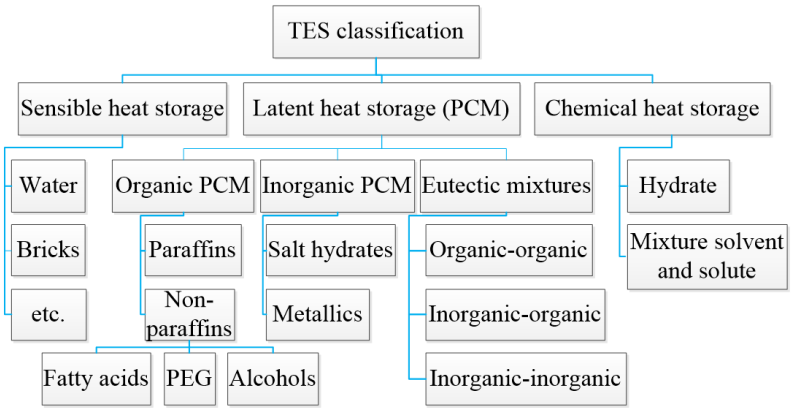

Figure 2.1. TES classifications [9, 10].

2.2.1. Sensible Heat Storage

Sensible heat storage is the most common method of heat and cold storage (see Figure 2.2(a)). Here energy is stored by changing the temperature of the employed materials, such as water, air, wood, bricks, or concrete. There is no phase change occurred when the sensible heat storage materials undergo an energy storage process. The amount of the sensible heat energy

stored in a material (Q) is determined by the mass of a storage medium, heat capacity, and the temperature variation in the form [11]:

$$Q = mC_p(T_f - T_i) \tag{2.1}$$

where m is the mass of storage material (kg), C_p is the specific heat of the storage material (J/kg·°C), T is the temperature (°C), which can be expressed as the difference between final instantaneous temperature T_f and initial instantaneous temperature T_i.

The main advantages of the sensible heat storage system are low cost and long working stability [9]. However, a large amount of the employed material is often needed to achieve desired thermal mass for building applications due to its relatively low heat storage capacity.

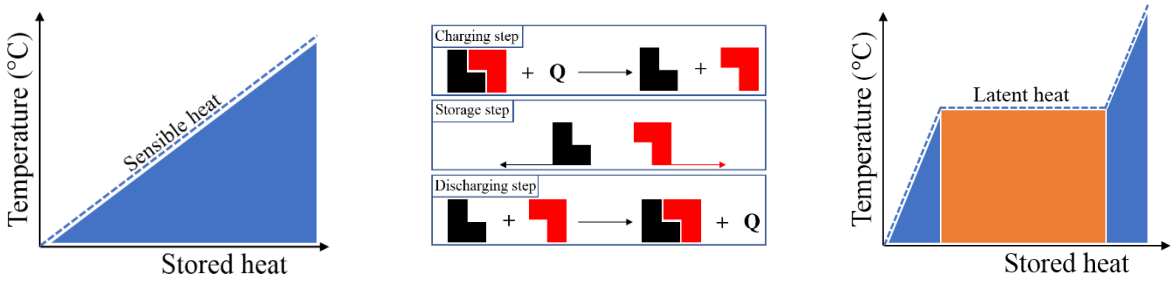

(a) (b) (c)

Figure 2.2. Methods of thermal energy storage (a) Sensible heat, (b) thermochemical reaction, and (c) latent heat (replotted from [12]).

2.2.2. Chemical Heat Storage

The second form of TES is chemical energy storage (see Figure 2.2(b)). Heat energy is absorbed or released during the reversible chemical reactions utilizing the formation and breaking of molecular bonds. The amount of the heat energy Q generated by a reaction can be expressed as [13],

$$Q = a_r m \Delta h_r \tag{2.2}$$

where a_r is the fraction reacted, m is the mass of the storage media (kg), and Δh_r is the endothermic heat of reaction. Yan et al. [14] presented an extensive review on the chemical reaction heat storage and provided a good insight into the advantages and drawbacks of this energy storage method. According to their summary, chemical heat storage shows a promising potential to be used in many applications owing to its high thermal energy storage density and long-term thermal energy storage with negligible heat loss. It possesses higher heat storage density than other TES forms including phase transition [15]. Nevertheless, this technology requires a bulky and complex chamber to complete chemical reactions and suffers from chemical hazards, therefore is not suitable for being used in building applications.

2.2.3. Latent Heat Storage

Latent heat thermal storage (LHTS) is when PCMs capture and release heat during the melting and solidification process [16]. It is an attractive technique and has taken increasing attention over the last decades for thermal management in buildings since it provides a high energy storage density and can store and release latent heat at a relatively constant temperature range (see Figure 2.2(c)). The heat energy storage capacity of a PCM (Q) can be expressed as [13],

$$Q = \int_{T_i}^{T_m} mC_p\, dT \; + m\Delta h_m + \; \int_{T_m}^{T_f} mC_p\, dT \tag{2.3}$$

$$Q = m[C_{sp}(T_m - T_i) + \Delta h_m + \; C_{lp}\big(T_f - T_m\big)] \tag{2.4}$$

where m is the mass of heat storage medium (kg), Δh_m is the heat of fusion per unit mass (J/kg), T_m is the melting temperature of the PCM (°C), C_{sp} is the average specific heat between T_i and T_m (J/kg·°C), and C_{lp} is the average specific heat between T_m and T_f (J/kg·°C). PCM is able to store much more heat energy than sensible heat storage material if the temperature range between T_f and T_i has covered the melting temperature of the PCM. This additional amount of

the energy is the latent heat thermal energy, which is determined by the heat of fusion h_m and mass of the storage material m. Compared with sensible heat energy storage, LHTS technique has proved to be a better engineering option due to its large energy storage capacity for a given mass or volume.

A comparison of the energy storage capacity achieved with different TES methods is shown in Table 2.1 [15]. One can see that chemical reactions can store much more heat energy than the sensible heat storage method and LHTS technique. However, the complexity of the reaction chamber and chemical hazard problem significantly limit its application, especially in the building industry. LHTS based on PCM shows great potential for building thermal management due to its safety and relatively high storage density, which is much higher than that of the sensible heat storage material. Devaux et al. [5] reported that PCM can store 5 to 14 times more heat per unit volume than sensible heat storage media such as masonry and rock. Therefore, PCM can accumulate much more heat or cold energy and overcome the mismatch between the supply and demand energy when being used for building space heating and cooling.

Table 2.1. Comparison of storage densities of different TES methods (adapted from [15]).

		MJ·m^{-3}	**kJ·kg^{-1}**	**Comments**
Sensible heat	Granite	50	17	ΔT= 20 °C
	Water	84	84	ΔT= 20 °C
Latent heat	Paraffins	180	200	$T_{melting}$= 5-130 °C
	Salt hydrates	300	200	$T_{melting}$= 5-130 °C
	Salts	600-1500	300-700	$T_{melting}$= 300-800 °C
Chemical reaction	H_2 gas (oxidation)	11	120000	300K, 1 bar
	H_2 gas (oxidation)	2160	120000	300K, 200 bar
	H_2 liquid (oxidation)	8400	120000	20K, 1 bar
	Fossil gas	32	-	300K, 1 bar
	Gasoline (petroleum)	33000	43200	(Diekmann et al.1997)

2.3. Phase Change Material Classifications and Applications

2.3.1. Classification of PCMs

PCMs can be any material that is capable of absorbing, storing, and releasing latent heat energy by changing the phase from one state to another. According to the phase change state, they fall into three categories: solid-solid, solid-liquid, and liquid-gas PCMs. Among them, the solid-liquid PCMs are most suitable for TES of buildings due to their suitable melting temperature range and low vapor pressure. A large number of solid-liquid PCMs are available in various melting temperature ranges and thermal storage densities. The classification of solid-liquid PCMs (organic, inorganic, and eutectic) is given in Figure 2.1 basing on chemical components.

2.3.1.1. Organic PCMs

Organic PCMs can be further classified as paraffin and non-paraffin. Paraffin consists of a mixture of a mostly straight chain of saturated hydrocarbons (n-alkanes) with the chemical formula of CH_3-(CH_2)-CH_3.The thermal properties of paraffin including melting point and latent heat of fusion both increase with the chain length. Paraffin PCMs have been utilized to reduce buildings' energy consumption for heating and cooling by many researchers [17-19]. The major advantage of using them as thermal energy storage material is their very little or no sub-cooling and non-corrosive nature [20]. The key issue that needs to be addressed is paraffin's low thermal conductivity which has limited their widespread utilization. The non-paraffins include a variety of organic materials such as fatty acids, esters, alcohols, and glycols [21]. They have generally excellent melting and freezing properties such as suitable melting points, high latent heat of fusion, and small volume changes during phase transition, however, they are reported to be three

times more expensive than paraffin [22], which becomes a major barrier in their application in buildings.

2.3.1.2. Inorganic PCMs

Inorganic PCMs generally show advantages over organic PCMs in terms of better thermal conductivity, economic benefit, higher heat of fusion, and non-flammable property. Research has primarily been concerned with the most common inorganic PCMs——salt hydrates, which require support and containment, and cannot be directly incorporated into building materials [23, 24]. One crucial question for utilizing these materials is how to choose a suitable container for a specific hydrate salt due to its corrosivity and degradation through phase change cycling. Most of the salt hydrates are corrosive, which may lead to the corrosion of the metals used in buildings. Moreover, they often undergo undesirable subcooling and phase decomposition during the phase transition process [25]. Subcooling appears when a salt hydrate starts to solidify at a temperature below its solidifying temperature (Figure 2.3). Several potential methods such as using nucleators to solve this problem can be found in publication [11].

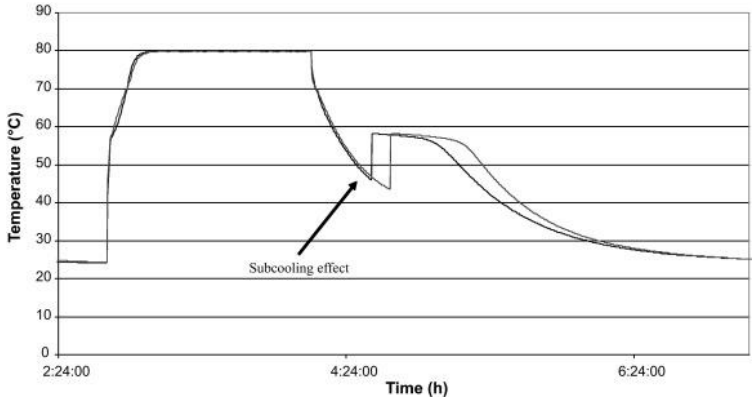

Figure 2.3. Subcooling effect of a salt hydrate [26].

2.3.1.3. Eutectics

Eutectics are mixtures of multiple solids which have definite melting/freezing temperature. They can be further classified as inorganic eutectics, organic eutectics, and organic-inorganic eutectics. Their behavior is reported similar to congruent PCMs and shows great potential for thermal energy storage applications [22]. Researchers have investigated and successfully prepared the fatty acid eutectic mixtures in the last decade [27-29]. It is found that the phase transition temperatures of fatty acid eutectics are more suitable for building applications than an individual fatty acid, but the heat of fusion of the mixtures can be maintained at a sufficient level. However, more research is still needed to supplement the currently available data on eutectics' thermal and physical properties.

2.3.2. Current Applications of PCMs

During the last decades, PCMs has been widely used as passive or active TES strategy in different fields to bridge the gap between the increasing energy consumption demand and the full utilization of renewable energy sources. PCMs offer the possibility of better thermal performance due to their high latent heat capacity and thermal inertia. Using them to store energy is an effective method to improve energy efficiency and benefit environmental protection. With proper physical and thermal properties, they could be used against heat and cold and smooth the temperature swing in a variety of applications. When being used in the solar energy system, PCM with high latent heat capacity can produce an increase in solar fraction and heat accumulation compared with the traditional water-based solar thermal system [25]. PCMs are also intensively integrated into the building elements to improve the building energy efficiency and thermal comfort of the occupants [30]. They show desirable qualities like smoothing out indoor temperature fluctuations and delaying the peak temperature occurrence, thus enhancing

the use of off-peak power. In addition, PCMs has got tremendous attention in their employment in the field of electronic cooling [31], industrial heat recovery [32], spacecraft thermal system[33], textiles [34], thermal protection of food [35], medical transport [36], etc. Among those uses, the application of PCM in buildings is emphatically discussed in section 2.4.

2.4. Review of Previous Studies of PCMs in Building Applications

A building envelope is a physical separator between the indoor and outdoor environment which provides resistance to inward heat and cold and maintains indoor thermal comfort. With the continuous improvement of living standards, the demand for indoor thermal comfort is increasing, resulting in more and more energy consumption by the HVAC system, especially in summer and winter when the transient outdoor condition is harsh. PCMs can be integrated into various building envelopes, such as walls, roof, and window as well as other building components like ceiling and floor to enhance the indoor thermal comfort and building energy efficiency [37]. In this section, studies (during the last two decades) investigating the incorporation of PCMs in buildings to enhance their thermal performance are reviewed, part of which concerned with the selection criteria of PCMs for building thermal management, thermo-physical properties of selected PCMs, the integration methods into different building components, and the corresponding thermal impact of PCMs are randomly selected and listed in Table 2.2.

2.4.1. Selection Criteria of PCMs for Building Applications

The PCM to be used in the design of thermal storage systems should possess desirable thermal, physical, kinetic, and chemical properties, that are recommended as follows [38, 39].

1) Thermal properties:

- congruent and suitable melting temperature closed to the thermal comfort temperature range of human beings,
- high latent heat storage capacity (heat of fusion) so that smaller masses and volumes are needed,
- high thermal conductivity to ensure faster and more efficient phase transition, which is usually positive for TES [40],
- high specific heat capacity that can be beneficial for the additional sensible heat storage.

2) Physical properties:

- small volume changes on phase transformation to prevent thermal expansion,
- low vapor pressure at operating temperature to reduce the containment issue,
- form stability to prevent leakage problems when converted into the liquid state, which can gradually decrease their latent heat capacity.

3) Chemical properties:

- long-term chemical stability to undergo enough freezing/melting cycles,
- non-corrosive to prevent deteriorating the container or enclosure,
- non-toxic, non-flammable, and non-explosive so that the system can meet safety requirement,

4) Kinetic properties:

- high nucleation rate to avoid super-cooling or sub-cooling during melting and solidifying processes,
- high rate of crystal growth to meet the demand of heat recovery from the storage system.

5) Economics

- large-scale availabilities in low cost-effective.

In the following section, several critical selection criteria are highlighted based on the summarize of studies listed in Table 2.2.

2.4.2. Critical Thermophysical Properties of PCM Used in Buildings

2.4.2.1. Organic Characteristic of the PCM Used in Buildings

There is a wide variety of PCMs on the market with different thermo-physical properties that can be used in buildings. By summarizing the category of those listed in Table 2.2, 85.9% of the investigations use organic PCMs to improve the thermal performance of buildings, which is much more than the utilization of inorganic PCMs (see Figure 2.4). Paraffins account for most of the selected organic PCMs due to their large availability in addition to relatively higher thermal conductivity over non-paraffins.

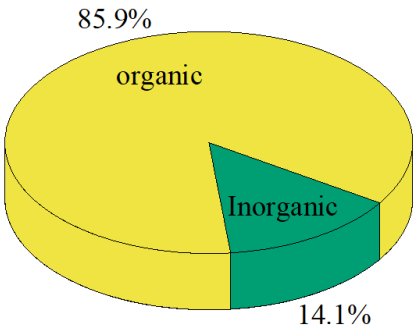

Figure 2.4. Distribution of PCM in building applications (summarized from Table 2.2).

There are several possible reasons leading to the wider use of organic PCMs in buildings. In general, they do not suffer from phase segregation and crystallize with little or no supercooling [41]. Moreover, organic PCM is noncorrosive and more compatible with building materials compared with inorganic PCMs like most salt hydrates. Another significant reason is the suitable phase change temperature range of organic PCMs, opening for use in buildings.

Figure 2.5 shows the difference in melting enthalpy and melting temperature for some of the most common materials used as PCMs. Both organic paraffin and inorganic salt hydrates or their mixtures are solid PCMs available in a large temperature range. Nevertheless, a large number of organic paraffin have covered the thermal comfort temperature range of human beings, making them the most common groups investigated by researchers for building-related applications. By contrast, the phase change temperature of most salt hydrates which are representative of inorganic PCMs is much higher than the thermal comfort temperature range. In addition, they often undergo incongruent melting, which may cause the anhydrous salt formed during the phase change process to sink to the bottom of the container and hinder the reversible phase change process. Overall, organic PCMs possess many advantages making them suited for building thermal management. However, they have some detrimental properties, such as being moderately flammable[13], which restricts them from being exposed to high temperatures, flames, and oxidizing substances. Fire retardant strategies are necessary when organic PCMs are used in the high-temperature scenarios, which are reviewed in [11].

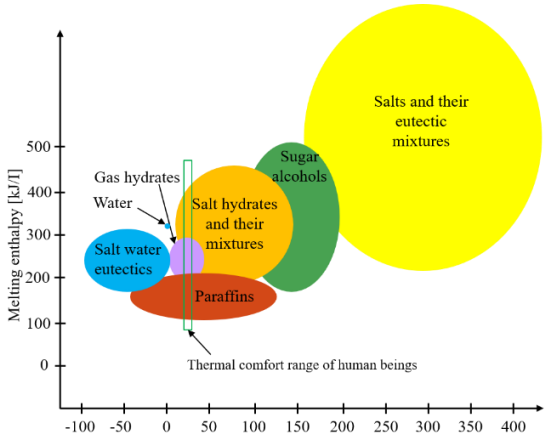

Figure 2.5. Melting enthalpy versus melting temperature for various materials used as PCMs, modified from [42][43].

2.4.2.2. Thermal Conductivity of the PCM Used in Buildings

Low thermal conductivity is considered to be the common defect for most PCMs, being around 0.2 $Wm^{-1}K^{-1}$ for paraffin and 0.5 $Wm^{-1}K^{-1}$ for salt hydrates [44], which significantly hinder their widespread applications. Figure 2.6 shows the general distribution tendency of thermal conductivity of PCMs listed in Table 2.2, covering a span of 0.083 $Wm^{-1}K^{-1}$ from 0.17 $Wm^{-1}K^{-1}$ to 0.253 $Wm^{-1}K^{-1}$. Up to 57.4% of the selected PCMs possess a thermal conductivity of 0.2 $Wm^{-1}K^{-1}$, which is closed to the mean value of this data set (0.205 $Wm^{-1}K^{-1}$). Notice that some special scenarios including a fraction of paraffin that possesses ever lower thermal conductivity (0.13 $Wm^{-1}K^{-1}$ to 0.15 $Wm^{-1}K^{-1}$) and salt hydrates with much higher thermal conductibility (0.5 $Wm^{-1}K^{-1}$ to 1.2 $Wm^{-1}K^{-1}$) are not shown in Figure 2.6.

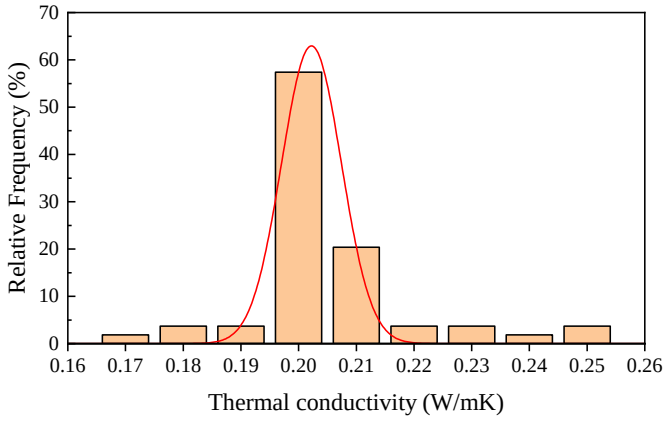

Figure 2.6. Thermal conductivity of PCMs in building applications (summarized from Table 2.2).

Low thermal conductivity of PCMs leads to low heat transfer rate, extending charging and discharging periods of the TES systems. In building applications, the thermal energy charging and discharging process is passively imposed by solar heating (daytime) and nature cooling (nighttime), which is supposed to be completed within a 24-hour cycle. Low thermal conductivity may prolong this process and influence the full utilization of the latent heat capacity of PCMs if they cannot be totally charged or discharged diurnally. Hence, improving the thermal

conductivity of PCMs is one of the focuses in their application in buildings during the last decade. Researchers have published review papers to summarize the heat transfer enhancement techniques, which can be divided into two groups: adding additives with high thermal conductivity and extending surface area by encapsulating PCMs [40, 45, 46] (Figure 2.7).

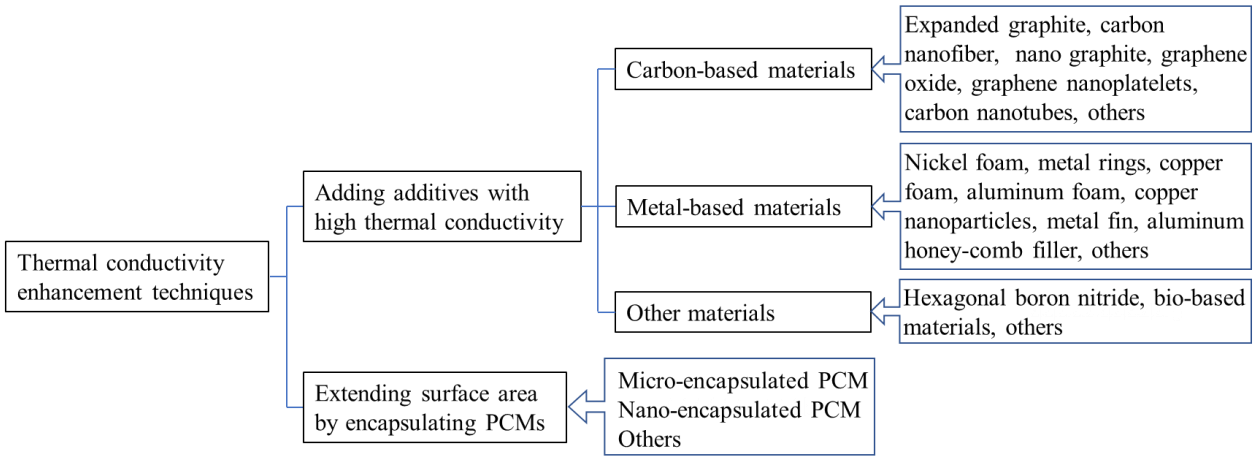

Figure 2.7. The techniques of thermal conductivity enhancement (adapted from [47]).

To improve the effectiveness of PCM-based buildings in response to environmental temperature changes, carbon-based materials are often used to enhance the heat transfer rate of PCMs due to their high thermal conductivities, low density, and chemical stability. Wu and Wang [48] developed a novel shape-stabilized PCM by impregnation of hydrated salts into expanded graphite (EG) and further coated with paraffin wax. The thermal conductivity of the achieved PCM composite was significantly increased to 3.643 $Wm^{-1}K^{-1}$ by adding 13 wt.% EG. The integration of metal-based material is another method proposed by various researchers to enhance the heat transfer rate of PCMs. It is well known that metals possess high thermal conductivity and strong mixing ability. Potential metal-based materials such as metal particles, fins, and metal foam can be incorporated into PCMs for building applications. Hussain et al. [49] designed a novel composite consisted of paraffin wax and nickel foam as a thermal management

system for high-powered lithium-ion batteries. The effective thermal conductivity of the nickel-paraffin composite is estimated at 1.16 $Wm^{-1}K^{-1}$, which is 5 to 6 times the pure paraffin used in this study. However, metal-based additives often suffer from high density, non-uniformity, and chemical incompatibility with the PCMs compared to the carbon-based additives, which significantly limits their extensive application in building thermal management.

The encapsulated PCMs (EPCMs) was discovered and developed by Barrett K Green of the National Cash Register Corporation (NRC) in the 1940s and 1950s [50]. Micro encapsulated PCMs (MEPCMs) or nano encapsulated PCMs (NEPCMs) refers to the core-shell structured particles, which usually consist of liquid PCMs enclosed by a polymer shell which can vary from millimeter to nano scale in size [51]. This method can not only solve the leakage problem during the phase transaction of PCMs but also provides a large heat exchange surface area for each PCM core, thus increasing the heat transfer area [52]. Wang et al. [53] used a self–assembly method to prepare a novel MEPCM with $CaCO_3$ as shell, while paraffin-based binary cores (RT 28, RT 42, and their mixtures) were used as core PCM. When the weight ratio of RT 28 to RT 42 is 10:0, 5:5, and 0:10, and the corresponding encapsulation efficiency is 36.6%, 44.8%, and 42.6%, respectively, the thermal conductivity of the MEPCM is magnified by 2.63, 2.18, and 2.41 times compared to that of the pure PCM. Both the enhanced thermal contact area and relatively high thermal conductivity (2.167 $Wm^{-1}K^{-1}$) of the $CaCO_3$ shell play an outstanding role in the overall thermal conductivity enhancement.

Although many studies reach an agreement on the positive effect of increasing PCM heat transfer rate on the building energy-saving improvement, there are some researchers who hold a different view on it. Xie et al.[54] mentioned that salt hydrate with a relatively high thermal conductivity may give rise to bad thermal insulation outcomes for buildings. They integrated salt

hydrate into vermiculite with thermal conductivity of 0.121 $Wm^{-1}K^{-1}$, resulting in a significant decrease in the thermal conductivity of the salt hydrate from 0.532 $Wm^{-1}K^{-1}$ to 0.192 $Wm^{-1}K^{-1}$ before integrating them in the wall board. Zhang et al. [55] used PCMs with thermal conductivity of 0.2, 0.5, 1.0 $Wm^{-1}K^{-1}$ to regulate the indoor air temperature in several days under the winter weather condition in Beijing. However, the thermal conductivity shows little effect on changing the peak of indoor air temperature. The author also investigated the impact of thermal conductivity on the thermal performance of the wall system in a previous study [56]. Figure 2.8 shows the instantaneous temperature history of the interior surface of the wall integrated with PCM with thermal conductivity ranging from 0.15 $Wm^{-1}K^{-1}$ to 2.0 $Wm^{-1}K^{-1}$. A similar conclusion with Zhang et al. [55] is drawn that the PCM thermal conductivity shows a little impact on the indoor temperature swing. A possible reason for this phenomenon is that the combined effect of the input temperature profile and wall configuration weakens the effect of the thermal conductivity. Since there is still conflict understanding on the optimal thermal conductivity of PCM when it is used in a certain building, more research is needed to further investigate the impact of PCM thermal conductivity on buildings subjected to various climatic conditions.

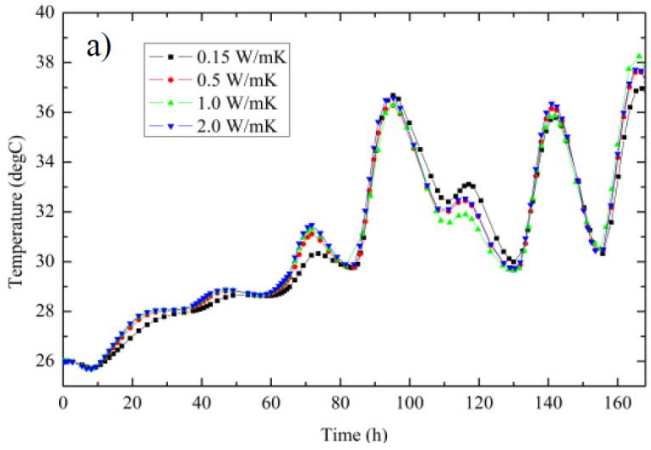

Figure 2.8. History of interior wall surface temperature over time [56].

2.4.2.3. Phase Change Temperature of the PCM Used in Buildings

The operation principle of PCMs in the scope of passive building thermal management can be explained as follows: when the PCM impregnated in the building envelope subjected to temperatures over its melting temperature range during the daytime, it absorbs and stores a large amount of the latent heat by changing from the solid to the liquid state, thus providing a buffering for the inward heat flux. Conversely, the stored heat is released when the outdoor temperature drops below the solidification temperature range of the PCM during the nighttime. This process results in a shift of the building heating/cooling load from peak to off-peak electricity consumption periods and better leveled indoor temperatures, which tend to be in the vicinity of the PCM's melting temperature [57]. A suitable phase change temperature is a desirable requirement for PCM, which directly influences its working efficiency in enhancing building energy savings.

Figure 2.9 shows the general distribution tendency of melting temperature of the PCMs in building applications. The melting temperature of the selected PCMs ranges from 16℃ to 40 ℃, covering a large temperature span up to 24℃. The big center of the Gaussian distribution curve fitted from the frequency distribution of different melting temperatures is 26.5℃. Researchers determine PCM's melting temperature mainly on the following basis that leads to this tendency. For building applications, the melting temperature of PCM should be in the vicinity of the human being's thermal comfort temperature (around 24℃), especially when PCM is integrated on the interior side of the building envelope [58, 59]. Furthermore, it needs to be closed to the middle of the operating temperature of the location assembled with PCM to guarantee it undergoes complete diurnal melting/solidifying cycles. Alawadhi [60] evaluated the efficiency of PCM melting temperature by comparing the heat flux at the indoor surface of the PCM-brick system

with three different PCMs to the reference brick without PCM. N-Octadecane, n-Eicosane, and P116 with melting temperatures of 27℃, 37℃, 47℃ respectively are explored, all of which are within the operating temperature of the system. Nevertheless, the melting point of n-Octadecane is closed to the lower limit of the operating temperature, while the melting point of P116 is closed to the upper limit of the operating temperature. Only n-Eicosane possesses a melting point that is closed to the middle of the operating temperature. The results show that n-Octadecane and P116 are almost ineffective in reducing the heat flux to the indoor space since the former with low melting temperature keeps in the liquid state and the latter in solid-state most of the test period. By contrast, n-Eicosane with proper melting temperature leads to a maximum heat flux reduction of 24.2%. Therefore, the melting temperature of the PCM should not only match the human being's thermal comfort temperature range but also be carefully adjusted to various operating temperatures when the building is subjected to different outdoor conditions. Only when the charging/discharging process is totally activated by the diurnal temperature swing, the latent heat of PCM can be fully utilized by the building system to save energy.

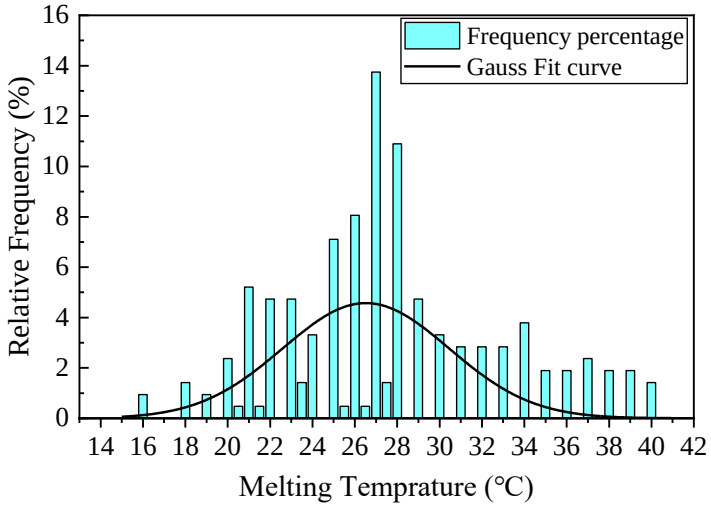

Figure 2.9. Melting temperature of PCMs in building applications (summarized from Table 2.2).

2.4.2.4. Thermal Reliability and Chemical Stability of the PCM Used in Buildings

Good thermal reliability and chemical stability over a long period is an important criterion for the successful application of proper PCMs for thermal energy storage in building systems. The economic feasibility of employing a TES system significantly depends on the total repeated melting/freezing cycles it can undergo. Many studies have been carried out on the investigation of the long-term stability of various PCMs. Figure 2.10 (a) shows the DSC result of paraffin wax after 200, 400, 600, 800, and 1000 thermal cycles [61].

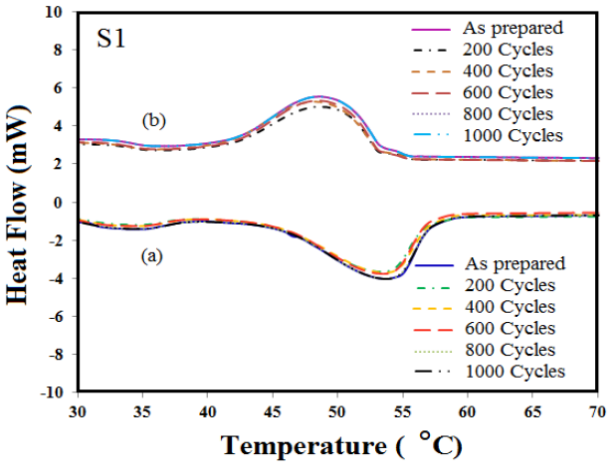

(a)

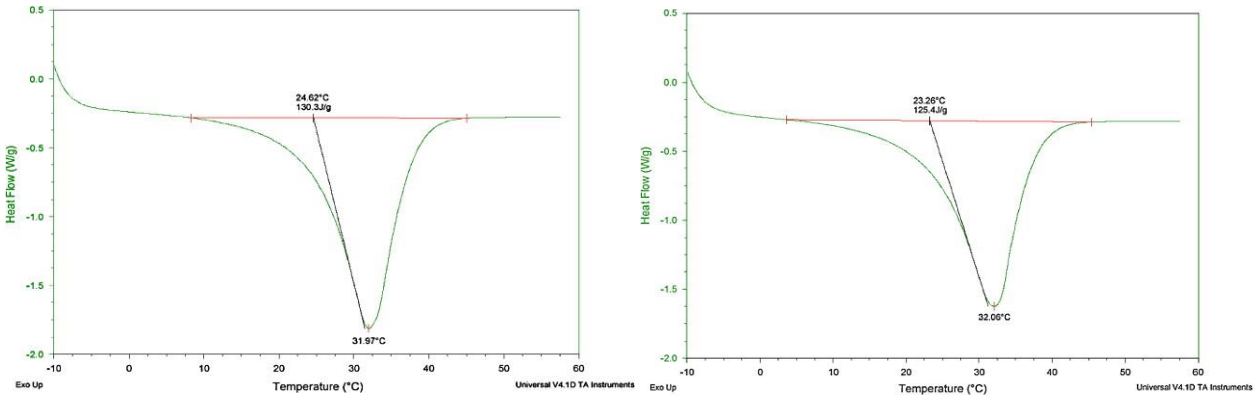

(b)

Figure 2.10. DSC measurement curve of (a) Paraffin [61] and (b) $CaCl_2 \cdot 6H_2O$[62] under different heating/cooling cycles.

It was found that congruent melting/freezing temperature and latent heat of fusion were distinguished after different cycles. Moreover, no supercooling or significant volume change was observed in this test. Tyagi and Buddhi [62] conducted the accelerated thermal cycle tests of calcium chloride hexahydrate ($CaCl2 \cdot 6H2O$) inorganic salt to illustrate its thermal stability as a latent heat storage material(see Figure 2.10(b)). As one can see from Figure 2.10 (b), it shows a good stability of thermal properties such as melting temperature and heat of fusion by comparing the DSC measurement curves of 200 and 1000 cycles.

Sharma et al. [63, 64] measured the melting point, latent heat, and specific heat of commercial-grade stearic acid, acetamide, and paraffin wax for 300 and 1500 repeated melt-freeze cycles, respectively. They concluded that there is no obvious change of thermal properties during thermal cycling for the commercial-grade of these materials. However, it has also been outlined that paraffin and acetamide have shown better stability as compared to stearic acid. Based on those literature survey, it can be noted that a comprehensive knowledge of the thermal stability of a PCM should be authenticated by thermal cycling testing to ensure long-term service life of the TES system in building application

Table 2.2. Application of PCMs in buildings for thermal energy efficiency enhancement.

PCM	Type	Thermal conductivity ($Wm^{-1}K^{-1}$)	Melting point (°C)	Heat of fusion (kJ/kg)	Density (kg/m^3)	Incorporation location (thickness of PCM)	Incorporation method	Outcomes	Ref
1.WALL									
Hydrated salt based PCM	Inorganic	-	24.79	140.7	-	Interior (2 mm)	sheet shield	Maximum heat flux reduction is 10.5%, and peak heat flux delay is 6.3h.	[65]
Hydrated salt based PCM	Inorganic	-	24.79	140.7	-	Center (2 mm)	sheet shield	Maximum heat flux reduction is 51.3%, and peak heat flux delay is 5h.	[65]
Hydrated salt based PCM	Inorganic	-	24.79	140.7	-	Exterior (2 mm)	sheet shield	Maximum heat flux reduction is 23.5%, and peak heat flux delay is 3h.	[65]
MEPCM	Organic	-	25	-	-	Interior	dispersed in plaster	Peak temperature reduction is about 3 °C.	[66]
n-octadecane ($C_{18}H_{38}$)	Organic	0.21 (solid) 0.15 (liquid)	28	180-195	-	-	MEPCM dispersed into cement	The insertion of PCM in cement increases its thermal inertia but reduces the effective thermal conductivity.	[67]
n-heptadecane ($C_{17}H_{36}$)	Organic	-	21.1	-	-	-	dispersed in gypsum board	The nano-PCM wallboard reduced the peak heat gains and delayed the heat flowing into the interior space.	[68]
n-Octadecane	Organic	0.358 (solid) 0.148 (liquid)	27	243.5	865(solid) 780 (liquid)	Center	integrated into holes in brick	ineffective	[60]
n-Eicosane	Organic	0.15	37	241	856(solid) 778 (liquid)	Center	integrated into holes in brick	Maximum heat flux reduction is 24.2%.	[60]
P116	Organic	0.24	47	225	830(solid) 773 (liquid)	Center	integrated into holes in brick	ineffective	[60]
PCM	-	0.2	23	330	800	Interior (12.5 mm)	-	Notable energy savings is achieved with proper selection of melting temperature.	[69]

Table 2.2. Application of PCMs in buildings for thermal energy efficiency enhancement (continued).

PCM	Type	Thermal conductivity ($Wm^{-1}K^{-1}$)	Melting point (°C)	Heat of fusion (kJ/kg)	Density (kg/m^3)	Incorporation location (thickness of PCM)	Incorporation method	Outcomes	Ref
Granular PCM	-	0.15	20-40	63	750	interior face of insulator (20 mm)	bounded with supporting structure	The amplitude and the maximum of the instantaneous heat flux are reduced with PCM integrated. Proper melting temperature should be selected basing on the season and wall orientation.	[70]
Granular PCM	-	0.15	20-40	63	750	Exterior face of insulator (20 mm)	bounded with supporting structure		[70]
Granular PCM	-	0.15	20-40	63	750	interior side of the wall without insulator (20 mm)	bounded with supporting structure		[70]
RT27	Organic	0.2	27	179	880 (solid) 760 (liquid)	Interior (1 mm)	integrated into the insulation cavity	Wall peak heat flux reduces by 0.18%.	[71]
RT27	Organic	0.2	27	179	880 (solid) 760 (liquid)	About 1/5 of the wall thickness to the wall interior face (1 mm)	integrated into the insulation cavity	Wall peak heat flux reduces by 2.29%.	[71]
RT27	Organic	0.2	27	179	880 (solid) 760 (liquid)	Center (1 mm)	integrated into the insulation cavity	Wall peak heat flux reduces by 0.13%.	[71]
RT27	Organic	0.2	27	179	880 (solid) 760 (liquid)	Exterior (1 mm)	integrated into the insulation cavity	Wall peak heat flux reduces by 0.53%.	[71]
RT27	Organic	0.2	27	179	880 (solid) 760 (liquid)	Interior (5 mm)	integrated into the insulation cavity	Wall peak heat flux reduces by 6.37%.	[71]
RT27	Organic	0.2	27	179	880 (solid) 760 (liquid)	About 1/5 of the wall thickness to the wall interior face (5 mm)	integrated into the insulation cavity	Wall peak heat flux reduces by 53.99%.	[71]
RT27	Organic	0.2	27	179	880 (solid) 760 (liquid)	Center (5 mm)	integrated into the insulation cavity	Wall peak heat flux reduces by about 7%.	[71]

Table 2.2. Application of PCMs in buildings for thermal energy efficiency enhancement (continued).

PCM	Type	Thermal conductivity ($Wm^{-1}K^{-1}$)	Melting point (°C)	Heat of fusion (kJ/kg)	Density (kg/m^3)	Incorporation location (thickness of PCM)	Incorporation method	Outcomes	Ref
RT27	Organic	0.2	27	179	880 (solid) 760 (liquid)	Exterior (5 mm)	integrated into the insulation cavity	Wall peak heat flux reduces by 1.29%.	[71]
RT27	Organic	0.2	27	179	880 (solid) 760 (liquid)	About 1/5 of the wall thickness to the wall interior face (7 mm)	integrated into the insulation cavity	Wall peak heat flux reduces by 56.11%.	[71]
RT27	Organic	0.2	27	179	880 (solid) 760 (liquid)	Center (7 mm)	integrated into the insulation cavity	Wall peak heat flux reduces by about 10.5%.	[71]
RT27	Organic	0.2	27	179	880 (solid) 760 (liquid)	Exterior (7 mm)	integrated into the insulation cavity	Wall peak heat flux reduces by 2.08%.	[71]
hydrated salt	Inorganic	-	25-34	140	-	Interior	integrated into the insulation cavity	Wall temperature range is 23.3-27.4 °C.	[72]
hydrated salt	Inorganic	-	25-34	140	-	About 1/5 of the wall thickness to the wall interior face	integrated into the insulation cavity	Wall temperature range is 25.6-29.4 °C.	[72]
hydrated salt	Inorganic	-	25-34	140	-	About 2/5 of the wall thickness to the wall interior face	integrated into the insulation cavity	Wall temperature range is 26.7-36.1 °C.	[72]
hydrated salt	Inorganic	-	25-34	140	-	About 3/5 of the wall thickness to the wall interior face	integrated into the insulation cavity	Wall temperature range is 25.1-42.8 °C.	[72]
n-octadecane	Organic	0.2	28	179	880 (solid) 750 (liquid)	Closed to the interior wall face	integrated into the plastic pouches	Maximum heat flux reduction is 10.7%.	[73]
n-octadecane	Organic	0.2	28	179	880 (solid) 750 (liquid)	Center	integrated into the plastic pouches	Maximum heat flux reduction is 6.7%.	[73]

Table 2.2. Application of PCMs in buildings for thermal energy efficiency enhancement (continued).

PCM	Type	Thermal conductivity ($Wm^{-1}K^{-1}$)	Melting point (°C)	Heat of fusion (kJ/kg)	Density (kg/m^3)	Incorporation location (thickness of PCM)	Incorporation method	Outcomes	Ref
n-octadecane	Organic	0.2	28	179	880 (solid)	Closed to the exterior wall face	integrated into the plastic pouches	Maximum heat flux reduction is 0.7%.	[73]
Fatty acid capric/myristic	Organic	-	21.4	162	-	Center	fill in the glass bricks	Maximum room temperature is reduced by 3.5-4°C for cooling.	[74]
Paraffin C18-20	Organic	-	25	170	-	Center	fill in the glass bricks	Maximum room temperature is reduced by 2-3°C for cooling.	[74]
Salt hydrate	Inorganic	-	27.5	194	-	Center	fill in the glass bricks	Maximum room temperature is d by 3.5-5°C for cooling.	[74]
paraffin	Organic	0.15	26	200	850	Exterior (10 mm)	shape-stabilized	Annual cooling load saving is 2.8%.	[75]
paraffin	Organic	0.15	25	200	850	Exterior (20 mm)	shape-stabilized	Annual cooling load saving is 3.5%.	[75]
paraffin	Organic	0.15	18	190	850	Interior (10 mm)	shape-stabilized	Annual cooling load saving is 9.9%.	[75]
paraffin	Organic	0.15	18	190	850	Interior (20 mm)	shape-stabilized	Annual cooling load saving is 12.4%.	[75]
CA–PA eutectic mixture	Organic	-	26.2	177	784	Interior (5 mm)	nano-encapsulated	Energy consumption for maintaining the interior temperature within comfort zone is reduced by 79%.	[76]
Micronal T23	Organic	0.2	22	132	-	Interior	microencapsulated	Indoor thermal comfort time is increased.	[6]
paraffin	Organic	0.142	20.78	147.4	881	Exterior (20 mm)	macro encapsulated in stainless steel box	Indoor temperature swing decreases by 29.2%.	[77]
paraffin	Organic	0.142	20.78	147.4	881	Center (20 mm)	macro encapsulated in stainless steel box	Indoor temperature swing decreases by 35.2%.	[77]
paraffin	Organic	0.142	20.78	147.4	881	Interior (20 mm)	macro encapsulated in stainless steel box	Indoor temperature swing decreases by 33.6%.	[77]
MEPCM	Organic	0.22	22	-	1019	Interior (5 mm)	microencapsulated	Indoor temperature fluctuation is decreased by 3.5°C.	[78]

Table 2.2. Application of PCMs in buildings for thermal energy efficiency enhancement (continued).

PCM	Type	Thermal conductivity ($Wm^{-1}K^{-1}$)	Melting point (°C)	Heat of fusion (kJ/kg)	Density (kg/m^3)	Incorporation location (thickness of PCM)	Incorporation method	Outcomes	Ref
fatty acid	Organic	-	20.394	150.305	-	Interior	absorbed in porous gypsum board	The maximum thermal flow is decreased by 13.3%.	[79]
MEPCM	Organic	0.21	20	180	860	-	microencapsulated	The maximum heat flux is decreased by 9.1%.	[80]
MEPCM	Organic	0.21	22	180	860	-	microencapsulated	The maximum heat flux is decreased by 12.3%.	[80]
MEPCM	Organic	0.21	28	180	860	-	microencapsulated	The maximum heat flux is decreased by 23.1%.	[80]
Micronal	Organic	-	26	110	-	Center (1.2 mm)	Microencapsulated	Thermal inertia of the wall is increased, resulting in lower inner temperature swing.	[81]
paraffin based PCM	Organic	0.2	26-28	147	870 (solid) 750 (liquid)	-	macro-encapsulated	Heat flux peak reduction is 37.5% in August 20.	[82]
paraffin based PCM	Organic	0.2	26-28	147	870 (solid) 750 (liquid)	-	macro-encapsulated	Heat flux peak reduction is 49% in August 20.	[82]
paraffin based PCM	Organic	0.2	26-28	147	870 (solid) 750 (liquid)	-	macro-encapsulated	Heat flux peak reduction is 40.4% in August 20.	[82]
paraffin based PCM	Organic	0.2	26-28	147	870 (solid) 750 (liquid)	-	macro-encapsulated	Heat flux peak reduction is 22.3% in August 20.	[82]
RT10	Organic	-	10	150	880	Interior	microencapsulated	Incorporation of hybrid PCM into plastering mortars shows potential to significantly reduce heating/cooling energy demands for maintaining the interior temperature within comfort levels.	[58]
MC24	Organic	-	24	162.4	-	Interior	microencapsulated		[58]
BSF26	Organic	-	26	110	350	Interior	microencapsulated		[58]
MC28	Organic	-	28	170.1	-	Interior	microencapsulated		[58]

Table 2.2. Application of PCMs in buildings for thermal energy efficiency enhancement (continued).

PCM	Type	Thermal conductivity ($Wm^{-1}K^{-1}$)	Melting point (°C)	Heat of fusion (kJ/kg)	Density (kg/m^3)	Incorporation location (thickness of PCM)	Incorporation method	Outcomes	Ref
$Na_2SO_4 \cdot 10H_2O$-$Na_2CO_3 \cdot 10H_2O$	Inorganic		25.41	195.3	-	Center (5 mm)	impregnated into expanded vermiculite	The composite can maintain the indoor comfort temperature range for a longer period.	[54]
Paraffin wax	Organic	0.13	44	174.12	830 (solid) 783 (liquid)	Interior (10 mm)	impregnated into aluminum frame	Indoor temperature and the cooling load are reduced by the PCM in hot summer.	[83]
RT PCM	Organic	0.2	16	250	880 (solid) 760 (liquid)	Exterior (20 mm)	-	The energy saving of 10582 kJ/m2year due to latent heat is attained in Erzurum, Turkey.	[84]
paraffin	Organic	0.21	21.7-22.7	161.6	786.1	Interior (10 mm)	impregnated into aluminum shell	Thermal performance of the building envelope is improved.	[85]
PCM	-	-	18-24	70	855.5	Interior (5.26 mm)	-	The PCM thermal storage system is effective during the whole year in a cold climate.	[86]
PCM	-	0.25 T<23°C 0.20 T>23°C	28	70-120	1100	Interior (10 mm)	-	PCM wallboard can be applied to shift the peak load to the off- peak period.	[87]
2. Multiple building elements									
Macro-encapsulated BioPCM	Organic	0.2	25	219	235	Center (20 mm)	impregnated into square pouches	Up to 34% reduction in thermal discomfort hours is achieved through the passive installation of PCM on the ceilings.	[88]
PCM eutectic mixture	Organic	0.28 (solid) 0.18 (liquid)	27.5	110	850 (solid) 780 (liquid)	Slab center	shape-stabilized and filled in the slab hole	The internal temperature of a building is regulated by PCM.	[89]
paraffin	Organic	0.15	19	150	800	Interior	shape-stabilized	Indoor temperature swing decreases by about 4%.	[90]
paraffin	Organic	0.15	21	150	800	Interior	shape-stabilized	Indoor temperature swing decreases by about 59%.	[90]
paraffin	Organic	0.15	23	150	800	Interior	shape-stabilized	Indoor temperature swing decreases by about 8%.	[90]

Table 2.2. Application of PCMs in buildings for thermal energy efficiency enhancement (continued).

PCM	Type	Thermal conductivity ($Wm^{-1}K^{-1}$)	Melting point (°C)	Heat of fusion (kJ/kg)	Density (kg/m^3)	Incorporation location (thickness of PCM)	Incorporation method	Outcomes	Ref
PCM	Organic	0.2	24	160	850	Interior (20 mm)	shape-stabilized	The daily maximum temperature is decreased by up to 2°C with the optimum PCM melting temperature of 26°C.	[91]
PCM	Organic	0.2	26	160	850	Interior (20 mm)	shape-stabilized		[91]
PCM	Organic	0.2	28	160	850	Interior (20 mm)	shape-stabilized		[91]
polyethylene glycol	Organic	-	21-25	148	1128	Interior (25 mm)	impregnated into PVC panel	The energy efficiency of PCM is remarkable with a reduction of the indoor temperature amplitude of approximately 20 °C in the test-cell	[92]
GR25	Inorganic	1.2	23.5	45.3	1310	Exterior (10 mm)	-	The improvement percentage of saving energy is 5% in Quito.	[93]
RT25–RT30	Organic	0.19	26.6	232	785	Exterior (10 mm)	-	The improvement percentage of saving energy is 25% in Quito.	[93]
n-Octadecane	Organic	0.19	27.7	243.5	865	Exterior (10 mm)	-	The improvement percentage of saving energy is 25% in Quito.	[93]
CaCl2–6H2O	Inorganic	1.09	29.9	187	1710	Exterior (10 mm)	-	The improvement percentage of saving energy is 5% in Quito.	[93]
BioPCM-Q21	Organic	0.21	21	225.6	235	Exterior (10 mm)	-	The improvement percentage of saving energy is 25% in Quito.	[93]
BioPCM-Q23	Organic	0.21	23	245.5	235	Exterior (10 mm)	-	The improvement percentage of saving energy is 25% in Quito.	[93]
BioPCM-Q25	Organic	0.21	25	236.9	235	Exterior (10 mm)	-	The improvement percentage of saving energy is 25% in Quito.	[93]
BioPCM-Q27	Organic	0.21	27	251.3	235	Exterior (10 mm)	-	The improvement percentage of saving energy is 25% in Quito.	[93]
BioPCM-Q29	Organic	0.21	29	260.7	235	Exterior (10 mm)	-	The improvement percentage of saving energy is 25% in Quito.	[93]

Table 2.2. Application of PCMs in buildings for thermal energy efficiency enhancement (continued).

PCM	Type	Thermal conductivity ($Wm^{-1}K^{-1}$)	Melting point (°C)	Heat of fusion (kJ/kg)	Density (kg/m^3)	Incorporation location (thickness of PCM)	Incorporation method	Outcomes	Ref
3. Roof									
PCM	-	0.2	23	330	800	Interior (12.5 mm)	-	Notable energy savings is achieved with proper selection of melting temperature.	[69]
paraffin wax	Organic	0.22 (solid) 0.18 (liquid)	23.4	71	850 (solid) 750 (liquid)	Closed to the ceiling (5 mm)	MEPCM enclosed in aluminum sheet	Temperature of the test cell is reduced by approximately 2°C.	[94]
Salt hydrate	Inorganic	1.09 (solid) 0.54 (liquid)	26-28	188	1640	Roof center (25 mm)	sealed in the panel	A double layer PCM incorporated in the roof is recommended for the purpose of narrowing indoor air temperature swing to suit for all seasons.	[95]
CaCl2·6H2O	Inorganic	0.6	28.11	159.85		Center	impregnated into expanded perlite	The PCM brick has the function of decreasing the indoor peak temperature.	[23]
paraffin	Organic	0.2	34-39	200	755	Exterior (0-30 mm)	shape-stabilized	The peak temperatures of the inner roof surface are all decreased by over 3.7°C.	[96]
4.Windows									
RT28HC	Organic	0.2	27-29	245	880 (solid) 770 (liquid)	Interior side	integrated into the window blade	Heat flux ranges reduce by about 60%.	[97]
Paraffin (MG29)	Organic	0.21	27-29	205	850	Center cavity of the window (5 mm)	fill in the double-pane (DP) window	Heat entered the DT+PCM window reduces by 16.6% in the sunny summer day compared to the TD+PCM window.	[98]
PCM eutectic mixture	Organic	0.28 (solid) 0.18 (liquid)	27	110	840 (solid) 771 (liquid)	Slab center	shape-stabilized and filled in the slab hole	The surface wall temperature amplitude is decreased.	[99]
PCM	Organic	-	40-55	150	850	Center (15-30 mm)	microencapsulated	The heating system consisted of PCM and electric setup can be used in various climates.	[100]
paraffin	Organic	2.1 (PCM+ concrete)	23	110	250-300		microencapsulated	The maximum indoor floor temperature reduces by 16 ± 2%.	[101]

Table 2.2. Application of PCMs in buildings for thermal energy efficiency enhancement (continued).

PCM	Type	Thermal conductivity ($Wm^{-1}K^{-1}$)	Melting point (°C)	Heat of fusion (kJ/kg)	Density (kg/m^3)	Incorporation location (thickness of PCM)	Incorporation method	Outcomes	Ref
5. Ceiling									
Eutectic mixture of lauric-stearic acid	Organic	0.5 (PCM-gypsum panel)	34	50.28	1500 (PCM-gypsum)	Interior (12.5 mm)	integrated with gypsum ceiling panel	The application of PCM ceiling panels could effectively reduce energy consumption through active cooling systems.	[102]
Micronal DS-5008X	Organic	0.17	23.5	102.6	-	Interior	microencapsulated	Substantial dumping of daily oscillations of air temperature is achieved.	[103]
Paraffin wax	Organic	0.13	44	174.12	830 (solid) 783 (liquid)	Interior (20 mm)	impregnated into aluminum frame	Indoor temperature and the cooling load are reduced by the PCM in hot summer.	[83]
6. Others									
Paraffin RT-20	Organic	-	22	160-180	750	-	contained in plastic balls	Total cost per day is decreased by 9.1% with paraffin.	[104]
MEPCM	Organic	-	26	100	-	-	sandwiched in panel	Thermal inertia is increased by PCM.	[105]

2.4.3. Integration of PCMs into Building Elements

PCM shows good performance in delaying peak electricity load, smothering indoor temperature fluctuations, improving thermal comfort, and saving energy consumed by buildings [40]. During the last decades, researchers try to integrate PCM into various building elements, such as walls, roofs, windows, ceilings, and other parts that composes the envelope of a building. By summarizing the applications listed in Table 2.2, it is found that 72.4% of them incorporate PCM into building wallboards and 27.6% of them choose other components (see Figure 2.11). This distribution tendency mainly owes to the implementation simplicity and cost-effectiveness of impregnating PCM in wallboards and the high energy efficiency since the wall element of the buildings presents the highest thermal gains and losses during the whole day [106]. Memon et al. [107] conducted indoor thermal performance tests of a porous light weight aggregate concrete containing macro encapsulated paraffin for wall application. The results of the indoor test reveal that the integration of macro encapsulated paraffin into the wall panel can decrease the interior temperature at the room center and on the internal surface of the panel by 4.7 ˚C and 7.5 ˚C, respectively. The economic evaluation of this PCM enhanced wall shows that the payback period is less than the average life span of a residential building in Hong Kong, which further corroborates the feasibility of using PCM to improve building thermal performance. The outcomes of including PCM into different building elements can be found in Table 2.2.

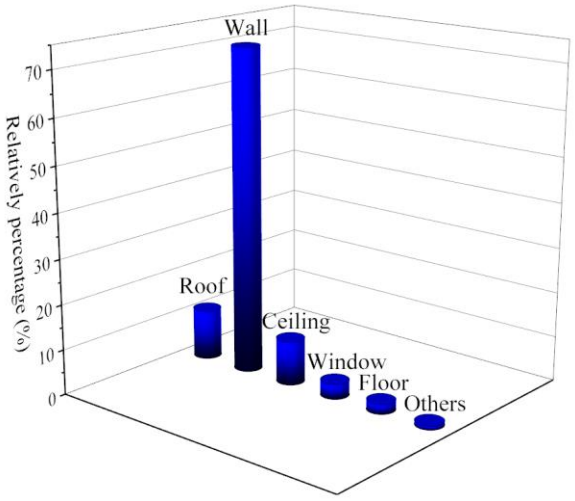

Figure 2.11. Building element that including PCM for thermal management (summarized from Table 2.2).

The energy efficiency of the building envelope depends on several factors, such as: (i) how and where the PCM is integrated; (ii) the orientation of the envelope; (iii) climatic conditions, (iv) direct solar gains; (v) internal gains; (vi) color of the envelope surface; (vii) ventilation rate; (viii) the PCM chosen and its phase-change temperature; (ix) the temperature range over which phase-change occurs; and (x) the latent heat capacity per unit area of the building envelope, etc [57]. By summarizing the tendency in Table 2.2, it is found that 51.1% of the studies choose to integrate the PCM layer closed to the interior surface of the building element, hence making it easier to keep the indoor air temperature closed to PCM's melting temperate. 23.9% and 25% of the studies prefer the exterior side and center of the building elements as their integration location, respectively (see Figure 2.12). Lee et al.[65] installed PCM thermal shield at various depths within the wall cavities, once a time, to experimentally explore the optimal location of the thin PCM layer. The thermal performance of south and west-facing walls outfitted with a thin PCM thermal shield was evaluated by comparing the heat flux reduction through the wall under full weather conditions. Their experimental results show that

the optimum location for the thin PCM layer in the south wall and the west wall would be between the wall interior surface and the center. In these locations, the peak heat flux reductions are 51.3% and 29.7% for the south wall and west wall, respectively, which are much higher than that of other locations. Jin et al.[71] conducted numerical analysis to estimate the optimal location of a thin PCM layer incorporated into frame walls, parallel to other wall assembly layers. It was found that an optimal location of this PCM layer can be estimated based on the thermal properties of PCM and the environmental conditions. They also draw the conclusion that the optimal locations for the PCM layer should be closer to the wall exterior surface when the thickness of PCM layer, the heat of fusion of PCM, and the PCM melting temperature are increased, while the optimal location should be closer to the interior surface of the wall when the interior surface temperature of the wall is increased. Zwanzig et al.[108] carried out similar studies to numerically investigate the optimal location for PCM placement within building envelope dependent upon the resistance values between the PCM layer and the exterior boundary conditions. The thermal performance of wall and roof systems with PCM in different locations was evaluated in this study. It was found that the centrally located PCM composite wallboard performed better than externally and internally located PCM composites in the multilayered wall systems during both the heating and cooling seasons.

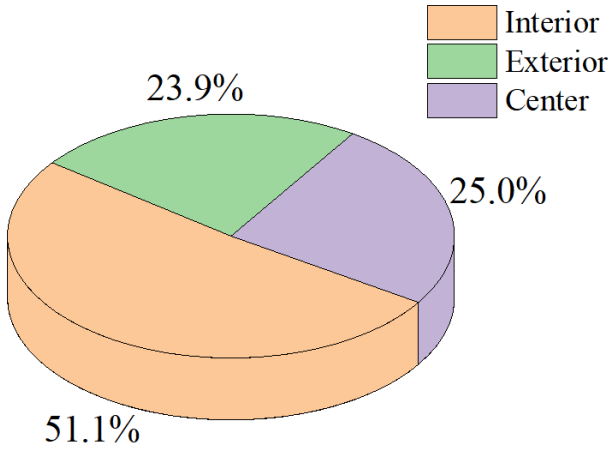

Figure 2.12. Integrating location of PCM in building elements (summarized from Table 2.2).

The thickness of the PCM layer integrated into the building elements varies a lot from 1mm to 30mm in the studies listed in Table 2.2. Theoretically, the fluctuation of indoor air temperature decreases with the increasing thickness of the PCM layer due to more latent heat of fusion it possesses [56]. Zhang et al. [55] studied the efficiency of PCM-enhanced wallboards to absorb solar energy to narrow the indoor temperature swing of a day in winter. Various thicknesses ranging from 10mm to 60mm were adopted. It was found that the indoor temperate swing tends to be gentle with increasing the thickness over 20mm. This is because, under this weather condition, the latent heat capacity of PCM thicker than 20mm cannot be fully utilized during the peak period. Therefore, selecting an optimal PCM thickness needs to relate to the environmental conditions that a building is subjected to. In addition, thermo-physical properties of PCM and the structural design requirements should also be taken into consideration.

2.4.4. Inclusion of PCMs into Building Elements

The utilization of PCM's latent heat in buildings relies on its phase reversible change between liquid and solid-state. Once the PCMs have been selected for a building based primarily on their thermo-physical properties and the operating temperature range of application, it is of great importance to determine how they could be included in the building elements to prevent

leakage. In 1993, Hawes et al. [109] introduced three traditional methods, including direct incorporation, immersion, and microencapsulation to include PCMs in conventional building materials. During recent two decades, new technologies including microencapsulation/nanoencapsulation, and shape-stabilized PCMs have been widely explored by researchers. The advantages and drawbacks of the conventional and new technologies are compared in Table 2.3.

Despite the possibility of direct incorporation and immersion that includes PCM into building structures or construction materials, these traditional methods have been replaced by some new technologies such as microencapsulation and shape-stabilized PCMs during recent years. This can be explained by the high potential of leaking during the phase change process of PCM from solid to liquid. Ramakrishnan et al.[110] prepared a paraffin/uncoated expanded perlite PCM composite and directly incorporated it into cementitious mixtures to study its stability. Significant loss of liquid paraffin from the supporting material was observed in their studies. To overcome the leakage problem, they developed a novel shape-stabilized PCM composite by impregnating paraffin into hydrophobic coated expanded perlite before being mixed with concrete. Macro encapsulation, which is the encapsulation of PCM in containers that usually larger than 1 cm in diameter, is another commonly used traditional technology for preventing liquid PCM from leaking and reacting with surrounding building materials [11]. It possesses the drawbacks of low thermal conductivity, complex installation into buildings, and a tendency of inhomogeneous solidification. Moreover, leakage may happen if the container is damaged by a building element cut or drilling.

Nowadays, microencapsulation and nanoencapsulation, which are enclosing PCMs in particles with sizes of micro and nano-level respectively, are drawing increasing attention due to

their good performance in preventing leakage of the melted PCM, increasing the heat transfer rate, controlling the volume change, and reducing the PCM reactivity with construction materials. Alkan et al. [111] prepared a microencapsulated docosane with polymethylmethacrylate as phase change material for thermal energy storage using emulsion polymerization method. Thermal analysis and thermal cycle tests reveal that the microencapsulated PCM possesses good chemical stability and thermal reliability, showing its good potential for thermal energy storage purposes such as building applications. However, MEPCM/NEPCM also suffers a few drawbacks that preventing their extensible application in building materials, such as reducing the mechanical strength of the construction materials [112]. Liu et al. [113] compared the compressive strength of mortar with and without MEPCM and found a 15.6 % strength loss with the addition of 3.0 wt.% of unsealed MEPCM. Shape-stabilized PCMs, in which the melted PCM is dispersed in the porous structure of supporting material to form a shape stable PCM composite has been investigated by numerous researchers. Xie et al. [54] prepared a new type of shape-stabilized PCM by impregnating eutectic salt hydrate ($Na_2SO_4 \cdot 10H_2O$-$Na_2CO_3 \cdot 10H_2O$ with 1:1 in mass ratio) into expanded vermiculite. They found that the molten hydrated salts can penetrate the interior gaps thanks to the capillary and surface tension force of the supporting expanded vermiculite, resulting in a successfully stable PCM composite even when the salt hydrates are liquid state. In addition to preventing leakage, supporting material with high thermal conductivity can benefit the heat transfer rate and homogeneity of the composite [28]. However, synthesis of PCM and the supporting material is needed before impregnating them into the building materials.

Table 2.3. Overview of advantages and drawbacks of different incorporation methods.

	Detail Methods	Advantages	Drawbacks
Conventional methods	Direct incorporation	-Simple -Economical -No extra equipment is needed	-Significant leakage -Poor compatibility with construction materials
	Immersion	-Simple	-Long term leakage -Eventual interaction with construction materials
	Macroencapsulation	-Leakage problem avoided -Less effect on construction materials	-Poor thermal conductivity -Tendency of inhomogeneous solidification -Complicated integration to building materials
New technologies	Microencapsulation Nanoencapsulation	-Prevent leakage -Reduced reaction with construction materials -Improve thermal conductivity by increasing heat exchange surface -Volume change avoided	-Supercooling problems -Affect the mechanical strength of building materials -Reduced latent heat storage capacity than pure PCM -High cost
	Shape-stabilized PCMs	-Prevent leakage -No extra device or container is needed -Suitable thermal conductivity -Long-term stability -Large apparent specific heat	-Synthesis of PCM and the supporting material increases operational complexity.

2.5. Numerical Simulation of Buildings with PCMs

2.5.1. Dynamic Simulation of PCM-based Buildings

Good knowledge of the thermal performance of buildings incorporating passive LHTES systems with PCMs is essential for building researchers to better understand the buildings' temperature response characteristics and the economic feasibility of using PCMs. Despite the

experimental works performed by various studies, the complex thermal transient nature of the building components with PCMs and the high cost of the set ups makes necessary the use of numerical models to deeply study the thermal performance of this system. The fundamental understanding of the working principle of this PCM-based building system is important to take further proper actions to make the most of PCMs to enhance indoor thermal comfort and the overall building energy efficiency.

2.5.2. Simulation Tools

Nowadays, there are many simulation tools for the building thermal performance assessment, such as EnergyPlus, ESP-r, TRNSYS, etc. EnergyPlus is an energy analysis and thermal load simulation program that models heating, cooling, ventilation, and other energy flows in buildings. Tardieu et al. [114] used EnergyPlus to predict the thermal performance of office size test rooms located in Auckland, New Zealand. The long-term measurements conducted for these test rooms showed a good agreement with the simulation results. They showed that PCM-gypsum wallboard provided significant heat energy storage capacity. The simulated results also showed that the additional thermal mass of the PCM can reduce the daily indoor temperature swing by up to 4 °C on a typical summer day. ESP-r is also an advanced building energy simulation tool that allows for a detailed thermal description of buildings. It can integrate the effect of a variety of factors including, weather, external shading, occupancy gains, HVAC systems, and many others. Schossig et al. [66] simulated the thermal performance of a lightweight office using ESP-r. They showed that the application of microencapsulated PCMs in the interior wall prevents overheating and reduces the cooling load in summer. The TRNSYS software is used for building dynamic simulation based on transfer functions technique, it is modular and contains many subroutines for various systems including building. Kuznik et al.

[115] developed and validated a new TRNSYS Type through experimental results, named Type 260, to model the thermal behavior of a PCM external wall. All the mentioned simulation tools above are highlighted for their versatility and reliability, however, based on the thermal performance of a whole building. Sharifi et al. [116] used COMSOL software to simulate temperature changes in structural elements enhanced with PCMs. To investigate the detailed thermal dynamics of building envelopes, this dissertation also utilizes COMSOL Multiphysics® software to develop the model, simulate the thermal dynamic behavior of the multilayer wall, and explore the complex interactions between different layers of the wall assembly.

2.6. Summary

Incorporating PCM into building elements enables a more dynamic use of thermal energy. In this chapter, previous studies on impregnating PCMs in various building elements for better thermal management have been reviewed. As a powerful alternative to the conventional building cooling/heating systems, PCMs with great heat energy storage density and isothermal nature can (i) take advantage of renewable sources like solar energy and natural cooling; (ii) shift the building load from peak to off-peak period; (iii) regulate the indoor temperature fluctuations and stabilize the temperature in the thermal comfort range for a longer time; and (iv) contribute to the energy saving.

PCMs are classified as organic, inorganic, and eutectic mixtures. By summarizing some current existing research, it was found 85.9% of them use organic PCM in buildings. It is because of their proper melting temperature, noncorrosive, no supercooling, and good compatibility with construction materials.

In addition to criteria concerning safety and reliability, the PCMs to be used in buildings also needs to meet the thermal criteria. It was found that currently used melting points range

from 16℃ to 40 ℃, covering a large temperature span up to 24℃ and centering the temperature of 26.5℃. The melting point is recommended to be close to occupants' thermal comfort temperature for the sake of saving energy. Moreover, the environmental conditions that a building is subjected to should also be taken into consideration when the phase change temperature of PCM is determined.

Among different building elements, it is recommended to integrate PCM into building walls due to the implementation simplicity and cost-effectiveness. In addition, the wall element is the main passageway for thermal gains and losses, therefore including PCM in it shows high potential to improve building energy efficiency. Another observation is that 51.1% of the investigated research choose to integrate the PCM layer closed to the interior side of the building element. 23.9% and 25% of the studies prefer the exterior side and center of the building elements, respectively.

In terms of incorporating PCM into building materials, new technologies (including microencapsulation, nanoencapsulation, and shape-stabilized) are preferred mainly due to their superiority in preventing leakage and enhancing heat transfer rate over the conventional methods (including direct incorporation, immersion, and macro-encapsulation).

2.7. References

[1] X. Li, H. Chen, H. Li, L. Liu, Z. Lu, T. Zhang, W.H. Duan, Integration of form-stable paraffin/nanosilica phase change material composites into vacuum insulation panels for thermal energy storage, Applied Energy 159 (2015) 601-609.

[2] J. Heier, C. Bales, V. Martin, Combining thermal energy storage with buildings – a review, Renewable and Sustainable Energy Reviews 42 (2015) 1305-1325.

[3] K.H. Khan, M.G. Rasul, M.M.K. Khan, Energy conservation in buildings: cogeneration and cogeneration coupled with thermal energy storage, Applied Energy 77(1) (2004) 15-34.

[4] R. Parameshwaran, S. Harikrishnan, S. Kalaiselvam, Energy efficient PCM-based variable air volume air conditioning system for modern buildings, Energy and Buildings 42(8) (2010) 1353-1360.

[5] P. Devaux M.M. Farid, Benefits of PCM underfloor heating with PCM wallboards for space heating in winter, Applied Energy 191 (2017) 593-602.

[6] G. Evola, L. Marletta, F. Sicurella, Simulation of a ventilated cavity to enhance the effectiveness of PCM wallboards for summer thermal comfort in buildings, Energy and Buildings 70 (2014) 480-489.

[7] Salyer, I. O., & Sircar, A. K. (1989). Development of PCM wallboard for heating and cooling of residential buildings (No. CONF-890351-). USDOE Assistant Secretary for Conservation and Renewable Energy, Washington, DC (United States). Office of Energy Management; Pacific Northwest Lab., Richland, WA (United States); Oak Ridge National Lab., TN (United States).

[8] M. Telkes, Solar energy storage, ASHRAE J, 16 (9) (1974) 38-44.

[9] T. Khadiran, M.Z. Hussein, Z. Zainal, R. Rusli, Advanced energy storage materials for building applications and their thermal performance characterization: A review, Renewable and Sustainable Energy Reviews 57 (2016) 916-928.

[10] A. Abhat, Low temperature latent heat thermal energy storage: Heat storage materials, Solar Energy 30(4) (1983) 313-332.

[11] L.F. Cabeza, A. Castell, C. Barreneche, A. de Gracia, A.I. Fernández, Materials used as PCM in thermal energy storage in buildings: A review, Renewable and Sustainable Energy Reviews 15(3) (2011) 1675-1695.

[12] De Gracia, A. and Cabeza, L.F., Phase change materials and thermal energy storage for buildings, Energy and Buildings 103 (2015) 414-419.

[13] A. Sharma, V.V. Tyagi, C.R. Chen, D. Buddhi, Review on thermal energy storage with phase change materials and applications, Renewable and Sustainable Energy Reviews 13(2) (2009) 318-345.

[14] T. Yan, R.Z. Wang, T.X. Li, L.W. Wang, I.T. Fred, A review of promising candidate reactions for chemical heat storage, Renewable and Sustainable Energy Reviews 43 (2015) 13-31.

[15] L. Navarro, A. de Gracia, S. Colclough, M. Browne, S.J. McCormack, P. Griffiths, L.F. Cabeza, Thermal energy storage in building integrated thermal systems: A review. Part 1. active storage systems, Renewable Energy 88 (2016) 526-547.

[16] P. Bose V.A. Amirtham, A review on thermal conductivity enhancement of paraffinwax as latent heat energy storage material, Renewable and Sustainable Energy Reviews 65 (2016) 81-100.

[17] C. Arkar S. Medved, Free cooling of a building using PCM heat storage integrated into the ventilation system, Solar Energy 81(9) (2007) 1078-1087.

[18] S. Medved C. Arkar, Correlation between the local climate and the free-cooling potential of latent heat storage, Energy and Buildings 40(4) (2008) 429-437.

[19] A. Lazaro, P. Dolado, J.M. Marín, B. Zalba, PCM–air heat exchangers for free-cooling applications in buildings: Experimental results of two real-scale prototypes, Energy Conversion and Management 50(3) (2009) 439-443.

[20] A. Waqas Z. Ud Din, Phase change material (PCM) storage for free cooling of buildings—A review, Renewable and Sustainable Energy Reviews 18 (2013) 607-625.

[21] R. Baetens, B.P. Jelle, A. Gustavsen, Phase change materials for building applications: A state-of-the-art review, Energy and Buildings 42(9) (2010) 1361-1368.

[22] S. M. Hasnain, Review on sustainable thermal energy storage technologies, Part I: heat storage materials and techniques, Energy conversion and management 39(11) (1998) 1127-1138.

[23] L. Fu, Q. Wang, R. Ye, X. Fang, Z. Zhang, A calcium chloride hexahydrate/expanded perlite composite with good heat storage and insulation properties for building energy conservation, Renewable Energy 114 (2017) 733-743.

[24] L. Erlbeck, P. Schreiner, F. Fasel, F.J. Methner, M. Rädle, Investigation of different materials for macroencapsulation of salt hydrate phase change materials for building purposes, Construction and Building Materials 180 (2018) 512-518.

[25] M. Kenisarin K. Mahkamov, Solar energy storage using phase change materials☆, Renewable and Sustainable Energy Reviews 11(9) (2007) 1913-1965.

[26] H. Mehling, L.F. Cabeza, Heat and cold storage with PCM. An up to date introduction into basics and applications, Springer-Verlag Berlin Heidelberg; Berlin (Germany) (2008).

[27] Y. Cai, H. Ke, L. Lin, X. Fei, Q. Wei, L. Song, Y. Hu, H. Fong, Preparation, morphology and thermal properties of electrospun fatty acid eutectics/polyethylene terephthalate form-

stable phase change ultrafine composite fibers for thermal energy storage, Energy Conversion and Management 64 (2012) 245-255.

[28] X. Tang, B. Zhu, M. Xu, W. Zhang, Z. Yang, Y. Zhang, G. Yin, D. He, H. Wei, X. Zhai, Shape-stabilized phase change materials based on fatty acid eutectics/expanded graphite composites for thermal storage, Energy and Buildings 109 (2015) 353-360.

[29] R. Wen, X. Zhang, Y. Huang, Z. Yin, Z. Huang, M. Fang, Y.g. Liu, X. Wu, Preparation and properties of fatty acid eutectics/expanded perlite and expanded vermiculite shape-stabilized materials for thermal energy storage in buildings, Energy and Buildings 139 (2017) 197-204.

[30] F. Agyenim N. Hewitt, The development of a finned phase change material (PCM) storage system to take advantage of off-peak electricity tariff for improvement in cost of heat pump operation, Energy and Buildings 42(9) (2010) 1552-1560.

[31] M. Li, N. Gong, J. Wang, Z. Lin , Phase Change Material for Thermal Management in 3D Integrated Circuits Packaging, International Symposium on Microelectronics (1) (2015) 000649-000653.

[32] J. Jia W.L. Lee, Applying storage-enhanced heat recovery room air-conditioner (SEHRAC) for domestic water heating in residential buildings in Hong Kong, Energy and Buildings 78 (2014) 132-142.

[33] W.F. Wu, N. Liu, W.L. Cheng, Y. Liu, Study on the effect of shape-stabilized phase change materials on spacecraft thermal control in extreme thermal environment, Energy Conversion and Management 69 (2013) 174-180.

[34] A. Shaid, L. Wang, S. Islam, J.Y. Cai, R. Padhye, Preparation of aerogel-eicosane microparticles for thermoregulatory coating on textile, Applied Thermal Engineering 107 (2016) 602-611.

[35] H.M. Hoang, D. Leducq, R. Pérez-Masia, J.M. Lagaron, E. Gogou, P. Taoukis, G. Alvarez, Heat transfer study of submicro-encapsulated PCM plate for food packaging application, International Journal of Refrigeration 52 (2015) 151-160.

[36] Y.J. Kim, B. Kim, J.W. Kim, G. Nam, H.S. Jang, S.W. Kang, U. Jeong, Combination of nanoparticles with photothermal effects and phase-change material enhances the non-invasive transdermal delivery of drugs, Colloids Surf B Biointerfaces 135 (2015) 324-331.

[37] H. Akeiber, P. Nejat, M.Z.A. Majid, M.A. Wahid, F. Jomehzadeh, I. Zeynali Famileh, J.K. Calautit, B.R. Hughes, S.A. Zaki, A review on phase change material (PCM) for sustainable passive cooling in building envelopes, Renewable and Sustainable Energy Reviews 60 (2016) 1470-1497.

[38] E. Osterman, V.V. Tyagi, V. Butala, N.A. Rahim, U. Stritih, Review of PCM based cooling technologies for buildings, Energy and Buildings 49 (2012) 37-49.

[39] V.V. Tyagi D. Buddhi, PCM thermal storage in buildings: A state of art, Renewable and Sustainable Energy Reviews 11(6) (2007) 1146-1166.

[40] M. Pomianowski, P. Heiselberg, Y. Zhang, Review of thermal energy storage technologies based on PCM application in buildings, Energy and Buildings 67 (2013) 56-69.

[41] M.K. Rathod J. Banerjee, Thermal stability of phase change materials used in latent heat energy storage systems: A review, Renewable and Sustainable Energy Reviews 18 (2013) 246-258.

[42] S.E. Kalnæs B.P. Jelle, Phase change materials and products for building applications: A state-of-the-art review and future research opportunities, Energy and Buildings 94 (2015) 150-176.

[43] J.H. Dieckmann, Latent heat storage in concrete, Technische UniversitätKaiserslautern, Kaiserslautern, Germany, http://www.eurosolar.org/new/pdfs neu/Thermal/IRES2006 Dieckmann.pdf (accessed 31.10.2013).

[44] D. Zhou, C.Y. Zhao, Y. Tian, Review on thermal energy storage with phase change materials (PCMs) in building applications, Applied Energy 92 (2012) 593-605.

[45] Z. Khan, Z. Khan, A. Ghafoor, A review of performance enhancement of PCM based latent heat storage system within the context of materials, thermal stability and compatibility, Energy Conversion and Management 115 (2016) 132-158.

[46] F. Agyenim, N. Hewitt, P. Eames, M. Smyth, A review of materials, heat transfer and phase change problem formulation for latent heat thermal energy storage systems (LHTESS), Renewable and Sustainable Energy Reviews 14(2) (2010) 615-628.

[47] Y. Lin, Y. Jia, G. Alva, G. Fang, Review on thermal conductivity enhancement, thermal properties and applications of phase change materials in thermal energy storage, Renewable and Sustainable Energy Reviews 82 (2018) 2730-2742.

[48] Y. Wu T. Wang, Hydrated salts/expanded graphite composite with high thermal conductivity as a shape-stabilized phase change material for thermal energy storage, Energy Conversion and Management 101 (2015) 164-171.

[49] A. Hussain, C.Y. Tso, C.Y.H. Chao, Experimental investigation of a passive thermal management system for high-powered lithium ion batteries using nickel foam-paraffin composite, Energy 115 (2016) 209-218.

[50] K.B. Green, Carbonless paper production. Ohio: NCR Corporation, NCR Corporation, Ohio (1953).

[51] H. Zhang, X. Wang, D. Wu, Silica encapsulation of n-octadecane via sol-gel process: a novel microencapsulated phase-change material with enhanced thermal conductivity and performance, J Colloid Interface Sci 343(1) (2010) 246-55.

[52] G. Alva, Y. Lin, L. Liu, G. Fang, Synthesis, characterization and applications of microencapsulated phase change materials in thermal energy storage: A review, Energy and Buildings 144 (2017) 276-294.

[53] T. Wang, S. Wang, R. Luo, C. Zhu, T. Akiyama, Z. Zhang, Microencapsulation of phase change materials with binary cores and calcium carbonate shell for thermal energy storage, Applied Energy 171 (2016) 113-119.

[54] N. Xie, J. Luo, Z. Li, Z. Huang, X. Gao, Y. Fang, Z. Zhang, Salt hydrate/expanded vermiculite composite as a form-stable phase change material for building energy storage, Solar Energy Materials and Solar Cells 189 (2019) 33-42.

[55] Y.P. Zhang, K.P. Lin, R. Yang, H.F. Di, Y. Jiang, Preparation, thermal performance and application of shape-stabilized PCM in energy efficient buildings, Energy and Buildings 38(10) (2006) 1262-1269.

[56] M. Li, G. Gui, Z. Lin, L. Jiang, H. Pan, X. Wang, Numerical Thermal Characterization and Performance Metrics of Building Envelopes Containing Phase Change Materials for Energy-Efficient Buildings, Sustainability 10(8) (2018) 2657.

[57] N. Soares, J.J. Costa, A.R. Gaspar, P. Santos, Review of passive PCM latent heat thermal energy storage systems towards buildings' energy efficiency, Energy and Buildings 59 (2013) 82-103.

[58] M. Kheradmand, M. Azenha, J.L.B. de Aguiar, J. Castro-Gomes, Experimental and numerical studies of hybrid PCM embedded in plastering mortar for enhanced thermal behaviour of buildings, Energy 94 (2016) 250-261.

[59] D. Zhou, G.S.F. Shire, Y. Tian, Parametric analysis of influencing factors in Phase Change Material Wallboard (PCMW), Applied Energy 119 (2014) 33-42.

[60] E.M. Alawadhi, Thermal analysis of a building brick containing phase change material, Energy and Buildings 40(3) (2008) 351-357.

[61] M. Silakhori, M.S. Naghavi, H.S.C. Metselaar, T.M.I. Mahlia, H. Fauzi, M. Mehrali, Accelerated Thermal Cycling Test of Microencapsulated Paraffin Wax/Polyaniline Made by Simple Preparation Method for Solar Thermal Energy Storage, Materials (Basel) 6(5) (2013) 1608-1620.

[62] V.V. Tyagi D. Buddhi, Thermal cycle testing of calcium chloride hexahydrate as a possible PCM for latent heat storage, Solar Energy Materials and Solar Cells 92(8) (2008) 891-899.

[63] A. Sharma, S.D. Sharma, D. Buddhi, Accelerated thermal cycle test of acetamide, stearic acid and paraffin wax for solar thermal latent heat storage applications, Energy Conversion and Management, 43(14) (2002) 1923-1930.

[64] S.D. Sharma, D. Buddhi, R.L. Sawhney, Accelerated thermal cycle test of latent heat-storage materials, Solar Energy, 66 (6) (1999) 483-490.

[65] K.O. Lee, M.A. Medina, E. Raith, X. Sun, Assessing the integration of a thin phase change material (PCM) layer in a residential building wall for heat transfer reduction and management, Applied Energy 137 (2015) 699-706.

[66] P. Schossig, H. Henning, S. Gschwander, T. Haussmann, Micro-encapsulated phase-change materials integrated into construction materials, Solar Energy Materials and Solar Cells 89(2-3) (2005) 297-306.

[67] T. Lecompte, P. Le Bideau, P. Glouannec, D. Nortershauser, S. Le Masson, Mechanical and thermo-physical behaviour of concretes and mortars containing phase change material, Energy and Buildings 94 (2015) 52-60.

[68] K. Biswas, J. Lu, P. Soroushian, S. Shrestha, Combined experimental and numerical evaluation of a prototype nano-PCM enhanced wallboard, Applied Energy 131 (2014) 517-529.

[69] M. Saffari, A. de Gracia, C. Fernández, L.F. Cabeza, Simulation-based optimization of PCM melting temperature to improve the energy performance in buildings, Applied Energy 202 (2017) 420-434.

[70] M.A. Izquierdo-Barrientos, J.F. Belmonte, D. Rodríguez-Sánchez, A.E. Molina, J.A. Almendros-Ibáñez, A numerical study of external building walls containing phase change materials (PCM), Applied Thermal Engineering 47 (2012) 73-85.

[71] X. Jin, M.A. Medina, X. Zhang, Numerical analysis for the optimal location of a thin PCM layer in frame walls, Applied Thermal Engineering 103 (2016) 1057-1063.

[72] X. Jin, S. Zhang, X. Xu, X. Zhang, Effects of PCM state on its phase change performance and the thermal performance of building walls, Building and Environment 81 (2014) 334-339.

[73] X. Jin, M.A. Medina, X. Zhang, On the placement of a phase change material thermal shield within the cavity of buildings walls for heat transfer rate reduction, Energy 73 (2014) 780-786.

[74] A. Bontemps, M. Ahmad, K. Johannès, H. Sallée, Experimental and modelling study of twin cells with latent heat storage walls, Energy and Buildings 43(9) (2011) 2456-2461.

[75] N. Zhu, P. Liu, P. Hu, F. Liu, Z. Jiang, Modeling and simulation on the performance of a novel double shape-stabilized phase change materials wallboard, Energy and Buildings 107 (2015) 181-190.

[76] M. Sayyar, R.R. Weerasiri, P. Soroushian, J. Lu, Experimental and numerical study of shape-stable phase-change nanocomposite toward energy-efficient building constructions, Energy and Buildings 75 (2014) 249-255.

[77] X. Shi, S.A. Memon, W. Tang, H. Cui, F. Xing, Experimental assessment of position of macro encapsulated phase change material in concrete walls on indoor temperatures and humidity levels, Energy and Buildings 71 (2014) 80-87.

[78] F. Kuznik, J. Virgone, J.-J. Roux, Energetic efficiency of room wall containing PCM wallboard: A full-scale experimental investigation, Energy and Buildings 40(2) (2008) 148-156.

[79] L. Shilei, Z. Neng, F. Guohui, Impact of phase change wall room on indoor thermal environment in winter, Energy and Buildings 38(1) (2006) 18-24.

[80] A.M. Thiele, G. Sant, L. Pilon, Diurnal thermal analysis of microencapsulated PCM-concrete composite walls, Energy Conversion and Management 93 (2015) 215-227.

[81] L.F. Cabeza, C. Castellón, M. Nogués, M. Medrano, R. Leppers, O. Zubillaga, Use of microencapsulated PCM in concrete walls for energy savings, Energy and Buildings 39(2) (2007) 113-119.

[82] K.O. Lee, M.A. Medina, X. Sun, X. Jin, Thermal performance of phase change materials (PCM)-enhanced cellulose insulation in passive solar residential building walls, Solar Energy 163 (2018) 113-121.

[83] M.I. Hasan, H.O. Basher, A.O. Shdhan, Experimental investigation of phase change materials for insulation of residential buildings, Sustainable Cities and Society 36 (2018) 42-58.

[84] M. Arıcı, F. Bilgin, S. Nižetić, H. Karabay, PCM integrated to external building walls: An optimization study on maximum activation of latent heat, Applied Thermal Engineering 165 (2020).

[85] Y. Liu, M. Wang, H. Cui, L. Yang, J. Liu, Micro-/macro-level optimization of phase change material panel in building envelope, Energy 195 (2020).

[86] F. Guarino, A. Athienitis, M. Cellura, D. Bastien, PCM thermal storage design in buildings: Experimental studies and applications to solaria in cold climates, Applied Energy 185 (2017) 95-106.

[87] A. Bastani, F. Haghighat, J. Kozinski, Designing building envelope with PCM wallboards: Design tool development, Renewable and Sustainable Energy Reviews 31 (2014) 554-562.

[88] H. Jamil, M. Alam, J. Sanjayan, J. Wilson, Investigation of PCM as retrofitting option to enhance occupant thermal comfort in a modern residential building, Energy and Buildings 133 (2016) 217-229.

[89] L. Royon, L. Karim, A. Bontemps, Optimization of PCM embedded in a floor panel developed for thermal management of the lightweight envelope of buildings, Energy and Buildings 82 (2014) 385-390.

[90] G. Zhou, Y. Zhang, X. Wang, K. Lin, W. Xiao, An assessment of mixed type PCM-gypsum and shape-stabilized PCM plates in a building for passive solar heating, Solar Energy 81(11) (2007) 1351-1360.

[91] G. Zhou, Y. Yang, X. Wang, S. Zhou, Numerical analysis of effect of shape-stabilized phase change material plates in a building combined with night ventilation, Applied Energy 86(1) (2009) 52-59.

[92] M. Ahmad, A. Bontemps, H. Sallée, D. Quenard, Thermal testing and numerical simulation of a prototype cell using light wallboards coupling vacuum isolation panels and phase change material, Energy and Buildings 38(6) (2006) 673-681.

[93] R.D. Beltrán J. Martínez-Gómez, Analysis of phase change materials (PCM) for building wallboards based on the effect of environment, Journal of Building Engineering 24 (2019).

[94] S. Guichard, F. Miranville, D. Bigot, B. Malet-Damour, H. Boyer, Experimental investigation on a complex roof incorporating phase-change material, Energy and Buildings 108 (2015) 36-43.

[95] A. Pasupathy R. Velraj, Effect of double layer phase change material in building roof for year round thermal management, Energy and Buildings 40(3) (2008) 193-203.

[96] J. Yu, Q. Yang, H. Ye, Y. Luo, J. Huang, X. Xu, W. Gang, J. Wang, Thermal performance evaluation and optimal design of building roof with outer-layer shape-stabilized PCM, Renewable Energy 145 (2020) 2538-2549.

[97] T. Silva, R. Vicente, F. Rodrigues, A. Samagaio, C. Cardoso, Development of a window shutter with phase change materials: Full scale outdoor experimental approach, Energy and Buildings 88 (2015) 110-121.

[98] S. Li, G. Sun, K. Zou, X. Zhang, Experimental research on the dynamic thermal performance of a novel triple-pane building window filled with PCM, Sustainable Cities and Society 27 (2016) 15-22.

[99] L. Royon, L. Karim, A. Bontemps, Thermal energy storage and release of a new component with PCM for integration in floors for thermal management of buildings, Energy and Buildings 63 (2013) 29-35.

[100] K. Lin, Y. Zhang, X. Xu, H. Di, R. Yang, P. Qin, Modeling and simulation of under-floor electric heating system with shape-stabilized PCM plates, Building and Environment 39(12) (2004) 1427-1434.

[101] A.G. Entrop, H.J.H. Brouwers, A.H.M.E. Reinders, Experimental research on the use of micro-encapsulated Phase Change Materials to store solar energy in concrete floors and to save energy in Dutch houses, Solar Energy 85(5) (2011) 1007-1020.

[102] N.A. Yahay H. Ahmad, Numerical Investigation of Indoor Air Temperature with the Application of PCM Gypsum Board as Ceiling Panels in Buildings, Procedia Engineering 20 (2011) 238-248.

[103] M. Jaworski, Thermal performance of building element containing phase change material (PCM) integrated with ventilation system – An experimental study, Applied Thermal Engineering 70(1) (2014) 665-674.

[104] N. Chaiyat, Energy and economic analysis of a building air-conditioner with a phase change material (PCM), Energy Conversion and Management 94 (2015) 150-158.

[105] C. Castellón, M. Medrano, J. Roca, L.F. Cabeza, M.E. Navarro, A.I. Fernández, A. Lázaro, B. Zalba, Effect of microencapsulated phase change material in sandwich panels, Renewable Energy 35(10) (2010) 2370-2374.

[106] R.D. Beltrán, I. Miño-Rodríguez, A. Lobato, A. Gallardo, C. Naranjo-Mendozac, Thermal comfort performance within heritage buildings subject to a change of use, Proceedings of the Mediterranean Green Building and Renewable Energy Forum (2015).

[107] S.A. Memon, H.Z. Cui, H. Zhang, F. Xing, Utilization of macro encapsulated phase change materials for the development of thermal energy storage and structural lightweight aggregate concrete, Applied Energy 139 (2015) 43-55.

[108] S.D. Zwanzig, Y. Lian, E.G. Brehob, Numerical simulation of phase change material composite wallboard in a multi-layered building envelope, Energy Conversion and Management 69 (2013) 27-40.

[109] D.W. Hawes, D. Feldman, D. Banu, Latent heat storage in building materials, Energy Build 20 (1993) 77-86.

[110] S. Ramakrishnan, J. Sanjayan, X. Wang, M. Alam, J. Wilson, A novel paraffin/expanded perlite composite phase change material for prevention of PCM leakage in cementitious composites, Applied Energy 157 (2015) 85-94.

[111] C. Alkan, A. Sarı, A. Karaipekli, O. Uzun, Preparation, characterization, and thermal properties of microencapsulated phase change material for thermal energy storage, Solar Energy Materials and Solar Cells 93(1) (2009) 143-147.

[112] J. Giro-Paloma, M. Martínez, L.F. Cabeza, A.I. Fernández, Types, methods, techniques, and applications for microencapsulated phase change materials (MPCM): A review, Renewable and Sustainable Energy Reviews 53 (2016) 1059-1075.

[113] F. Liu, J. Wang, X. Qian, Integrating phase change materials into concrete through microencapsulation using cenospheres, Cement and Concrete Composites 80 (2017) 317-325.

[114] A. Tardieu, S. Behzadi, J.J.J. Chen, M.M. Farid, Computer simulation and experimental measurements for an experimental PCM-impregnated office building, Proceedings of Building Simulation, Sydney, Australia (2011).

[115] F. Kuznik, J. Virgone, K. Johannes, Development and validation of a new TRNSYS type for the simulation of external building walls containing PCM, Energy and Buildings 42(7) (2010) 1004-1009.

[116] N.P. Sharifi, G.E. Freeman, A.R. Sakulich, Using COMSOL modeling to investigate the efficiency of PCMs at modifying temperature changes in cementitious materials – Case study, Construction and Building Materials 101 (2015) 965-974.

3. EXPERIMENTAL STUDY ON THE THERMAL PERFORMANCE OF PCM INTEGRATED INTO LABORATORY-SCALE PROTOTYPES

3.1. Introduction

As a thermal storage technology, PCM has been widely researched in buildings in the last two decades. Building applications of PCMs can be divided into passive systems and active systems [1]. In the passive system, PCM integrated into the building envelopes is used to increase their thermal mass, which is especially beneficial in lightweight building envelopes with low thermal inertia [2]. The possible envelopes that can be enhanced by PCM include wallboards, floors, roofs, windows, etc. Among different incorporation methods, the shape-stabilized PCM consisted of PCM and supporting material has attracted much research interest due to its advantages of keeping the shape during the phase change process, no need for the container, and large thermal energy storage capacity [3][4].

Paraffin is one of the most promising components of shape-stabilized PCM for building applications due to its many advantages, including large latent heat capacity, low cost, non-toxicity, good thermal and chemical stability, and good compatibility with other construction materials [5]. However, the low thermal conductivity (about 0.24 W/mK) of paraffin limits its widespread application because of the inefficient charging and discharging rate when absorbing or releasing thermal energy. The thermal conductivity of paraffin is therefore needed to be modified to improve its thermal performance when being used for building thermal management. In addition, there exists a leakage problem during the phase transition process of paraffin that needs to be solved.

Among various heat transfer enhancement strategies, such as adding additives with high thermal conductivity and extending surface area by encapsulating PCMs [6-8], incorporating

expanded graphite (EG) into paraffin has been considered promising due to EG's low density, high thermal conductivity, low cost, and compatibility with the paraffin [9]. Moreover, the porous structure of EG can be used as a carrier to absorb paraffin to form a stabilized-shape phase change material, which can prevent the paraffin from leaking out during the process of melting. Zhang and Fang [10] prepared a paraffin/EG composite phase change thermal energy storage material by mixing the EG into the liquid paraffin at 65 °C. They found that the weight percentage of paraffin can reach up to 85.6% of the total weight of the composite without leakage, and the latent heat of the resulted composite is 161.45 J/g, which can significantly increase the thermal mass when being used in the building envelopes. Yang et al. [11] also synthesized a paraffin/EG composite retaining up to 93.1% of paraffin, which was tested chemically compatible, thermally stable, and reliable.

Several studies have investigated the feasibility of applying paraffin/EG composite into the building envelopes for thermal energy storage. Guo et al. [12] prepared the thermal energy storage composite by employing EG stabilized paraffin as PCM and wood flour/high-density polyethylene as the matrix. Their results show that this TES composite has the efficient temperature-regulated ability and the satisfying thermal performance and acceptable mechanical property indicating this composite can be used as a building material for temperature conditioning. Frąc et al. [13] added the paraffin/EG grains into the cement composites in a ratio of 10-30 wt% of cement to investigate their application in accumulative heating systems. When being installed in a heat chamber, these composites were found to maintain a desirable are temperature inside of the chamber for a longer time, indicating that the cement composites with paraffin/EG composite could be effectively used to enhance the building energy efficiency. Composites of this kind are therefore considered in this study.

The objective of this experimental study is to investigate the thermal performance of a novel shape-stabilized composite PCM that consists of paraffin and EG and the feasibility of applying this composite in building envelopes for better thermal management. To achieve this goal, a paraffin/EG composite was prepared by absorbing liquid paraffin into the pores of expanded graphite that has excellent absorbability and good thermal conductivity. To explore the microstructure and thermal properties of the materials, appropriate measurements and characterizations were performed. Then the thermal performance of two laboratory-scale prototypes with and without the paraffin/EG composite has been tested under the sample input loading conditions, which can provide deeper knowledge about the advantages of using PCMs in buildings.

3.2. Experimental Description

3.2.1. Materials

Technical-grade paraffin blend purchased from Microtek Laboratories, Inc. is used as the PCM in this study. Expandable graphite provided by Asbury Carbon, Inc is used to produce the required expanded graphite (EG). Grade 3772 of the expandable graphite with an average particle size of 300 μm is selected to derive expanded graphite as the supporting material of paraffin and the heat exchanger to enhance the thermal conductivity of the PCM composite.

3.2.2. Preparation of EG

EG used as the supporting material was obtained by rapid expansion and exfoliation of expandable graphite in a high-temperature furnace. Before the expansion, expandable graphite was placed in a vacuum drying oven at a constant temperature of 60 °C for 24 hours to ensure it is completely dried. The expandable graphite was then heated for 14 seconds in a muffle furnace that was preheated to 850 °C (1562 ºF). During expansion, the flaky expandable graphite showed

in Figure 3.1(a) produces different sizes of pores between its flake structure and yields the expanded graphite with the worm-like structure (Figure 3.1(b)). After being expanded, the size of EG can reach up to around 2mm.

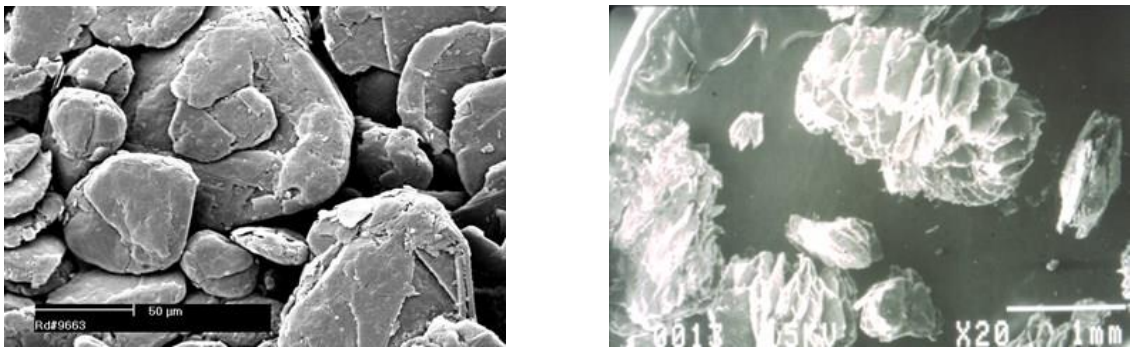

(a) (b)

Figure 3.1. Scanning electron microscopy (SEM) images of (a) flaky expandable graphite and (b) worm-like expanded graphite [14].

3.2.3. Preparation of Paraffin/EG Composite PCMs

Figure 3.2 shows the fabrication process of the paraffin/EG composites, in which the melt blending method was used to prepare the mixture. Pre-weighed paraffin was heated on the hot plate at 60 °C to ensure it was completely liquified, and the EG of mass fractions ranges from 5 wt% to 20 wt% were then submerged in the liquid paraffin. The mixture was stirred mechanically for 3 hours at 60 °C and then put in the vacuum oven for 24 hours at the same temperature to ensure the liquid paraffin can be completely absorbed into the micropores of the EG. In order to investigate the effects of the expansion conditions on the sorption capacity of EG for paraffin, different heating temperatures and times in the muffle furnace were used to prepare the EG samples. The maximum sorption capacity was determined based on the saturated state of EG particles, at which no excess paraffin is observed at the bottom and interior wall of the mixing container.

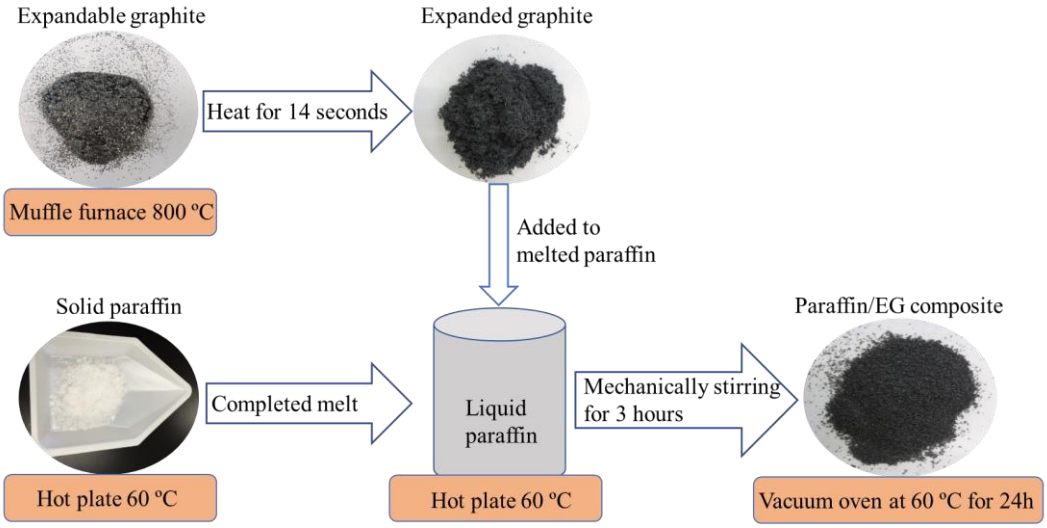

Figure 3.2. The fabrication process of paraffin/EG composite.

3.2.4. Characterization of Paraffin/EG Composites

A scanning Electron Microscope (SEM) was used to measure the surface morphology of the pure EG and paraffin/EG composite. The Fourier Transform Infra-Red (FTIR) and Brunauer–Emmet–Teller (BET) surface area and pore size distribution tests were also conducted to explore the absorption mechanism between paraffin and EG. The phase transition temperatures and latent heat capacity of pure paraffin and paraffin/EG composite were obtained by differential scanning calorimeter (DSC). Approximately 10 mg of each sample was sealed in an aluminum crucible and heated in a nitrogen atmosphere from 0 °C to 50 °C at a heating rate of 5 °C/min. Latent heat values were calculated for each sample based on the test results.

3.2.5. Thermal Energy Storage Test

A thermal energy storage test was conducted using 2×2×2 inches cubic samples to explore the heat transfer performance of the paraffin/EG composite. Those samples were made from paraffin/EG composites with the same weight but different paraffin and EG ratios. PCM composite specimens with 70 wt%, 80 wt%, and 90 wt% of paraffin were tested. As shown in

Figure 3.3 (a), a hot plate was used to provide a high-temperature environment on the bottom of the apparatus up to 80 °C. One steel block with the size of 2×2×0.74 inches was placed between the hot plate and the PCM sample to ensure the sample is heated uniformly on the bottom side. Since this test was conducted at room temperature (23.6°C), the phase transition temperature of the paraffin selected was 38°C to ensure it can undergo the phase transition process from solid to the liquid state. As shown in Figure 3.3 (b), PCM samples were wrapped around with the thermal insulating material except for the top and bottom side during the tests, so that the heat can only transfer in the vertical direction. Two thermal couplers (thermo-coupler K type) were placed on top and bottom of the test sample to measure its instantaneous temperature. A data logger was used to collect and record the temperature with time.

(a) (b)

Figure 3.3. Thermal energy storage test.

3.2.6. Thermal Performance Test of Prototypes

In order to assess the thermal effect of embedding paraffin/EG composite PCM into the building wallboard as the thermal inertia enhancement strategy, two laboratory-scale prototypes were built as shown in Figure 3.4. The prototypes are two hollow cubic boxes that hold six 0.6 m × 0.6 m wall panels. The top and bottom panels of both prototypes are the same, consisting of a

40 mm insulating layer sandwiched by two 12 mm oriented strand boards (OSB). From inside to outside, the wall of the tested prototype with a PCM layer consisted of a 12 mm OSB, a 12 mm PCM layer, a 20 mm insulating layer, and a 12 mm OSB. The PCM layer is a 12 mm cavity filled with the paraffin/EG composite with 90 wt.% of paraffin. The phase transition temperature of paraffin is 24 ℃ (75.2ºF), which is closed to the thermal comfort range of human beings. The reference wall without PCM layer consisted of a 12 mm OSB and a 20 mm insulating layer followed by another 12 mm OSB. The composition of the test cells is similar to a typical one in building envelopes but with smaller thickness. In fact, the target in this study was to have two small-sized prototypes, with relatively thin walls, which would however highlight the effect of PCM to show its thermal behavior.

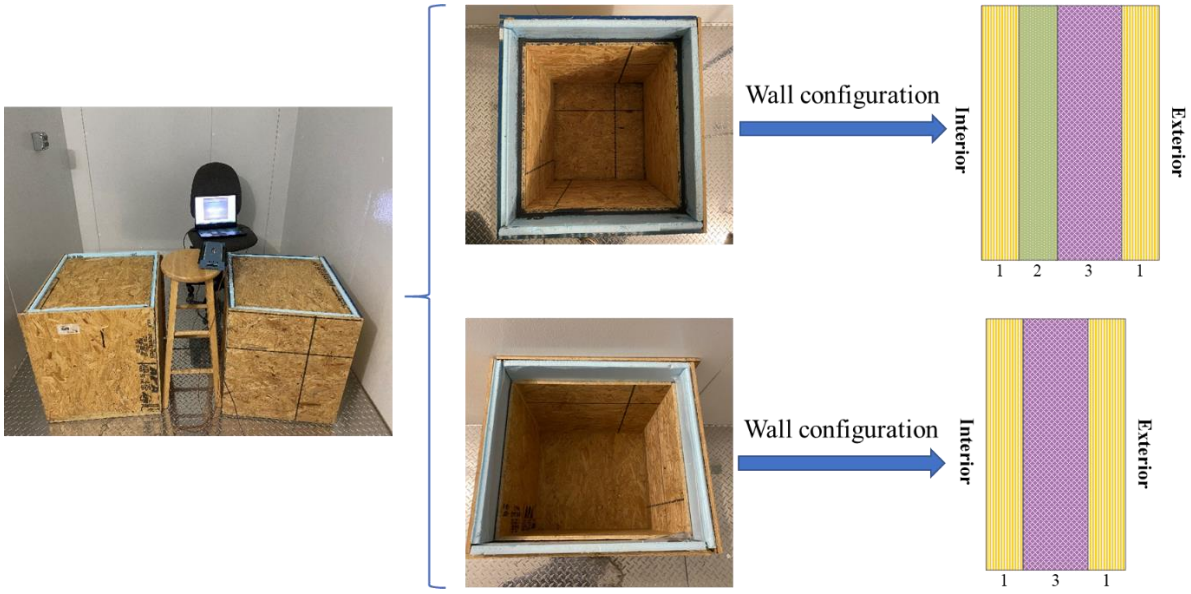

Figure 3.4. Test prototypes and schematic representation of wall configurations. 1: oriented strand board (OSB), 2: PCM composite, and 3: insulating layer.

In regard to the input temperature loading conditions, the test cells were located in an air-conditioned climatic chamber which was programmed to follow temperature cycles that matched the sol-air temperature for a vertical wall facing west. Under this arrangement, the interior of the

prototypes represents the interior space of a building, while the exterior of the prototypes represents the exterior environment of a building. The prototypes were tested in cycles of 4.5 hours each, where the chamber was turned on to simulate the solar-air temperature coupling the effect of both solar radiation and the ambient temperature. The simulated typical weather conditions were based on the temperature swing of early June in Chicago, Illinois, USA. The temperature profiles of the exterior surfaces of the test cells obtained during the experiments were intended to be as similar as possible to the temperature profiles of exterior wall surfaces facing west. Under these conditions, the thermal loads imposed by the chamber on the exterior surfaces of the prototypes were considerably relevant to those that occur in buildings surfaces exposed to the elements.

Four thermal couplers (thermo-coupler K type) were installed on the interior surface of each wallboard and one at the center of each test cell. Another four thermal couplers were installed on the exterior surface of each wallboard to collect the real input loading conditions. The temperature uncertainty of the thermocouple was 0.4 ℃. The average of the temperatures collected by the “interior” and “exterior” thermal couplers were calculated as the final room and environment temperatures, respectively. The thermal behavior of both prototypes was tested and compared to evaluate the thermal effect of PCM composites.

3.3. Results and Discussions

3.3.1. Paraffin Absorption into EG Samples

3.3.1.1. Comparison of the Paraffin Absorbing Capacity of EG Samples

Table 3.1 shows the maximum sorption capacity of the EG samples obtained at different heating temperatures and times. It can be seen from Table 3.1 that the mass percentage of paraffin in the PCM composites gradually increases with increasing the temperature of the

muffle furnace until it reaches 850 ℃. The maximum mass percentage of paraffin reaches 90.8% for the EG prepared under a muffle furnace temperature of 850 ℃ for 14 s. It has been observed that building took place during the treatment of the expandable graphite powder in the muffle furnace with a temperature over 850 ℃ for 16 s. At 850 ℃, the expandable graphite powder was found not completely expanded with a heating time shorter than 14 s, while with an increased treating time over 14 s, the expandable graphite tended to become over-expanded and some wormlike particles were broken due to the partially burning. Both conditions result in a decrease in the sorption capacity of EG.

Table 3.1. The maximum sorption capacity of different EG samples.

Muffle furnace temperature (℃)	**Heating time (s)**	**Mass ratio of paraffin in the composite (%)**
700	14	70.5
750	14	78.0
800	14	83.3
850	10	84.5
850	12	87.4
850	14	90.8
850	16	88.6
900	12	88.4
900	14	86.1

3.3.1.2. FTIR Analysis of the Prepared Samples

To explore the sorption mechanism of the EG with different preparation conditions, the FTIR spectroscopy of the natural expandable graphite (NEG) and EG samples was investigated in the frequency range of 500 to 4000 cm^{-1} with a resolution of 4 cm^{-1}. Figure 3.5 shows the FTIR spectra of the NEG and EG samples which were heated for 14 s in the muffle furnace with three temperatures including 300 ℃, 500 ℃, and 850 ℃. As can be seen from the results, the band at 3430 cm^{-1} and 1077 cm^{-1} is attributed to O-H stretching vibrations of phenolic or

alcoholic functional groups presented on all samples including the NEG [15], caused by intercalation of H_2SO_4 or HSO_4^- [16]. The presence of carboxyl functional groups can also be detected at around 1630 cm^{-1}. The absorption peak of S=O in EG is at 1160 cm^{-1}, but there are wide superimposed peaks in the range of 1160 to 1000 cm^{-1} in the FTIR of EG, and it is because the absorption peaks of S=O and P=O both appear in the range of 1350–1000 cm^{-1}. The results announce the intercalation of the intercalator. Compared to NEG, more functional groups such as a large number of hydroxyl, carboxyl, fat alkyl, and other active functional groups were produced caused by the oxidation intercalation during high-temperature exfoliation, which may contribute to the absorbing capacity of paraffin. However, increasing the exfoliation temperature from 300 ℃ to 850 ℃ has not led to significant degradation of SP2 carbon structure of EG [17]. The different sorption capacity between EG samples prepared under different heating temperatures may be caused by their different porous structures.

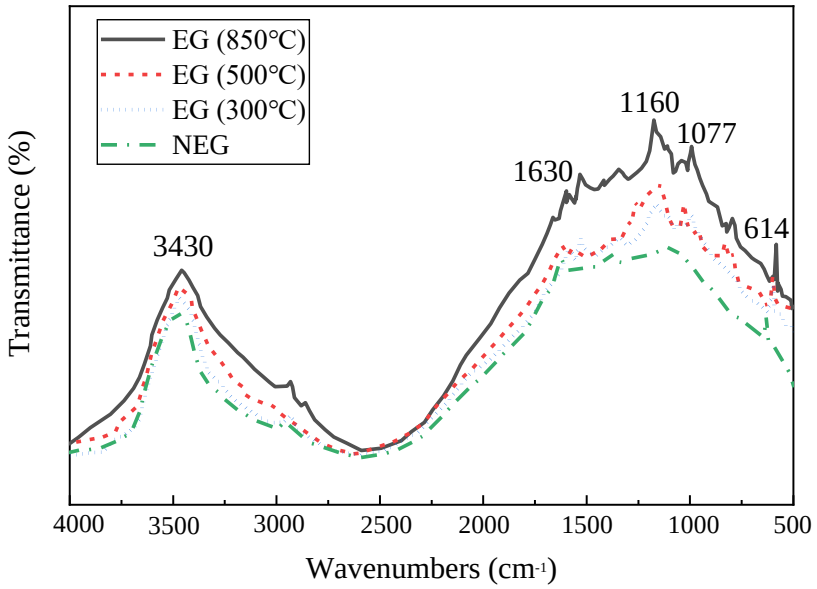

Figure 3.5. FTIR spectra of the EG prepared under different heating temperatures and NEG.

3.3.1.3. BET Surface Area and Pore Size Distribution of EG

The surface area and the pore size distribution of the EG heated in the muffle furnace at 850 ℃ were measured using an auto N_2 absorption method to further investigate the absorbability of the prepared EG specimen. The measurement results showed that the BET surface area of the EG was 32.89 m^2/g. Figure 3.6 shows the pore size distribution of the EG sample, which covers a wide pore size distribution ranges from 0.01 to 25.8 μm. Those mesopores and macropores caused by the exfoliation of NEG contribute to the easy absorption of organic compounds into EG [18]. Therefore, the prepared EG shows high absorption capacity to paraffin and can be used as a good matrix for the shape-stabilized PCM composite.

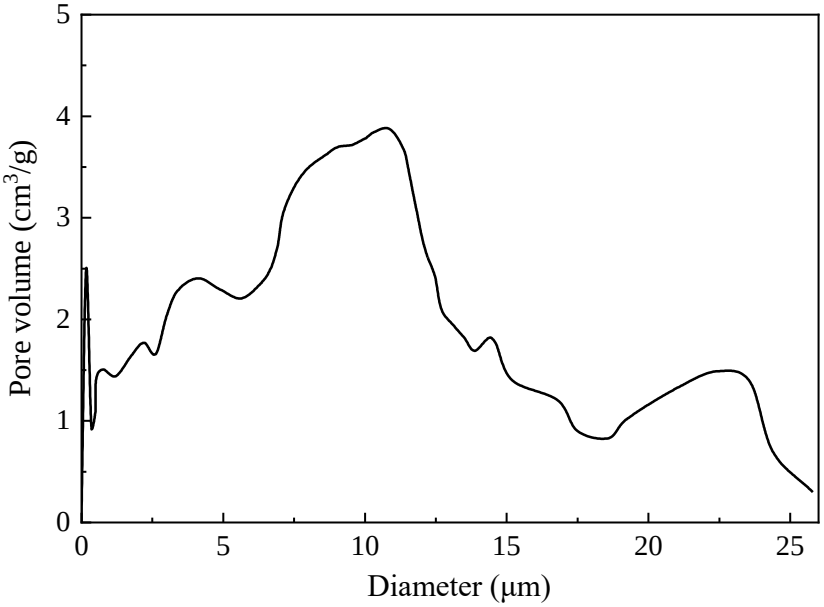

Figure 3.6. Pore size distribution of EG.

3.3.1.4. Surface Morphology of EG and the Paraffin/EG Composite

Surface morphology of EG and paraffin/EG composite were observed by SEM with an acceleration voltage of 2 kV. All samples were gold-coated and glued to the sample stage before observation. Figure 3.7 (a) shows the SEM image of EG under different magnifications. One can

see the loose and porous structure of worm-like expanded graphite, which was obtained after high-temperature heating. This porous structure resulted in its extremely low density. Meanwhile, the rapid heating led to a rough microstructure exhibited as an irregular honeycomb network, which enables the little amount of EG to significantly improve the heat transfer rate of the paraffin/EG composite.

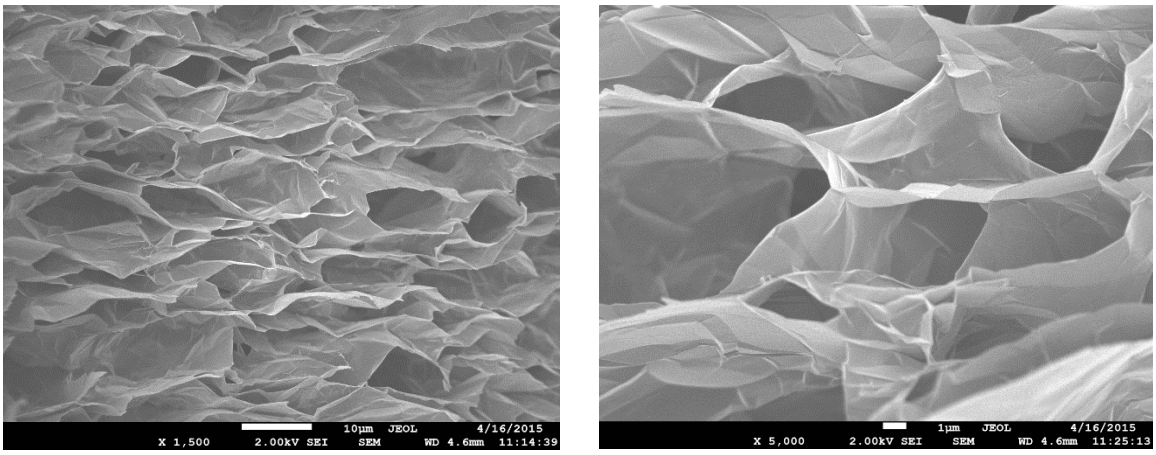

(a)

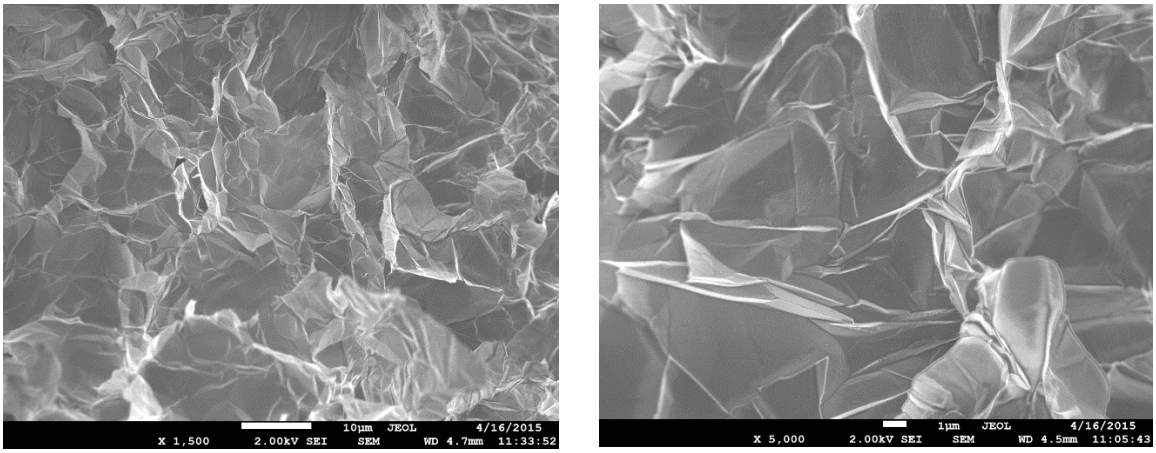

(b)

Figure 3.7. SEM images of (a) EG and (b) paraffin/EG composite.

As shown in Figure 3.7 (b), after the paraffin was absorbed into the pores of the EG, the EG remained in the worm-like structure. The porous structure of EG was filled with paraffin due

to absorption. The paraffin matrix was divided into numerous small areas by the space network structure of the expanded graphite and exhibited a uniform distribution in the paraffin/EG composite. The absorption properties of the PCM composite are caused by the unique network porosity, capillary force, high surface tension of the graphite microcrystalline, and the functional groups produced during the expansion process of EG. In addition to the unique structure, EG with non-polar properties is likely to absorb non-polar materials like paraffin [19]. Therefore, EG is a promising supporting media for paraffin to keep its form-stability and meanwhile enhance its thermal conductivity.

3.3.2. The Phase-change Temperature and the Latent Heat of Phase-change

Figure 3.8 shows the DSC curves of the pure paraffin and the paraffin/EG composites with 90 wt.% and 85 wt.% of paraffin, respectively. The nominal melting temperature of the paraffin used in this test was 24 °C, which is closed to the thermal comfort temperature of human beings. One can see that in addition to the solid-liquid phase change, there is a solid-solid phase change below the melting temperature of paraffin-based PCM. The solid-solid phase change is actually an internal structure variation of paraffin, and the solid-solid phase-change peak is a crystal transition peak. The solid-solid phase-change temperature of the pure paraffin is around 20.9°C, and its solid-liquid phase change temperature is around 24.2 °C. During the solid-liquid phase change process, only the paraffin in the composites becomes liquid, while expanded graphite maintains the original morphology and the spatial structure. The solid-liquid phase change temperatures of the paraffin/EG composites were found slightly less than that of the pure paraffin. Specifically, the melting point of PCM composite with 90 wt.% of paraffin was 23.9 °C and that of the composite with 85 wt.% of paraffin was 23.7 °C. The possible reason is that paraffin belongs to amorphous materials. It softens only in the vicinity of the solid-liquid melting

temperature and gradually transforms into liquid. In the composites, the heat transfer rate was increased because of the existence of graphite microcrystalline. Compared with pure paraffin, the softening speed was therefore increased. As a result, the temperature at which the composites are completely transformed into a liquid was lowered.

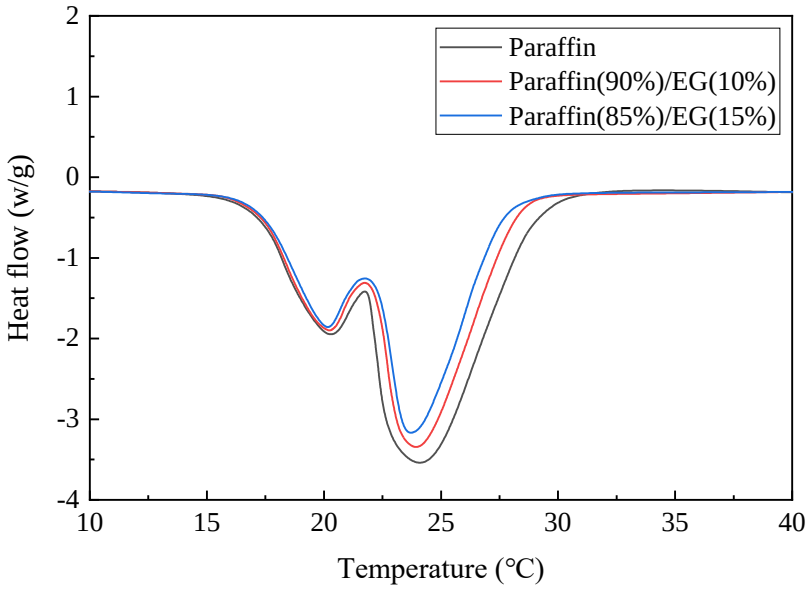

Figure 3.8. DSC curves of the pure paraffin and paraffin/EG composites.

The latent heat of the paraffin and paraffin/EG composites were obtained as the total area under the peaks of the solid-solid and solid-liquid transitions of the paraffin in the composite by numerical integration. The total latent heat of the pure paraffin is 180.5 J/g, and that of the composite PCM with 90 wt.% and 85 wt.% of paraffin is 161.8 J/g and 152.3 J/g, respectively. It can be seen the total latent heat of PCM is in direct proportion to the paraffin content in the composite.

3.3.3. Thermal Storage and Heat Transfer of Paraffin/EG Composite

Figure 3.9 shows the instantaneous temperature on the top surface of the PCM composite with 90 wt.% of paraffin and 10 wt.% of EG during the paraffin melting cycle. When the temperature of the specimen is below about 35°C and over 41°C, it shows a trend that is similar

to a sensible heat storage system, in which the thermal energy is stored on the basis of rapid temperature increase. On the other hand, the temperature increase became much slower from 900 to 3600 seconds, displaying similarities to a typical latent heat storage system with relatively constant temperature characteristics. During the phase change process, the solid PCM started to melt with a large amount of the latent heat stored within a small temperature change interval due to its isothermal nature, which formed the plateau on the instantaneous temperature curve. The phase change process of the specimen started when its temperature reaches around 35 °C and ended at around 41°C, which centers on the melting temperature of the paraffin (38 °C). During this phase change period, a large amount of the latent heat energy can be stored for later use. This property enables PCM composites to keep the ambient temperature relatively constant at its melting temperature. PCM with a melting point that is closed to human being's thermal comfort temperature shows high potential to downsize the use of HVAC systems and enhance the building energy efficiency.

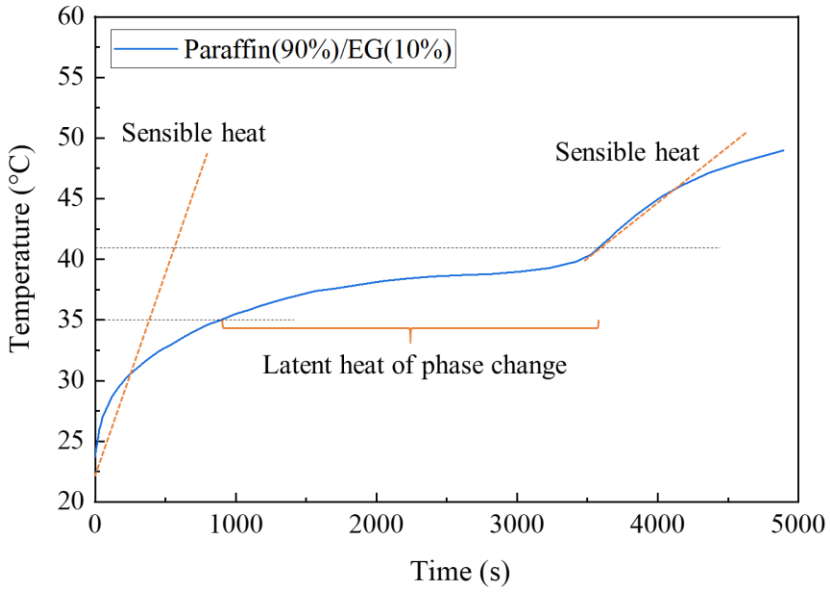

Figure 3.9. Thermal storage and heat transfer of paraffin/EG composite.

Figure 3.10 shows the thermal behavior comparison graph between the paraffin/EG composite with 70 wt.%, 80 wt.%, and 90 wt.% of paraffin during the heating cycle. One can see that the composite with higher EG content demonstrates greater heat transfer capabilities. For the PCM composite with 90 wt.% of paraffin and 10 wt.% of EG, it takes 4000 s to complete the charging process from room temperature to 45 ℃. While for the composites with 20 wt.% and 30 wt.% of EG, the charging time decreases to 2590 s and 1680 s respectively reaching the same temperature. The slope of the temperature curves increases with the EG content at every phase of the heating cycle, which demonstrates that expanded graphite can significantly enhance the heat transfer rate of paraffin. Another observation is that the total area under the phase change period of the composite decreases with the increase in the EG content, indicating that the EG content increase affects the composite's overall heat storage capacity in a negative way. However, the phase change temperature was not affected much by the content ratio of paraffin and EG. When being used as a building thermal management strategy, the ratio of paraffin and EG needs to be comprehensively determined by considering several factors, such as the thermal loading conditions, the desired time of completing a phase change cycle, the necessity for the latent heat storage capacity and so on.

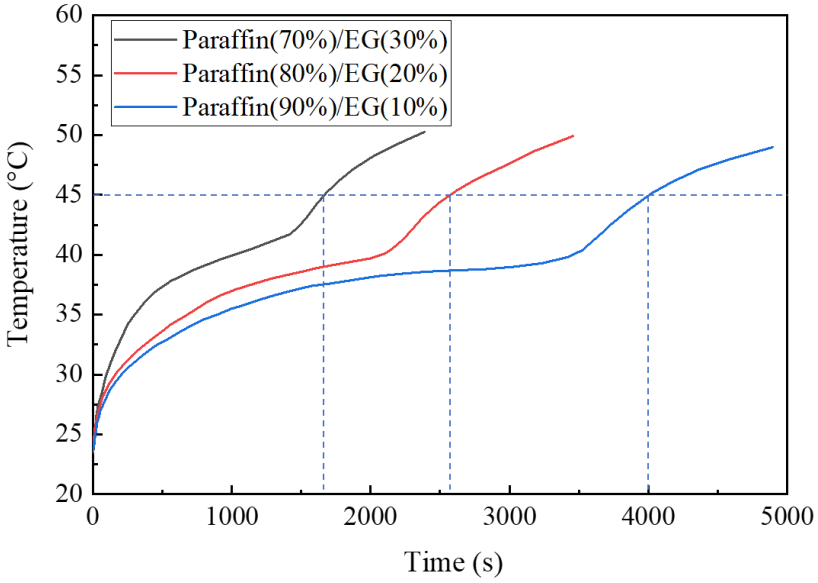

Figure 3.10. Thermal behavior of paraffin/EG composites with different paraffin contents.

3.3.4. Thermal Performance of Prototypes

Figure 3.11 presents the evolution of the "outdoor" and "indoor" temperatures of the test prototypes (with and without PCM layer). It can be seen that when the chamber temperature changed between 15 ℃ and 31℃ periodically, the temperature inside the reference cell without PCM oscillated between 17.81 and 27.43 ℃, resulting in a fluctuation of 9.62 ℃. For the test cell equipped with PCM composite, the temperature inside oscillated between 18.52 ℃ and 25.77 ℃, resulting in a fluctuation of 7.25 ℃. This temperature interval has covered the melting point of the paraffin, indicating that the PCM has fulfilled its function of heat absorber. The maximum temperature fluctuation of the test cell decreased by 2.37 ℃ due to the existence of PCM. When the inside temperature increased from 18.52 ℃ to 25.77 ℃, the paraffin installed in the cell wall changed from solid to liquid state, absorbed and stored part of the inward thermal energy, and hindered the inside temperature increase. This process corresponds to the daytime when the exterior surface temperature of a building increases. When the inside temperature decreased from 25.77 ℃ to 18.54 ℃, the PCM liquified and released its stored heat

automatically to hinder the inside temperature decrease. This process corresponds to the nighttime when the exterior surface temperature of a building drops. Therefore, if the building envelope is integrated with PCM which possesses proper melting temperature that can be covered by the temperature fluctuation of the envelope, the PCM is able to store and release thermal energy automatically to regulate the indoor temperature and downsize the use of the HVAC system.

In addition to the improvement of the room thermal amplitude reduction, another observation concerns the time delay in the maximum temperature inside of the test cell. Compared with that of the reference test cell, the maximum "indoor" temperature of the test cell integrated with PCM delayed about 0.67 hours as shown in Figure 3.11. This delay phenomenon is due to the fact that the paraffin/EG composite is not sensitive to the temperature variations during its phase-change processes. The PCM composite can provide considerable thermal mass for the building envelopes, which acts as a thermal battery to shift the heating or cooling load to an off-peak time of day when the electricity costs are lower.

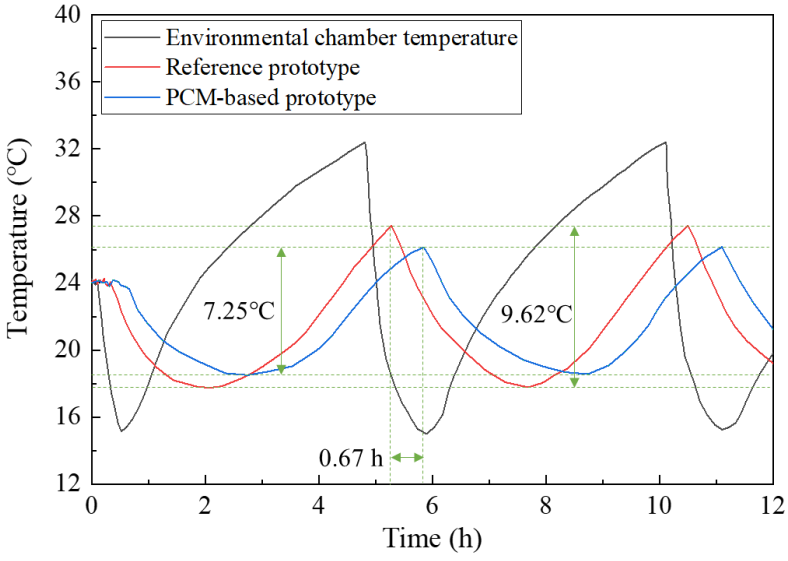

Figure 3.11. Instantaneous temperature of the chamber and the inside of the prototypes as a function of time.

3.4. Summary

In this study, a novel form-stabilized PCM composite prepared from paraffin and EG was experimentally investigated. Among different exfoliating conditions, heating the expandable graphite in the muffle furnace at 850 ℃ for 14 seconds resulted in completely expanded EG with the maximum sorption capacity for paraffin (90.8 wt.%). The FTIR analysis demonstrated that many functional groups were produced during the exfoliation process of NEG caused by the oxidation intercalation during high-temperature exfoliation. In addition, the prepared EG has a wide pore size distribution that consisted of mesopores and macropores. Both the functional groups and the porous structure produced may contribute to the absorbing capacity of paraffin. SEM images showed that the porous structure of EG was filled with paraffin uniformly due to absorption, making it a promising supporting media for paraffin to keep its form-stability and meanwhile enhance its thermal conductivity.

The DSC results showed that the total latent heat of the pure paraffin is 180.5 J/g, and that of the composite PCM with 90 wt.% and 85 wt.% is 161.8 J/g and 152.3 J/g, respectively. Therefore, the total latent heat of PCM is in direct proportion to the paraffin content in the composite. The solid-liquid phase change temperatures of the paraffin/EG composites were found slightly less than that of the pure paraffin due to the increased heat transfer rate by EG.

The thermal storage and heat transfer test with the cubic specimen showed that the paraffin/EG composite possessed favorable thermal energy storage ability to be used for enhancing building energy efficiency. EG can significantly enhance the heat transfer rate of paraffin, but the EG content increase affected the composite’s overall heat storage capacity negatively.

The thermal performance test of prototypes indicated that the integration of PCM in the test cell walls led to the improvement of room thermal performance in two ways. On one hand, the maximum temperature fluctuation of the test cell reinforced by PCM was reduced by 2.37 ℃ compared to the reference test cell without PCM. On the other hand, the maximum "indoor" temperature of the test cell integrated with PCM was delayed about 0.67 hours. Both improvements indicate that the proposed PCM composite possesses the high potential to be used in building envelopes for saving energy and downsizing electricity costs.

3.5. References

[1] Kong, X., Jie, P., Yao, C. and Liu, Y., 2017. Experimental study on thermal performance of phase change material passive and active combined using for building application in winter. Applied energy, 206, pp.293-302.

[2] Kalnæs, S.E. and Jelle, B.P., 2015. Phase change materials and products for building applications: A state-of-the-art review and future research opportunities. Energy and Buildings, 94, pp.150-176.

[3] Ye, H., Long, L., Zhang, H. and Zou, R., 2014. The performance evaluation of shape-stabilized phase change materials in building applications using energy saving index. Applied energy, 113, pp.1118-1126.

[4] Zhou, D., Zhao, C.Y. and Tian, Y., 2012. Review on thermal energy storage with phase change materials (PCMs) in building applications. Applied energy, 92, pp.593-605.

[5] Zhang, B., Tian, Y., Jin, X., Lo, T.Y. and Cui, H., 2018. Thermal and mechanical properties of expanded graphite/paraffin gypsum-based composite material reinforced by carbon fiber. Materials, 11(11), p.2205.

[6] Z. Khan, Z. Khan, A. Ghafoor, A review of performance enhancement of PCM based latent heat storage system within the context of materials, thermal stability and compatibility, Energy Conversion and Management 115 (2016) 132-158.

[7] M. Pomianowski, P. Heiselberg, Y. Zhang, Review of thermal energy storage technologies based on PCM application in buildings, Energy and Buildings 67 (2013) 56-69.

[8] F. Agyenim, N. Hewitt, P. Eames, M. Smyth, A review of materials, heat transfer and phase change problem formulation for latent heat thermal energy storage systems (LHTESS), Renewable and Sustainable Energy Reviews 14(2) (2010) 615-628.

[9] Karaipekli, A., Biçer, A., Sarı, A. and Tyagi, V.V., 2017. Thermal characteristics of expanded perlite/paraffin composite phase change material with enhanced thermal conductivity using carbon nanotubes. Energy conversion and management, 134, pp.373-381.

[10] Zhang, Z. and Fang, X., 2006. Study on paraffin/expanded graphite composite phase change thermal energy storage material. Energy Conversion and Management, 47(3), pp.303-310.

[11] Yang, H., Memon, S.A., Bao, X., Cui, H. and Li, D., 2017. Design and preparation of carbon based composite phase change material for energy piles. Materials, 10(4), p.391.

[12] Guo, X., Zhang, S. and Cao, J., 2018. An energy-efficient composite by using expanded graphite stabilized paraffin as phase change material. Composites Part A: Applied Science and Manufacturing, 107, pp.83-93.

[13] Frąc, M., Pichór, W., Szołdra, P. and Szudek, W., 2021. Cement composites with expanded graphite/paraffin as storage heater. Construction and Building Materials, 275, p.122126.

[14] https://asbury.com/resources/education/science-of-graphite/expandable-flake-graphite/

[15] Wang, Z., Qi, R., Wang, J. and Qi, S., 2015. Thermal conductivity improvement of epoxy composite filled with expanded graphite. Ceramics International, 41(10), pp.13541-13546.

[16] Zhao, H., Pang, X. and Zhai, Z., 2015. Preparation and antiflame performance of expandable graphite modified with sodium hexametaphosphate. Journal of Polymers, 2015.

[17] Goudarzi, R. and Motlagh, G.H., 2019. The effect of graphite intercalated compound particle size and exfoliation temperature on porosity and macromolecular diffusion in expanded graphite. Heliyon, 5(10), p.e02595.

[18] Inagaki, M. and Suwa, T., 2001. Pore structure analysis of exfoliated graphite using image processing of scanning electron micrographs. Carbon, 39(6), pp.915-920.

[19] Zhao, J., Guo, Y., Feng, F., Tong, Q., Qv, W. and Wang, H., 2011. Microstructure and thermal properties of a paraffin/expanded graphite phase-change composite for thermal storage. Renewable Energy, 36(5), pp.1339-1342.

4. NUMERICAL THERMAL CHARACTERIZATION AND PERFORMACE METRICS OF BUILDING ENVELOPES CONTAINING PHASE CHANGE MATERIALS FOR ENERGY-EFFICIENT BUILDINGS[1]

4.1. Introduction

Improving the energy efficiency of buildings is drawing significant interest in recent two decades to address concerns about the increasing energy consumption and the global climatic changes [1]. A recent energy consumption survey provided by the United States Energy Information Administration reveals that residential and commercial buildings consumed over 38 quadrillion BTUs (energy unit), about 39% of total USA energy use in 2017. Over the past decades, the development of advanced engineered materials and the improvement in design specifications [2-4] have spurred tremendous progress in energy-efficient building envelopes (e.g., walls, roofs, and foundation) to reduce space heating and cooling loads. Among them, phase change materials (PCMs), due to their superior latent heat energy storage capacity, have been gaining much interest in applications to building envelopes in recent years [5-7]. For instance, literature reviews [8, 9] show that wall assemblies reinforced by PCM layers offer improved thermal comfort for indoor environments in terms of reducing temperature fluctuation, and cut significant costs through shifting the cooling load to off-peak electricity load.

Significant efforts [10] have been made in the implementation of PCMs in building envelopes through either experimental, analytical, or numerical studies. Lei et al. [11] simulated building envelopes integrated with a PCM layer using the software EnergyPlus® (National

[1] This chapter describes the thermodynamics of PCM-enabled building envelopes using numerical investigation. Most of the contents of this chapter has been published in M. Li, G. Gui, Z. Lin, L. Jiang, H. Pan, X. Wang, Numerical Thermal Characterization and Performance Metrics of Building Envelopes Containing Phase Change Materials for Energy-Efficient Buildings, Sustainability 10 (8) (2018) 2657. Mingli Li had primary responsibility for building the numerical model and conducting the parametric analysis. Mingli Li also drafted and revised all versions of this chapter. Zhibin Lin served as proofreader and checked the mathematical model used in the simulation conducted by Mingli Li.

Renewable Energy Laboratory, USA) and evaluated the energy performance of the building system for cooling load reduction in tropical Singapore. Their results showed that PCM can effectively reduce heat gains through building envelopes throughout the whole year, indicating the significant advantage of using PCMs in buildings located in hot circumstances. Seong and Lim [12] investigated the energy-saving potentials in buildings with PCMs in a lightweight building envelope and found both the peak heating load and highest indoor temperature decreased when various PCMs with different phase change temperatures were applied. Wang et al. [10] experimentally evaluated the year-round applicability of an exterior wall with PCM bricks and found a reduction of 0.2 °C for the maximum interior wall surface temperature and a time delay of about 1–2 h under summer seasons. Izquierdo-Barrientos et al. [13] studied the performance of external building wall assemblies containing a PCM layer. They concluded that the influencing factors included the orientation of the wall, the position of the PCM layer, and the phase change temperature. Jin et al. [14] numerically analyzed the effects of the location of a thin PCM layer placed in frame walls. They stated that the optimal locations of the PCM layer should be near to the exterior surface of the wall, if using thicker PCM layers, the higher the heat of fusion, and the higher the melting temperature. Different from the observation by Jin et al. [14], Zwanzig et al. [15] found that that the centrally located PCM composite wallboard performed better under both the heating and cooling seasons, as compared to either externally or internally located PCM walls. In general, these studies [10] have demonstrated the improvement of energy efficiency through the use of PCMs for a building environment. Due to different focuses in those previous studies, each investigation may be conducted on the PCM-enabled buildings using one or two variables, such as the location of PCM or its melting temperature. Moreover, some conclusions may conflict with each other. For instance, there are still open

questions about how to select melting temperature for a PCM layer and where the optimal location for a PCM layer is. It necessitates comprehensive parametric studies, as proposed in this study, that could efficiently assist the building community and stakeholders, from builders, designers, building manufacturers, and to state/local governments, to identify better design.

Correspondingly, it is significant to select proper performance metrics to evaluate the robustness of building envelope design and elucidate critical factors affecting its energy efficiency. Reduction of peak temperature and temperature shifting hours are currently used through a comparison to determine the effectiveness of building envelopes with and without PCMs. Cabeza et al. [16] experimentally studied energy saving by using microencapsulated PCM in concrete walls and found that air temperature in the room with PCM could lead to a reduction by up to 2 °C, as compared to conventional walls. Moreover, Kuznik and Virgone [17] introduced a decrement factor defined as the ratio between the amplitude of the indoor air temperature in the cell with and without PCM to evaluate their energy efficiency. Some argued that such performance metrics could only provide discrete/local information while ignoring the temporal data representation over time and detailing of the PCMs' impacts on building comfort. To improve performance metrics, Evola et al. [18, 19] developed comprehensive assessment methods, including the evaluation of the intensity of thermal discomfort, frequency of thermal comfort, frequency of activation, and storage efficiency of the PCMs. Thus, as a key step, we will evaluate the existing performance metrics in determining the implementation techniques for PCMs and their installation patterns to minimize the energy demand of a building.

Therefore, the objectives of this study aim to numerically investigate the thermodynamics of PCM-enabled building envelopes. A comprehensive and systematic study is conducted on external wall assemblies reinforced by a PCM layer as a representative under summer weather

and solar radiation. A parametric study focuses on identified critical variables, including the location and thickness of the PCM layer, the latent heat of PCMs, the melting temperature of PCMs, and the thermal conductivity of PCMs. Four metrics, the temperature swings, the peak temperature reduction, the intensity of thermal discomfort for overheating, and frequency of thermal comfort, are accordingly selected to assess building efficiency.

4.2. PCMs for Building Envelopes and Building Systems

4.2.1. Critical Factors Affecting the Thermodynamics and Energy Efficiency of PCM-Enabled Building Envelopes

The improvement in the energy efficiency of PCM-enabled building envelopes has been observed by many researchers [20]. Izquierdo-Barrientos et al. [13] stated the importance of these variables: (a) the position of the PCM layer and (b) the phase change temperature. Jin et al. [14] and Zwanzig et al. [15] recognized the contribution of the location of PCM layers the building energy efficiency. Jing [20] compared the energy-saving performance of building envelopes with PCMs and traditional building materials and drew the conclusion that the energy-saving efficiency increased by 27.56% when PCM was integrated into the buildings. Kuznik et al. [21] studied the effect of PCM thickness on the thermal behavior of the building wall and provided an optimal PCM thickness value for the construction. Lee et al. [22] assessed the impact of the location of the PCM layer in a residential building wall on the heat transfer reduction of the wall and found that the optimal location for a PCM layer is the middle part of the wall. Xu et al. [23] investigated several design variables, such as melting temperature and thermal conductivity of the PCM. It was found that for a given position or weather condition, the melting temperature of PCM should be selected to near the average indoor air temperature of sunny winter days, and the thermal conductivity should be larger than 0.5 W/(mK). Zhu et al.

[24] explored the effect of melting temperature and corresponding thickness of the PCM-based wall in typical climate regions of China. Jayalath et al. [25] illustrated that the amount of PCM integrated in the building material, corresponding to different heat of fusion, also has an obvious effect on the thermodynamics of the wall. The maximum indoor temperature decreases with the increase of the heat of fusion.

To sum up, these factors, such as the location of the PCM layer, the thickness of the PCM layer, the latent heat of PCM, melting temperature of PCM, and thermal conductivity of PCM, could be used as design variables for understanding their impacts on the building efficiency, as studied in detail in the following sections.

4.2.2. Performance Metrics for Assessing Energy Efficiency of the Building System

In this section, we briefly introduce four different performance metrics that could quantitatively evaluate the effectiveness of the PCM for the energy savings of a building. Note that each metric could provide different perspectives to assist engineers to understand PCMs for building applications.

Performance metrics are crucial to assess PCM potential for building energy efficiency. The existing performance metrics could be summarized as (a) temperature swings/shift; (b) maximum instantaneous temperature reduction; (c) intensity of thermal discomfort for overheating (ITD_{over}); and (d) frequency of thermal comfort (FTC). Figure 4.1 displays the definition of both ITD_{over} and FTC.

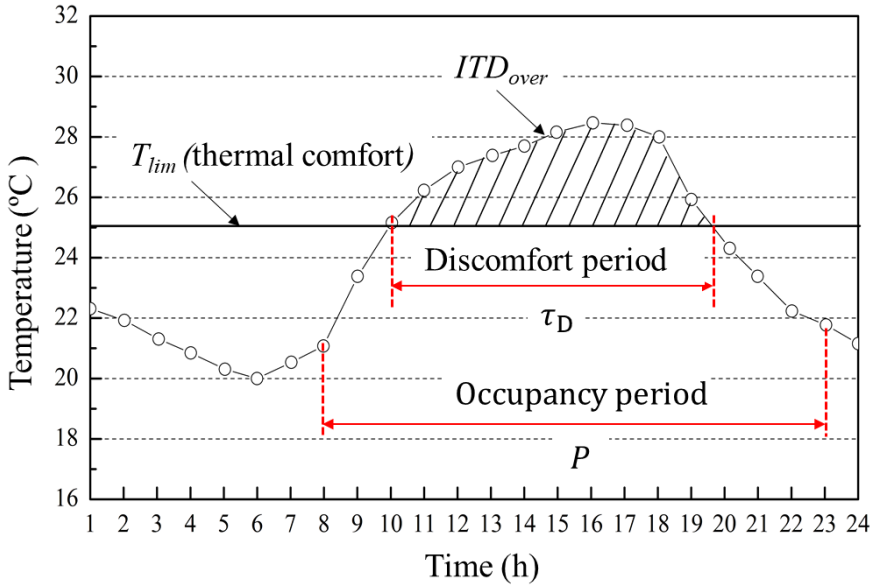

Figure 4.1. *ITD*$_{over}$ and *FTC*: graphic definition (replotted from [18]).

The *ITD*$_{over}$ is defined as the time integral, over the occupancy diurnal period P, of the positive difference between the current temperature and the upper threshold for comfort [18]:

$$ITD_{\text{over}} = \int_P \Delta T^+(\tau) \cdot d\tau \tag{4.1}$$

where,

$$\Delta T^+(\tau) = \begin{cases} T_{op}(\tau) - T_{\text{lim}} \; if \; T_{\text{op}}(\tau) \geq T_{\text{lim}} \\ 0 \; if \; T_{\text{op}}(\tau) < T_{\text{lim}} \end{cases} \tag{4.2}$$

where T_{op} is the current operative temperature of a certain moment within the occupancy period, τ is the time interval between two operative temperature, T_{lim} is the upper limit of comfort temperature as defined, which is usually determined based on thermal comfort associated with the local climate [26]. Consider there are potentially multiple discrete discomfort periods over the occupancy diurnal period P, the *ITD*$_{over}$ in Equation (4.1) can be generalized as the summation of the effects over the discrete multiple periods, $\sum \tau_D$:

$$ITD_{over} = \sum \int_{\tau_D} \Delta T^+(\tau) \cdot d\tau \tag{4.3}$$

As illustrated in Figure 1, the *FTC* is defined as the percentage of a discomfort period, τ_{D}, over the entire occupancy time:

$$FTC = \frac{P-\tau_{\mathrm{D}}}{P} \tag{4.4}$$

within a given diurnal period, during which the indoor thermal comfort conditions are met. Accordingly, the generalized can be revised from Equation (4.4) to account for the summation over the multiple discrete periods:

$$FTC = \frac{P-\sum \tau_{\mathrm{D}}}{P} \tag{4.5}$$

4.3. Simulation of Thermodynamics of Building Envelopes Using Exterior Walls Reinforced by PCMs

In this section, a mathematical formalization of heat transfer of PCM-enabled building walls is introduced, and the model is then numerically implemented using the COMSOL Multiphysics® software [27], where the material, loading conditions, and boundary conditions are provided. A case in the literature [13] is used to calibrate the mathematic model employed in this investigation.

4.3.1. Modeling the Thermodynamics of Building Envelopes in COMSOL

4.3.1.1. Overview of Formulation of the 2-D Heat Transfer

A multi-layered wall is widely used in residential and commercial building envelopes in the United States and herein is selected as a typical representative. To characterize the dynamics of building envelopes, such as the heat transfer through a wall assembly, the transient thermal behavior of a solid could be formulated by the partial differential equation as follows:

$$\frac{\partial}{\partial x}\left(\lambda \frac{\partial T}{\partial x}\right) + \frac{\partial}{\partial y}\left(\lambda \frac{\partial T}{\partial y}\right) = \rho C_P \frac{\partial T}{\partial t} \tag{4.6}$$

where T is the temperature (K), λ is the thermal conductivity of the material (W/m K), ρ is the density of the material (kg/m^3), and C_P is the specific heat of the material (J/kg K). Analytical or numerical methods, such as finite difference methods, have been found in the literature through Equation (4.6) to formulate the heat transfer in the wall assemblies. In this study, a commercially available multi-physics software, COMSOL, was used for modeling two-dimensional (2D) heat transfer of the wall assembly [28]. For simplicity, contact resistance between different wall layers is ignored. The dynamics of the phase change process from phase I (solid) to phase II (liquid) in PCM material was modeled in the COMSOL using:

$$\rho_{PCM} = \rho_{phase\ I}\beta + \rho_{phase\ II}(1-\beta) \tag{4.7a}$$

$$\lambda_{PCM} = \lambda_{phase\ I}\beta + \lambda_{phase\ II}(1-\beta) \tag{4.7b}$$

$$C_{p,PCM} = \frac{1}{\rho_{PCM}}\left(\rho_{phase\ I}C_{p,phase\ I}\beta + \rho_{phase\ II}C_{p,phase\ II}(1-\beta)\right) + L\frac{\partial \alpha_m}{\partial T} \tag{4.7c}$$

where C_p is the specific heat (J/kg K), L is the latent heat of fusion (J/kg), and α_m is:

$$\alpha_m = \frac{1}{2}\frac{\rho_{phase\ II}(1-\beta)-\rho_{phase\ I}\beta}{\rho_{phase\ II}(1-\beta)+\rho_{phase\ I}\beta} \tag{4.8}$$

where L is the latent heat of fusion (J/kg); β is the volume fraction of PCM at initial solid-phase I; the transition interval of PCM material between solid and liquid phase is not ideally zero, and is usually determined by actual material results, 5 °C by default in the COMSOL if not available.

4.3.1.2. COMSOL Implementation: Material, Loading, and Boundary Conditions

The wall assembly is idealized as homogenous and isotropic materials in each layer, and thus its heat transfer is one-dimensional through the wall thickness. Consider there are identical properties in solid and liquid phases, the volume fraction or thermal conductivity of the PCM in Equations (4.7a) and (4.7b):

$$\rho_{PCM} = \rho_{phase1} = \rho_{phase2} \tag{4.9a}$$

$$\lambda_{PCM} = \lambda_{phase1} = \lambda_{phase2} \tag{4.9b}$$

As a result, the α_m in Equation (4.8) could be reduced to −0.5 and introducing them in Equation (4.7c) yields

$$C_{p,PCM} = C_p + L\frac{\partial \alpha_m}{\partial T} \tag{4.10}$$

Exterior boundary condition in the numerical simulation has accounted for the surface temperature and solar radiation data that are generated from the typical meteorological year weather data from a collection station under summer seasons in Austin, Texas. Input files containing hourly values of outdoor dry air temperature and solar radiation in the first week of June in Austin are shown in Figure 4.2. Note that the weather data used herein are just for demonstration, while more thermal performance could be carried out similarly under the different climate zones in the United States.

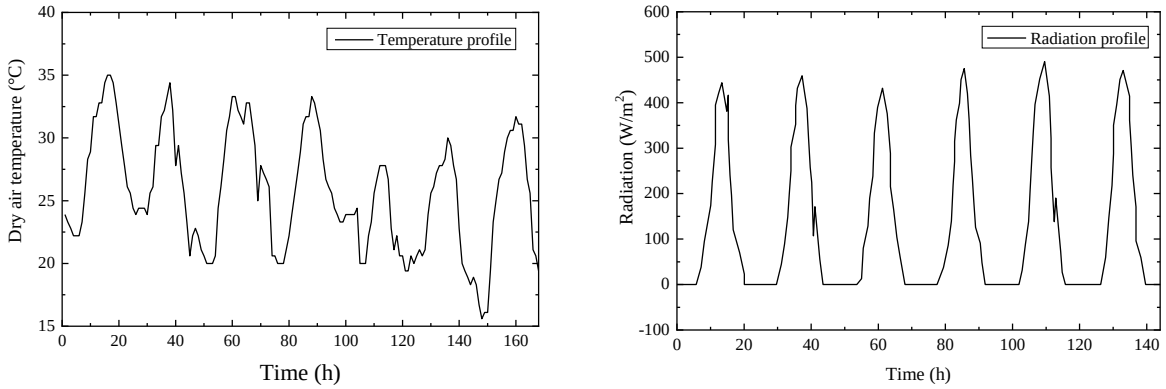

(a) (b)

Figure 4.2. Loading conditions of Austin, Texas (a) External dry air temperature and (b) radiation on the external surface of the wall.

4.3.2. Validation of the Model

A multi-layered wall configuration in the literature was used to calibrate the effectiveness of the numerical thermal analysis using the multi-physics COMSOL. As illustrated in Figure 4.3(a), the 2D wall configuration with a PCM layer was plotted and the predicted results were

compared to data found in the literature [13], where the heat transfer of the wall was mathematically formulated and solved by the finite difference method. The wall illustrated in Figure 4.3(b) was subjected to one-dimensional heat transfer under both top and bottom sides ideally insulated.

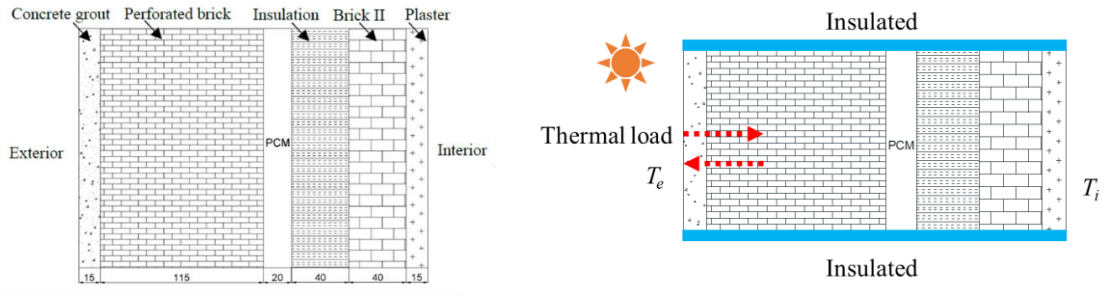

(a) (b)

Figure 4.3. The wall assembly used for the calibration.

The thermal and physical properties of materials used in each wall layer are shown in Table 4.1. The heat of fusion of PCM used in this investigation is 63000 J/kg and its melting point is 24 °C, which is closed to the thermal comfort temperature of human beings.

Table 4.1. Thermal and physical properties of materials [13].

Materials	**Density (kg/m^3)**	**Specific heat capacity (kJ/(kg K))**	**Thermal conductivity (W/m K)**
Concrete grout	1900	1000	1.3
Perforated brick	900	1000	0.5
PCM	750	1500	0.15
Insulation	32	840	0.038
Brick II	920	1000	0.4
Plaster	1100	1000	0.57

The loading conditions used for model validation are shown in Figure 4.4, which have accounted for the combined action of both dry air temperature and solar radiation. These weather profiles were applied on the wall exterior surface as the boundary condition. The indoor

temperature is fixed at 26 °C for summer. As the continuous heat or cold going inward, the temperature on each layer of the wall assembly will change accordingly. The instantaneous temperature of the wall achieved from this study is recorded and compared with the result in the literature for model validation.

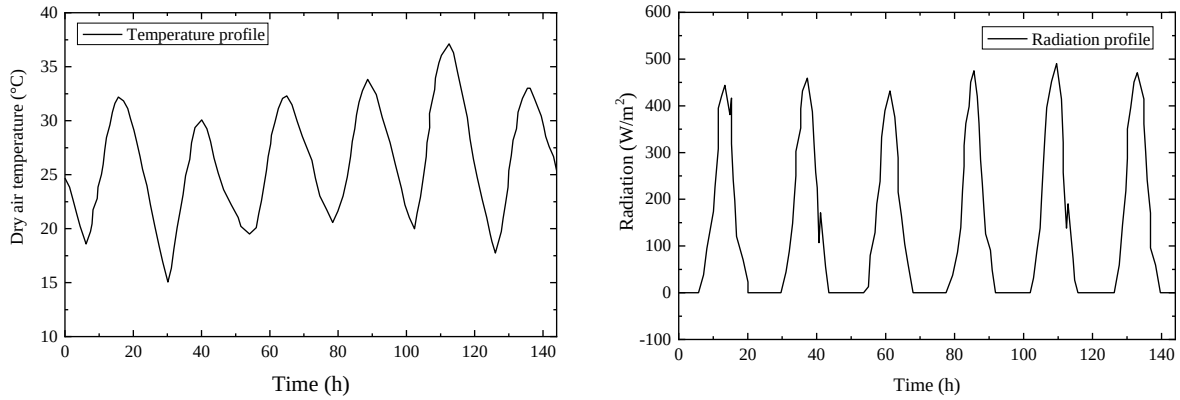

(a) (b)

Figure 4.4. Input loading condition for validation (a) External dry air temperature and (b) radiation on the external surface of the wall (replotted from [13]).

Figure 4.5 shows the temperature comparison of the referred and the proposed studies when the input temperature and radiation are applied for 20 h. One can see that the instantaneous temperature along the wall thickness of the proposed model is in good agreement with that of the referred model in the literature [13] at both examined moments. Therefore, the proposed model in COMSOL can be used to simulate the thermodynamics of the multi-layered wall system with PCM.

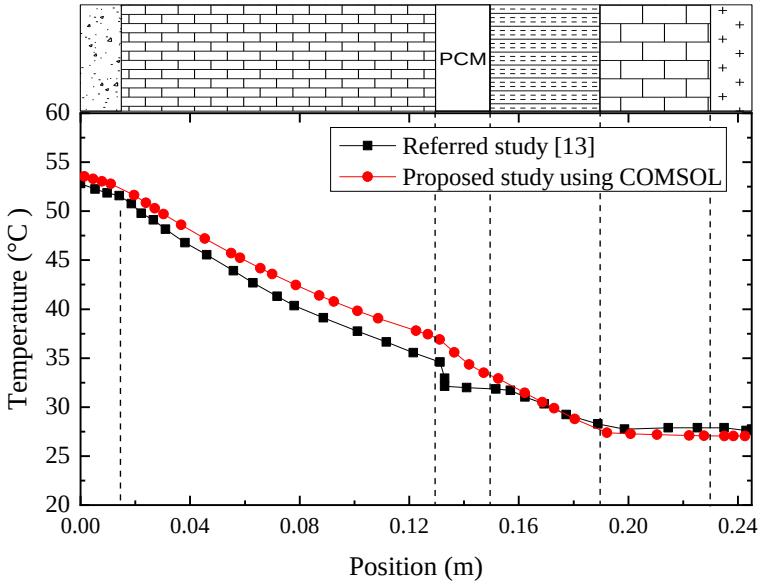

Figure 4.5. Temperature profile through the wall thickness at 20 h.

4.3.3. Characterization of Thermodynamics of the Wall Assembly

A comprehensive study was herein conducted to gain a deep understanding of the thermodynamics of a building envelope reinforced with PCM layers under transition temperature and to elucidate the impacts of the five different factors, including the location of the PCM layer, the thickness of the PCM layer, latent heat of the PCM, melting temperature of the PCM, and thermal conductivity of the PCM, on energy efficiency.

4.3.3.1. Prototype of the Wall Assembly

As illustrated in Figure 4.6, a typical multi-layered wall from the literature [29] was selected as the prototype of this study. The wall assembly consisted of a 100-mm thick cement grout layer on the outside, a 100-mm perforated brick layer, a 40-mm layer of thermal insulation, and a 30-mm layer of PCM followed by a 20-mm oriented strand board (OSB) inside. Note that the parameters of a building in terms of thickness of thermal insulation or other layers should be designed to account for different locations based on climate maps through hydrothermal analysis

with the help of software like TRNSYS® (Thermal Energy System Specialists, LLC, Madison, USA).

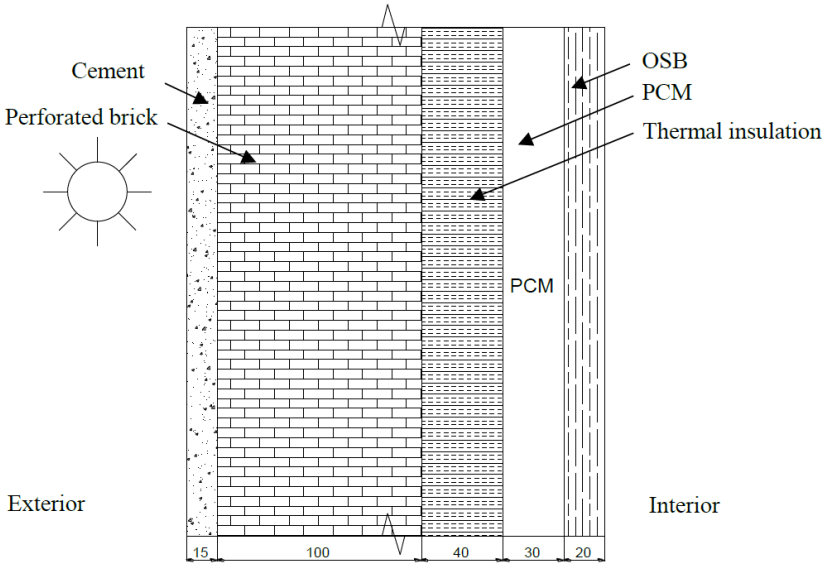

Figure 4.6. A schematic diagram showing the wall assemblies of a typical external wall (unit: mm).

To perform thermal simulations using COMSOL, the thermophysical properties of each layer in the wall assembly are defined from the literature, as listed in Table 4.2.

Table 4.2. Thermal and physical properties of materials used in the building envelope assembly.

Materials	**Specific Heat Capacity (J/kg K)**	**Thermal Conductivity (W/(mK))**	**Density (kg/m³)**	**Thickness (mm)**
Concrete grout	1000	1.3	1900	15
Perforated brick wall	1000	0.5	900	100
PCM	1500	0.15	750	30
Thermal insulation	840	0.038	32	40
OSB	1210	0.13	650	20

The melting point of the PCM is 28 °C, and its heat of fusion is 63000 J/kg. During the heat transient process, the entire domain is initially assumed to be 26 °C.

4.3.3.2. Design of Test Cases for the Parametric Study and Performance Assessment

A comprehensive parametric study is then conducted to explore the effect of several critical factors, including the location, thickness, heat of fusion, melting point, and thermal conductivity of the PCM on the thermal performance of the wall assembly. The cases concerned in this study are illustrated in Table 4.3.

Table 4.3. Test matrix of the building envelope under varying design parameters.

Case Design	Label	PCM Thickness (mm)	Heat of Fusion (J/kg)	Melting Point (°C)	Thermal Conductivity (W/(mK))	Specific Heat Capacity (J/kg K)	Density (kg/m³)
Variability associated with PCM location	**EX**-MT24-D30	30	63,000	28	0.15	1500	750
	MD-MT24-D30	30	63,000	28	0.15	1500	750
	IN-MT24-D30	30	63,000	28	0.15	1500	750
Variability associated with melting point	IN-**MT24**-D30	30	63,000	**24**	0.15	1500	750
	IN-**MT26**-D30	30	63,000	**26**	0.15	1500	750
	IN-**MT28**-D30	30	63,000	**28**	0.15	1500	750
	IN-**MT30**-D30	30	63,000	**30**	0.15	1500	750
	IN-**MT32**-D30	30	63,000	**32**	0.15	1500	750
	IN-**MT34**-D30	30	63,000	**34**	0.15	1500	750
	IN-**MT36**-D30	30	63,000	**36**	0.15	1500	750
	IN-**MT38**-D30	30	63,000	**38**	0.15	1500	750
	IN-**MT45**-D30	30	63,000	**45**	0.15	1500	750
Variability associated with wall thickness	IN-MT28-**D00**	**0**	63,000	28	0.15	1500	750
	IN-MT28-**D08**	**7.5**	63,000	28	0.15	1500	750
	IN-MT28-**D15**	**15**	63,000	28	0.15	1500	750
	IN-MT28-**D30**	**30**	63,000	28	0.15	1500	750
	IN-MT28-**D50**	**50**	63,000	28	0.15	1500	750
	IN-MT28-**D70**	**70**	63,000	28	0.15	1500	750
	IN-MT28-**D100**	**100**	63,000	28	0.15	1500	750
Variability associated with heat of fusion	IN-MT24-D30-C1	30	**0**	**24**	0.15	1500	750
	IN-MT24-D30-C2	30	**63,000**	**24**	0.15	1500	750
	IN-MT24-D30-C3	30	**150,000**	**24**	0.15	1500	750
	IN-MT24-D30-C4	30	**210,000**	**24**	0.15	1500	750
	IN-MT28-D30-C1	30	**0**	**28**	0.15	1500	750
	IN-MT28-D30-C2	30	**63,000**	**28**	0.15	1500	750
	IN-MT28-D30-C3	30	**150,000**	**28**	0.15	1500	750
	IN-MT28-D30-C4	30	**210,000**	**28**	0.15	1500	750
Variability associated with thermal conductivity	IN-MT28-D30-C5	30	63,000	28	**0.15**	1500	750
	IN-MT28-D30-C6	30	63,000	28	**0.3**	1500	750
	IN-MT28-D30-C7	30	63000	28	**0.5**	1500	750
	IN-MT28-D30-C8	30	63000	28	**1**	1500	750

Note: EX = exterior (the location of the PCM layer, see Figure 4.7a), MD = middle (Figure 4.7b), and IN = interior (Figure 4.7c). MT = melting temperature; D = thickness.

A total of 31 cases are designed to address the thermodynamics of building envelopes with and without PCM layers. All cases are consistently labeled in such a way that the first term of the labels denotes the location of the PCM, the second term “MT” denotes the melting point, and the third term “D” denotes the thickness of the PCM layer, unless otherwise stated. For

example, IN-MT28-D100 represents the wall assembly including a 100-mm PCM layer with a melting point of 28 °C on the wall interior side.

To elucidate the variables that may impact the building energy efficiency, the investigated cases are classified into five categories: (a) variability associated with the location of the PCM layer: the PCM layer was placed at different locations (i.e., exterior, middle, or interior layer of the wall) as labeled by **EX**-MT24-D30, **MD**-MT24-D30, **IN**-MT24-D30, respectively (see Figure 4.7); (b) variability associated with the melting point of the PCM layer: the melting point of the PCM was herein selected with a wide range from 24 °C to 45 °C to address their impacts on the energy efficiency of a building envelope; (c) variability associated with the thickness of the PCM layer: its range varied from zero to 100 mm; (d) variability associated with the heat of fusion of the PCM, and (e) variability associated with the thermal conductivity of PCM.

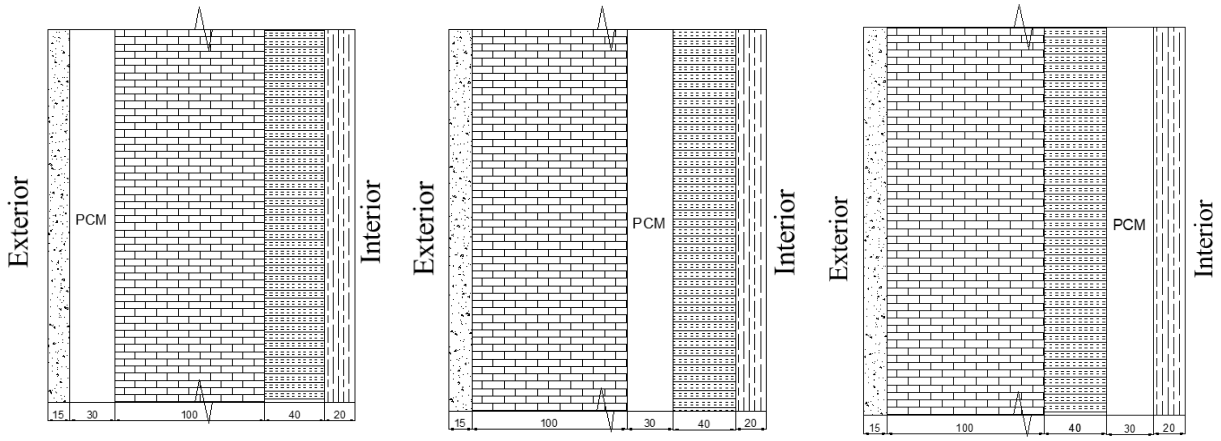

(a) Exterior (EX-MT24-D30) (b) Middle (MD-MT24-D30) (c) Interior (IN-MT24-D30)

Figure 4.7. Different schematic diagrams showing the investigated wall configurations.

4.4. Results and Discussions

4.4.1. Thermodynamics of Building Walls under Instantaneous Loading Conditions

The design of energy-efficient building envelopes necessitates a deep understanding of their dynamic interaction with the ambient environment. In this sub-section, the first attempt was made to unveil the heating and cooling processes of the multi-layered wall responding to the applied loading conditions associated with the dry air temperature and solar radiation of Austin in summer, as shown in Figure 4.2.

The thermodynamics of the wall of Case IN-MT24-D30 was investigated and the results are presented in Figure 4.8 to demonstrate the temperature of the wall over its thickness under different test periods. Both the heating and cooling processes of the wall are presented. During the heating process, the temperature of the wall exterior surface is increasing under the combined effect of environmental temperature and solar radiation, resulting in a temperature gradient through the wall thickness. Take the temperature curve of 30 h showed in Figure 4.8 (a) as an example. At this moment, the temperature of the wall exterior surface is about 35 °C, while that of the wall interior surface is about 25 °C which can be seen in the temperature contour of the same moment showed in Figure 4.9 (a). If the ambient temperature is higher than the originally solid PCM, its latent heat storage can be triggered, and a large amount of inward heat will be absorbed. During this process, the temperature of PCM is relatively stabled at its melting temperature, hindering the rapid increase in the room temperature. On the other hand, when the outside temperature drops until it’s lower than the room temperature, the cooling process starts by delivering the inward cold energy. Take the temperature curve of 10 h showed in Figure 4.8 (b) as an example, when the temperature of the wall exterior surface is about 26 °C, lower than that of the wall interior surface which is about 40 °C (see Figure 4.9 (b)). As the ambient

temperature drops to the solidifying point of the PCM, the stored thermal energy can be released and hinder the rapid decrease of the room temperature. Such heating and cooling process of the wall cyclically repeats accompanied by the charge and discharge of the PCM layer, showing great potential to downsize the use of HVAC systems and thus enhance the building energy efficiency.

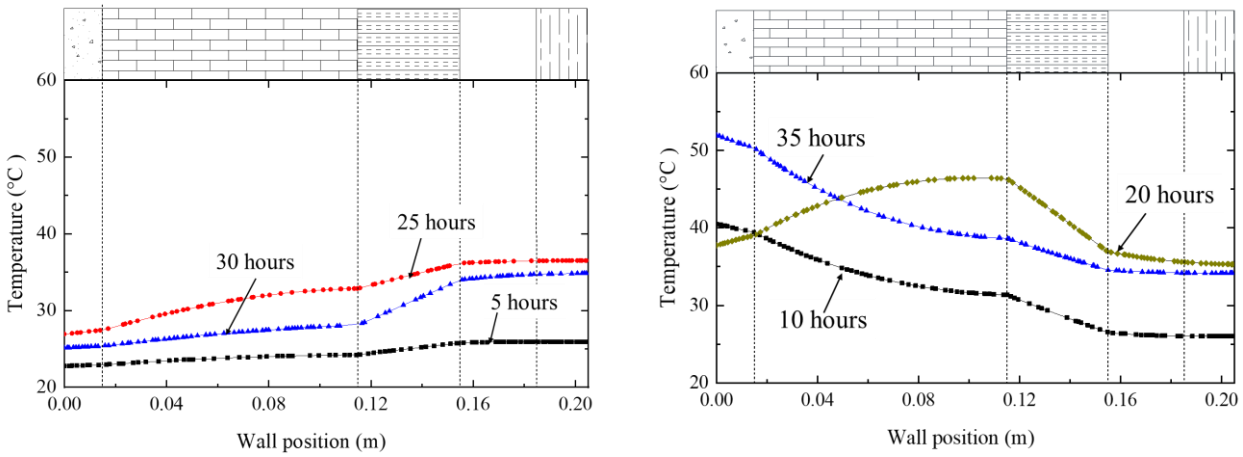

Figure 4.8. Thermodynamics of the (a) heating and (b) cooling processes through the temperature profile over the wall thickness.

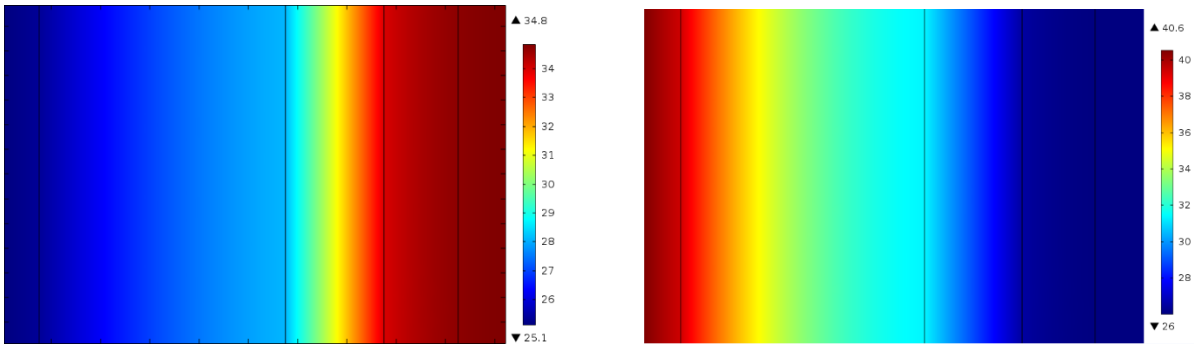

Figure 4.9. Thermal contour over the wall thickness under different test periods: (a) 30 h and (b) 10 h.

4.4.2. Effect of the Location of the PCM Layer within the Wall Assembly on the Thermal Performance

Previous studies [15] have shown that the PCM layer can be embedded within different locations of the wall assembly. This section is to address three different placements of the PCM layer, illustrated in Figure 4.7, and the impact of the placement/location of the PCM layer on the wall energy efficiency.

Figure 4.10 shows the transient temperature profiles and the peak temperature of the interior wall surface over time. As a comparison, the wall exterior surface temperature that directly responded to air temperature and solar radiation was also plotted in the dashed line. All three cases showed the time delay response to the outdoor ambient temperature due to multiple layers of wall assemblies serving as thermal mass and PCM effects as well. The peak temperature swings for the three cases were 12 °C, 15 °C, and 7 °C during the 7-day test period, respectively. The PCM layer that was located near the interior of the wall, labeled as IN-MT28-D30, had the smallest temperature swings over time and the lowest maximum instantaneous temperature, as compared to the other two cases (i.e., EX-MT28-D30 and MD-MT28-D30). The maximum instantaneous temperature of the IN-MT28-D30 was only 36 °C, 13% and 16% smaller than their counterparts (41 °C for the EX-MT24-D30 and 43 °C for the MD-MT28-D30) at the first 24 h, respectively. Thus, the case of IN-MT28-D30 exhibited the most effective way to reduce the indoor temperature swings (see Figure 4.10 (a)) and the peak temperatures (see Figure 4.10 (b)) during both heating and cooling stages.

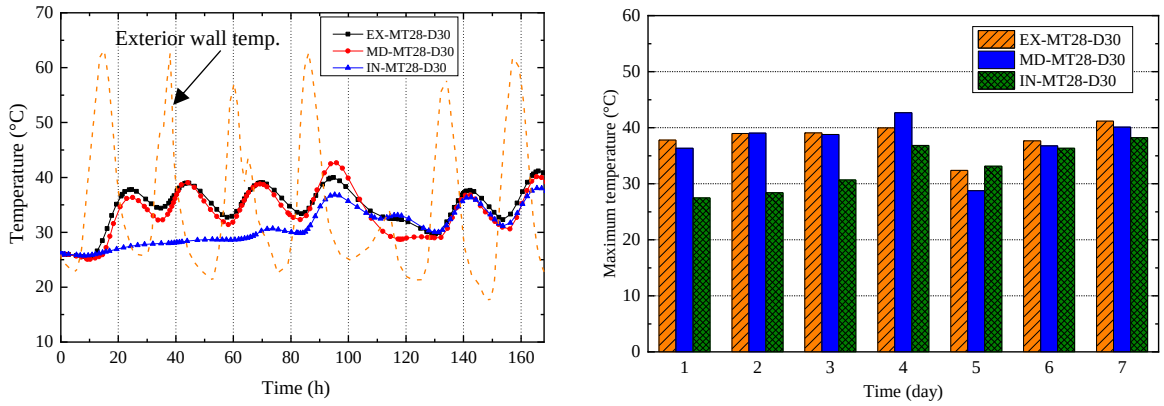

(a) (b)

Figure 4.10. History of interior wall surface temperature over time: (a) transient temperature and (b) peak temperature.

As defined in Equations 4.1 to 4.5, the generalized performance metrics, ITD_{over} and *FTC*, were used from different perspectives to quantitatively evaluate the thermal performance of a wall. Figure 4.11(a) displays the results of the ITD_{over} overtime to cover the discomfort periods for occupants when the upper threshold for the thermal comfort T_{lim} was set to 27 °C. The case of IN-MT28-D30 well outperformed the other two cases throughout all of the time, particularly during the first and second days, which was confirmed by the values of the *FTC*, frequency of thermal comfort. It reveals that IN-MT28-D30 reached up to 95% of the thermal comfort, while the other two cases also reached about 60% of the thermal comfort, suggesting that about 40% of the time remained in the discomfort period during the first day. Such efficiency further dropped to as low as 10% of the period within the thermal comfort at seven days. It is mainly because the use of passive PCM layers in the building envelopes in these three cases could reduce the peak temperature to certain levels but may not meet the thermal comfort demand (e.g., 27 °C) in the given hot weather in Texas, which usually requires cooling through the input of HVAC systems and/or supplementary windows open at nighttime. If the upper-temperature threshold of the thermal comfort is set up to a higher value like 35 °C, the impacts of PCM location on the

thermal performance of a building wall can be theoretically reassessed, as shown in Figure 4.11 (b).

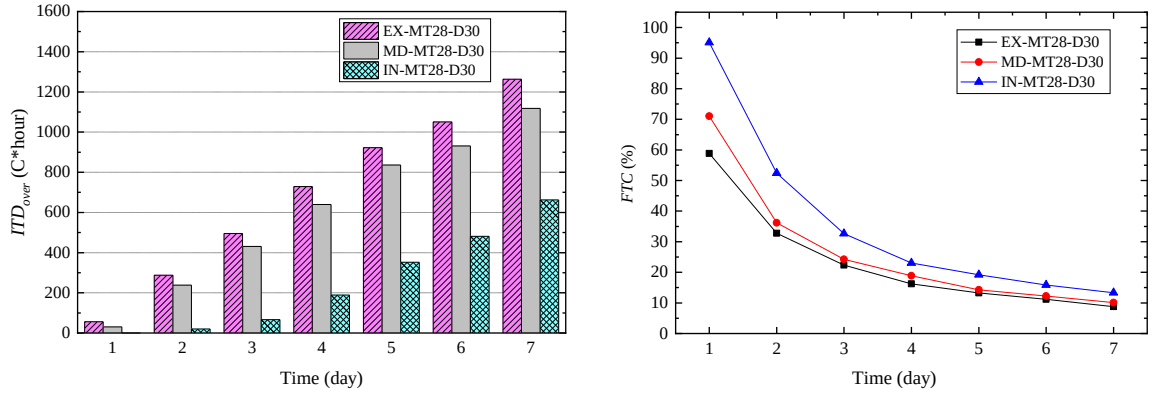

(a) T_{lim}=27 °C

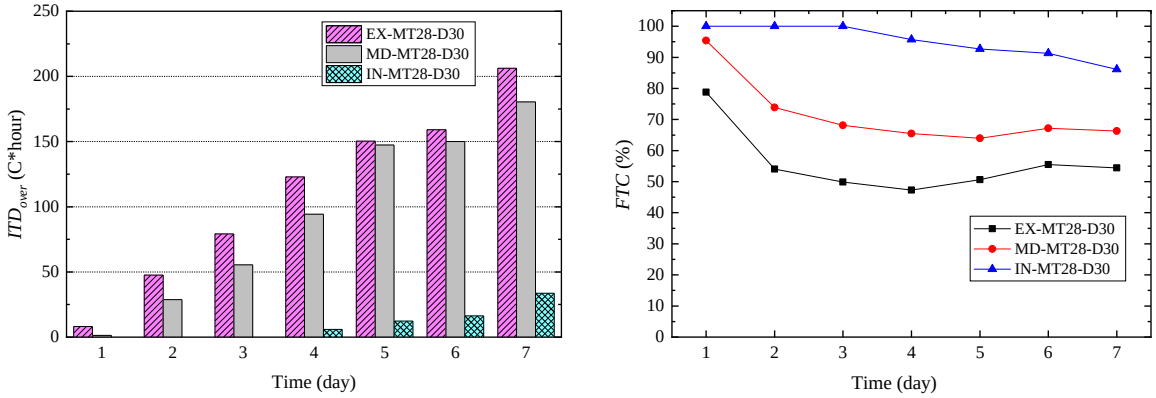

(b) T_{lim}=35 °C

Figure 4.11. Performance metrics ITD_{over} and *FTC* under different placements of the PCM layer.

All three cases offered high efficiency with above 80% of thermal comfort at 35 °C on the first day while remaining above 50% or higher for the rest of the days. It also confirmed the previous observation that IN-MT28-D30 could achieve the most efficiency for thermal performance. One can see that installing the PCM layer on the interior side of the wall shows more potential to enhance the building energy efficiency.

4.4.3. Effect of the Melting Point of PCM on the Thermal Performance

The selection of the proper melting point of the PCM used for the multi-layered wall systems is one of the key properties of interest. In this section, a wide range of the melting points varying from 24 °C to 45 °C were selected to account for their impacts, while maintaining other design parameters as listed in Table 4.3, including the thickness of the PCM layer of 30 mm located in the interior layer, named as IN-MD**-D30.

Figure 4.12 shows the instantaneous temperature of the wall interior surface over time when different melting temperatures of the PCM were used. The controlling wall without PCM layers had the highest temperature swings, ranging from 26 °C to 46 °C during the 7-day test period. A reduction of peak temperature was observed in all the walls reinforced with the PCM layer, though each case displayed different trends. Specifically, the performance curve of the wall with a PCM layer at a melting point of 24 °C, IN-MD24-D30, was not effective to mitigate the temperature fluctuation, which was identical to the performance of IN-MD45-D30 (i.e., melting point of 45 °C). This suggests that the PCM could not be as effective as expected if the melting point was too high or too low. When the melting point of the PCM varied from 28 °C to 32 °C, a significant reduction of the maximum instantaneous temperature and the temperature swings over the test periods were observed. Particularly, IN-MD28-D30 presented the best improvement, as compared to all other cases.

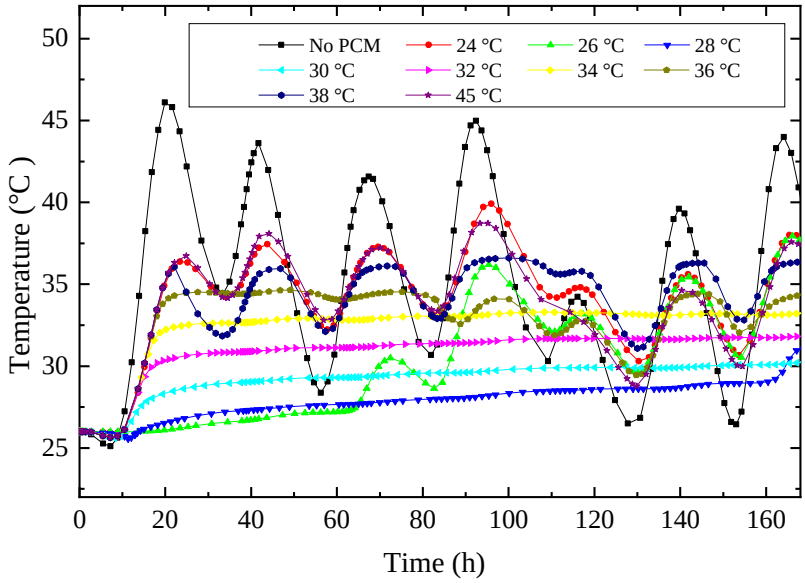

Figure 4.12. Transient temperatures of the interior wall surface over time.

Further quantitative assessments were conducted using the ITD_{over}, as plotted in Figure 4.13, where four different test periods were selected as the representatives. It shows that the IN-MD28-D30 with a melting point of 28 °C exhibited much better performance than the others, leading to the shortest discomfort period on the first day and still maintaining the higher performance as compared to other melting temperatures over time. This may be caused by the higher utilization rate in the heat capacity of the PCM with a melting point of 28 °C under the investigated loading conditions.

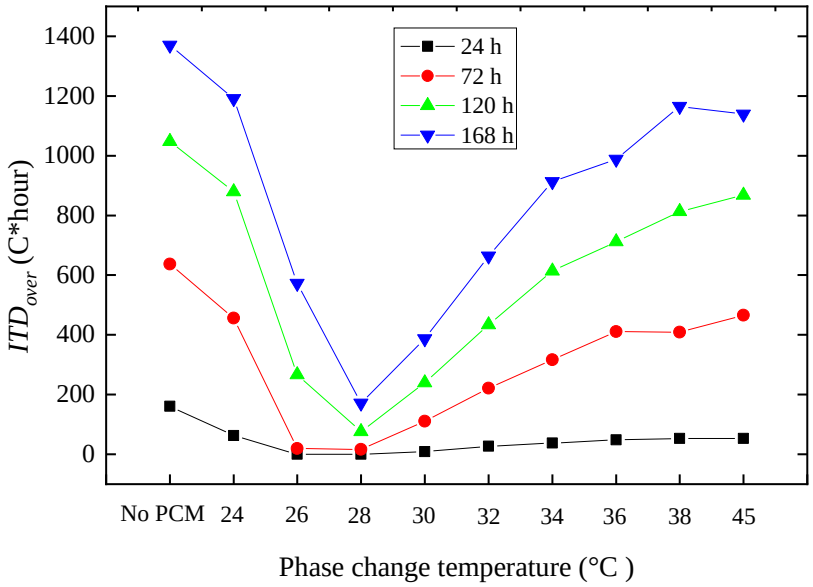

Figure 4.13. ITD_{over} under different melting points of the PCM layer.

4.4.4. Effect of the Thickness of PCM Layer on the Thermal Performance

Another piece of critical information for building designers and engineers is the determination of the thickness of PCM layers for building envelopes. Seven scenarios using three different thicknesses of PCM layers, from 7.5 mm to 100 mm, as well as the controlling sample without PCM, were investigated to address their effects on the thermal performance of the multi-layered wall system.

As shown in Figure 4.14 (a), the model of IN-MD28-D30 achieved a reduction of 7 °C at the peak temperature and had a temperature fluctuation ranging from 25 °C to 35 °C, about a 55% reduction as compared to the controlling wall without PCM. Further reduction in terms of temperature swings over time and the maximum instantaneous temperature was observed with an increase of the thicknesses. During the seven-day test period, the temperature swings of these scenarios, IN-MD28-D15, IN-MD28-D30, and IN-MD28-D50, were 10 °C, 5.8 °C, and 4.0 °C, respectively. A comparison further demonstrated that the maximum instantaneous temperature reductions were 30%, 55%, and 60%, respectively, as shown in Figure 4.14 (b), suggesting that

the thicker the PCM layer, the more latent heat of fusion it possesses, which in turn results in larger thermal energy storage capacity.

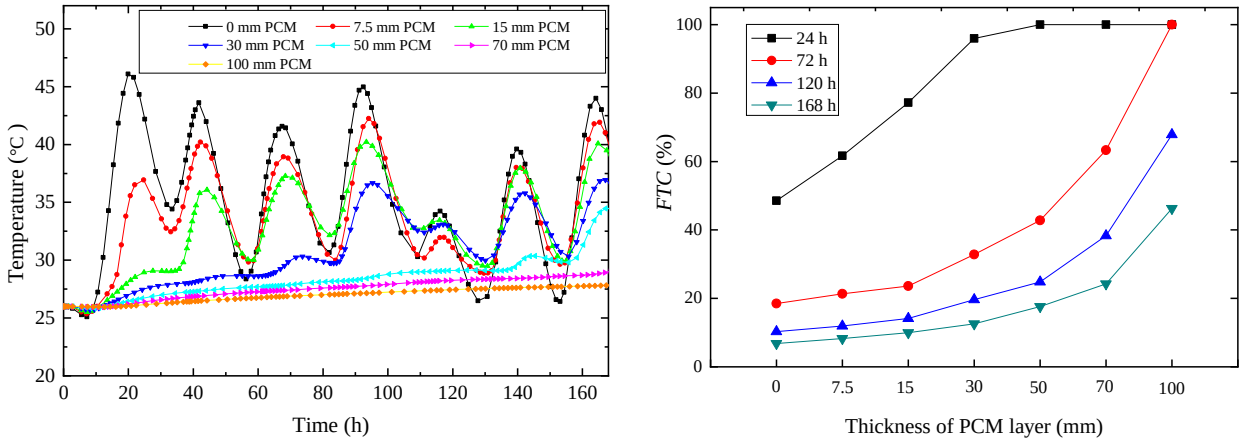

(a) (b)

Figure 4.14. History of interior wall surface temperatures over time: (a) transient temperatures and (b) *FTC* results.

Figure 4.15 shows the results using the performance metric ITD_{over} under different scenarios when the upper temperature threshold T_{lim} was 27 °C. The seven-day ITD_{over} of the PCM layers with different thicknesses ranging from 15 mm to 50 mm exhibited a considerable reduction in the discomfort periods, from 29% to 79%, as compared to the controlling one during the first day, respectively. It reveals that a thicker PCM layer can exponentially improve building energy efficiency in terms of shortening discomfort periods.

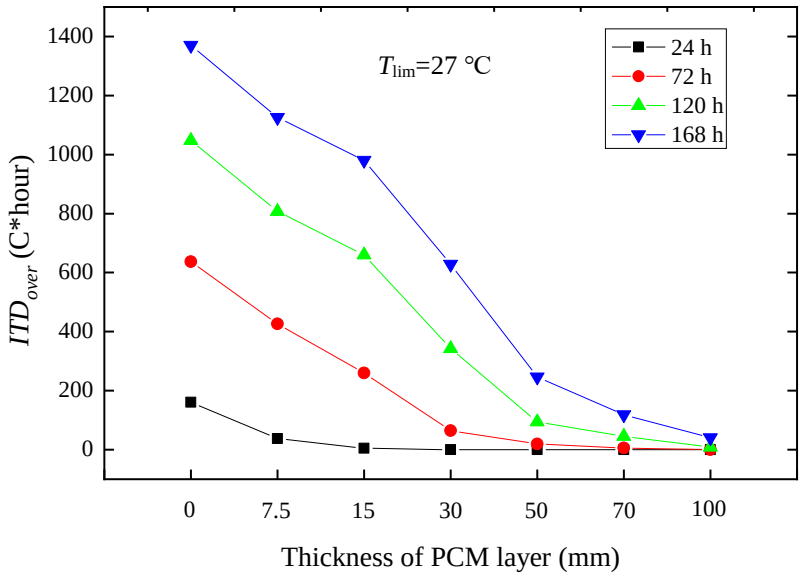

Figure 4.15. ITD_{over} under different thicknesses of the PCM layer.

4.4.5. Effect of the Latent Heat of PCM on the Thermal Performance

The latent heat of PCM represents the capacity of energy storage, and thus selection of high latent heat of fusion could potentially provide better thermal comfort to the building systems. In this section, four different latent heat of fusions of the PCM including 0, 63, 150, and 210 kJ/kg were used. The thickness of the PCM layer remained 30 mm. PCM with two different melting points including 24 °C and 28 °C were used for comparison.

As shown in Figure 4.16 (a), no considerable difference was observed for the various latent heat of fusions when the melting point of the PCM was 24 °C. During the seven-day test period, the temperature swings of the four cases with different heat of fusions were not influenced much by the heat of fusion of the PCM. Compared with that of the reference model with 0 kJ/kg of the latent heat, the maximum instantaneous temperature of the wall with 63, 150, and 210 kJ/kg of latent heat reduced by 1.5%, 1.6%, and 4.1 at the fourth day. When the PCM with a melting point of 28 °C was used, a significant enhancement of the indoor thermal comfort is achieved by using higher heat of fusions, as shown in Figure 4.16 (b). When the highest heat

of fusion was used, the wall exhibited the smallest temperature swings over time and the lowest maximum instantaneous temperature.

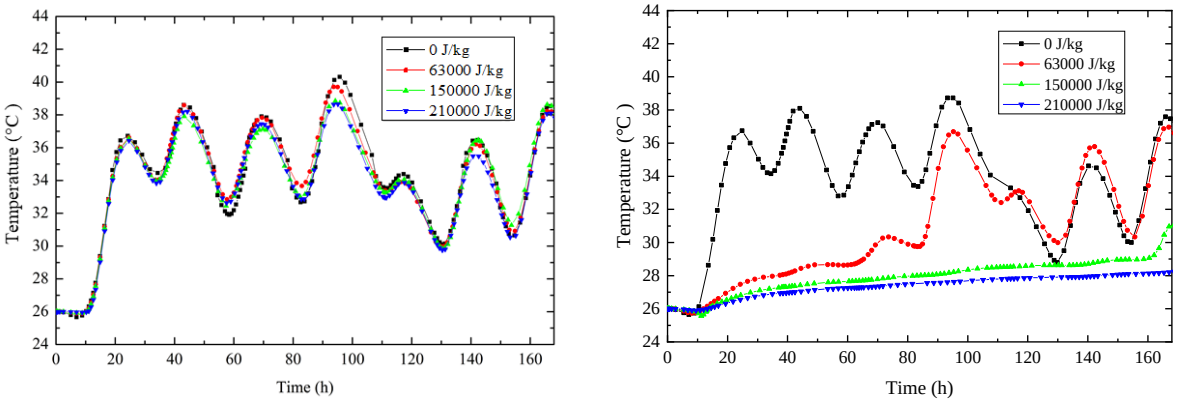

Figure 4.16. Time history of interior wall surface temperature with under different melting points of the PCM layer: (a) 24 °C and (b) 28 °C.

Figure 4.17 shows the results of the ITD_{over} and *FTC* when the upper threshold of the thermal comfort was at 27 °C and the melting point of PCM was 28 °C. The seven-day ITD_{over} of the cases with the heat of fusions of 63, 150, and 210 kJ/kg displayed a considerable decrease, by 47%, 83%, and 92%, respectively compared to the controlling model with 0 kJ/kg. The higher the heat of fusion of the PCM was, the smaller value the ITD_{over} was, suggesting that shorter discomfort periods were achieved by using the PCM with a higher latent heat of fusion. The *FTC* values of the investigated model are shown in Figure 4.17(b). Higher energy efficiency is achieved when the PCM with larger heat of fusions was employed. One can see that different parameters may affect each other concerning the thermal performance of PCM. Specifically, the utilization of latent heat capacity of PCM is highly affected by the melting points of PCM. The environment temperature is supposed to trigger the diurnal latent heat storage and release

process, in which scenario the PCM-based wall system can make full use of the latent heat capacity of the PCM.

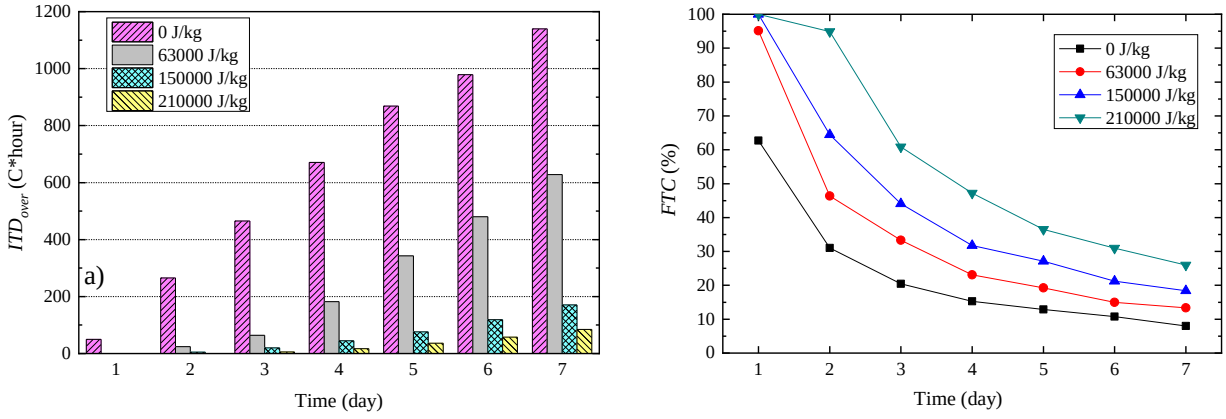

(a) (b)

Figure 4.17. Performance metrics of the models with different heat of fusions of the PCM: (a) ITD_{over} and (b) *FTC*.

4.4.6. Effect of the Thermal Conductivity of PCM on the Thermal Performance

Figure 4.18 shows the effect of the thermal conductivity of PCM on the thermal performance of the multi-layered wall system. The investigation focused on the thermal conductivity of the PCM layer ranging from 0.15 W/mK to 1.0 W/mK.

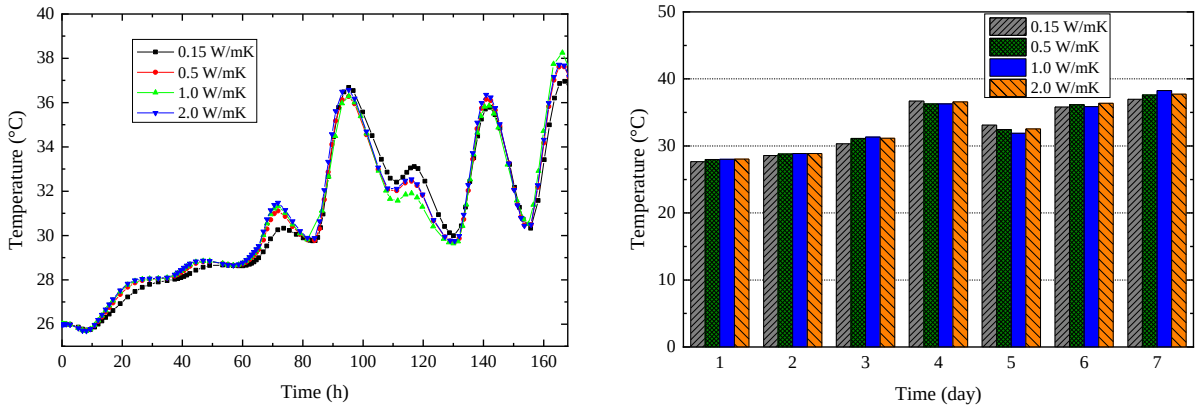

(a) (b)

Figure 4.18. History of interior wall surface temperatures over time: (a) transient temperature and (b) peak temperature.

Figure 4.18 (a) shows that there were identical trends for the interior wall surface temperature of different models. Figure 4.18 (b) reveals that the maximum instantaneous temperatures for all four scenarios were identical, suggesting that the thermal conductivity of the PCM layer shows little impact on the thermal performance of the wall system under the investigated loading conditions.

4.5. Summary

This study numerically investigated the thermal performance of a multi-layered PCM-enabled wall assembly and its thermodynamics under various design variables, including the installing location and thickness of the PCM layer and the properties of PCM (e.g., latent heat, melting temperature of PCM, and thermal conductivity). The results were quantitatively evaluated using four performance metrics: temperature swing, maximum instantaneous temperature, the intensity of thermal discomfort for overheating (ITD_{over}), and frequency of thermal comfort (*FTC*). Four performance metrics could provide different perspectives for the evaluation of building energy efficiency. As compared to discrete peak temperature or temperature swings, the ITD_{over} and *FTC* can provide systematic information of discomfort period over time, and thus be effective tools for quantifying the thermal performance of a PCM-enabled building.

Each design variable exhibited high variation in attributing to building energy savings in terms of reducing peak temperature and temperature swings. The melting point, thickness, and heat of fusion of PCM were found as crucial parameters to affect building energy efficiency, but it was not influenced much by the thermal conductivity of PCM. Specifically, the selection of the proper melting point is highly associated with the local climate zones and thermal comfort demand. The effect of thickness, location, and heat of fusion of PCM on the thermal behavior of

the wall was influenced by its melting point. A proper melting point of PCM is necessary to trigger its latent heat storage and release process so that its latent heat capacity can be made full use of. In the context of placement of PCM layer in a building envelope assembly, researchers have not reached a consensus on which is an optimal solution when subjected to the ambient environment. For the design of a single layer of PCM in a building envelope, this study showed that placing the PCM closed to the interior wall surface could achieve better energy efficiency than other locations.

4.6. References

[1] Kheradmand, M., Azenha, M., de Aguiar, J.L. and Castro-Gomes, J., Experimental and numerical studies of hybrid PCM embedded in plastering mortar for enhanced thermal behaviour of buildings. Energy, 94 (2016) 250-261.

[2] R. Baetens, B.P. Jelle, A. Gustavsen, Phase change materials for building applications: A state-of-the-art review, Energy and Buildings 42(9) (2010) 1361-1368.

[3] S. Ramakrishnan, J. Sanjayan, X. Wang, M. Alam, J. Wilson, A novel paraffin/expanded perlite composite phase change material for prevention of PCM leakage in cementitious composites, Applied Energy 157 (2015) 85-94.

[4] D. Zhou, C.Y. Zhao, Y. Tian, Review on thermal energy storage with phase change materials (PCMs) in building applications, Applied Energy 92 (2012) 593-605.

[5] S.A. Memon, Phase change materials integrated in building walls: A state of the art review, Renewable and Sustainable Energy Reviews 31 (2014) 870-906.

[6] A.M. Khudhair M.M. Farid, A review on energy conservation in building applications with thermal storage by latent heat using phase change materials, Energy Conversion and Management 45(2) (2004) 263-275.

[7] H. Akeiber, P. Nejat, M.Z.A. Majid, M.A. Wahid, F. Jomehzadeh, I. Zeynali Famileh, J.K. Calautit, B.R. Hughes, S.A. Zaki, A review on phase change material (PCM) for sustainable passive cooling in building envelopes, Renewable and Sustainable Energy Reviews 60 (2016) 1470-1497.

[8] N. Zhu, Z. Ma, S. Wang, Dynamic characteristics and energy performance of buildings using phase change materials: A review, Energy Conversion and Management 50(12) (2009) 3169-3181.

[9] A. Sharma, V.V. Tyagi, C.R. Chen, D. Buddhi, Review on thermal energy storage with phase change materials and applications, Renewable and Sustainable Energy Reviews 13(2) (2009) 318-345.

[10] X. Wang, H. Yu, L. Li, M. Zhao, Experimental assessment on the use of phase change materials (PCMs)-bricks in the exterior wall of a full-scale room, Energy Conversion and Management 120 (2016) 81-89.

[11] J. Lei, J. Yang, E.-H. Yang, Energy performance of building envelopes integrated with phase change materials for cooling load reduction in tropical Singapore, Applied Energy 162 (2016) 207-217.

[12] Y.-B. Seong J.-H. Lim, Energy Saving Potentials of Phase Change Materials Applied to Lightweight Building Envelopes, Energies 6(10) (2013) 5219-5230.

[13] M.A. Izquierdo-Barrientos, J.F. Belmonte, D. Rodríguez-Sánchez, A.E. Molina, J.A. Almendros-Ibáñez, A numerical study of external building walls containing phase change materials (PCM), Applied Thermal Engineering 47 (2012) 73-85.

[14] X. Jin, M.A. Medina, X. Zhang, Numerical analysis for the optimal location of a thin PCM layer in frame walls, Applied Thermal Engineering 103 (2016) 1057-1063.

[15] S.D. Zwanzig, Y. Lian, E.G. Brehob, Numerical simulation of phase change material composite wallboard in a multi-layered building envelope, Energy Conversion and Management 69 (2013) 27-40.

[16] L.F. Cabeza, C. Castellón, M. Nogués, M. Medrano, R. Leppers, O. Zubillaga, Use of microencapsulated PCM in concrete walls for energy savings, Energy and Buildings 39(2) (2007) 113-119.

[17] F. Kuznik J. Virgone, Experimental assessment of a phase change material for wall building use, Applied Energy 86(10) (2009) 2038-2046.

[18] G. Evola, L. Marletta, F. Sicurella, A methodology for investigating the effectiveness of PCM wallboards for summer thermal comfort in buildings, Building and Environment 59 (2013) 517-527.

[19] G. Evola L. Marletta, The Effectiveness of PCM Wallboards for the Energy Refurbishment of Lightweight Buildings, Energy Procedia 62 (2014) 13-21.

[20] Y.H. Jing, Research on the Application and Energy-Saving Assessment of Phase Change Materials in Intelligence Architectural, Applied Mechanics and Materials 416-417 (2013) 1741-1745.

[21] F. Kuznik, J. Virgone, J. Noel, Optimization of a phase change material wallboard for building use, Applied Thermal Engineering 28(11-12) (2008) 1291-1298.

[22] K.O. Lee, M.A. Medina, E. Raith, X. Sun, Assessing the integration of a thin phase change material (PCM) layer in a residential building wall for heat transfer reduction and management, Applied Energy 137 (2015) 699-706.

[23] X. Xu, Y. Zhang, K. Lin, H. Di, R. Yang, Modeling and simulation on the thermal performance of shape-stabilized phase change material floor used in passive solar buildings, Energy and Buildings 37(10) (2005) 1084-1091.

[24] N. Zhu, F. Liu, P. Liu, P. Hu, M. Wu, Energy saving potential of a novel phase change material wallboard in typical climate regions of China, Energy and Buildings 128 (2016) 360-369.

[25] A. Jayalath, R. San Nicolas, M. Sofi, R. Shanks, T. Ngo, L. Aye, P. Mendis, Properties of cementitious mortar and concrete containing micro-encapsulated phase change materials, Construction and Building Materials 120 (2016) 408-417.

[26] R. Zeinelabdein, S. Omer, G. Gan, Critical review of latent heat storage systems for free cooling in buildings, Renewable and Sustainable Energy Reviews 82 (2018) 2843-2868.

[27] COMSOL – Multiphysics Modeling and Simulation Software. Multiphysics Modeling and Simulation Software; 2021. <http://www.comsol.com>.

[28] N.P. Sharifi, G.E. Freeman, A.R. Sakulich, Using COMSOL modeling to investigate the efficiency of PCMs at modifying temperature changes in cementitious materials – Case study, Construction and Building Materials 101 (2015) 965-974.

[29] Fang, Y., 2009. A comprehensive study of phase change materials (PCMs) for building walls applications (Doctoral dissertation, University of Kansas).

5. EFFECT OF MELTING POINT ON THERMODYNAMICS OF THIN PCM REINFORCED RESIDENTIAL FRAM WALLS IN DIFFERENT CLIMATE ZONES[2]

5.1. Introduction

Residential and commercial buildings consume over 38 quadrillion BTUs (energy units), contributing to 39% of the total USA energy use in 2017 [1]. Space heating and cooling account for over one-third of all energy consumed in U.S. commercial buildings, while this proportion for residential buildings could even reach up to as much as 50%. Therefore, increasing building energy efficiency and indoor thermal comfort is nowadays a prime objective for energy policy worldwide. This goal can be achieved by taking advantage of sustainable energy conservation technologies such as thermal energy storage (TES) [2-4]. The utilization of the TES system shows high potential for better energy conservation through storing unconsumed thermal energy and releasing it later when needed. As illustrated in Figure 5.1, thermal energy can be stored in a material in the form of sensible heat, latent heat, thermochemical, or a combination of them [5].

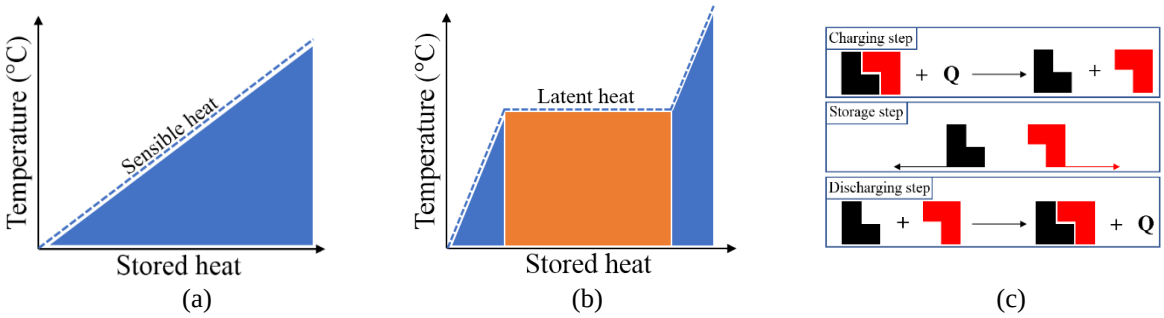

Figure 5.1. Methods of thermal energy storage (a) Sensible heat, (b) latent heat, and (c) thermochemical reaction (replotted from [6]) .

[2] This chapter presents the study that numerically investigates the optimal PCM melting temperature when being used to improve the thermal performance of multi-layered residential walls. Most of the contents of this chapter has been published in M. Li, Q. Cao, H. Pan, X. Wang, Z. Lin, Effect of melting point on thermodynamics of thin PCM reinforced residential frame walls in different climate zones, Appl. Therm. Eng. 188 (2021) 116615. Mingli Li had primary responsibility for building the numerical model and conducting the parametric study. Mingli Li also drafted and revised all versions of this chapter. Zhibin Lin served as proofreader and checked the mathematical model used in the simulation conducted by Mingli Li.

Sensible heat energy storage capacity, Q, of a certain material is determined by the mass of the medium (m), specific heat (C_p), and temperature variation ($T_f - T_i$) in the form [7].

$$Q = mC_p(T_f - T_i) \tag{5.1}$$

The commonly used building materials such as cement, concrete, and sand, are capable of storing certain levels of sensible heat energy. The main drawback of its application lies in its low thermal storage capacity, which makes it impractical to use a large amount of sensible heat based material to meet desired thermal energy demand for a building [8]. Differently, latent heat storage depends on the heat absorption or release when the phase of material changes from one state to another (e.g., solid to liquid or vice versa). As illustrated in Figure 5.1 (b), the heat energy storage capacity Q of a PCM consists of sensible heat energy and latent heat energy as described by [7].

$$Q = m[\underbrace{C_{sp}(T_m - T_i) + C_{lp}(T_f - T_m)}_{\text{Sensible heat energy}} + \underbrace{a_m \Delta h_m}_{\text{Latent heat energy}}] \tag{5.2}$$

where, C_{sp} and C_{lp} are the averaged specific heat in solid and liquid states, respectively; a_m and $\Delta h_m$are fraction melted and heat of fusion of PCM, respectively; T_m is the melting temperature of the PCM. Equation (5.2) reveals that, besides the sensible heat at the first term, PCMs enable offering much higher energy storage capacity through absorbing and releasing a considerably large amount of the latent heat during the phase transition process. Unlike sensible heat storage, the heat of isothermal behavior during the latent heat storing and its recovery process renders PCMs ability to prevent temperature swings. As such, PCMs can significantly increase building energy efficiency, thermal inertia, economic benefits, and thermal comfort of the occupants [9-11].

The effect of PCMs on the thermal performance of buildings has been extensively studied [12-17], as well as the investigation of PCMs on enhancing indoor temperature and reducing heating and cooling loads [18-21]. Castell et al. [11] experimentally studied the introduction of PCM-based bricks into the walls in Spain and reported that the PCM reduced the indoor peak temperature up to 1.0 °C and smoothed out the daily fluctuations. They found that the integration of PCM helped to reduce the cooling load of the building by about 15% in summer 2018. Alam et al. [19] numerically investigated the potential of PCMs in reducing the energy consumption of residential houses and their results demonstrated that PCM integrated buildings located in major Australian cities saved an annual heating/cooling load by 17~23%. Another numerical study on a passive house duplex located in Oregon, USA, confirmed that the integration of the PCM could cut half of the annual overheated hours [22]. Literature revealed that PCMs were introduced into multiple building components, including wall [23-27], ceiling [28], window and shutter [29-31], floor [32, 33], and roof [34], to prevent rapid changes of the indoor temperature and thus reduce heating/cooling energy consumption of the building envelope. Diaconu and Cruceru [35] conducted a year-round simulation of a room built with the PCM-reinforced walls and revealed that those walls contributed to annual energy savings and reduce the peak value of the cooling/heating loads. Halford and Boehm [36] demonstrated that using the latent heat of PCMs provided promising thermal mass for the building walls and shifted the energy demand from peak hours to off-peak hours. Thus, the rush hour electric supply pressure can be released, and the power utilization can be optimized. Also, residents and businesses may save on their electricity bills by consuming less on-peak electricity for the HVAC equipment.

Despite great efforts in the integration of PCM in building envelopes, how to select proper PCMs for various building envelopes under different climate zones still post high

challenges. Several attempts have been conducted through the determination of proper PCM melting temperature, in order to improve the efficiency of the latent heat energy released by PCMs. Tyagi and Buddhi [37] recommended that PCMs with melting temperatures between 20°C and 32°C can be used for thermal energy storage in terms of heating and cooling in buildings. Zhou et al. [38] indicated that PCMs with phase change temperatures ranging from 18°C to 30°C were preferred to meet the need for thermal comfort in the building applications since they covered the thermal comfort range of human beings. Neeper [39] investigated the thermal performance of PCM-based wallboard that was subjected to the diurnal variation of room temperature without solar radiation. They reported that the maximum thermal energy storage occurred when the melting temperature of PCM was close to the average room temperature in most circumstances. Zhang et al. [40] studied the ability of PCM-enhanced wallboard and find that the suitable melting temperature of PCM should be a little higher than the average indoor air temperature of the room without PCM for the period of sunshine. There were high variances among these studies and more importantly, these investigations limited their applications to specific cases, in which few attempted to address the impacts of wide ranges of climate zones. Saffari et al. [41, 42] presented a simulation-based optimization methodology to enhance the heating and cooling energy performance of a residential building enhanced with PCM concerning both short and long terms. They concluded that PCM with the melting point, ranging from 26°C to 27°C, could achieve higher energy savings in cooling dominant climates, while PCM with lower melting temperature ranging from 22°C to 23°C appears to be more effective for heating dominant climates. Considering that the efficiency of the latent heat energy of PCMs could be affected by multiple critical factors, including the thickness of PCM layer, PCM heat of fusion, and thermal conductivity of PCM. The existing studies that often discussed

one or two variables fell in short to systemically explore the thermal dynamics of a structure element under specific and realistic temperature profiles for various U.S. cities. Lack of information is unable to comprehensively address the factors affecting the selection of PCMs for a building envelope, to adopt various climate zones.

To fill the need, this study aims to numerically investigate the thermal performance of multi-layer residential walls reinforced with PCMs and unveil the impacts of various factors on the optimal PCM melting temperature under different climate zones over the U.S. cities. The COMSOL Multiphysics® software is selected to simulate the walls. Actual temperature profiles from different climate zones are extracted from Typical Meteorological Year (TMY) databases of various U.S. cities, and then applied to the wall external surface. The developed model is used to explore the influence of PCM location, thickness, and loading conditions associated with different climate zones and months on the selection of PCM melting point for building thermal management system.

5.2. Numerically Modeling of PCM-based Building Wall System

5.2.1. Wall Types as Thermal Enclosure Commonly Used for the Residential Buildings

The external wall of the residential building constitutes a major part of the building envelope and receives a large amount of direct solar radiation. A “perfect” external wall should be an environmental separator—it must possess various layers to control heat flow, rain, air, and vapor. Among them, thermal insulation is a significant technology to reduce energy consumption in buildings by providing resistance to heat flow through the building’s external walls. A well-insulated building can prevent heat loss in buildings in a cold climate and reduce excess heat in a warmer climate, effectively minimizing the requirement for HVAC system to keep the inside room temperature in the thermal comfort zone of occupants.

Thermal insulation can be integrated into different typical configurations of exterior walls, such as masonry, wood frame, and steel frame walls (Figure 5.2). As shown in Figure 5.2 (a), the masonry wall consists of exterior brick veneer, exterior rigid insulation layer, concrete block, and interior gypsum board. All layers above have some resistance to heat flow, however, the insulation layer with much lower thermal conductivity and density can endow building assembly better ability to retard the heat flow through the wall enclosing the conditioned space. Although masonry construction has advantages over steel and wood frame walls such as high strength, fire resistance, and termite resistance, it suffers from higher cost, longer build-time, and less thermal insulation due to its relatively high density and thermal conductivity. As shown in Figure 5.2 (b), instead of employing concrete block, the steel framing wall uses metal studs as the main structure, making the wall lighter, easier to install, and more sustainable since most structural steel can be reused and recycled. Nevertheless, the steel stud with high thermal conductivity can provide thermal bridges and allow considerable heat flow through the wall. This can be avoided if the wall is constructed with a thermal break or gap. In addition to the thermal insulation layer, an air gap with a thermal conductivity of about 0.025 W/m K constructed in the steel stud cavity can also be used to enhance thermal insulation performance. Using air gaps is sufficient for buildings in mild climate conditions but not enough for buildings in hot or cold regions. By contrast, better thermal insulation can be achieved by a wood frame wall with the cavity between wood studs filled with insulation materials (see Figure 5.2 (c)). Moreover, wood frame wall also offers several added benefits, such as cost-effectiveness, less build-time, and simplicity to remodel, which make it popular for being used in U.S. residential buildings.

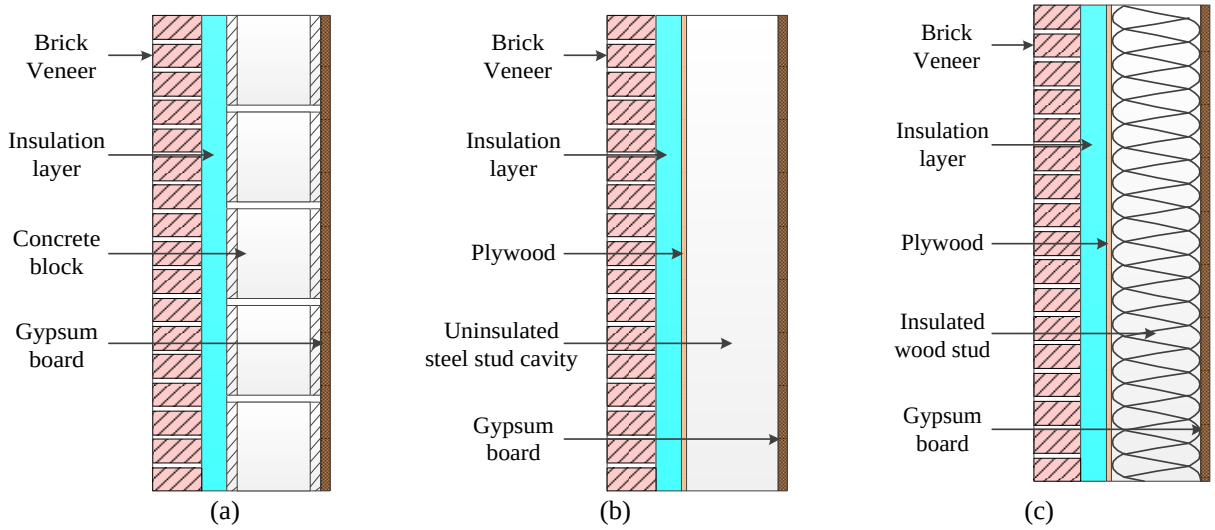

Figure 5.2. Typical configurations of exterior walls (a) Masonry wall, (b) steel frame wall, and (c) wood frame wall (replotted from [43]).

Thermal transmittance or *U*-value is generally used to express the thermal insulation performance of a multilayer wall by calculating the heat flow that passes through a unit area of a complex component or inhomogeneous material due to a temperature gradient equal to 1 K [44]. The maximum acceptable thermal transmittance of the building enclosure is specified to design energy-efficient buildings located in different climate zones by USA and EU regulations [45]. Several types of insulation measures exist to lower *U*-value and meet the thermal insulation requirement. A commonly used method is fixing the thermal insulating materials into the wall cavity as an internal insulation layer during the construction phase. They can resist heat flow as a result of the countless microscopic dead air-cells, which suppresses convective heat transfer. Mineral fibre, cellular plastic, and plant or animal derived products are often used as industrial insulation materials in building envelope. The choice of proper insulation material type and form depends on the application as well as the desired materials thermal, physical, and other properties.

For the last few decades, predominantly keeping the *U*-value of the building envelope as low as possible based on high insulation levels is regarded as the most important strategy to improve the thermal performance of the building envelope. However, in recent years, taking thermal inertia into account turns out to be an attractive criterion to enhance building thermal comfort conditions and reduce heating and cooling energy demands of buildings [46]. N. Aste et al. [47] demonstrate the importance of having a building envelope with high thermal inertia for saving energy and indoor comfort, particularly in the hot summer. The integration of PCM in the building envelope allows promising enhancement of the thermal inertia of the buildings. Kuznik et al. [23] demonstrate that a 1-cm PCM wallboard allows a doubling of the thermal inertia of the building with a total wall thickness increased by 4%. Cabeza et al. [48] study an innovative concrete with PCM on thermal aspects, and their results show that the encapsulation of the PCMs-based concrete in the walls leads to improved thermal inertia as well as lower inner temperatures in June. Following the literature review, it is found that PCMs bring more benefits for building envelope during all-year-round external conditions. To evaluate these benefits, we have chosen to investigate the thermal behavior of multilayer wall board reinforced with a PCM layer under simulated hourly external temperature and solar radiations.

5.2.2. Description of the Multilayer Frame Walls

The physical frame wall system considered is a typical North American residential wall, which is schematically shown in Figure 5.3 [49]. This wall consists of an interior layer of 12.7-mm gypsum wallboard followed by a 20.5-mm oriented strand board (OSB) with an 89-mm insulating layer between them. To evaluate the thermal performance of PCMs in the system, simulation results of this reference wall are compared with results obtained for a wall incorporated with a thin PCM layer in various locations. In the model, different PCM melting

points are utilized as the input variable to investigate the optimal ones for various loading conditions associated with different climate zones and months.

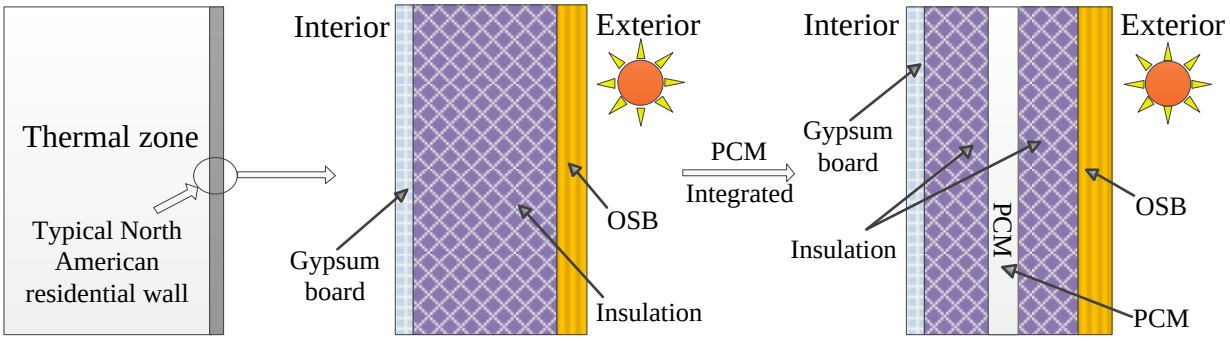

Figure 5.3. Schematics of residential wall systems strengthened by thin PCM layer.

5.2.3. Numerical Procedure for the PCM-based Multilayer Wall System

5.2.3.1. Mathematical Model and Boundary Conditions

A two-dimensional (2D) multi-layered transient conduction model is developed with the COMSOL Multiphysics® software [50] to simulate the thermal behavior of the typical North American residential wall system reinforced with PCM. This software is used to create and mesh the geometrical model of the multilayer wall and to solve the heat equation. In the simulation, the transient thermal response of both solid and liquid PCMs is involved due to the heat transfer caused by their "phase change" behavior. Only conduction heat transfer mode is considered inside the wall, even during the PCM melting or solidifying processes. Convection in the liquid phase is not considered in this simulation because it's not significant during liquid forms of PCM in this case [49, 51]. In addition, other layers like the gypsum board and insulating layer that tightly enclosing the PCM prevent natural convection inside the PCM [52]. The transient thermal behavior of a solid is governed by the partial differential equation as follows [53]:

$$\frac{\partial}{\partial x}\left(\lambda \frac{\partial T}{\partial x}\right) + \frac{\partial}{\partial y}\left(\lambda \frac{\partial T}{\partial y}\right) = \rho C_P \frac{\partial T}{\partial t}, \tag{5.3}$$

where T is the temperature (K), λ is the thermal conductivity of the material (W/m K), ρ is the density of the material (kg/m^3), and C_P is the specific heat of the material (J/kg K).

For simplicity, the model of the wall is established under the following assumptions: (a) All layers of the wall system are assumed to be homogenous and isotropic; (b) The heat transfer through the wall is one-dimensional (1D); (c) The thermal expansion of the materials is not considered; (d) The thermophysical properties of the materials are constant except the density of the PCM in the solid and liquid phase, and (e) For multi-layered wall systems, the contact resistance between different layers is negligible. Since the thermal conductivity is assumed to be constant through each material, and the system is isolated in direction, Eq. (5.3) can be reduced to a 1D heat transfer equation as shown in Eq. (5.4) [54],

$$\frac{\partial^2 T}{\partial x^2} = \frac{\rho C_P}{\lambda}\frac{\partial T}{\partial t}, \tag{5.4}$$

In COMSOL Multiphysics® software, the dynamics of the phase change process from phase I (solid) to phase II (liquid) in PCM is taken into consideration using the equation below [54]:

$$\rho_{PCM} = \rho_{phase1}\beta + \rho_{phase2}(1-\beta), \tag{5.5 a}$$

$$\lambda_{PCM} = \lambda_{phase1}\beta + \lambda_{phase2}(1-\beta), \tag{5.5 b}$$

$$C_{p,PCM} = \frac{1}{\rho_{PCM}}\left(\rho_{phase1}C_{p,phase1}\beta + \rho_{phase2}C_{p,phase2}(1-\beta)\right) + L\frac{\partial \alpha_m}{\partial T}, \tag{5.5 c}$$

where C_p is the specific heat (J/kg K), L is the latent heat of fusion (J/kg). Given the PCM is assumed to have an identical thermal conductivity in solid and liquid phases, Eq. (5.5 b) can be rewritten as:

$$\lambda_{PCM} = \lambda_{phase1} = \lambda_{phase2}, \tag{5.6 a}$$

and α_m is:

$$\alpha_m = \frac{1}{2}\frac{\rho_{phase2}(1-\beta)-\rho_{phase1}\beta}{\rho_{phase2}(1-\beta)+\rho_{phase1}\beta}, \quad (5.6\ b)$$

where β is the volume fraction of PCM at initial phase I (solid); α_m represents the mass percentage of PCM that is transferred from phase 1 to phase 2. The transition interval of PCM material between solid and liquid phase is not ideally zero, and a narrow temperature range of 5 °C is considered according to [55] in this simulation.

In this analysis, a typical North American residential building wall system across various climate zones under certain monthly conditions is examined. Appropriate exterior and interior boundary conditions are required for the simulation models. For the exterior side, data from the latest TMY3 weather files provided by National Solar Radiation Data Base (NSRDB) are used. On the interior side, an initial room temperature of 24°C is used and the subsequent heat gains and losses at the interior wall surface are recorded to explore the impact of PCM melting point on the thermal performance of the PCM–reinforced wall system.

5.2.3.2. Mesh Generation and Grid Check

Figure 5.4 shows the computational domain meshing of the multilayer wall system. The 2D model is chosen for the numerical analysis. For the subdomains and boundaries of the numerical model, triangular elements are used to apply the finite element method. Under the investigated temperature loading conditions, a mesh convergence study is carried out to ensure the accuracy of the finite element results. For the same numerical model, different non-uniform grid systems are checked and shown in Table 5.1. The supervising parameter considered is the average temperature of the boundary between the interior gypsum board and the insulating layer as marked in red in Figure 5.4 (a). Results of three different instants including 24h, 48h, and 96h are captured respectively to ensure the accuracy of the mesh sensitivity study.

Table 5.1. Grid sensitivity check for the numerical model.

Size of meshing	**Coarse**	**Normal**	**Fine**	**Extra fine**	**Extremely fine**
Element number	785	884	925	3110	10885
Time of solution (s)	15	17	19	30	44
Temperature at 24h (°C)	22.62	22.21	21.96	21.91	21.89
Temperature at 48h (°C)	22.18	21.70	21.52	21.45	21.43
Temperature at 96h (°C)	20.69	21.39	21.74	21.85	21.89

As shown in Figure 5.4(b), no significant change in supervising temperature is observed for the three tested instants when the meshing changes from coarse to extremely fine, showing the meshing insensibility of the investigated model. Given the accuracy of extra fine meshing can reach 99.8% of that of the extremely fine meshing save 31.8% of the time of solution under the same calculating system configuration, the former is adopted for the numerical simulations of PCM-based wall modules in this study. The model is a mesh that consists of 3110 triangular elements as shown in Figure 5.4(a).

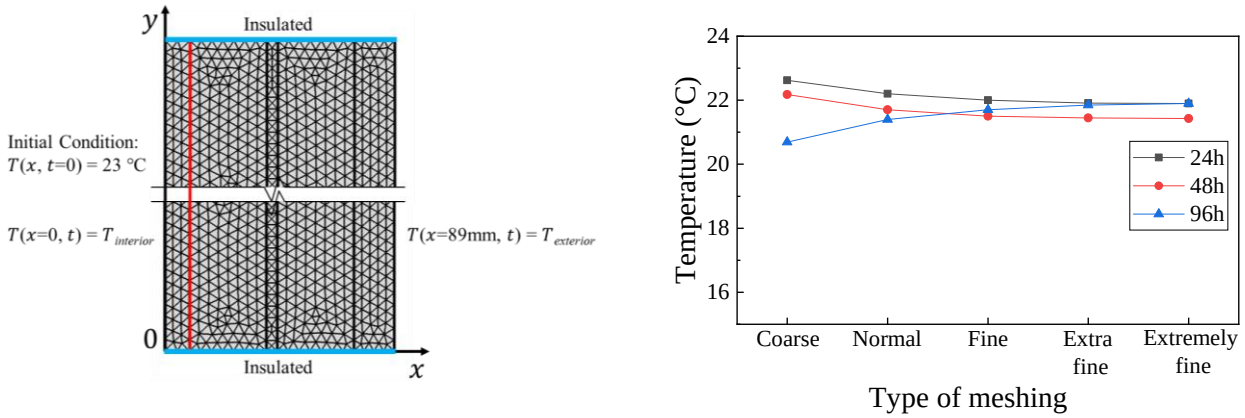

(a) (b)

Figure 5.4. COMSOL heat transfer model (a) geometry, mesh and boundary conditions and (b) mesh sensitivity study.

5.3. Validation of the Numerical Model

5.3.1. A Multilayer Wall Building in the Literature

As illustrated in Figure 5.5(a), a cubic box simulator consists of six 1.19m by 1.19m multilayer wall panels provided by the literature (Fang et al. [56]) is used to validate the mathematical model built in the COMSOL Multiphysics® software. Figure 5.5(b) shows the panel structure when the PCM layer is located in the center of the insulating layer, which is selected as the representative scenario for the model verification. The basic thermophysical properties of the materials used in each layer are listed in Table 5.2.

Table 5.2. Thermal properties of materials [49].

Materials	**Density (kg/m^3)**	**Specific heat capacity (kJ/(kg K))**	**Heat of fusion (kJ/kg)**	**Melting point (°C)**	**Thermal conductivity (W/m K)**
Gypsum board	800	1.09	/	/	0.16
Insulating layer	12.7	0.84	/	/	0.045
OSB	650	1.21	/	/	0.13
PCM	880 (solid) 760 (liquid)	2.0	179	27	0.20

In the tests, the transient temperature at the location between the interior gypsum board and the insulating layer and the heat flux value through the wall are collected to reveal the thermal behavior of the multilayer walls. Corresponding wall structure possessing the same assembly and materials with the experiments is mathematically analyzed in COMSOL to validate the accuracy of the numerical model. The wall is subjected to 1D heat transfer in the horizontal direction with both top and bottom sides thermally insulated. Wall assemblies with PCM layers in different locations are numerically investigated and similar results are generated.

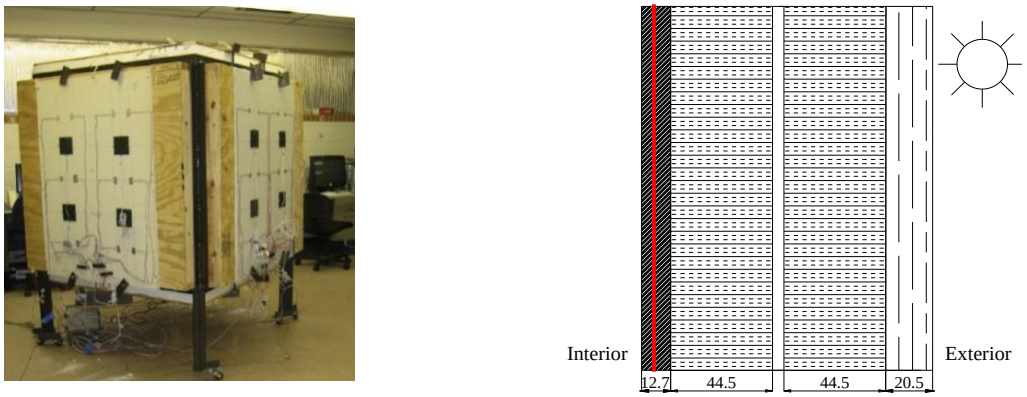

Figure 5.5. The multilayer wall (a) dynamic wall simulator in the laboratory test [49] and (b) schematic diagram showing the wall assembly.

5.3.2. Loading Conditions Associated with the Weather

The simulated typical weather applied on the exterior surface of the wall panel is based on the summer weather conditions in Lawrence, Kansas, USA [49]. The simulator is located in an airconditioned laboratory with a temperature range between 22-24°C. A test period of 96 hours (4 days) is adopted in the experiments. Figure 5.6 shows the temperature profile captured from the interior and exterior wall surface, which are used as the loading conditions in this study. The original temperature set for the structure in COMSOL Multiphysics® software is 23°C to match the experimental setup.

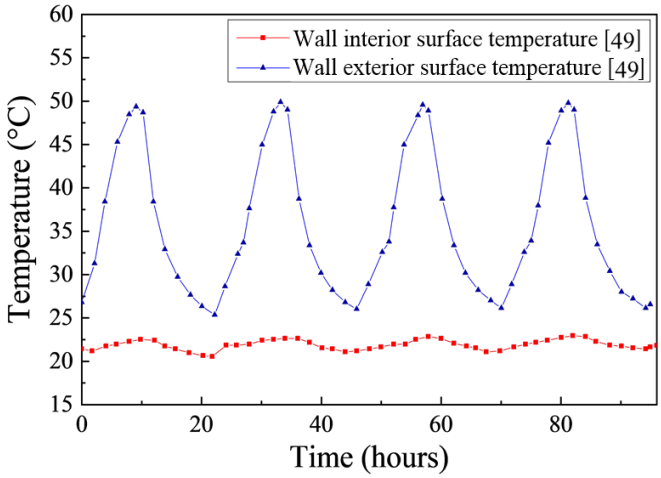

Figure 5.6. The boundary conditions of the multilayer wall.

5.3.3. Model Calibration and Discussion

Figure 5.7 (a) shows the comparison of the numerical temperature values with the tested temperature values [49] of the same location between the interior gypsum board and insulating layer, which is marked in red in Fig. 5(b). Figure 5.7 (b) shows the comparison between numerical and measured heat flux results through the wall. As shown in both comparisons, a good agreement between the results generated from the proposed study and the test results can be noted. The maximum temperature deviation between them is 0.52 °C, and the maximum heat flux deviation is 1.31W/m^2. These deviations may be caused by the chain of aspects that the numerical model does not consider, such as the continuum contact resistance between different layers and the anisotropic characteristic of the tested material. In the model validation, even though a slight difference between the numerical and experimental data still exists, it is acceptable based on the assumption made in this analysis. Therefore, the mathematical model using COMSOL Multiphysics® software can be used to analyze the thermal behavior of the PCM-reinforced multilayer wall.

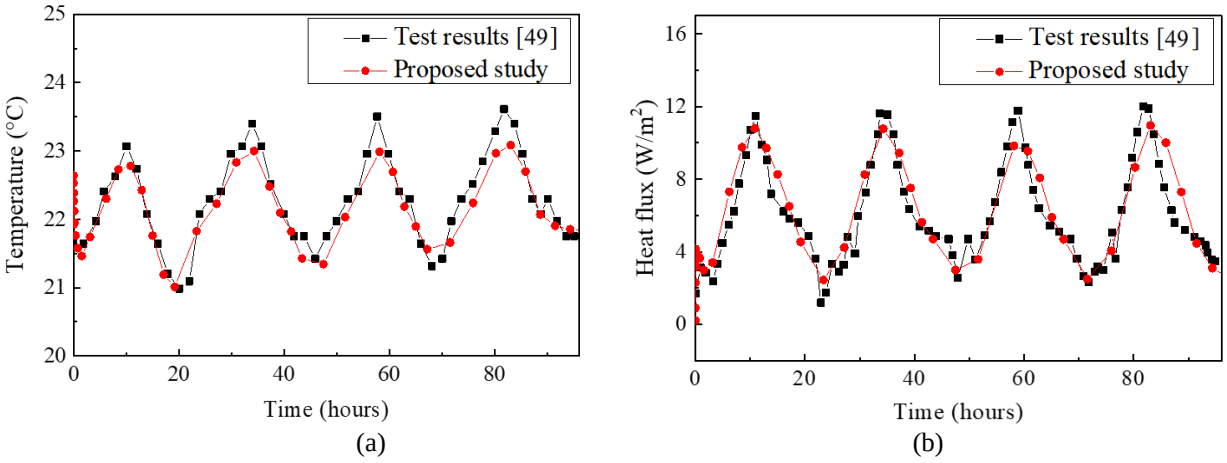

Figure 5.7. Comparison of test results and proposed study (a) transient temperature result (b) heat flux result.

5.4. Parametric Studies Using the Model

5.4.1. Prototype of the Frame Wall

As shown in Figure 5.8(a), a multilayer frame wall is considered for this comprehensive study to gain a deep understanding of the thermodynamics of a building envelope reinforced with PCM. The basic wall assembly used in this analysis consists of the first layer of a 12.7-mm gypsum board on the interior side of the wall, an 89-mm thermal insulating layer in the center, and followed by a 20.5-mm OSB on the exterior side. PCM layers with different melting points are integrated into various locations of the wall. The thermophysical properties of each layer are defined from the literature (see Table 5.2). As illustrated in Figure 5.8(b), the wall is subjected to 1D heat transfer with both top and bottom sides ideally insulated.

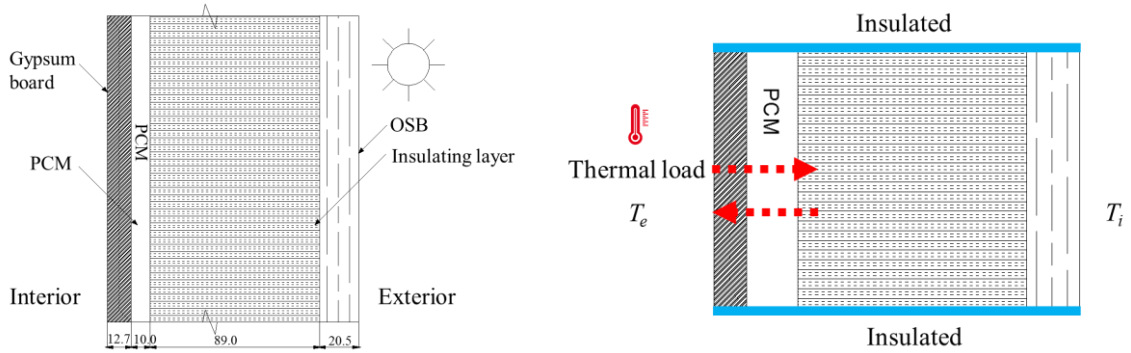

Figure 5.8. A schematic diagram showing (a) the assembly of the investigated external wall (unit: mm) and (b) boundary conditions.

5.4.2. Design of Test Cases for the Parametric Study

A comprehensive parametric study is conducted to explore the impacts of four critical factors, including the location of the PCM layer, the thickness of the PCM layer, loading conditions associated with different climate zones, and loading conditions associated with

different months on the selection of the PCM melting point. During the heat transient process, the initial temperature of the entire domain is assumed to be 24 °C.

An equivalent solar-air temperature ($T_{sol-air}$) as a combined action of the environment temperature and solar radiation generated from the TMY3 weather data files are used as the wall exterior boundary condition. External environment temperature and solar radiation are the major sources of the heat energy absorbed by the external surface of a building. As a commonly used loading condition, the external surface temperature of the wall can be calculated by means of the equivalent solar-air temperature for which, in the absence of solar radiation, the wall external surface received the same amount of heat energy compared with the scenario under the combinational effect of environment temperature and the solar radiation. In this study, a clear-sky solar radiation model considering clear-sky direct normal irradiance and diffuse solar irradiances is used to generate $T_{sol-air}$ according to the following equation:

$$T_{sol-air} = T_e + \frac{\alpha I_t}{h_e}, \tag{5.7}$$

where T_e is the external environment temperature (°C); α is the solar radiation absorption coefficient of the exterior surface; h_e is the heat transfer coefficient of exterior surface (W/m^{2}K); and I_t is the total solar radiation (W/m^2) [57]. The hourly external environment temperature of different cities in the U.S. can be obtained from the TMY weather database. For a building envelope that using OSB as the exterior layer, the solar radiation absorption coefficient (α) is considered as 0.7 in this study [58]. The heat transfer coefficient of the exterior surface (h_e) is considered as 22.7 W/m^{2}K for summer and 34.0 W/m^{2}K for winter according to the technical standard ASHRAE. The total solar radiation (I_t) can be calculated according to Eq. (5. 8) shown as follows:

$$I_t = I_D + I_d + I_{Earth}, \tag{5.8}$$

where I_D is the direct solar irradiance (W/m^2); I_d is the diffuse horizontal irradiance (W/m^2); and I_{Earth} is the ground-reflected irradiance (W/m^2). The value of I_t depends on the building's geographical location (latitude and longitude), the wall's orientation, and the sun's position in the sky associated with the local standard time. Figure 5.9 shows the global horizontal solar radiation, external environment temperature, and the sol-air temperature of the first week of July in Chicago. One can see that a significant difference between the external environment temperature and the solar-air temperature is observed because of the notable heating function of the solar radiation.

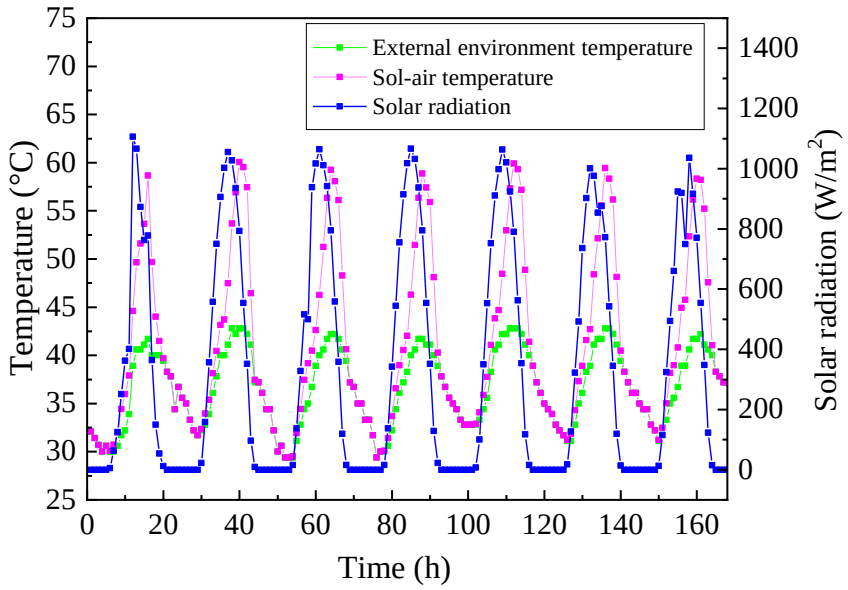

Figure 5.9. Evolution of the temperature at the first week of July in Chicago.

In this analysis, four variables are designed to explore the thermodynamic behavior of the multilayer walls reinforced with PCM layers. For each variable, different cases are consistently labeled in such a way that the first term of the label ——"L" denotes the location of the PCM, which is followed by a location number (see Figure 5.10). The second term "D" denotes the thickness of the PCM layer, unless otherwise stated. For example, L0-D5 in Table 5.3 represents a 5-mm PCM layer embedded next to the gypsum board.

5.4.2.1. Variability Associated with the Location of the PCM Layer

Figure 5.10 shows five configurations of the wall systems with a 5-mm PCM layer embedded in different locations. In the model, the insulating layer is assumed to be divided into 4 parts evenly, in which /4L, where 0≤ ≤4, is defined as the distance between any PCM layer in the nth location from the internal surface of the gypsum board and L is the total thickness of the insulating layer. For example, when the distance between the internal surface of the gypsum board and the PCM layer is ¼ of the thickness of the insulating layer, its location number equates to 1, which is shown in Fig. 10(b). In this simulation, the TMY weather data of Chicago on the first week of July is applied on the exterior surface of each wall configuration to investigate the impact of PCM layer location on the selection of its melting point.

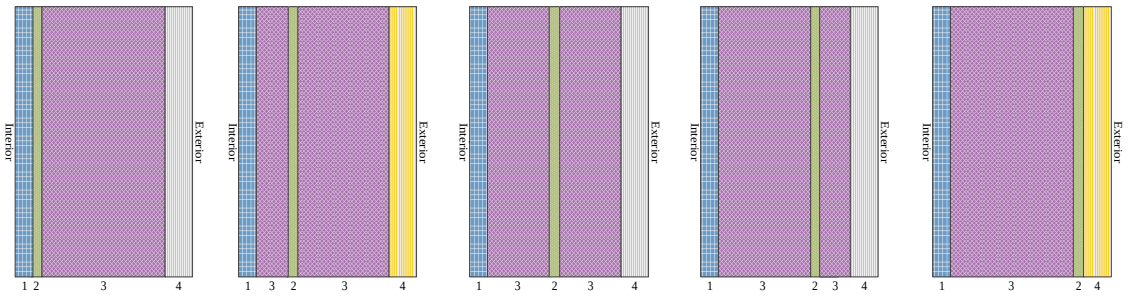

(a) L0-D5 (b) L1-D5 (c) L2-D5 (d) L3-D5 (e) L4-D5

Figure 5.10. Schematic of wall systems with different PCM layer locations. For the numbers in the schematics, 1: gypsum board, 2: PCM layer, 3: insulating layer, 4: OSB.

5.4.2.2. Variability Associated with the Thickness of the PCM Layer

In the previous study [1] conducted by the author, the thickness of the PCM layer shows a promising influence on the heat energy storage capacity of the multilayer wall reinforced with PCM. To address its impact on the selection of the PCM melting point, PCM layers with five different thicknesses are integrated into the wall and their thermal performance are numerically investigated. Note that the previous study demonstrates that the placement of the PCM near the interior wall surface can lead to higher energy efficiency [1]. In this study, the PCM layers are

embedded between the most interior gypsum board and the insulating layer to achieve better thermal performance. Other information on the investigated walls is shown in Table 5.3. In this simulation, the TMY weather data of Chicago in July is again applied on the exterior surface of each wall configuration to investigate the impact of PCM layer thickness on the selection of its melting point.

Table 5.3. Test matrix of the building envelope under varying design parameters.

Case Design	Label	Location	PCM Thickness (mm)	City	Month
Variability associated with wall thickness	L0-D0	0	**0**	Chicago	July
	L0-D2.5	0	**2.5**	Chicago	July
	L0-D5.0	0	**5.0**	Chicago	July
	L0-D7.5	0	**7.5**	Chicago	July
	L0-D10	0	**10**	Chicago	July
	L0-D15	0	**15**	Chicago	July

5.4.2.3. Variability of Loading Conditions Associated with Different Climate Zones

The thermal performance of PCM is influenced by the imposed climate conditions [59]. As shown in Figure 5.11, eight climate zones across the U.S. are specified based on different climate conditions by the "International Energy Conservation Code" (2012).

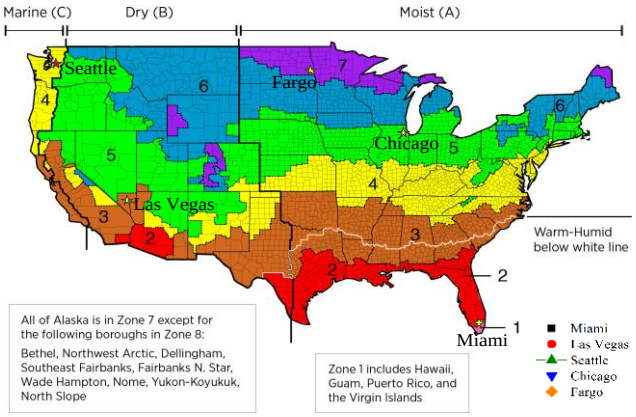

Figure 5.11. Map of different climate zones.

Simulations are carried out regarding the buildings located in five typical cities that belong to five different climate zones respectively in the U.S., including Miami (climate zone 1), Las Vegas (climate zone 3), Seattle (climate zone 4), Chicago (climate zone 5), and Fargo

(climate zone 7). Table 5.4 shows the average temperature and solar radiation applied on a west wall in those cities in January and July of the typical meteorological year. The data is summarized from the real temperature and solar radiation information provided by NSRDB. It can be found the average temperature and solar radiation in Miami and Las Vegas are relatively higher than those in other cities, while the average temperature and solar radiation in the higher climate zone like Fargo and Chicago tend to be relatively low during the investigated period. The thermal performance of the PCM-based building wall located in those cities is investigated to explore the impact of the loading conditions associated with different climate zones on the selection of PCM melting point.

Table 5.4. The climate characteristics of typical cities in different climate zones.

Climate zone	**Typical City**	**Average temperature of January (°C)**	**Average temperature of July (°C)**	**Average radiation of January (W/m^2)**	**Average radiation of July (W/m^2)**
Zone 1	Miami	19.42	28.13	145.17	250.29
Zone 3	Las Vegas	7.74	33.07	121.47	327.12
Zone 4	Seattle	4.50	17.67	42.25	259.62
Zone 5	Chicago	-4.65	24.13	74.50	257.37
Zone 7	Fargo	-14.50	21.43	62.48	262.79

5.4.2.4. Variability of Loading Conditions Associated with Different Months

Given that the monthly loading condition of a city varies all year round, simulations are carried out for different months to address their impact on the selection of PCM melting point. In this section, weather conditions in two typical hot and cold city including Austin (climate zone 2) and Minneapolis (climate zone 6) are adopted respectively. Figure 5.12 shows the annual loading conditions consist of the dry-bulb temperature and solar radiation of both cities. Both temperature and solar radiation in Austin are much higher than that of Minneapolis all year round.

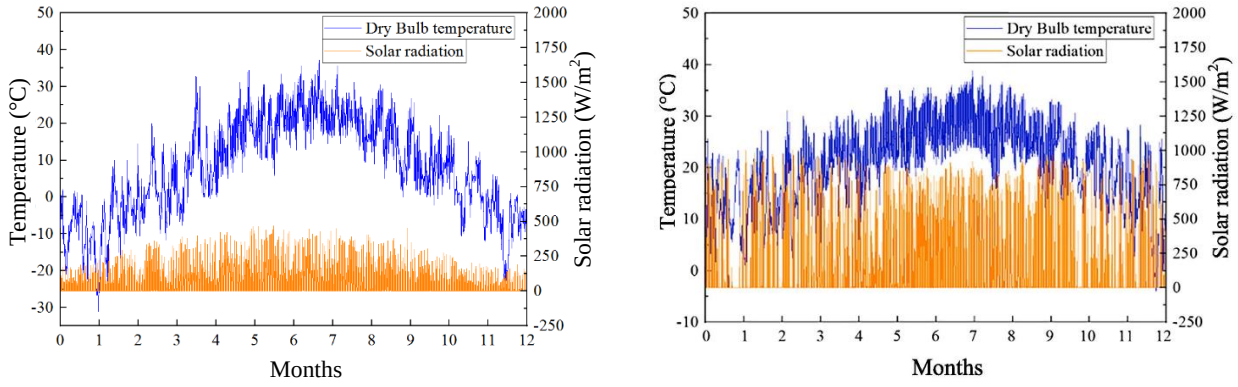

Figure 5.12. Weather conditions of (a) Minneapolis and (b) Austin.

5.4.3. Performance Indexes for Assessing Thermal Performance of the Multilayer Wall System

In this study, two different performance indexes including (a) indoor instantaneous temperature fluctuation, and (b) intensity of thermal discomfort (*ITD*) are used to comprehensively evaluate the thermal performance of the PCM-based wall system. ITD_{up} and ITD_{down} reflect the intensity of thermal discomfort for overheating and overcooling, respectively. Figure 5.13 displays the definition of terms used to calculate ITD_{up} and ITD_{down}. Note that the thermal comfort range of human beings is defined as 22°C to 28°C [58].

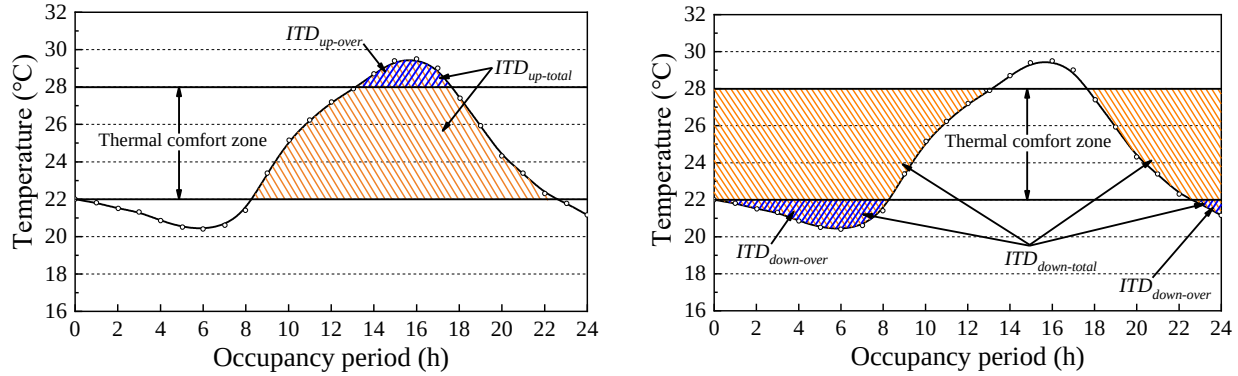

Figure 5.13. Graphic definition of (a) ITD_{up} and (b) ITD_{down} (adapted from [60]).

The ITD_{up} value can be presented as Eq. (5.9) shown below:

$$ITD_{up} = \frac{ITD_{up-total} - ITD_{up-over}}{ITD_{up-total}} \tag{5.9}$$

where the $ITD_{up\text{-}total}$ is defined as the time integral, over the investigated occupancy period P, of the positive difference between the current temperature and the lower threshold of the thermal comfort zone:

$$ITD_{up-total} = \int_P \ \Delta T^+(\tau) \cdot d\tau \tag{5.10a}$$

where

$$\Delta T^+(\tau) = \begin{cases} T_{op}(\tau) - T_{lower-lim} & if\ T_{op}(\tau) \geq T_{lower-lim} \\ 0 & if\ T_{op}(\tau) < T_{lower-lim} \end{cases} \tag{5.10b}$$

$T_{lower-lim}$ is the upper limit of the thermal comfort zone, which is determined as 22°C in this study. $ITD_{up\text{-}over}$ is defined as the time integral, over the investigated occupancy period P, of the positive difference between the current temperature and the upper threshold of the thermal comfort zone:

$$ITD_{up-over} = \int_P \ \Delta T^+(\tau) \cdot d\tau \tag{5.11a}$$

where

$$\Delta T^+(\tau) = \begin{cases} T_{op}(\tau) - T_{upper-lim} & if\ T_{op}(\tau) \geq T_{upper-lim} \\ 0 & if\ T_{op}(\tau) < T_{upper-lim} \end{cases} \tag{5.11b}$$

$T_{upper-lim}$ is the upper limit of the thermal comfort zone, which is determined as 28°C.

Similarly, the ITDdown value can be presented as Eq. (5.12) shown below:

$$ITD_{down} = \frac{ITD_{down-total} - ITD_{down-over}}{ITD_{down-total}} \tag{5.12}$$

where the $ITD_{down\text{-}total}$ is defined as the time integral, over the investigated occupancy period P, of the positive difference between the current temperature and the upper threshold of the thermal comfort zone:

$$ITD_{down-total} = \int_P \Delta T^+(\tau) \cdot d\tau \tag{5.13a}$$

where

$$\Delta T^+(\tau) = \begin{cases} T_{op}(\tau) - T_{upper-lim} & if\ T_{op}(\tau) \le T_{upper-lim} \\ 0 & if\ T_{op}(\tau) > T_{upper-lim} \end{cases} \tag{5.13b}$$

$ITD_{down\text{-}over}$ is defined as the time integral, over the investigated occupancy period P, of the positive difference between the current temperature and the lower threshold of the thermal comfort zone:

$$ITD_{down-over} = \int_P \Delta T^+(\tau) \cdot d\tau \tag{5.14a}$$

where

$$\Delta T^+(\tau) = \begin{cases} T_{op}(\tau) - T_{lower-lim} & if\ T_{op}(\tau) \le T_{lower-lim} \\ 0 & if\ T_{op}(\tau) > T_{lower-lim} \end{cases} \tag{5.14b}$$

One can see that within a given occupancy period, higher ITD_{up} and ITD_{down} value corresponds to the scenario that the indoor temperature is kept in the thermal comfort zone (22°C - 28°C) for a longer duration. Therefore, they are used as one performance index to assess the thermal performance of the building envelope in this study.

5.5. Results and Discussion

5.5.1. Effects of the PCM Location on the Selection of the PCM Melting Point

Chapter 4 illustrates that the PCM location within the building envelope has a significant effect on the thermal performance of the building envelope [1]. The objective of this section is to address the relationship between PCM melting point and PCM locations inside the wall. As illustrated in Figure 5.14, a 5-mm PCM layer with melting points ranging from 20°C to 32°C is integrated into five various locations of the wall as an internal layer. For each wall assembly, the thermal performance of the PCM-reinforced wall system is evaluated when it's subjected to the

representative summer week of Chicago by comparing their indoor transient temperature with the reference wall without PCM.

Figure 5.14 shows the transient temperature profiles of the interior surface of five different walls over a 7-day test interval. In general, all wall systems with PCM layers show a reduced peak indoor temperature when compared with the reference wall without PCM. The peak indoor temperature of the reference wall is 37.9°C appeared on the fifth day. During the same day, case L0-D5 (Figure 5.14 (a)) shows the most significant reduction (2.4°C) in peak thermal load while case L4-D5 (Figure 5.14 (e)) shows the smallest reduction (0.4°C). Therefore, installing PCM closed to the interior side of the wall can achieve better thermal performance, which is consistent with the previous study [1]. On the other hand, the instantaneous temperature of the five wall assemblies shows different evolution tendencies. In the case of L0-D5, the indoor temperature stays in human beings' thermal comfort zone (22-28°C [58]) during most of the test period for the scenario that the PCM melting point ranges from 24°C to 28°C. As the location of the PCM layer getting closer to the wall exterior surface, the "comfort time" is getting shorter. This phenomenon is due to the change in the interaction between the PCM layer and the insulating layer. With the PCM layer getting closer to the wall exterior surface, the insulating layer outside the PCM layer is getting thinner, thus making the PCM more directly exposed to the outdoor environment. Therefore, the PCM is more easily to melt and get heat saturated with the continuous heat energy input during the hot summer. If all the incorporated PCM turns to liquid and cannot further provide the latent heat energy storage capacity, the air-conditioner is needed to regulate the indoor temperature until it falls in the thermal comfort zone. Therefore, the optimal location of the PCM layer should be close to the wall interior surface to make sure that more inward heat is blocked by the insulating layer.

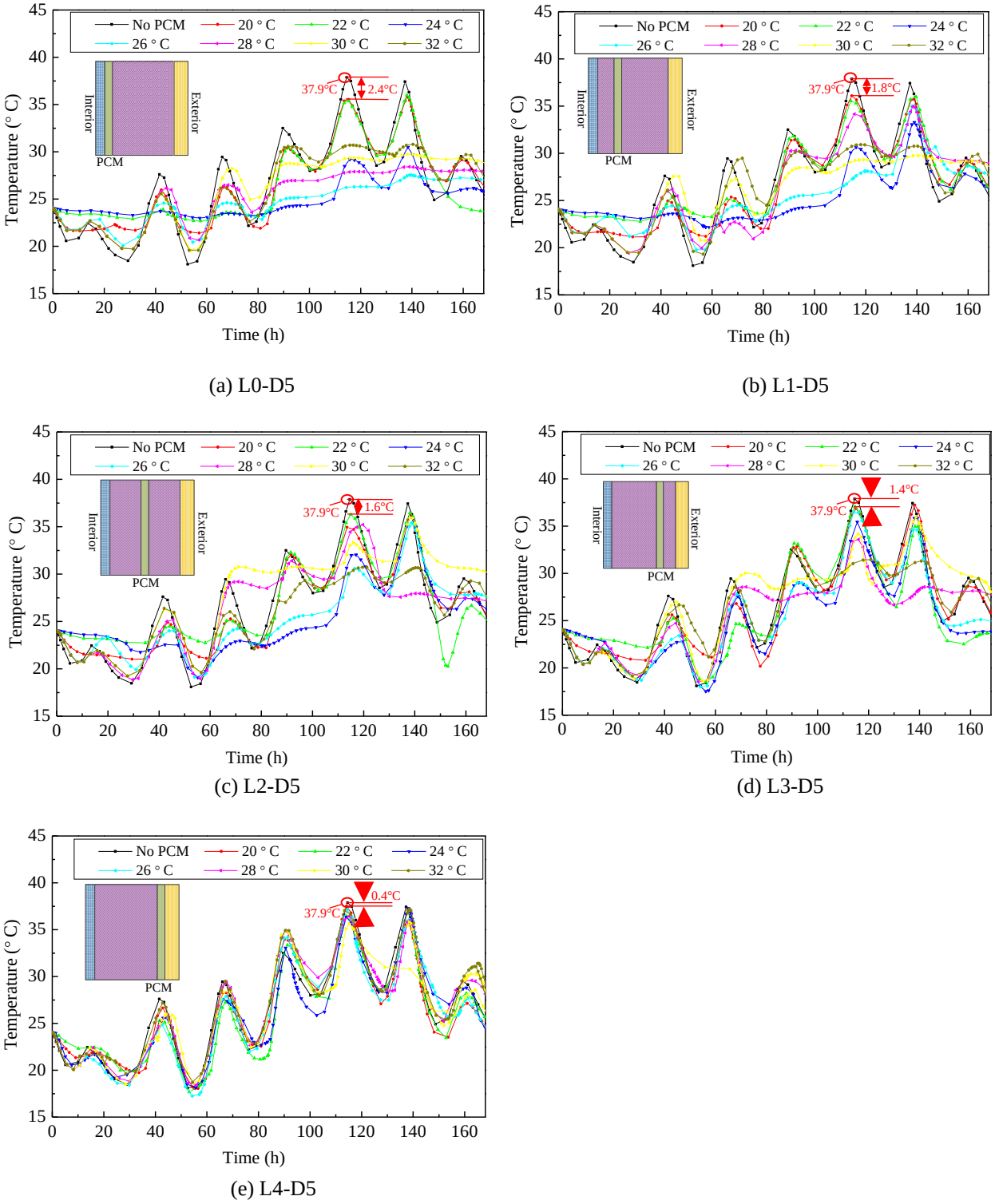

(a) L0-D5

(b) L1-D5

(c) L2-D5

(d) L3-D5

(e) L4-D5

Figure 5.14. Transient temperature of the interior wall surface over time.

Figure 5.15 shows a comparison of the *ITD* value of cases L0-D5 and L4-D5. One can see that changing the location of the PCM layer from interior to exterior of the wall results in a considerable reduction of both ITD_{up} and ITD_{down} value. For example, when the PCM is installed on the wall interior side, the ITD_{up} value of the 7-days occupancy period is almost 100% when the PCM melting point ranges from 24°C to 28°C. This number drops to about 84% when the same PCM is installed on the wall exterior side.

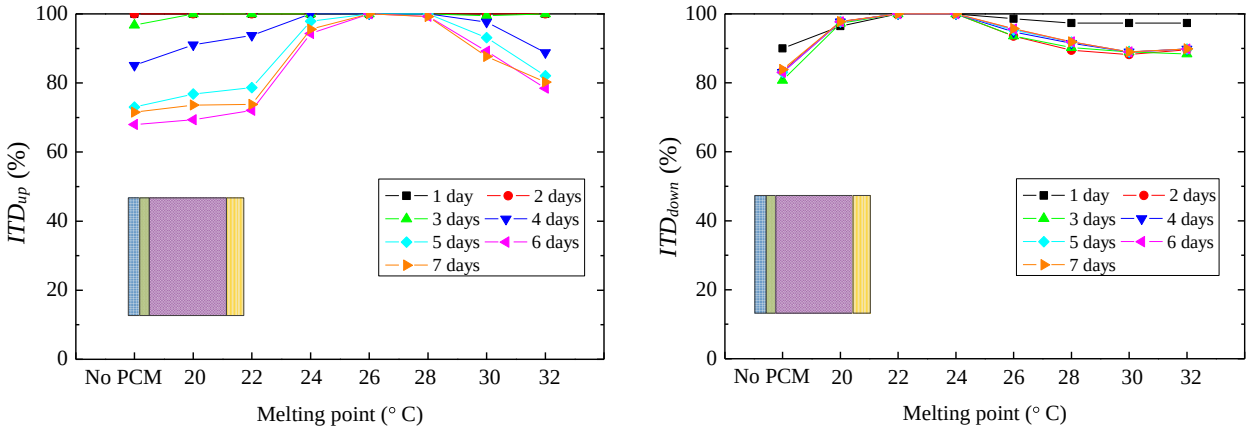

(a) ITD_{up} and ITD_{down} value of L0-D5

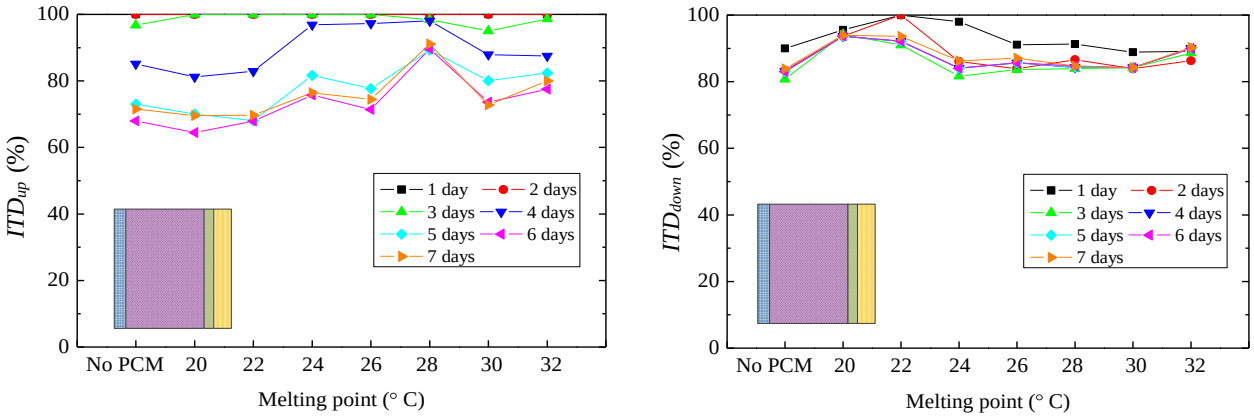

(b) ITD_{up} and ITD_{down} value of L4-D5

Figure 5.15. *ITD* values of (a) L0-D5 and (b) L4-D5.

Similarly, the ITD_{down} value of all the occupancy periods is 100% when the PCM melting temperature ranges from 22°C to 24°C is being installed on the wall interior side, but this number drops up to 18% when it's installed on the wall exterior side. Therefore, a similar

conclusion can be reached out that the PCM layer located on the wall interior side can achieve better energy efficiency to keep the inside temperature closer to the thermal comfort zone.

ITD distribution contour for different cases is also generated to quantitively evaluate the thermal performance of all wall assemblies. Figure 5.16 reveals that the ITD_{up} value of a certain wall system is affected by the PCM melting point, test period, and location of the PCM layer. As shown in Fig. 16(a), the maximum ITD_{up} value is 100%, corresponding to the scenario that the PCM layer is located on the wall interior side and the PCM melting point is between 24°C and 28°C. The contour in Fig. 16(b) represents the ITD_{up} distribution of the 4-days test period. The evolution of the ITD_{up} values shows a decreasing trend with the PCM location changed from the interior to the exterior side of the wall. The maximum ITD_{up} value corresponding to the 100% thermal comfort appears when PCM with a melting point of 26°C is installed on location 1 (wall interior side). In addition, the melting point about 2°C lower than the upper threshold temperature of human beings' thermal comfort zone (28°C) can benefit more for the cooling efficiency of the PCM-based building envelope investigated.

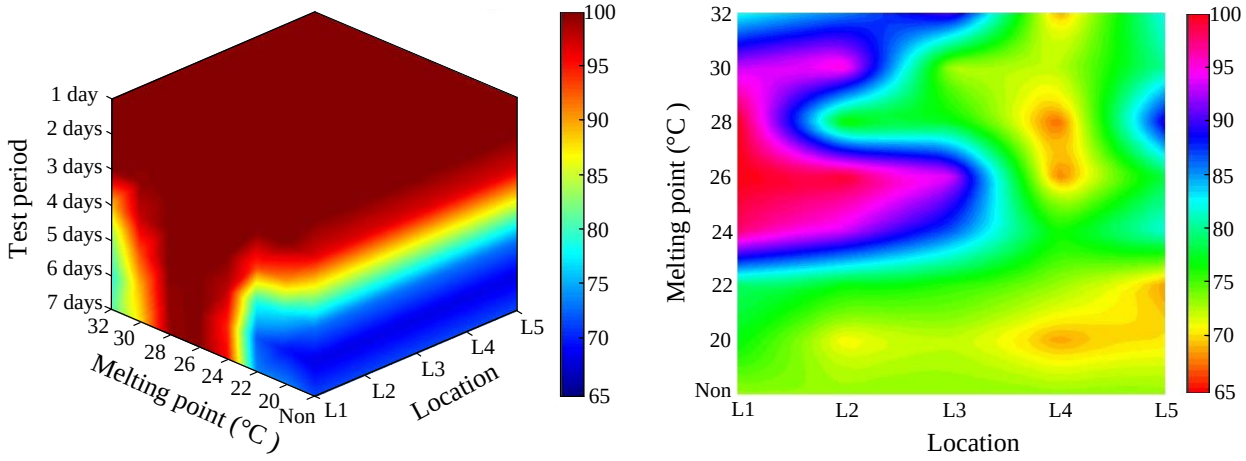

(a) (b)

Figure 5.16. ITD_{up} contour of (a) whole test period and (b) 4-days test period.

As shown in Figure 5.17, the optimal PCM location is also close to the wall interior surface in regard to increasing the ITDdown value. The optimal PCM melting point to maximize the ITD_{down} value is 22°C to 24°C, lower than the optimal PCM melting point to maximize the ITD_{up} value (26°C). It is because as a passive heating strategy, PCM with a relatively lower melting point possesses a greater opportunity to fully melt during the daytime, thus making full use of the latent heat capacity of the PCM under the given loading condition. Moreover, the ITD_{down} value is found to reduce with the increase of the test period. It is mainly because using PCM only for passive heating cannot meet the thermal comfort requirement in the given loading condition in Chicago. An HVAC system can be used as a supplement to the passive thermal regulation provided by PCM to further improve indoor thermal comfort.

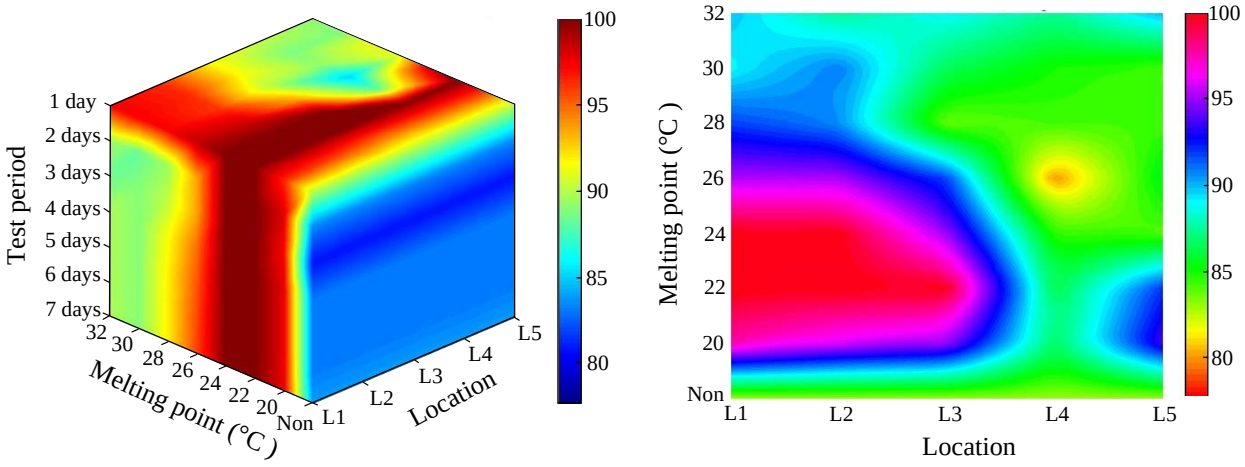

(a) (b)

Figure 5.17. ITD_{down} contour of (a) whole test period and (b) 4-days test period.

5.5.2. Effects of the PCM Thickness on the Selection of PCM Melting Point

PCM with thicknesses ranging from 2.5-15 mm is integrated into the wall as an internal layer respectively. The instantaneous temperature profiles of the wall interior surface are also generated to assess the effect of PCM thickness on the selection of the PCM melting point. Figure 5.18 shows that both peak temperature reduction and trough temperature rise increase

gradually with the PCM layer getting thicker. As a result, the wall with a 15-mm PCM layer proves its superiority on the thermal performance with a maximum peak temperature reduction of 8.8% and a maximum trough temperature increase of 16.7% compared with the wall reinforced by 2.5-mm PCM layer. It is because a thicker PCM layer contributes more to the heat energy storage capacity and thermal inertia of the wall system, thus reducing the indoor temperature swing during the test period.

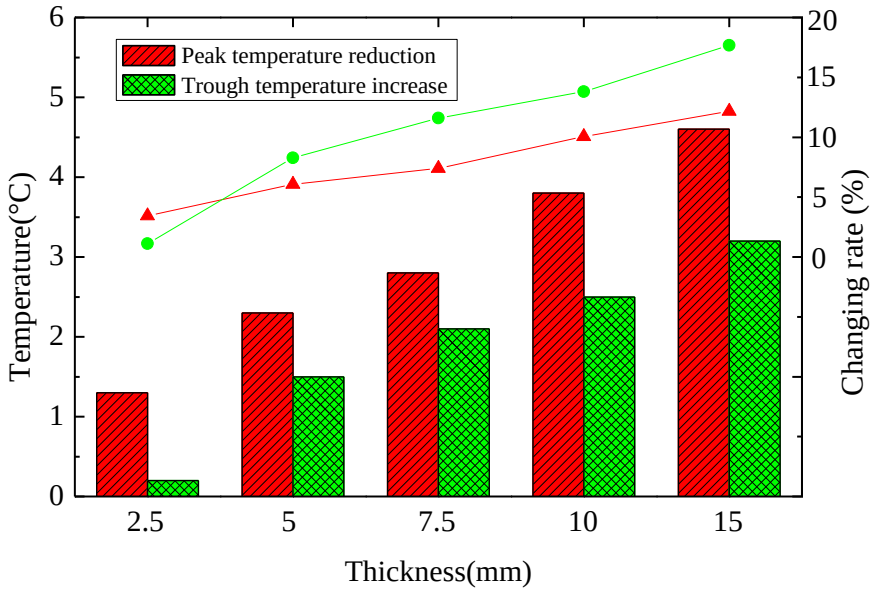

Figure 5.18. Temperature changes over thickness.

The effect of PCM layer thickness on the selection of PCM melting point is further explored by comparing the *ITD* value as a function of PCM thickness, melting points, and test periods when the PCM layer is placed in the walls. Figure 5.19 (a) shows that the ITD_{up} value is 100% during the first three days for all cases. As more heat energy is accumulated in the PCM, the ITD_{up} value starts to reduce from the fourth day and only the wall reinforced by PCM with melting points ranging from 26°C to 28°C can maintain the inside temperature within the thermal comfort zone for the following four days. This is mainly because that PCMs with melting points from 26°C to 28°C possess a higher conversion rate between solid and liquid and

the latent heat capacity of these PCMs tends to be made full use of under such a loading condition. In Figure 5.19 (b), the PCM with a melting point of 22°C can benefit most on the ITD_{down} value and thus increasing the thermal comfort duration. Note this temperature is lower than that to maximize ITD_{up} value.

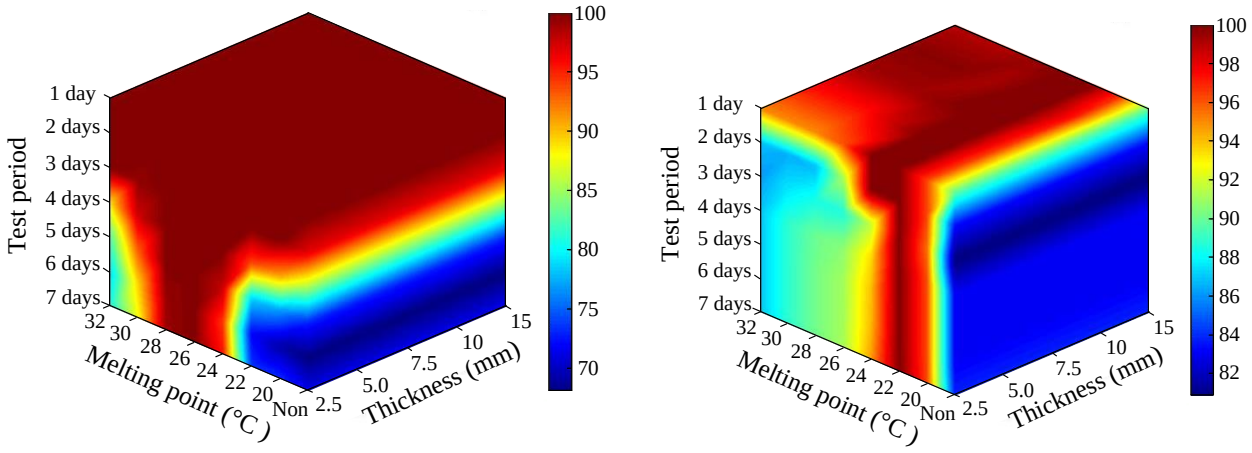

(a) ITD_{up} value (b) ITD_{down} value

Figure 5.19. *ITD* contour showing the effectiveness of PCM layer thickness.

To have a closer view of the effect of PCM thickness, a more detailed analysis is presented by comparing the *ITD* value of 1 day, 4 days, and 7 days. On can see from Figure 5.20 and Figure 5.21 that the envelope of 100% ITD_{up} and ITD_{down} value is slightly enlarged with an increased PCM layer thickness in different test periods. This is because more PCM possesses higher latent heat capacity, endorsing it more potential to keep the indoor temperature in the comfort zone. Therefore, the thickness of the PCM layer shows little impact on the selection of PCM melting point. It's also found that the most effective PCM melting point is 26°C-28°C to "cool down" the building envelope and 22°C to "heat" the indoor air, showing the feasibility of utilizing PCM with different melting points in the building envelope. On the other hand, the optimal PCM melting point range to achieve the higher ITD_{up} and ITD_{down} value becomes smaller

as the test period increases from 1 day to 7 days due to the decreased thermal energy storage capacity over time under the investigated loading condition.

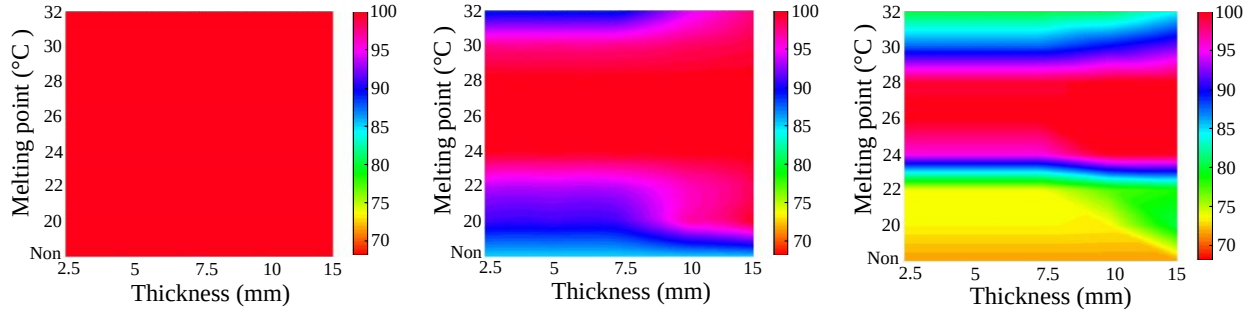

(a) (b) (c)

Figure 5.20. ITD_{up} contour of different test period (a) 1 day, (b) 4 days, and (c) 7 days.

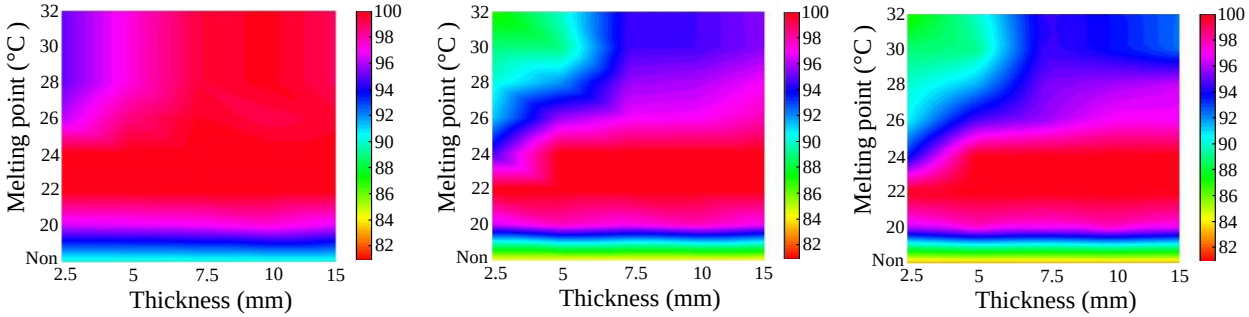

(a) (b) (c)

Figure 5.21. ITD_{down} contour of the different test periods (a) 1 day, (b) 4 days, and (c) 7 days.

5.5.3. Effects of the Loading Conditions Associated with Climate Zones on the Selection of the PCM Melting Point

Residential and commercial buildings located in the "hot" area are expected to increase the demand for energy consumption during the hot summer. Given the climate diversity of the United States, the equivalent sol-air temperature ($T_{sol-air}$) of five typical U.S. cities shown in Figure 5.22 are applied on the wall exterior surface to investigate the effect of loading conditions associated with climate zones on the selection of the PCM melting point. The test period ranges from July 1st to July 7th, representing the particularly hot days in a year. The selected cities can

be divided into three categories: hot, moderate, and cold according to their thermal loading conditions. The “hot” category contains Miami and Las Vegas, with maximum temperatures of 46.7°C and 61.8°C respectively during the test period. The “moderate” category includes Chicago and Fargo, with the minimum temperature about 10°C lower than Miami. Seattle can be categorized as a “cold” climate since it has the lowest maximum and minimum temperature during the first week of July. Those cities are considered to cover the main U.S. climate zones according to the U.S. Department of Energy classification.

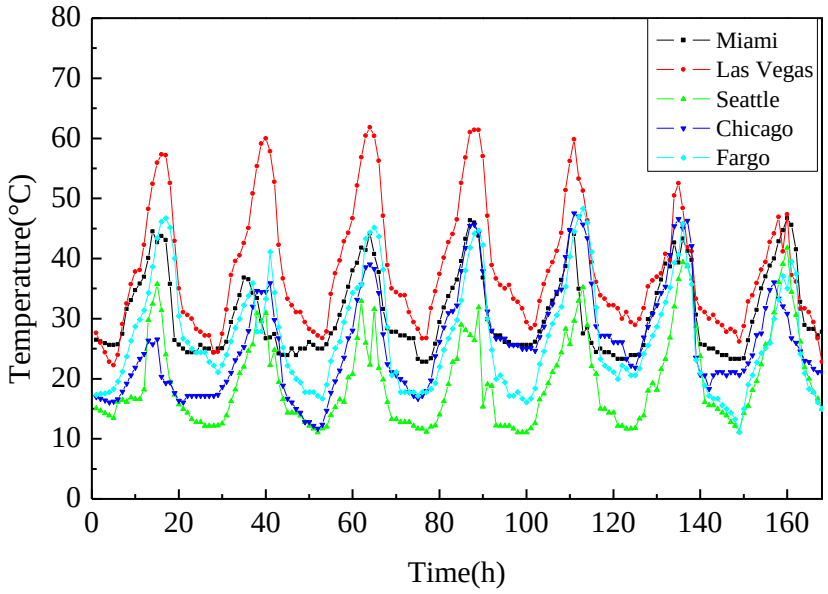

Figure 5.22. The equivalent sol-air temperature of five typical U.S. cities.

To determine the thermal performance of the walls located in different cities, the temperature profiles of the wall interior surface are numerically generated (Figure 5.23). As shown in Figure 5.23(a) and (b), the general temperature evolution trends of Miami and Las Vegas are similar, with all the indoor instantaneous temperatures above the lower threshold temperature of the thermal comfort zone (22°C) due to the hot weather. The maximum temperatures of the reference wall without PCM located in Miami and Las Vegas are 38.0°C and 48.9°C, respectively. After introducing PCM into the wall, the indoor peak temperature reduces

at different levels. It is because when the outside temperature increases, the inward heat can be absorbed and stored by the PCM due to its large heat storage capacity, thus preventing the indoor temperature from increasing drastically. As shown in Figure 5.23(a), the most effective PCM melting point to decrease the indoor peak temperature is 28°C for the thermal loading condition of Miami. Nevertheless, this optimal melting point increases to 36°C for Las Vegas. This is because the applied instantaneous of Las Vegas is much higher than Miami so that PCM with a higher melting point possesses a greater opportunity to turn to solid during the night and make it possible to provide "cooling energy" for the following day. Another observation is that the PCM with a melting point of 24°C can effectively keep the inside temperature in the thermal comfort zone for the first four days in Miami. The indoor temperature starts to exceed the upper threshold temperature of the occupied comfort zone from the fifth day. This is because the inward heat continuously charges the PCM and turns it into a liquid phase, but the inward cold during the night in Miami is not low enough to discharge it, thus reducing the effectiveness of the cooling function of the PCM.

For the "moderate" temperature category including Chicago (Figure 5.23(c)) and Fargo (Figure 5.23 (d)), the oscillation of the indoor temperature of the reference wall is relatively closer to the thermal comfort zone in the selected test period. In this scenario, PCM can effectively regulate the indoor temperature and make it fall into the thermal comfort zone for a longer time, and therefore decrease the energy demand for the HVAC system. Concerning the thermal comfort length during the 7-days test period, the optimal PCM melting point for Chicago and Fargo is 24°C to 26° C, lower than that of the cities in the "hot" area. For Fargo showed in Figure 5.23(d), when the melting point of the integrated PCM is 26°C, the wall interior temperature is kept in the thermal comfort zone for the whole test period, which is 34.5% and

75% longer than Miami and Las Vegas respectively when the same PCM is used. It can be noted that PCM with proper melting point plays a more significant role when being used under the "moderate" loading conditions. This is because building envelope subjected to "moderate" loading conditions needs less HVAC input to keep thermal comfort and PCM may have enough heat energy storage capacity to regulate the indoor transient temperature as a passive thermal management strategy.

Figure 5.23(e) shows the temperature profile of the wall interior surface under the summer weather in Seattle, which is classified as the "cold" category. The indoor temperature of the reference wall is lower than the upper threshold temperature of the thermal comfort zone (28°C) during nearly the whole test period and even below the lower threshold temperature (22°C). The PCM integrated into the wall here is mainly used to absorb heat energy during the daytime and release the stored energy to heat the indoor air during the night when the room temperature drops down. The result reveals that PCM with a melting point of 22°C tends to keep the room temperature closer to the thermal comfort zone, which is lower than the optimal PCM melting point for "hot" and "moderate" cities. If PCM with a high melting point is utilized in such a "cold" city, the inward heat energy is not able to fully charge it during the daytime, in which scenario there's not enough energy stored to heat the indoor air during the following night. By comparing the results of different cities, it can be concluded that the optimal PCM melting point is in direct proportion to the input loading conditions, suggesting that a higher PCM melting point is needed for a building envelope subjected to higher input temperature associated with climate zones. The selection principle is making sure the diurnal service effectiveness of the PCM by converting between solid and liquid totally under a certain loading condition.

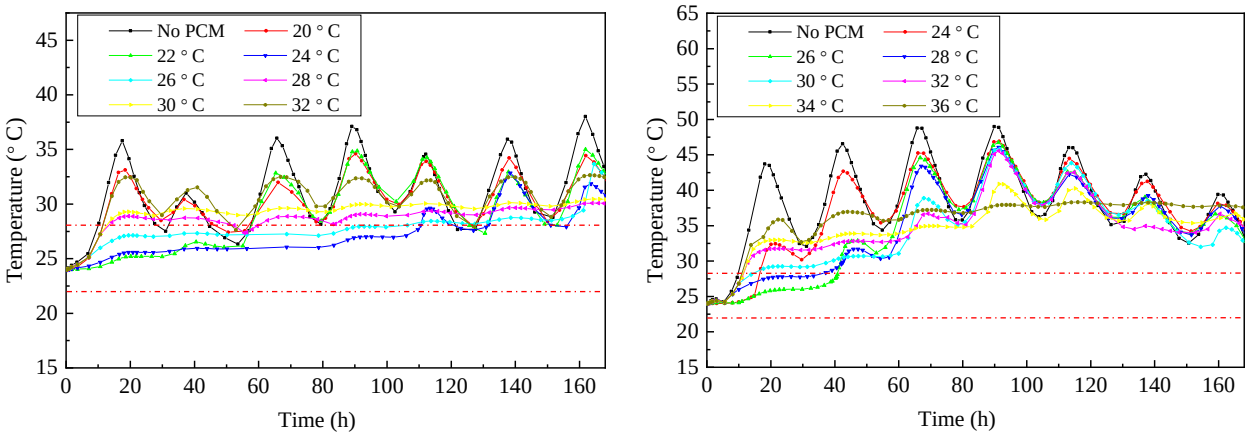

(a) Miami

(b) Las Vegas

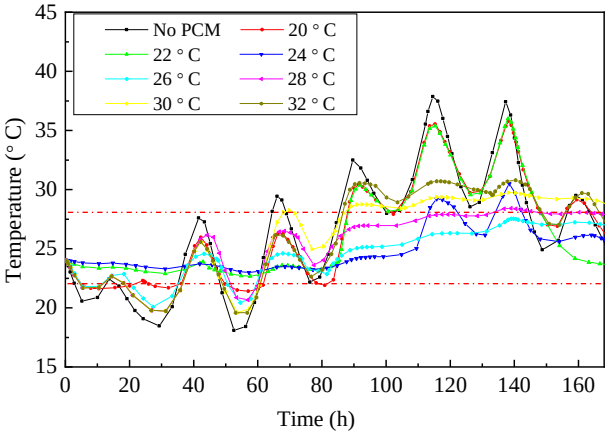

(c) Chicago

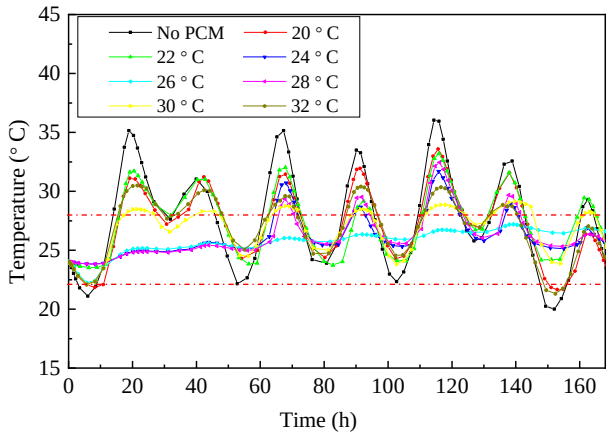

(d) Fargo

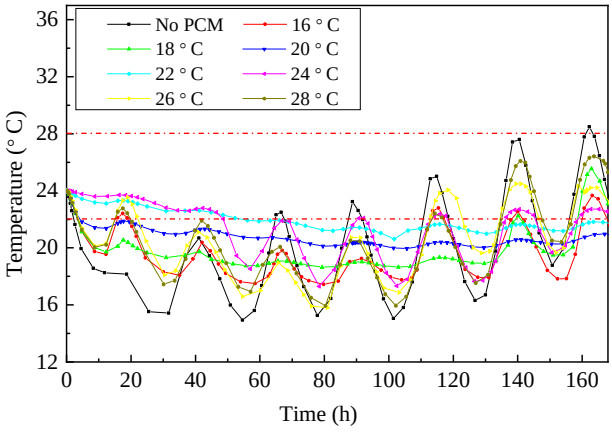

(e) Seattle

Figure 5.23. Indoor transient temperature of the wall located in different cities over time.

A more detailed analysis by comparing the *ITD* value of the above cities is conducted to further explore the impact of loading conditions associated with climate zones. Figure 5.24

shows the 7-days ITD_{up} and ITD_{down} value results of the walls subjected to summer weather in those cities as a function of the melting point and test period. As shown in Figure 5.24(a) and (b), Miami and Las Vegas possess relatively low ITD_{up} values since their indoor temperatures exceed the upper threshold of the thermal comfort zone (28°C) most of the test period due to the hot weather. The most effective melting point interval to increase the ITD_{up} value is about 24°C to 26°C for Miami. A higher melting point ranging from 26 °C to 30°C is needed for Las Vegas to achieve maximum ITD_{up} value, which is consistent with the conclusion drawn previously. The ITD_{down} value of both "hot" cities is 100% since the indoor temperatures are higher than the lower threshold of the thermal comfort zone (22 °C) during the whole test period. For Chicago and Fargo belonging to the "moderate" category (Figure 5.24(c) and (d)), the optimal melting point interval to increase the ITD_{up} value is 24°C to 28°C. For Chicago, the optimal melting point interval to increase the ITD_{down} value is 20°C to 24°C. This interval increases to a wider range for Fargo due to its "hotter" weather than Chicago. The indoor temperatures of all the PCM-based walls subjected to the weather of Fargo are over the lower threshold temperature of thermal comfort. For Seattle, the representative city of the "cold" category, ITD_{up} value for all the PCM-based walls is 100% during the test period due to the relatively cold weather. The feasible melting point interval to keep the indoor air warmer and the ITD_{down} value higher is from 20°C to 24°C. The PCM with melting points higher than 24°C cannot totally turn to liquid during the daytime under such cold weather and thus not enough heat energy can be stored in the PCM. On the other hand, the PCM with melting points lower than 20 °C cannot solidify totally during the night and provide enough cooling energy for the following daytime to store heat energy.

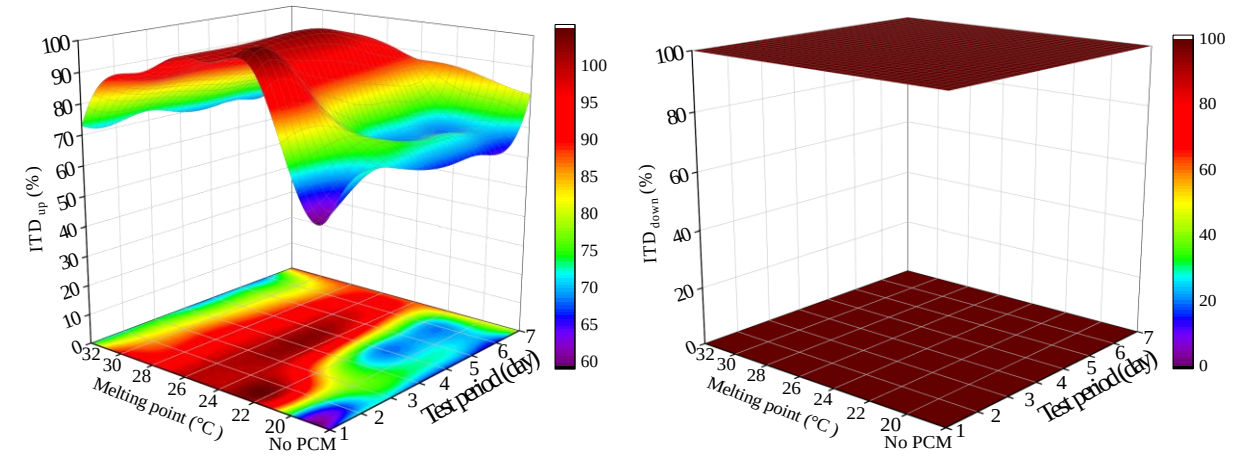

(a) Miami

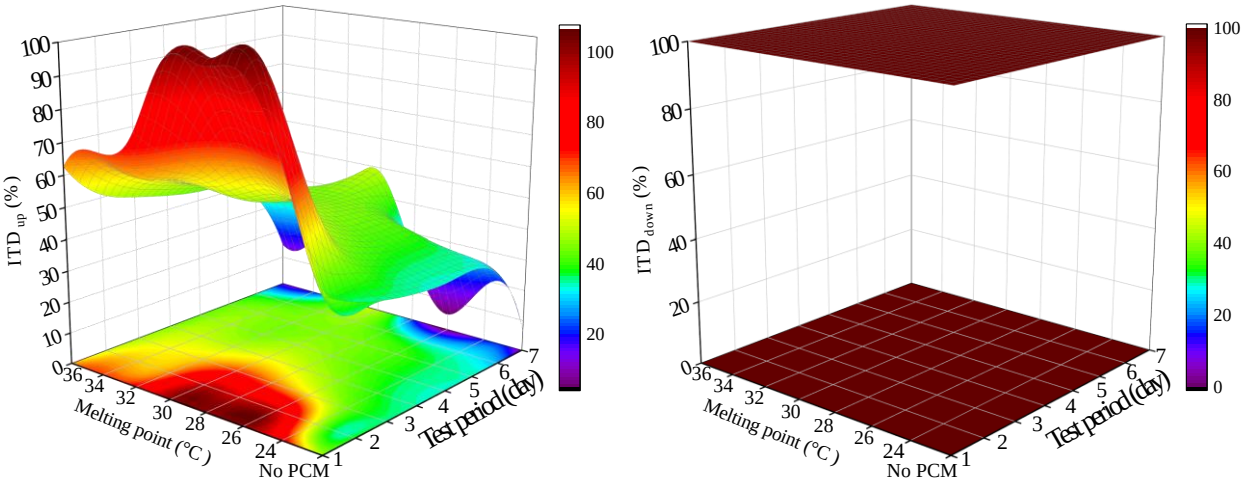

(b) Las Vegas

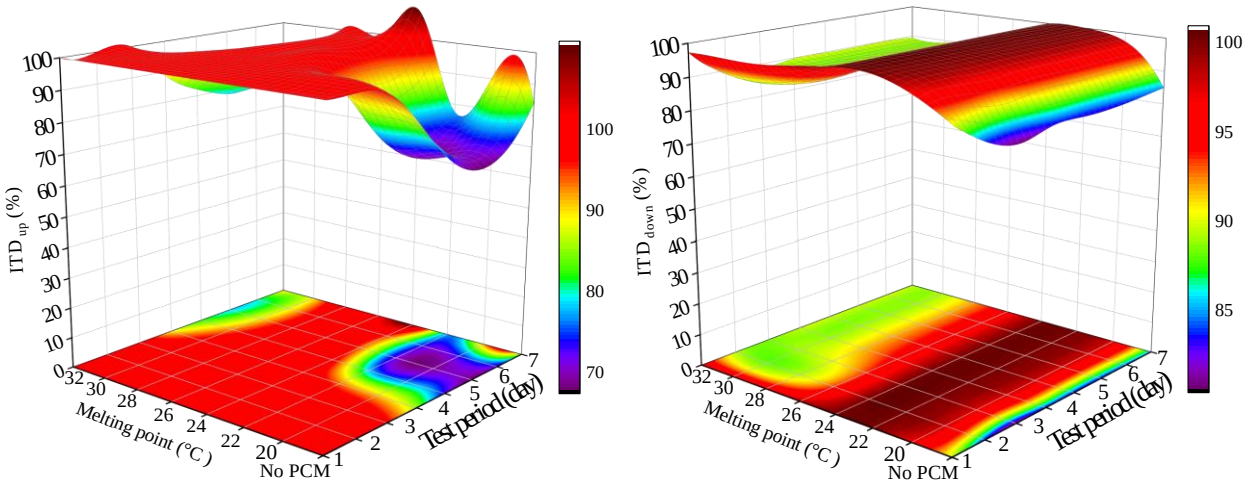

(c) Chicago

Figure 5.24. *ITD* contour of different cities.

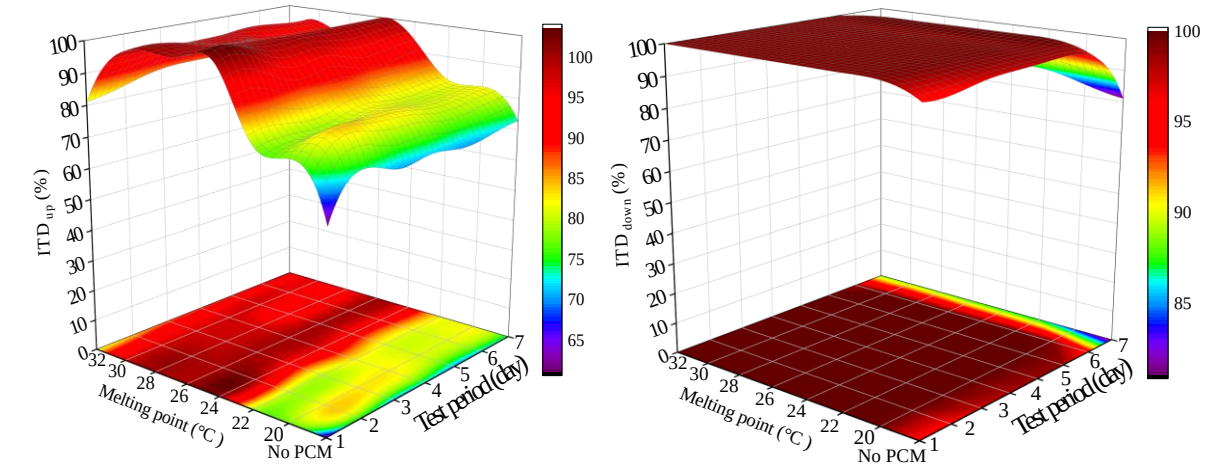

(d) Fargo

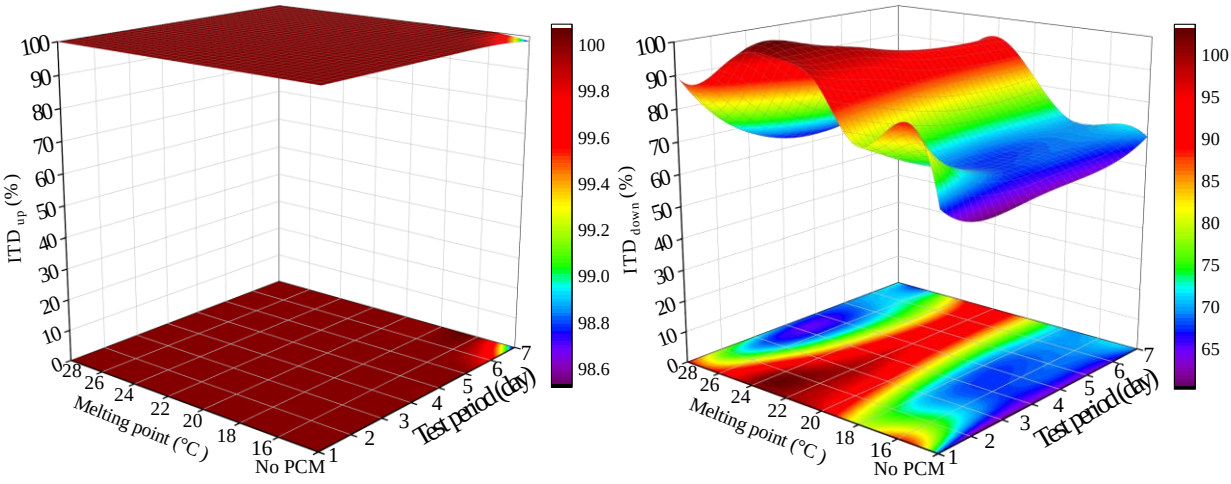

(e) Seattle

Figure 5.24. *ITD* contour of different cities (continued).

5.5.4. Effects of the Loading Conditions Associated with Different Months on the Selection of the PCM Melting Point

More energy is supposed to be consumed by the buildings for the hottest and coldest months than the moderate ones to maintain the indoor temperature in human beings' thermal comfort zone. To highlight the effect of the loading conditions associated with different months on the selection of the PCM melting point, the monthly thermal performance of the PCM-based wall located in Austin and Minneapolis is numerically explored. They are two U.S. cities

representing the “hot” and “cold” categories. The hourly temperature profile of the wall interior surface for the first week of each month is obtained respectively for both cities.

5.5.4.1. Loading Conditions Associated with Different Months in Austin

Figure 5.25 presents the indoor transient temperature profile of the wall subjected to the first week of three typical months in Austin, including January, May, and August. As shown in Figure 5.25(a), for January represents the cold months, the indoor temperature of nearly all the wall assemblies reinforced by PCM with various melting points are below the lower threshold temperature of the thermal comfort zone during the whole test period. The main function of the PCM integrated into the wall here is to absorb and store heat energy during the daytime and release it to increase the room temperature during the night. One can observe that the indoor instantaneous temperature is relatively even and close to the thermal comfort zone during the whole test period when PCM with a melting point of 16°C is integrated. Nevertheless, an HVAC system is still needed as a supplement to further increase the indoor temperature due to the cold weather. PCM with melting points over 24°C is unable to provide heat of fusion in this scenario since it stays in solid phase during the whole test period. For May that belongs to the “moderate” months (see Figure 5.25(b)), the indoor temperature of the reference wall without PCM oscillates from 15.4°C to 30.5°C, centering on the thermal comfort zone. The integration of the PCM with melting points ranging from 22°C to 24°C is found to effectively reduce the oscillation and keep the indoor temperature in the thermal comfort zone for most of the test period. Therefore, the oscillation centering on the thermal comfort zone tends to make full use of the latent heat capacity of the PCM with a melting point within the thermal comfort zone. The indoor temperature evolution over the first week of August is shown in Figure 5.25(c). In contrast to January, the indoor temperature of nearly all the wall assemblies is over the upper threshold

temperature of the thermal comfort zone for most of the test period. Even though the indoor temperature is kept in the thermal comfort zone when PCM with a melting point of 26°C is used, it starts to exceed 28°C from the third day due to the continuous heat energy input. In such a hot month in Austin, the natural cooling during the night is not enough to discharge the liquid PCM, and one possible strategy is discharging it with the help of an air conditioner during the off-peak period, thus provide more heat energy storage capacity for the next day.

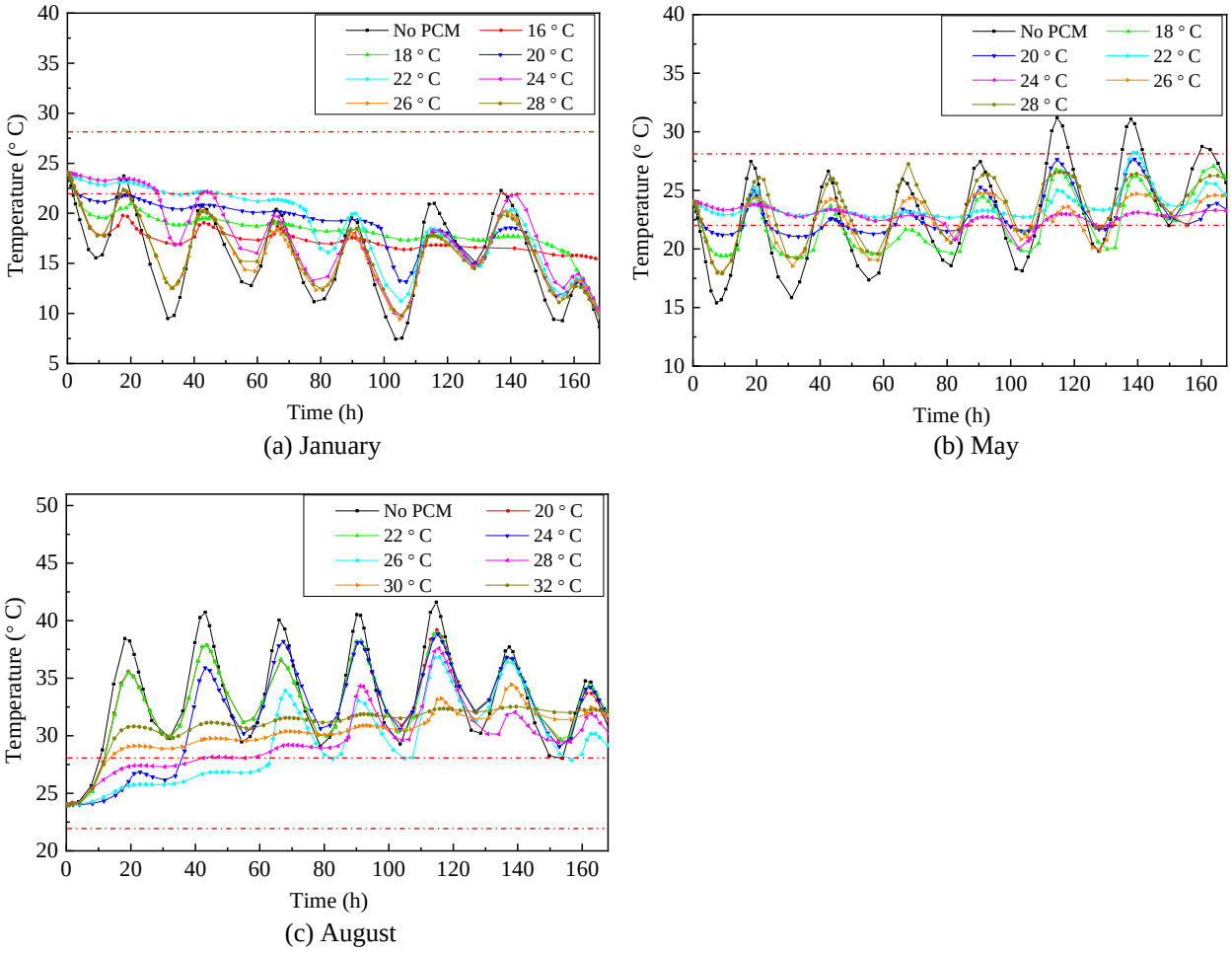

Figure 5.25. Indoor transient temperature over the first week of different months in Austin.

The feasibility of PCM and optimal PCM melting point on keeping the indoor thermal comfort is also assessed by comparing the indoor temperature amplitude of the reference wall and the wall reinforced by PCM with the optimal melting point (see Figure 5.26). Under the

same loading condition in Austin, the indoor temperature oscillation of the wall with proper PCM is found to be smaller and closer to the thermal comfort zone than the reference wall. Therefore, less energy input for the HVAC system is needed by the PCM-reinforced wall to keep the indoor thermal comfort due to its heat energy storage capacity and isothermal nature. For the cold months including December, January, and February, the optimal melting points range from 18°C to 20°C, which is below the lower threshold temperature of the thermal comfort zone. For the moderate months including March, April, May, October, and November, the optimal melting point interval increases to 22°C to 26°C, and the corresponding room temperature tends to be maintained in the thermal comfort zone for a longer time. For Jun, July, August, and September that are categorized as the hot months, the optimal PCM melting point interval is found to rise as high as 28°C to 30°C. In this scenario, even though the maximum indoor temperature of the PCM-based wall can be lowered, it still exceeds the upper threshold temperature of the thermal comfort zone due to the hot weather. Therefore, for both cold months and hot months, using PCM alone for passive heating or cooling is not enough to keep the indoor temperature in the comfort zone. An HVAC system is also needed to further regulate the room temperature.

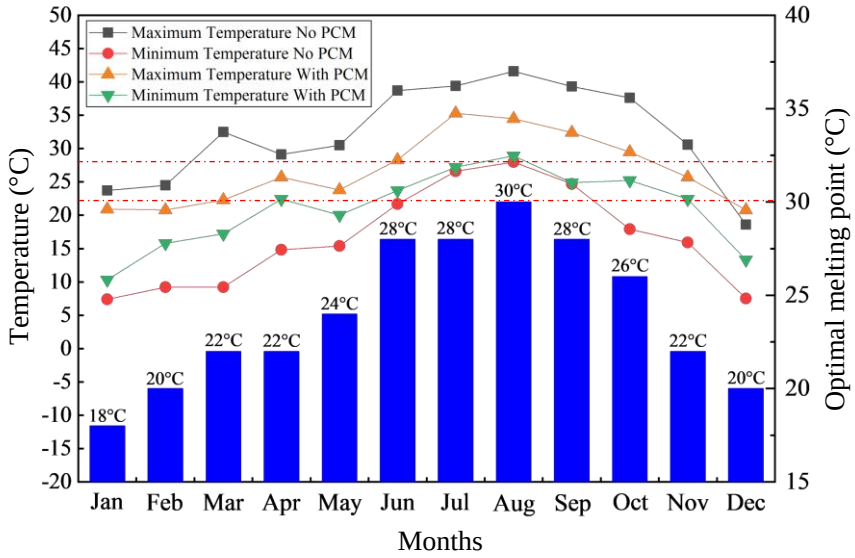

Figure 5.26. Optimal PCM melting point for different months in Austin.

Monthly ITD_{up} and ITD_{down} value of the PCM-based and reference wall are also generated and compared. As shown in Figure 5.27(a), the ITD_{up} value of both walls is 100% in January, February, and December since their indoor temperature is below the upper threshold temperature of the thermal comfort zone due to the cold weather. From March to November, the ITD_{up} value is significantly increased by incorporating proper PCM with an increased rate ranging from 2.7% to 56.5%. This confirms that theoretically, adjustable melting points per month could significantly amplify the best efficiency of latent heat energy of PCMs and achieve the optimal building energy saving. Note that this parametric study is merely based on theoretical assumptions, and there are currently few studies that enable addressing this gap. The evolution of ITD_{down} value (Figure 5.27(b)) further shows the feasibility of using PCM for "heating" the indoor air during cold months. The ITD_{down} value increases by 0.2% to 37.2% when PCM with optimal melting point is integrated. ITD_{down} value is not governing in the cases of hot months ranging from July to September, because the PCM incorporated in those hot months is used to reduce the indoor temperature and increase the ITD_{up} value.

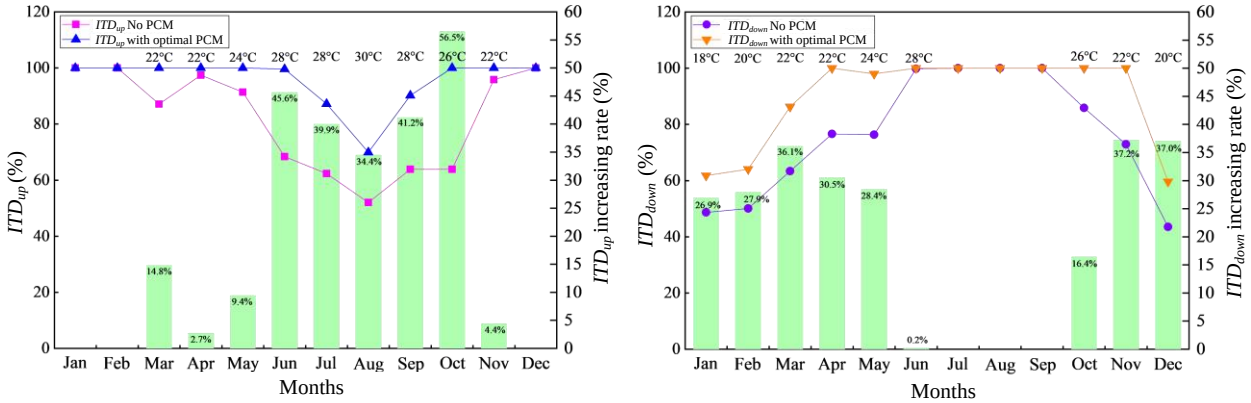

(a) ITD_{up} (b) ITD_{down}

Figure 5.27. Monthly ITD_{up} and ITD_{down} value of the PCM-based and reference wall.

5.5.4.2. Loading Conditions Associated with Different Months in Minneapolis

As a comprehensive analysis, the thermal performance of the PCM-reinforced wall and the reference wall is also investigated based on the monthly loading conditions of Minneapolis, which is chosen as the representative for cities located in the "cold" region. The indoor temperature profile of the wall subjected to typical months including January and August is generated. For January (see Figure 5.28(a)), the indoor temperature of all wall assemblies drops rapidly to 0 °C or lower within the test period owing to the extremely cold weather. The optimal melting point of the PCM to increase the minimum temperature is about -10 °C, which is far below the lower threshold temperature of the thermal comfort zone. For these months ranging from November to April, the utilization of PCM plays a negligible role in enhancing the thermal comfort of the buildings and downsizing the heating equipment. For the result of August that represents the hot months showed in Figure 5.28(b), the indoor temperature of the reference wall swings between 18.5 °C and 39.3 °C. The integration of PCM with melting points ranging from 26 °C to 28 °C diminishes the amplitude of the indoor temperature notably and effectively limits the indoor temperature oscillation within the thermal comfort zone for most of the test period.

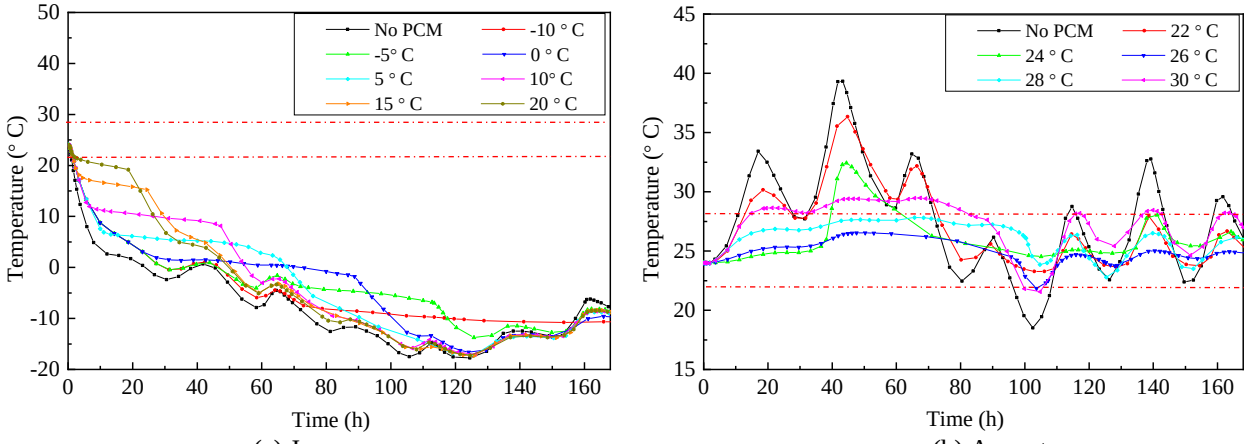

(a) January (b) August

Figure 5.28. Transient temperature of the interior wall surface over time in Minneapolis.

The optimal PCM melting point on keeping the indoor thermal comfort for different months of Minneapolis is also explored by comparing the indoor temperature amplitude of the reference wall and the wall reinforced by PCM with the optimal melting point. Only the results for the months ranging from May to October are presented in Figure 5.29 since the single utilization of PCM for passive heating for the rest of extremely cold months is useless. In contrast with the reference wall, the maximum and minimum indoor temperature of the PCM-based wall are limited within the thermal comfort zone from June to October due to the temperature regulation function provided by PCM. In addition, the optimal melting point of the PCM integrated for the hottest months including July and August is 28 °C, higher than the ones for other cooler months. Therefore, the optimal melting point of the PCM increases with the rise of the loading conditions. This conclusion is consistent with the one drawn from Austin.

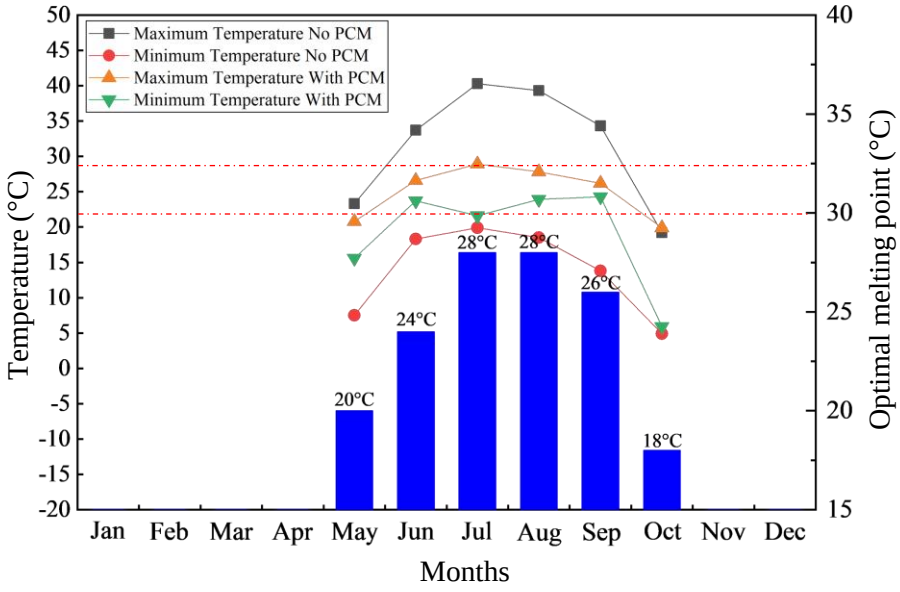

Figure 5.29. Optimal PCM melting point for different months in Minneapolis.

Monthly ITD_{up} and ITD_{down} value of the PCM-based and the reference wall located in Minneapolis are further explored to assess the impact of integrated PCM with different melting points. As shown in Figure 5.30(a), compared with that of the reference wall, the ITD_{up} value

increases by 17.2% to 49.5% when PCM with optimal melting point is integrated as an internal layer of the building wall. In Figure 5.30(b), the ITD_{down} value of the PCM-based wall is kept as high as 100% for nearly all the moderate months ranging from June to September, revealing the effectiveness of PCM in diminishing the energy consumption by the HVAC system. When PCM with optimal melting point is integrated, the corresponding ITD_{down} value increases by 5.6% to 32.6% from May to October. Therefore, the use of heating equipment can also be downsized by making the most of the latent heat capacity of PCM.

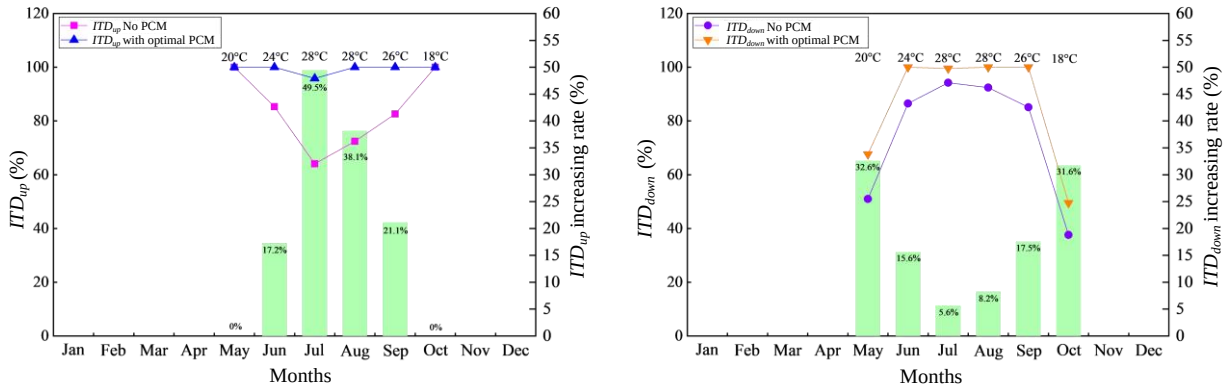

(a) ITD_{up} (b) ITD_{down}

Figure 5.30. Monthly ITD_{up} and ITD_{down} value of the PCM-based and reference wall.

5.6. Summary

The objective of this research is to elucidate the relationship between the optimal PCM melting point and critical design parameters including PCM layer location, thickness, and the loading conditions associated with different climate zones and months. A numerical model of a frame wall integrated with a thin PCM layer with different melting points is built-in COMSOL Multiphysics® software and validated by experimental data. A few specific conclusions, which might be useful for the utilization of the PCM-based building envelope in different climate regions, are listed below:

The optimal location of the PCM layer should be close to the wall interior surface to make sure it is not directly exposed to the external environment. The ITD_{up} and ITD_{down} value of the wall assembly with PCM installed on the wall interior side drop from 100% to 84% and 82% respectively when the same PCM is installed on the wall exterior side. Enough thermal insulation outside the PCM can block a considerable amount of inward heat or cold so that the PCM is able to provide a longer service time without being easily saturated.

In the investigated thickness ranging from 2.5 to 15 mm, increasing the thickness of the PCM layer leads to better building energy efficiency due to its contribution to the heat energy storage capacity and thermal inertia of the frame wall. For specific, the wall with a 15-mm PCM layer proves its superiority on the thermal performance with a maximum peak temperature reduction of 8.8% and a maximum trough temperature increase of 16.7% compared with the wall reinforced by 2.5-mm PCM layer. Nevertheless, the thickness of the PCM layer only shows little impact on the optimal PCM melting point.

The selection of the PCM melting point for a certain building envelope is highly dependent on the thermal loading conditions. The optimal PCM melting point is in direct proportion to the input loading conditions, suggesting that a higher PCM melting point is needed for a building envelope subjected to higher input temperature. Specifically, for the buildings located in cities with a hot climate like the summer of Las Vegas, the optimal PCM melting point ranges from 26 °C to 30 °C to “cool down” the indoor air; for the buildings located in cities with a moderate climate like the summer of Fargo, the optimal PCM melting point is about 24 °C to improve the indoor thermal comfort; for the buildings located in cities with a relatively cold climate like the summer of Seattle, the optimal PCM melting point is about 20 °C to 24 °C to “warm-up” the indoor air. The selection principle for the optimal PCM melting point is making

sure the diurnal service effectiveness of the PCM through a maximized converting between solid and liquid under a certain loading condition.

PCM with a melting point within the occupant thermal comfort zone (22 °C to 28 °C) can increase indoor thermal comfort duration more effectively for the “moderate” loading conditions. For example, when the PCM melting point is about 26 °C, the indoor temperature can be kept in the thermal comfort zone for the whole test period in Fargo with moderate loading conditions, which is 34.5% and 75% longer than Miami and Las Vegas respectively when the same PCM is used. The utilization of PCM in areas or months with extremely high or low thermal loading conditions does not exhibit high efficiency.

5.7. References

[1] M. Li, G. Gui, Z. Lin, L. Jiang, H. Pan, X. Wang, Numerical Thermal Characterization and Performance Metrics of Building Envelopes Containing Phase Change Materials for Energy-Efficient Buildings, Sustainability 10 (8) (2018) 2657.

[2] M.R. Anisur, M.H. Mahfuz, M.A. Kibria, R. Saidur, I.H.S.C. Metselaar, T.M.I. Mahlia, Curbing global warming with phase change materials for energy storage, Renew. Sustain. Energy Rev. 18 (2013) 23-30.

[3] L. Navarro, A. De Gracia, S. Colclough, M. Browne, S.J. McCormack, P. Griffiths, L.F. Cabeza, Thermal energy storage in building integrated thermal systems: A review. Part 1. active storage systems, Renew. Energy 88 (2016) 526-547.

[4] G. Bakan, B. Gerislioglu, F. Dirisaglik, Z. Jurado, L. Sullivan, A. Dana, C. Lam, A. Gokirmak, H. Silva, Extracting the temperature distribution on a phase-change memory cell during crystallization, J. Appl. Phys. 120 (2016) 164504.

[5] L.M. Bal, S. Satya, S. N. Naik, V. Meda, Review of solar dryers with latent heat storage systems for agricultural products, Renew. Sustain. Energy Rev. 15 (2011) 876-880.

[6] De Gracia, A. and Cabeza, L.F., Phase change materials and thermal energy storage for buildings, Energy and Buildings 103 (2015) 414-419.

[7] A. Sharma, V.V. Tyagi, C.R. Chen, D. Buddhi, Review on thermal energy storage with phase change materials and applications, Renew. Sustain. Energy Rev. 13 (2) (2009) 318-345.

[8] L. F. Cabeza, A. Castell, C. D. Barreneche, A. De Gracia, A. I. Fernández, Materials used as PCM in thermal energy storage in buildings: A review, Renew. Sustain. Energy Rev. 15 (2011) 1675-1695.

[9] G. Alva, Y. Lin, G. Fang, An overview of thermal energy storage systems, Energy 144 (2018) 341-378.

[10] L. Navarro, A. de Gracia, D. Niall, A. Castell, M. Browne, S.J. McCormack, P. Griffiths, L.F. Cabeza, Thermal energy storage in building integrated thermal systems: A review. Part 2. Integration as passive system, Renew. Energy, 85 (2016) 1334-1356.

[11] A. Castell, I. Martorell, M. Medrano, G. Pérez, L.F. Cabeza, Experimental study of using PCM in brick constructive solutions for passive cooling, Energy Build. 42 (4) (2010) 534-540.

[12] F. Souayfane, F. Fardoun, P.H. Biwole, Phase change materials (PCM) for cooling applications in buildings: A review, Energy Build. 129 (2016) 396-431.

[13] V. D. Cao, S. Pilehvar, C. Salas-Bringas, A. M. Szczotok, J. F. Rodriguez, M. Carmona, N. Al-Manasir,A.L. Kjøniksen, Microencapsulated phase change materials for enhancing

the thermal performance of Portland cement concrete and geopolymer concrete for passive building applications, Energy Convers. and Manage. 133 (2017) 56-66.

[14] Y. Konuklu, M. Ostry, H.O. Paksoy, P. Charvat, Review on using microencapsulated phase change materials (PCM) in building applications. Energy Build. 106 (2015) 134-155.

[15] S.E Kalnæs, B.P. Jelle, Phase change materials and products for building applications: A state-of-the-art review and future research opportunities, Energy Build. 94 (2015) 150-176.

[16] B. Gerislioglu, G. Bakan, R. Ahuja, J. Adam, Y.K. Mishra, A. Ahmadivand, The role of Ge2Sb2Te5 in enhancing the performance of functional plasmonic devices, Mater. Today Phys. 12 (2020) 100178.

[17] A. Ahmadivand, B. Gerislioglu, N. Pala, Active control over the interplay between the dark and hidden sides of plasmonics using metallodielectric Au– Ge2Sb2Te5 unit cells, J. Phys. Chem. C, 121 (36) (2017) 19966-19974.

[18] X. Xu, Y. Zhang, K. Lin, H. Di, R. Yang, Modeling and simulation on the thermal performance of shape-stabilized phase change material floor used in passive solar buildings, Energy Build. 37 (10) (2005) 1084-1091.

[19] M. Alam, H. Jamil, J. Sanjayan, J. Wilson, Energy saving potential of phase change materials in major Australian cities, Energy Build. 78 (2014) 192-201.

[20] J. Lei, J. Yang, E.H. Yang, Energy performance of building envelopes integrated with phase change materials for cooling load reduction in tropical Singapore, Appl. energy 162 (2016) 207-17.

[21] L. Karim, F. Barbeon, P. Gegout, A. Bontemps, L. Royon, New phase-change material components for thermal management of the light weight envelope of buildings, Energy Build. 68 (2014) 703-706.

[22] J.S. Sage-Lauck, D.J. Sailor, Evaluation of phase change materials for improving thermal comfort in a super-insulated residential building, Energy Build. 79 (2014) 32-40.

[23] F. Kuznik, J. Virgone, J. Noel, Optimization of a phase change material wallboard for building use, Appl. Therm. Eng. 28 (11-12) (2008) 1291-1298.

[24] F. Kuznik, J. Virgone, Experimental assessment of a phase change material for wall building use, Appl. energy, 86 (10) (2009) 2038-2046.

[25] F. Kuznik, D. David, K. Johannes, J.J. Roux, A review on phase change materials integrated in building walls, Renew. Sustain. Energy Rev. 15 (1) (2011) 379-391.

[26] S.A. Memon, Phase change materials integrated in building walls: A state of the art review, Renew. Sustain. Energy Rev. 31 (2014) 870-906.

[27] F. Berroug, E.K. Lakhal, M. El Omari, M. Faraji, H. El Qarnia, Thermal performance of a greenhouse with a phase change material north wall, Energy Build. 43 (11) (2011) 3027-3035.

[28] L. Erlbeck, P. Schreiner, F. Fasel, F.J. Methner, M. Rädle, Investigation of different materials for macroencapsulation of salt hydrate phase change materials for building purposes, Constr. Build. Mater. 180 (2018) 512-518.

[29] K. Zhong, S. Li, G. Sun, S. Li, X. Zhang, Simulation study on dynamic heat transfer performance of PCM-filled glass window with different thermophysical parameters of phase change material, Energy Build. 106 (2015) 87-95.

[30] T. Silva, R. Vicente, F. Rodrigues, A. Samagaio, C. Cardoso, Performance of a window shutter with phase change material under summer Mediterranean climate conditions, Appl. Therm. Eng. 84 (2015) 246-256.

[31] E.M. Alawadhi, Using phase change materials in window shutter to reduce the solar heat gain, Energy Build. 47 (2012) 421-429.

[32] K. Nagano, S. Takeda, T. Mochida, K. Shimakura, T. Nakamura, Study of a floor supply air conditioning system using granular phase change material to augment building mass thermal storage—heat response in small scale experiments, Energy Build. 38 (5) (2006) 436-446.

[33] X. Jin, X. Zhang, Thermal analysis of a double layer phase change material floor, Appl. Therm. Eng. 31 (10) (2011) 1576-1581.

[34] A. Pasupathy, R. Velraj, Effect of double layer phase change material in building roof for year round thermal management, Energy Build. 40 (3) (2008) 193-203.

[35] B.M. Diaconu, M. Cruceru, Novel concept of composite phase change material wall system for year-round thermal energy savings, Energy Build. 42 (10) (2010) 1759-1772.

[36] C.K. Halford, R.F. Boehm, Modeling of phase change material peak load shifting, Energy Build. 39 (3) (2007) 298-305.

[37] V.V. Tyagi, D.P.C.M. Buddhi, PCM thermal storage in buildings: a state of art, Renew. Sustain. Energy Rev. 11 (6) (2007) 1146-1166.

[38] D. Zhou, C.Y. Zhao, Y. Tian, Review on thermal energy storage with phase change materials (PCMs) in building applications, Appl. energy, 92 (2012) 593-605.

[39] D.A. Neeper, Thermal dynamics of wallboard with latent heat storage, Solar energy 68 (5) (2000) 393-403.

[40] Y.P. Zhang, K.P. Lin, R. Yang, H.F. Di, Y. Jiang, Preparation, thermal performance and application of shape-stabilized PCM in energy efficient buildings, Energy Build. 38 (10) (2006) 1262-1269.

[41] M. Saffari, A. De Gracia, C. Fernández, L.F. Cabeza, Simulation-based optimization of PCM melting temperature to improve the energy performance in buildings, Appl. Energy 202 (2017) 420-434.

[42] M. Saffari, A. de Gracia, S. Ushak, L.F. Cabeza, Economic impact of integrating PCM as passive system in buildings using Fanger comfort model, Energy Build. 112, (2016) 159-172.

[43] M. Saffari, A. de Gracia, S. Ushak, L.F. Cabeza, Economic impact of integrating PCM as passive system in buildings using Fanger comfort model, Energy Build. 112, (2016) 159-172.

[44] S. Schiavoni, F. Bianchi, F. Asdrubali, Insulation materials for the building sector: A review and comparative analysis, Renew. Sustain. Energy Rev. 62 (2016) 988-1011.

[45] B. Rodríguez-Soria, J. Domínguez-Hernández, J.M. Pérez-Bella, J.J. del Coz-Díaz, Review of international regulations governing the thermal insulation requirements of residential buildings and the harmonization of envelope energy loss, Renew. Sustain. Energy Rev. 34 (2014) 78-90.

[46] Y. Feng, Thermal design standards for energy efficiency of residential buildings in hot summer/cold winter zones, Energy Build. 36 (12) (2004) 1309-1312.

[47] N. Aste, A. Angelotti, M. Buzzetti, The influence of the external walls thermal inertia on the energy performance of well insulated buildings, Energy Build. 41 (11) (2009) 1181-1187.

[48] L.F. Cabeza, C. Castellon, M. Nogues, M. Medrano, R. Leppers, O. Zubillaga, Use of microencapsulated PCM in concrete walls for energy savings, Energy Build. 39 (2) (2007) 113-119.

[49] X. Jin, M.A. Medina, X. Zhang, Numerical analysis for the optimal location of a thin PCM layer in frame walls, Appl. Therm. Eng. 103 (2016) 1057-1063.

[50] COMSOL Multiphysics®, version5.2a < https://www.comsol.com/>.

[51] H. Fayaz, N.A. Rahim, M. Hasanuzzaman, A. Rivai, R. Nasrin, Numerical and outdoor real time experimental investigation of performance of PCM based PVT system, Solar Energy 179 (2019) 135-150.

[52] L. Royon, L. Karim, A. Bontemps, Thermal energy storage and release of a new component with PCM for integration in floors for thermal management of buildings, Energy Build. 63 (2013) 29-35.

[53] T.L. Bergman, F.P. Incropera, A.S. Lavine, D.P. DeWitt, Introduction to heat transfer, John Wiley & Sons 2011.

[54] N.P. Sharifi, G.E. Freeman, A.R. Sakulich, Using COMSOL modeling to investigate the efficiency of PCMs at modifying temperature changes in cementitious materials – Case study, Constr. Build. Mater. 101 (2015) 965-974.

[55] M. Rady, Granular phase change materials for thermal energy storage: Experiments and numerical simulations, Appl. Therm. Eng. 29 (14-15) (2009) 3149-3159.

[56] Y. Fang, A comprehensive study of phase change materials (PCMs) for building walls applications, PhD diss., University of Kansas, 2009.

[57] B.M. Marino, N. Muñoz, L.P. Thomas, Calculation of the external surface temperature of a multi-layer wall considering solar radiation effects, Energy Build. 174 (2018) 452-463.

[58] R. Ye, W. Lin, K. Yuan, X. Fang, Z. Zhang, Experimental and numerical investigations on the thermal performance of building plane containing CaCl2· 6H2O/expanded graphite composite phase change material, Appl. energy 193 (2017) 325-335.

[59] A. Sharma, C.R. Chen, N. Vu Lan, Solar-energy drying systems: A review, Renew. Sustain. Energy Rev. 13 (6-7) (2009) 1185-1210.

[60] G. Evola, L. Marletta, F. Sicurella, A methodology for investigating the effectiveness of PCM wallboards for summer thermal comfort in buildings, Build. Environ. 59 (2013) 517-527.

6. A NOVEL RESIDENTIAL FRAME WALL CONTAINING PCM WITH HYBRID MELTING POINTS FOR ENERGY-EFFICIENT BUILDINGS

6.1. Introduction

The building industry is globally responsible for more than one-third of overall energy demand and is expected to keep its increasing trend [1]. Therefore, improving the energy efficiency of buildings is one of the major topics for energy saving at the international level. One of the solutions, which has attracted researchers and engineers, is to introduce thermal energy storage (TES) systems into building envelopes to realize sustainable and renewable energy utilization [2]. Energy storage can be classified as sensible heat, latent heat, and chemical energy or products in a reversible chemical reaction[3]. To date, most of the researchers investigating TES have focused on latent heat storage which can be implemented with the thermal energy charge and discharge of phase change material (PCM) due to its significant reduction in storage volume. PCM such as calcium chloride hexahydrate can store/release 193 kJ/kg of heat on the phase transition process, as compared to conventional building materials like concrete, having a sensible heat capacity of about 1.0 kJ/kg [4]. A further advantage of the latent heat storage is that the phase transition process of PCM occurs over a narrow temperature range corresponding to its melting temperature, resulting in a reduced temperature fluctuation in building applications.

Much research has proven that integrating PCM into building envelopes shows promising enhancement of the building energy performance and thereby reducing the environmental impact related to energy use [5, 6]. Being integrated into different building components (e.g., wallboards, concrete blocks, ceilings, and floors), the PCMs can store a large amount of heat by a change of phase from solid to liquid as the ambient temperature increases above their melting point when the exterior temperature and solar radiation increase. This whole process can be

completed over a limited temperature range and the PCMs act as an isothermal reservoir of heat [7]. When the ambient temperature drops below their freezing point, the thermal energy stored can be released automatically to heat the indoor air by changing the phase of PCMs from liquid to solid.

In recent years, investigation on design parameters of the PCM-based building envelopes buildings has drawn more and more attention, aiming to improve thermodynamic response and energy efficiency of building envelope. Research has shown that choosing the PCM melting temperature in different climate conditions is a key factor to improve the energy performance in buildings. Saffari et al. [8] studied the thermal performance of buildings reinforced with PCM that has different melting points. They found that in Madrid climate zone, PCM with 27 °C achieved higher energy savings in summer (cooling period) whereas PCM with 23 °C was most effective in winter (heating period). Tunçbilek et al. [9] conducted research to enhance the thermal behavior of a standard-sized hollow brick by filling it with PCM for the Marmara Region in Turkey. Locating the PCM near the interior and increasing the quantity of PCM reduced the cooling load by 17.6%. The annual optimum phase transition temperature was found to be 18 °C. Sovetova et al. [10] evaluated the thermal performance and energy efficiency performance of PCM integrated residential buildings located in eight different cities (Abu-Dhabi, Dubai, Faisalabad, Mecca, Jodhpur, Nouakchott, Cairo, and Biskra) from hot desert climate zone was with thirteen different PCMs in EnergyPlus. They concluded that except for Cairo and Biskra, the best PCM were close to the cooling set point suggesting that in the hot desert climate, PCM with higher melting points perform better. One can see that the existing studies have made a great effort to determine the optimal PCM melting point for building envelopes subjected to different weather conditions. However, most of the previous studies were trying to find an annual

optimal PCM melting point for a building without considering the dynamic change of the weather condition applied on the same building during different seasons and months.

To comprehensively address the factors affecting the selection of PCM melting point for a building envelope, the author has investigated the thermal performance of PCM-based building envelopes subjected to various loading conditions associated with different locations (climate zones) and months in Chapter 5. It was found that the selection of the PCM melting point for a certain building envelope is highly dependent on the thermal loading conditions. The optimal PCM melting point is in direct proportion to the input loading conditions, suggesting that a higher PCM melting point is needed for a building envelope subjected to higher input temperature. For the buildings located in cities like Minneapolis and Austin which experience significant temperature changes in different months, the optimal PCM melting points vary from 18 °C to 30 °C, depending on the input loading conditions. Expected annual energy savings are not achievable if PCM with a fixed melting point is integrated, because the exploitation of latent heat can be maximized in certain months while ineffective for other months. For example, 28 °C was found to be the optimal melting point for June to September in Austin. If PCM with this melting point was integrated, the low ambient temperature in months like December, January, and February which was below the PCM melting point temperature prevented the PCM to absorb heat to reach its melting point temperature and melt. In this case, the maximum annual savings cannot be achieved since the low utilization rate of latent heat of the PCM.

U.S. Department of Energy is conducting research on preparing solid-state PCM with tunable thermal energy storage [11]. Some researchers are also proposing to prepare the composite PCMs with tunable melting points with a large temperature interval instead of a particular temperature point, and the composite exhibits a relatively high thermal storage

capacity at the same time [12][13]. The research provides a possibility of utilizing PCM with tunable melting points in "smart" building envelopes that can adjust its melting temperature with the dynamic loading conditions and achieve the maximum utilization of its latent heat.

So far, limited studies have explored the feasibility of using PCM with different melting points in the same building to improve the indoor thermal comfort for both heating and cooling dominant climates. To fill this need, this study aims to numerically investigate the potential of integrating PCMs with more than one melting point in a multi-layer residential wall to maximize the yearly activation period of PCMs' latent heat and thus further enhance building energy efficiency. The thermodynamics of both models are simulated using COMSOL Multiphysics® software.

6.2. Problem Description

6.2.1. Description of the Multilayer Frame Walls

The reference frame wall systems considered are derived from a typical North American residential wall [14], which is schematically shown in Figure 6.1. From the interior to the exterior side, reference wall 1(RW1) consists of a 12.7-mm gypsum wallboard, a 30-mm insulating layer, and a 20.5-mm oriented strand board (OSB). Reference wall 2 (RW2) has the identical assembly with RW1, but a 10-mm PCM layer is added between the gypsum board and insulating layer. Note the thickness of the insulating layer was reduced from 89 mm in Chapter 5 to 30 mm to allow more heat or cold penetration through the wall and thus highlight the thermal performance of PCM. The melting point of the PCM integrated into RW2 is fixed at 24 °C which is closed to the thermal comfort temperature of human beings. To evaluate the thermal performance of the wall system including PCMs with more than one melting point, two different cases are studied to determine its potential benefits.

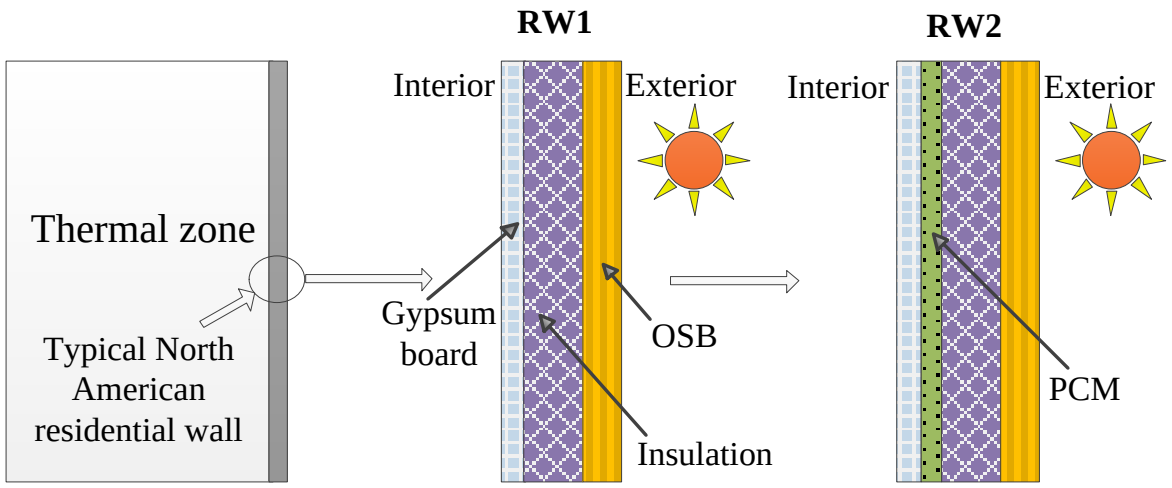

Figure 6.1. Schematics of reference wall systems.

6.2.2. Case One—Multilayer Wall Including Composite PCM with Hybrid Melting Points

The investigated model of case one is shown in Figure 6.2 (a). This wall is assembled with the same composition as the RW2 shown in Figure 6.1, but the PCM layer is replaced with a composite PCM that consists of three equal amounts of PCMs with a melting point of 16 °C, 24 °C, and 32 °C, respectively. The PCM used is consistently labeled in such a way that the number after PCM denotes its melting point. For example, PCM24 refers to the PCM with a melting point of 24 °C. The selected melting points aim to adapt to various loading conditions including cold, mild, and hot months. The total volume of the composite PCM is the same as that of the PCM integrated into RW2. In the analysis, the same time-history loading conditions are applied on all walls to determine the thermal performance by integrating PCM with hybrid melting points into building envelopes.

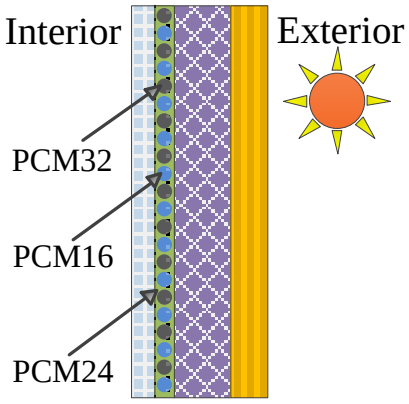

Figure 6.2. Schematics of wall systems including PCMs with hybrid melting points.

6.2.3. Case Two—PCM Blocks with Different Melting Points

In order to comprehensively analyze the working mechanism of the composite PCM, a 10 mm×10 mm of composite PCM block consisted of an equal amount of PCMs is isolated from the wall structure (see Figure 6.3). Composite 1 consists of PCM24 and PCM30 (denoted by PCM24-30) with a latent heat of 180 J/g, and composite 2 consists of PCM27 and PCM27 (denoted by PCM27-27) with a latent of 180 J/g. To evaluate the impact of latent heat, the thermal performance of PCM24-30 with a latent of 360 J/g is also investigated. The heat transfer behavior of all composite PCM blocks is explored in detail under the same loading condition. The original temperature of the blocks is 18 °C and the input temperature is assumed to be constant at 35°C.

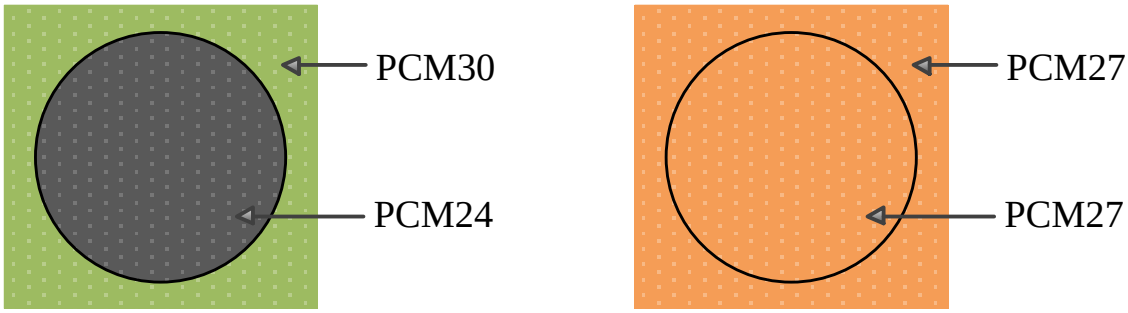

Figure 6.3. Schematics of PCM blocks with (a) hybrid melting point and (b) single melting point.

6.3. Methodology

6.3.1. Mathematical Model

A two-dimensional (2D) multi-layered transient conduction model is developed with the COMSOL Multiphysics® software [15] to simulate the thermal behavior of the multilayer wall system reinforced with PCM. This software is used to create and mesh the geometrical model of the multilayer wall and to solve the heat transfer equation. In the simulation, the transient thermal response of both solid and liquid PCMs is involved due to the heat transfer caused by their "phase change" behavior. Only conduction heat transfer mode is considered inside the wall, even during the PCM melting or solidifying processes. Convection in the liquid phase is not considered in this simulation because it's not significant during liquid forms of PCM in this case [14, 16]. In addition, other layers like the gypsum board and insulating layer that tightly enclosing the PCM prevent natural convection inside the PCM [17]. The transient thermal behavior of a solid is governed by the partial differential equation as follows [18]:

$$\frac{\partial}{\partial x}\left(\lambda \frac{\partial T}{\partial x}\right) + \frac{\partial}{\partial y}\left(\lambda \frac{\partial T}{\partial y}\right) = \rho C_P \frac{\partial T}{\partial t}, \tag{6.1}$$

where T is the temperature (K), λ is the thermal conductivity of the material (W/m K), ρ is the density of the material (kg/m^3), and C_P is the specific heat of the material (J/kg K).

For simplicity, the model of the wall is established under the following assumptions: (a) All layers of the wall system are assumed to be homogenous and isotropic; (b) The heat transfer through the wall is one-dimensional (1D); (c) The thermal expansion of the materials is not considered; (d) The thermophysical properties of the materials are constant except the density of the PCM in the solid and liquid phase, and (e) For multi-layered wall systems, the contact resistance between different layers is negligible. Since the thermal conductivity is assumed to be constant through each material, and the system is isolated in direction, Eq. (5.3) can be reduced

to a 1D heat transfer equation as shown in Eq. (6.2) [19], in which the thermal and physical properties of each material used in this study are shown in Table 6.1.

$$\frac{\partial^2 T}{\partial x^2} = \frac{\rho C_P}{\lambda}\frac{\partial T}{\partial t}, \tag{6.2}$$

Table 6.1. Thermal properties of materials [14].

Materials	**Density (kg/m^3)**	**Specific heat capacity (kJ/(kg K))**	**Thermal conductivity (W/m K)**
Gypsum board	800	1.09	0.16
Insulating layer	12.7	0.84	0.045
OSB	650	1.21	0.13
PCM*	880 (solid)/760 (liquid)	2.0	0.20

* The heat of fusion and melting point of PCM is specified in each investigated section.

In COMSOL Multiphysics® software, the dynamics of the phase change process from phase I (solid) to phase II (liquid) in PCM is taken into consideration using the equation below [19]:

$$\rho_{PCM} = \rho_{phase1}\beta + \rho_{phase2}(1-\beta), \tag{6.3 a}$$

$$\lambda_{PCM} = \lambda_{phase1}\beta + \lambda_{phase2}(1-\beta), \tag{6.3 b}$$

$$C_{p,PCM} = \frac{1}{\rho_{PCM}}\left(\rho_{phase1}C_{p,phase1}\beta + \rho_{phase2}C_{p,phase2}(1-\beta)\right) + L\frac{\partial \alpha_m}{\partial T}, \tag{6.3 c}$$

where C_p is the specific heat (J/kg K), L is the latent heat of fusion (J/kg). Given the PCM is assumed to have an identical thermal conductivity in solid and liquid phases, Eq. (6.3 b) can be rewritten as:

$$\lambda_{PCM} = \lambda_{phase1} = \lambda_{phase2}, \tag{6.4 a}$$

and α_m is:

$$\alpha_m = \frac{1}{2}\frac{\rho_{phase2}(1-\beta) - \rho_{phase1}\beta}{\rho_{phase2}(1-\beta) + \rho_{phase1}\beta}, \tag{6.4 b}$$

where β is the volume fraction of PCM at initial phase I (solid); α_m represents the mass percentage of PCM that is transferred from phase 1 to phase 2. The transition interval of PCM material between solid and liquid phase is not ideally zero, and a narrow temperature range of 5 °C is considered according to [20] in this simulation.

6.3.2. Boundary Conditions

The boundary conditions of the governing equation are

$$T\ (0, t) = T_i\ (x = 0) \tag{6.5 a}$$

$$T\ (\delta, t) = T_e\ (x = \delta) \tag{6.5 b}$$

where T is the temperature, t is time, t is the thickness of the wall, T_i is the interior surface temperature of the wall, and T_e is the exterior solar-air temperature of the wall, respectively.

The initial condition needed to solve the system of equations is a constant temperature for the whole wall that is equal to the interior temperature (24 °C). Figure 6.4 shows the artificial solar-air temperature that follows the sine function for 28 days covering 7 days in typical loading conditions including cold, mild, and hot scenarios. On a typical cold season, the temperature applied on the wall exterior surface is assumed to swing between 4 °C to 24 °C centering at 14 °C. On a typical mild season, the temperature is assumed to swing between 14 °C to 34 °C centering 24 °C. In contrast, in a typical hot season, the temperature is higher, which is assumed to swing between 24 °C to 44 °C centering 34 °C. The overall temperature profile of the input loading condition consisted of four 7-day temperature fragments following the order of mild-hot-mild-cold to simulate a seasonal temperature change. Under this loading condition, the instantaneous temperature of the interior surface of the gypsum board is recorded to assess the efficiency of latent heat of PCM with different melting points. For the heat transfer analysis of PCM blocks, the initial temperature of the whole block is set to 18 °C and a constant temperature

of 35 °C is applied on the exterior surface of the blocks. The instantaneous temperature of the interior surface of the two investigated blocks is recorded and compared to explore the working mechanism of PCM.

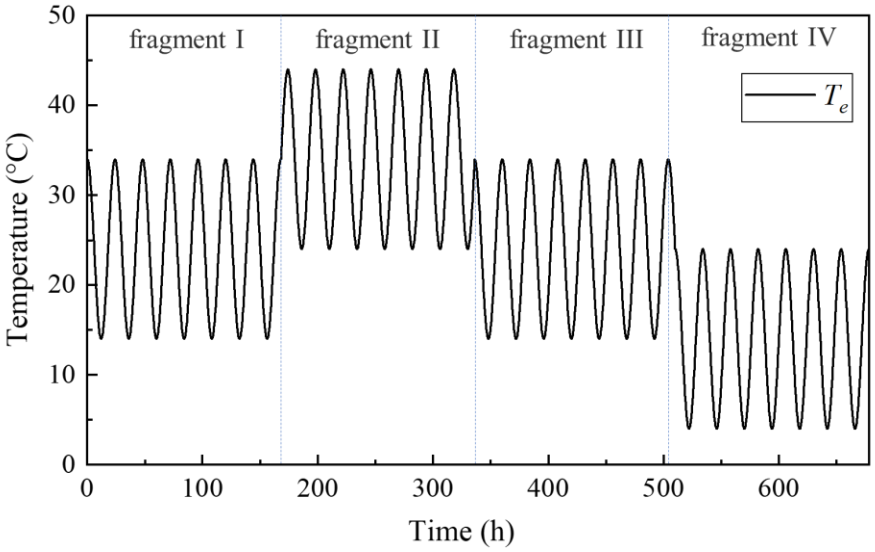

Figure 6.4. Solar-air temperature applied on the wall exterior surface.

6.3.3. Grid Sensitivity Check and Model Calibration

The mesh generation and grid check are presented in Chapter 5 and "extra fine" meshing is used in this study because of its high accuracy up to 99.8%. The numerical model in COMSOL is also validated in Chapter 5 and will not be presented in this chapter again due to the redundancy.

6.3.4. Performance Indexes for Assessing Thermal Performance of the Multilayer Wall System

In this study, performance indexes including decrement, increment factor, and the intensity of thermal discomfort (*ITD*) are used to evaluate the thermal performance of the PCM-based wall system. The decrement is defined as the reducing percentage of the maximum indoor temperature of the wall assembly compared to that of RW1. The increment is defined as the

increasing percentage of the minimum indoor temperature of the wall assembly compared to that of RW1. ITD_{up} and ITD_{down} reflect the intensity of thermal discomfort for overheating and overcooling, respectively, which are defined in Chapter 5 in detail. Combination use of those performance indexes aims to comprehensively assess the thermodynamics of PCM.

6.4. Results and Discussion

6.4.1. Case One—Multilayer Wall Including Composite PCM with Hybrid Melting Points

In this section, the thermal performance of an external building wall incorporating PCM with hybrid melting points is studied considering the dynamic year-round loading conditions. The artificial solar-air temperature profile with four temperature fragments shown in Figure 6.4 is applied on the wall exterior surface of RW1, RW2, and the proposed wall, respectively. The instantaneous temperature of the gypsum board interior face of each wall is obtained and discussed.

6.4.1.1. Decrement and Increment Factor

Figure 6.5 shows the instantaneous temperature profile of RW1, RW2, and the proposed wall under the same loading condition. It is evident that the incorporation of PCM (shown in red and blue) decreases the indoor temperature swing due to the activated latent heat storage capacity of PCM. The room temperature of the wall equipped with PCM is retained in the thermal comfort zone (22 °C to 28 °C as marked by dashed lines) for a longer time during the 28 days test period. This is consistent with the results of Li et al. [21] and Kim et al. [22] who demonstrated that embedding PCM into a wall helps maintain comfortable room temperature during intermittent heating operation, and extends this finding to cooling operation.

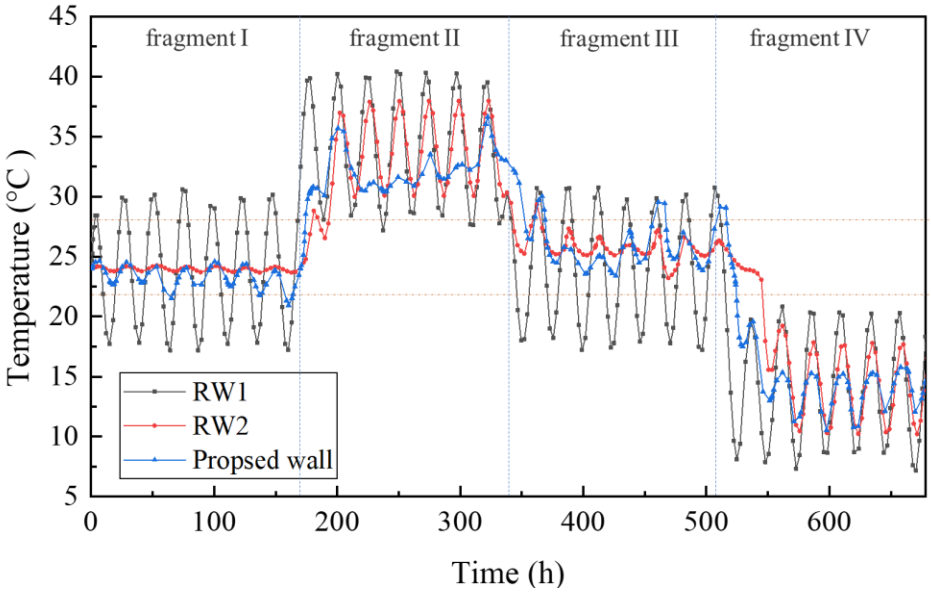

Figure 6.5. Instantaneous indoor temperature of RW1, RW2, and the proposed wall.

In Figure 6.6, the histogram shows the 7-days' average maximum and the minimum peak of the instantaneous temperature of all walls in each temperature fragment; the scatter gram shows the decrement and increment factor (ø) of RW2 and the proposed wall, which are also presented on the top of the corresponding column. As shown in Figure 6.6(a), the maximum indoor temperature of RW1 is 40.4 °C which appears in fragment II due to the high input temperature. When the 10-mm PCM with a melting point of 24 °C and latent heat capacity of 180 J/g is integrated, the corresponding maximum indoor temperature decreases to 37.8 °C, resulting in a decrement factor of 6.4% owing to the temperature regulation function of PCM. By contrast, the maximum indoor temperature of the proposed wall incorporating PCM with hybrid melting points (16 °C, 24 °C, and 32 °C) and an identical amount of latent heat with RW1 decreases to 32.9 °C, resulting in a decrement factor of 18.5%. One can see that a remarkable reduction in the maximum indoor temperature is achieved when the PCM with hybrid melting points is integrated. This is because, under the investigated hot dominant loading condition, it is easy for the PCM with a single point of 24 °C to get energy saturated and turn to a liquid state

quickly. For the scenario of using PCM with hybrid melting points, even though the total latent heat capacity is the same with RW1, the inward heat tends to be absorbed and stored as latent heat continuously. PCM32 can provide the temperature regulation service and hinder the indoor temperature increase after PCM16 and PCM24 getting energy saturated.

As shown in Figure 6.6(b), the minimum indoor temperature of RW1 is 7.9 °C which appears in fragment IV due to the low input temperature. For RW1, this number increases to 10.6 °C, resulting in an increment factor of 34.2% owing to the temperature regulation function of PCM. By contrast, it increases to 12.0 °C for the proposed wall, leading to an increment factor of 51.9%. A 17.7% increase in the minimum indoor temperature is achieved when the melting temperature of PCM changes from a single number 24 °C to the hybrid melting points (16 °C, 24 °C, and 32 °C). Under the low input loading condition in fragment IV, when the PCM24 and PCM32 turn to solid, PCM16 in the proposed wall can still release thermal energy and heat the indoor temperature.

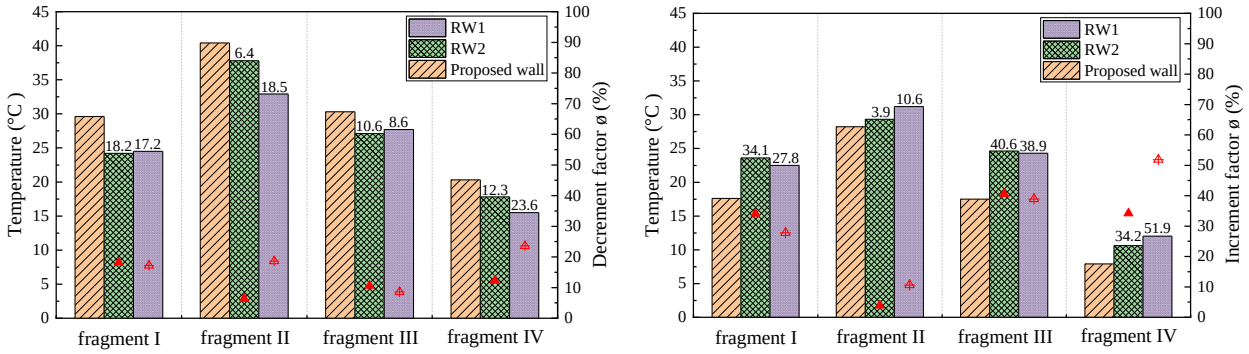

(a) (b)

Figure 6.6. (a) Maximum and (b) minimum peak of the instantaneous temperature of each wall.

Another observation is that in fragment I and fragment II when the mild loading condition centering 24 °C is applied, the thermal performance of RW1 is better than that of the proposed wall regarding the regulation on the maximum indoor temperature swing. This is

because the amount of PCM24 in RW1 is three times that in the proposed wall, providing more latent heat capacity to maintain the indoor temperature closed to 24 °C. One can see that the indoor temperature of the proposed wall can still be retained in the thermal comfort range over most of the test period of fragment I and fragment II. Therefore, the PCM with hybrid melting points shows high potential to improve the thermal management of buildings subjected to dynamic loading conditions covering cold to hot scenarios. It allows reaching the comfortable room temperature more rapidly than in the case of RW1 after the air conditioner is turned on.

6.4.1.2. ITD Value

The intensity of indoor thermal comfort of different wall configurations is evaluated in this section. The *ITD* value of RW1, RW2, and the proposed wall are summarized in Table 6.2. Within a given occupancy period, a higher *ITD* value (including ITD_{up} and ITD_{down}) corresponds to the scenario that the indoor temperature is kept in the thermal comfort zone (22°C - 28°C) for a longer duration.

As shown in Table 6.2, the ITD_{up} value of RW2 and the proposed wall is 92.9% and 94.1%, respectively for the whole test period, which is much higher than that of RW1 (84.4%). Similarly, the ITD_{down} value of RW2 and the proposed wall is 92.7% and 93.9%, respectively, which are also higher than that of RW1 (79.5%). One can see that the ITD_{up} and ITD_{down} value of RW2 and the proposed wall are also much higher than RW1 in each temperature fragment. This comparison further proves the indoor temperature regulation function of PCM, which is consistent with the results of Section 1.4.1.1.

One can see that for temperature fragment I and fragment III when the mild loading condition is applied, the ITD_{up} and ITD_{down} value of RW2 are the same or higher than that of the proposed wall, demonstrating the conclusion that higher heat storage capacity provides more

indoor thermal comfort. Meanwhile, the ITD_{up} and ITD_{down} value of the proposed wall is higher than those of RW2 for temperature fragment II and fragment IV as well as the whole test period, indicating that PCM with hybrid melting points can provide more indoor thermal comfort than the PCM with a single point under the changeable loading conditions.

Table 6.2. *ITD* value of RW1, RW2, and the proposed wall.

	ITD_{up} (%)			ITD_{down}(%)		
	RW1	**RW2**	**Proposed wall**	**RW1**	**RW2**	**Proposed wall**
fragment I	86.5	100	100	79.9	100	98.9
fragment II	65.7	74.7	85.2	100	100	100
fragment III	85.2	96.9	94.5	78.6	100	100
fragment IV	100	100	96.7	59.4	77.4	76.5
Total	84.4	92.9	94.1	79.5	92.7	93.9

6.4.1.3. The Impact of Latent Heat Capacity of PCM

In Chapter 4, it was found that the latent heat capacity shows a negligible impact on the thermal performance of the wall if the PCM melting point is out of the input temperature range. Increasing the PCM latent heat capacity is expected to improve the thermal performance of the external wall if its latent heat is fully activated. In order to distinguish the contribution of latent heat, the thermal performance of the proposed walls with the same hybrid melting points but different latent heat capacities are investigated under the same loading condition.

Figure 6.7 shows the instantaneous temperature profile of the proposed wall incorporating PCMs with 180 J/g and 360 J/g, respectively. For the PCM with the latent heat capacity of 180 J/g, the indoor temperature oscillates between 10.5 °C and 36.7 °C in the whole test period, formulating a maximum temperature fluctuation of 26.2 °C. For the PCM with the latent heat capacity of 360 J/g, the indoor temperature oscillates between 11.0 °C and 31.7 °C, formulating a maximum temperature fluctuation of 20.7 °C. Doubling the latent heat capacity of

the PCM leads to a 20.9% reduction in the maximum indoor temperature fluctuation. The duration of indoor thermal comfort is also increased by about 17.6%. Another observation is that the peak of the maximum and minimum indoor temperature averagely shifts about 3 hours due to the increase in the thermal inertia of the wall caused by the increased latent heat. Therefore, if proper melting points are selected, the increased latent heat can further benefit the thermal performance of building envelopes by increasing the indoor thermal comfort and shaping thermal demand.

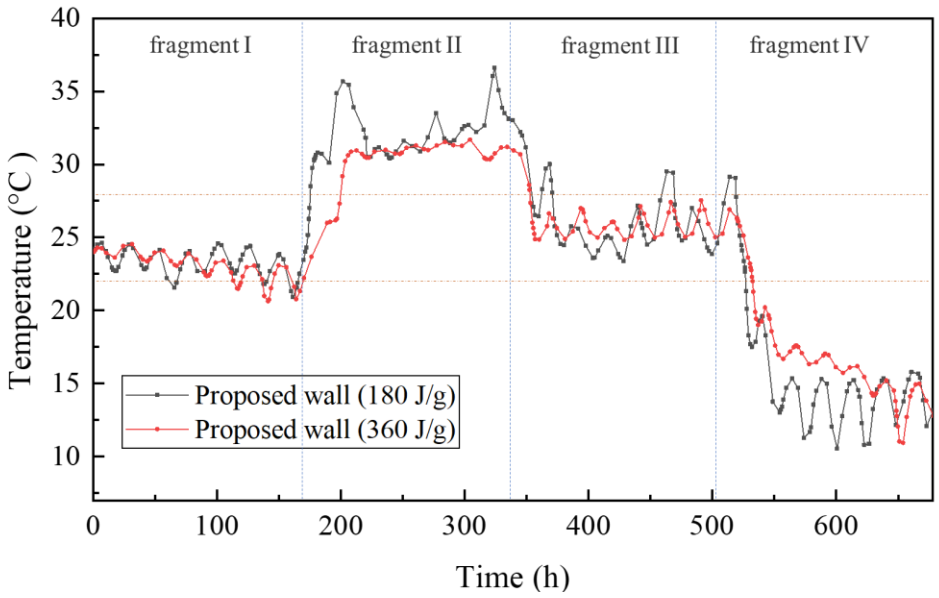

Figure 6.7. Instantaneous indoor temperature of the proposed wall incorporating PCMs with 180 J/g and 360 J/g, respectively.

6.4.2. Case Two—Thermal Performance of PCM Blocks

The thermal performance of the PCM blocks with hybrid melting points and identical melting points is investigated. For PCM24-30, both 180 J/g and 360 J/g are assigned as the latent heat of the PCM to examine its impact on the thermal behavior of the tested block. Figure 6.8 shows the instantaneous temperature of the interior surface of each block, which changes from 18 °C initially to the equilibrium state at 35 °C. As the temperature of PCM increases, its

increasing speed starts to slow down when the phase change process occurs, indicating the relatively steady-state temperature step appeared on the curves within the range of 18 °C to 35 °C corresponds to the phase change interval of the PCM. One can see that PCM27-27 has only one melting point (about 27 °C), and there are two steady-state temperature steps on the curve of PCM24-30 blocks, corresponding to their melting points of 24 °C and 30 °C, respectively. Even though the melting temperature varies, the time that PCM27-27 (180 J/g) and PCM24-30 (180 J/g) used to reaches 35 °C is the same, which is 34 minutes. This is because that they possess the same latent heat capacity, meaning they can absorb and store the same amount of latent heat. By contrast, it takes PCM24-30 (360 J/g) about 52 minutes to reach 35 °C. The doubled latent heat of PCM leads to an increase in the amount of thermal energy storage and a 52.9% of the peak temperature shift. Therefore, the thermal performance of building envelopes can be optimized by integrating PCM with proper melting points and heat storage capacity.

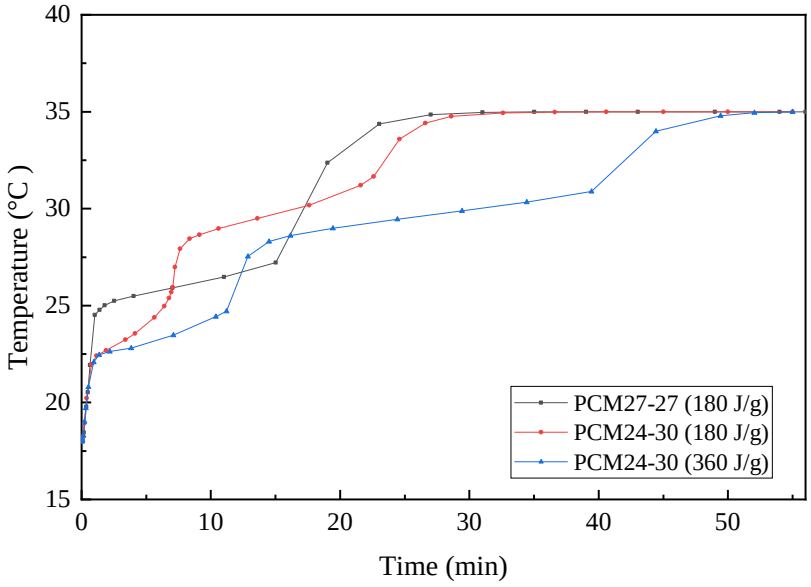

Figure 6.8. Instantaneous temperature of the PCM blocks with various melting points and latent heat capacities.

Figure 6.9 displays the temperature contours in the computational domain of PCM24-30 (180 J/g) and PCM27-27 (180 J/g) when the temperature of the block center is 19 °C, 24 °C, 27°C, 30 °C, and 34 °C, respectively. At 19 °C as shown in Figure 6.9(a) and (b), both PCM24-30 and PCM27-27 remain in the solid-state since the melting point temperature is not reached. The isothermal lines of both PCMs are straight in the vertical direction, indicating the heat penetration passes inward the domain uniformly.

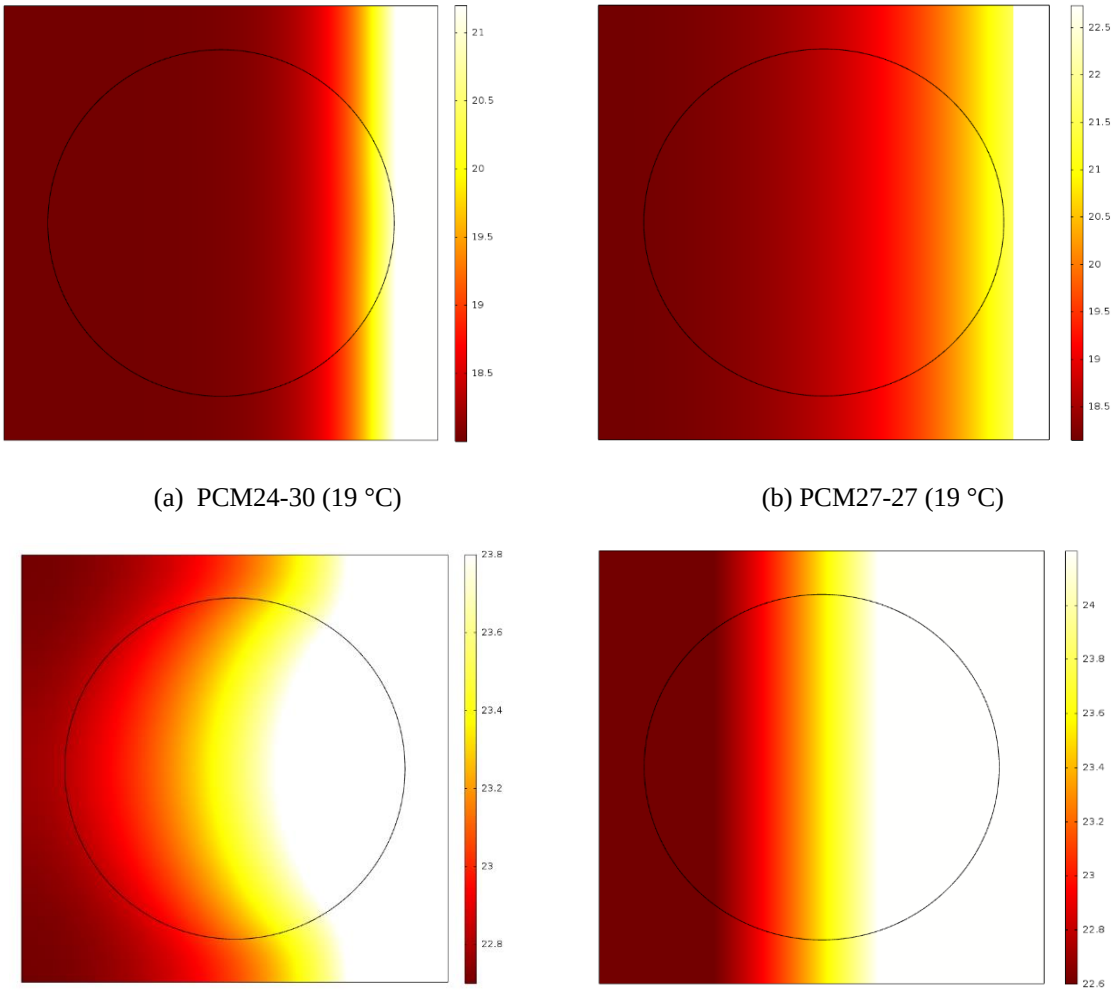

(a) PCM24-30 (19 °C)

(b) PCM27-27 (19 °C)

(c) PCM24-30 (24 °C)

(d) PCM27-27 (24 °C)

Figure 6.9. Temperature contour of PCM blocks at different center temperatures.

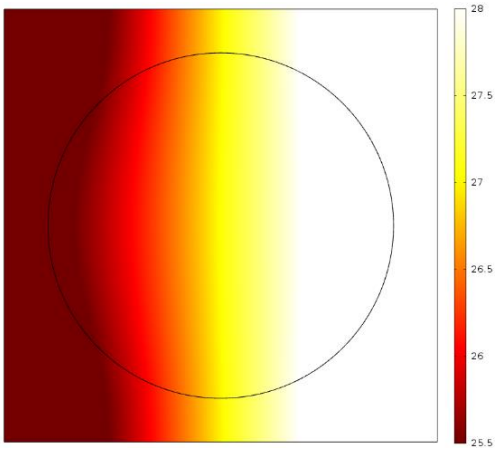

(e) PCM24-30 (27 °C)

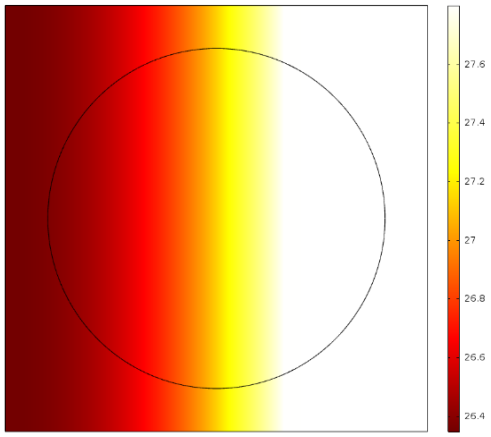

(f) PCM27-27 (27 °C)

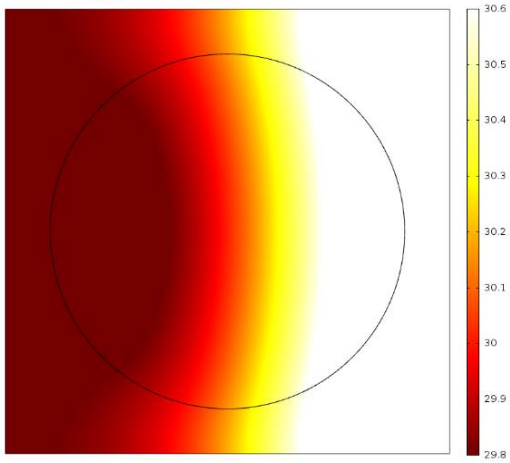

(g) PCM24-30 (30 °C)

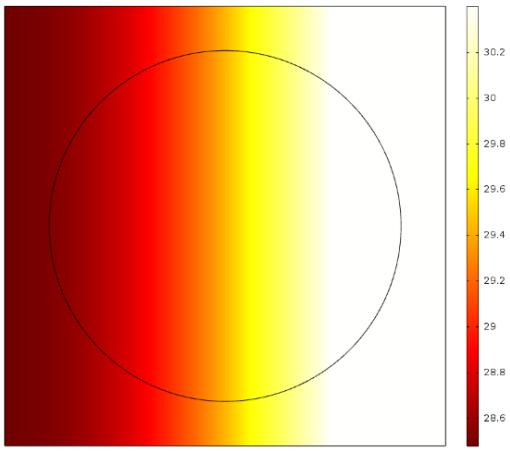

(h) PCM27-27 (30 °C)

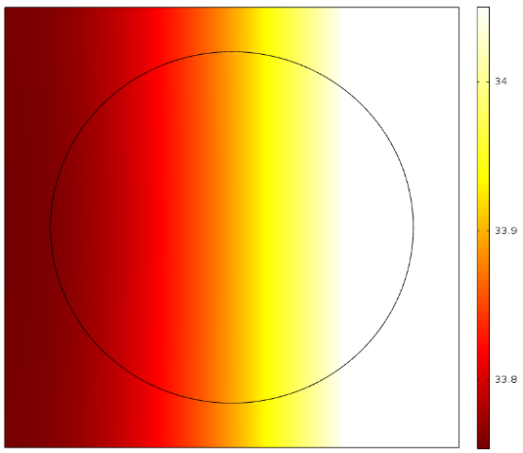

(i) PCM24-30 (34 °C)

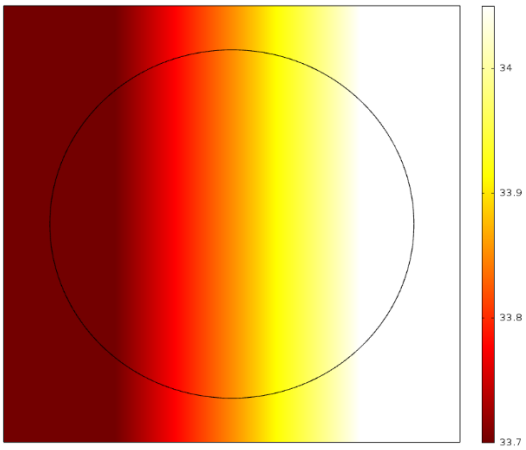

(j) PCM27-27 (34 °C)

Figure 6.9. Temperature contour of PCM blocks at different center temperatures (continued).

At 24 °C as shown in Figure 6.9(c) and (d), the isothermal line of PCM27-27 remains straight due to the uniform heat penetration. However, the isothermal line of PCM24-30 becomes inward concave in the center due to the uneven increase speed of the temperature. At this temperature, PCM24 in the outside domain starts to melt and absorb heat, and therefore hinders the rapid temperature increase; PCM30 in the circle domain keeps its solid-state with a steady increase in the temperature.

At 27 °C as shown in Figure 6.9(e), the PCM24 in the outside domain completed the phase change from solid to liquid, and the PCM30 in the circle domain keeps solid. No phase change process occurs at this moment and the temperature increases evenly in the whole block, so the isothermal line turns straight. As shown in Figure 6.9(f), even though the phase change process occurs in PCM27-27, the isothermal line keeps straight since the temperature increase of the inside and outside domains are the same due to their same melting point.

At 30 °C as shown in Figure 6.9(g), the isothermal line of PCM24-30 becomes outward concave in the center due to the uneven increase speed of the temperature. At this temperature, PCM24 in the outside domain already turns to liquid totally and keeps a constant temperature increase; however, PCM30 in the circle domain starts to melt and absorb heat with a decelerated growth in the temperature. In Figure 6.9(f), the isothermal line still keeps straight due to the identical thermal property of the whole domain. At 34 °C as shown in Figure 6.9(i) and (j), the isothermal lines of PCM24-30 and PCM27-27 are both straight since the PCM in the whole domain are in the identical liquid state.

By observing the results from Figure 6.8 and Figure 6.9, one can see that PCM with hybrid melting points provides more flexibility in the use of its latent heat capacity. When the

ambient temperature changes within a relatively large interval covering cold, mild, and hot loading conditions, the melting point of PCM can be optimized accordingly to shape the thermal demand and thus save the building energy for the long term.

6.5. Summary

A numerical study has been conducted to observe the potential thermal comfort benefits of integrating PCM with more than one melting point into an external wall of the residential building. The impact of latent heat capacity of the PCM on the thermal performance of the investigated domain is also investigated. The simulations on the multilayer wall system were conducted under an artificial solar-air temperature that follows the sine function for 28 days covering 7 days in typical loading conditions including cold, mild, and hot scenarios. A composite block consisted of PCM with different melting points is also simulated under constant input temperature. The obtained conclusions in this study are highlighted below:

Compared to the reference wall without PCM, the integration of a 10-mm PCM with a melting point of 24 °C and latent heat capacity of 180 J/g leads to a 6.4% of reduction in the maximum indoor temperature and 34.2% increase in the minimum indoor temperature. When the PCM with hybrid melting points (16 °C, 24 °C, and 32 °C) is integrated, the corresponding decrement and increment factors increase to 18.5% and 51.9% respectively. The integration of PCM with multiple melting points can benefit more in the indoor thermal comfort than using the PCM with a single melting under the investigated loading condition.

For the mild loading condition, the *ITD* value of RW2 is the same or higher than that of the proposed wall, demonstrating the conclusion that higher heat storage capacity provides more indoor thermal comfort. For the loading conditions covering cold and hot scenarios, PCM with

hybrid melting points can provide more indoor thermal comfort than the PCM with a single point.

Doubling the latent heat capacity of the PCM leads to a 20.9% reduction in the maximum indoor temperature fluctuation and a 3-hour peak temperature shift. The duration of indoor thermal comfort is also increased by about 17.6%. If proper melting points are selected, the increased latent heat can benefit the thermal performance of building envelopes by increasing the indoor thermal comfort and shaping thermal demand.

PCM with hybrid melting points provides more flexibility in the use of its latent heat capacity. When the ambient temperature changes within a relatively large interval covering cold, mild, and hot loading conditions, the melting point of PCM can be optimized accordingly to shape the thermal demand and thus save the building energy for the long term. In this way, the proposed PCM-based wall can adapt to the input loading conditions in different seasons and months, and its latent heat can remain active for a longer period of the year.

6.6. References

[1] International Energy Agency, Market Report Series – Energy Efficiency 2019, IEA Publications, 2019.

[2] Rathore, P.K.S. and Shukla, S.K., 2021. Enhanced thermophysical properties of organic PCM through shape stabilization for thermal energy storage in buildings: A state of the art review. Energy and Buildings, p.110799.

[3] F. Agyenim, N. Hewitt, P. Eames, M. Smyth, A review of materials, heat transfer and phase change problem formulation for latent heat thermal energy storage systems (LHTESS), Renewable and Sustainable Energy Reviews 14(2) (2010) 615-628.

[4] J. Giro-Paloma, M. Martínez, L.F. Cabeza, A.I. Fernández, Types, methods, techniques, and applications for microencapsulated phase change materials (MPCM): A review, Renewable and Sustainable Energy Reviews 53 (2016) 1059-1075.

[5] M. Song, F. Niu, N. Mao, Y. Hu, S. Deng, Review on building energy performance improvement using phase change materials, Energy and Buildings 158 (2018) 776-793.

[6] K. Du, J. Calautit, Z. Wang, Y. Wu, H. Liu, A review of the applications of phase change materials in cooling, heating and power generation in different temperature ranges, Applied Energy 220 (2018) 242-273.

[7] N. Soares, J.J. Costa, A.R. Gaspar, P. Santos, Review of passive PCM latent heat thermal energy storage systems towards buildings' energy efficiency, Energy and Buildings 59 (2013) 82-103.

[8] Saffari, M., de Gracia, A., Ushak, S. and Cabeza, L.F., 2016. Economic impact of integrating PCM as passive system in buildings using Fanger comfort model. Energy and Buildings, 112, pp.159-172.

[9] Tunçbilek, E., Arıcı, M., Bouadila, S. and Wonorahardjo, S., 2020. Seasonal and annual performance analysis of PCM-integrated building brick under the climatic conditions of Marmara region. Journal of Thermal Analysis and Calorimetry, 141(1), pp.613-624.

[10] Sovetova, M., Memon, S.A. and Kim, J., 2019. Thermal performance and energy efficiency of building integrated with PCMs in hot desert climate region. Solar Energy, 189, pp.357-371.

[11] https://www.energy.gov/eere/buildings/articles/solid-state-tunable-thermal-energy-storage-smart-building-envelopes

[12] Cao, F., Zheng, Y., Chen, C.H. and Bonner, R., 2018. Thermal energy storage with tunable melting point phase change materials. In International Heat Transfer Conference Digital Library. Begel House Inc..

[13] Wei, H., Wang, C., Yang, S., Han, J., Yang, M., Zhang, J., Lu, Y. and Liu, X., 2019. A strategy for designing microencapsulated composite phase change thermal storage materials with tunable melting temperature. Solar Energy Materials and Solar Cells, 203, p.110166.

[14] X. Jin, M.A. Medina, X. Zhang, Numerical analysis for the optimal location of a thin PCM layer in frame walls, Applied Thermal Engineering 103 (2016) 1057-1063.

[15] COMSOL Multiphysics®, version5.2a,

[16] H. Fayaz, N.A. Rahim, M. Hasanuzzaman, A. Rivai, R. Nasrin, Numerical and outdoor real time experimental investigation of performance of PCM based PVT system, Solar Energy 179 (2019) 135-150.

[17] L. Royon, L. Karim, A. Bontemps, Thermal energy storage and release of a new component with PCM for integration in floors for thermal management of buildings, Energy and Buildings 63 (2013) 29-35.

[18] Introduction to heat transfer, 1996

[19] N.P. Sharifi, G.E. Freeman, A.R. Sakulich, Using COMSOL modeling to investigate the efficiency of PCMs at modifying temperature changes in cementitious materials – Case study, Construction and Building Materials 101 (2015) 965-974.

[20] M. Rady, Granular phase change materials for thermal energy storage: Experiments and numerical simulations, Applied Thermal Engineering 29(14-15) (2009) 3149-3159.

[21] Li, Y., Long, E., Jin, Z., Li, J., Meng, X., Zhou, J., Xu, L. and Xiao, D., 2019. Heat storage and release characteristics of composite phase change wall under different intermittent heating conditions. Science and Technology for the Built Environment, 25(3), pp.336-345.

[22] Kim, T., Ahn, S. and Leigh, S.B., 2014. Energy consumption analysis of a residential building with phase change materials under various cooling and heating conditions. Indoor and Built Environment, 23(5), pp.730-741.

7. NUMERICAL INVESTIGATION OF THE THERMAL PERFORMANCE OF BUILDING ENVELOPES COUPLING THERMAL INSULATION AND STORAGE STRATEGIES[3]

7.1. Introduction

Rapid growths in world population and economy have led to tremendous energy consumption (e.g., uses of fossil fuels) while producing a large amount of waste and greenhouse gas emissions [1]. According to the data from the International Energy Agency, the buildings and building construction sectors combined were responsible for 36% of global final energy consumption and nearly 40% of total CO_2 emissions [2]. In 2018, the residential and commercial buildings consumed about 40% of the total U.S. energy [3], in which space heating and cooling are responsible for half of all energy [4]. Therefore, desirably airtight insulating materials are in great demand for a building envelope to achieve high energy savings in both existing and new-constructed buildings.

One of the attractive solutions to tackle the challenge appears to be the utilization of vacuum insulation panels (VIPs) in building envelopes. By using superiorly low thermal conductivity core material with vacuumed air, VIPs display a notably low thermal conductivity (4-8 mW/(mK)), a factor of four to eight times smaller than the conventional insulation materials (≥30 mW/(mK)) [5] (see Figure 7.1). VIPs are currently with applications to broader engineering, such as shipping containers, temperature-sensitive products, and refrigerators.

[3] This chapter presents the study that numerically investigates the optimal PCM melting temperature when being used to improve the thermal performance of multi-layered residential walls. Most of the contents of this chapter is submitted for publication and is currently under review. The submitted article is coauthored by Mingli Li, Hong Pan, Qi Cao, and Zhibin Lin. Mingli Li had primary responsibility for building the numerical model and conducting the analysis. Mingli Li also drafted and revised all versions of this chapter. Zhibin Lin served as proofreader and checked the mathematical model used in the simulation conducted by Mingli Li.

Introducing VIPs to the building sector, such as floors, walls, and roofs has become an area of international interest to meet the growing building thermal resistance requirements. Nussbaumer et al. [6] conducted both experimental and numerical studies on the thermal performance of an exterior wall system mounted with VIPs embedded in expanded polystyrene (EPS) foam-forming insulation boards. Their results showed that a thermal improvement of over 95% was realized by adding a layer of 60 mm insulation boards containing 40 mm thick VIPs, equivalent to a 212-mm thick conventional insulation material if assuming identical thermal transmittance (*U*-value). Their results revealed that the VIPs are not only a great insulation material, but also could save a lot of space due to high thermal-to-mass ratio, as compared to conventional building materials.

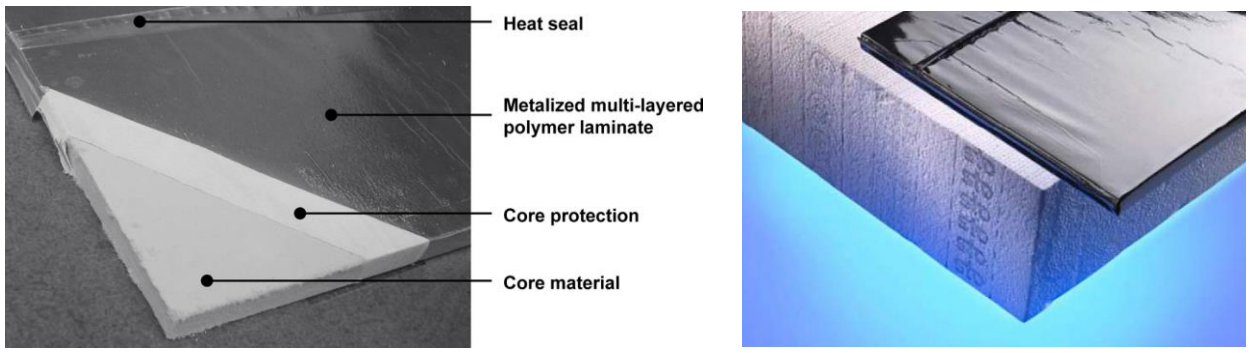

(a) (b)

Figure 7.1. Typical VIP structure showing (a) the main components [7], and (b) a comparison of equivalent thermal resistance thickness between traditional thermal insulation and VIP [8].

Rather than the use of materials with low thermal conductivity, enhancement of the thermal mass of a building is another strategy for energy saving. For instance, the incorporation of phase change materials (PCMs) can effectively enhance the building energy efficiency due to their ability to increase the thermal mass of the building envelope, reduce the indoor temperature oscillations, and delay the electricity load from peak to off-peak operation period [9, 10]. This tendency is confirmed by extensive papers available in the literature over the recent two decades.

For a review, see in Ref. [11, 12][13] and more recently [14] [15]. PCMs can be outfitted into building envelopes either by being directly integrated into commonly used building materials, such as concrete [16] and gypsum boards [17], or by using a separate layer of shape stabilized PCMs in the wall assembly [18]. In various applications, PCM-reinforced building envelopes are proven successful in enhancing building energy efficiency. Cabeza et al. [16] found that compared with a conventional concrete wall, the wall reinforced by encapsulating PCMs exhibited improved thermal inertia, resulting in smaller indoor temperature fluctuations. Sharifi et al. [17] conducted a numerical study aiming to evaluate the efficiency of PCM-impregnated gypsum boards on improving building thermal performance. They found that the integrated PCM effectively delayed and reduced the indoor peak temperature, increased the indoor thermal comfort duration, and decreased the cost and energy required by the heating, ventilation, and air conditioning (HVAC) system to keep the inside temperature in human beings' thermal comfort range.

Thus, as proposed in this study, coupling PCMs and VIPs could effectively combine the PCMs' thermal energy storage capacity and VIPs' super insulation to further increase the thermal performance of the building envelope system. On one hand, PCMs with high latent heat storage capacity can provide promising thermal mass to the system as a complement for the VIPs; on the other hand, the integration of the VIP on the exterior side of the PCM layer can block a considerable amount of inward heat or cold, rending PCMs longer phase transition time to get energy saturated. So far, there is limited research investigating the coupling effect of VIPs and PCMs, on the thermal dynamics of the building envelope. Ahmad et al. [19] tested the thermal dynamics of a test-cell enclosing both VIPs and PCMs to improve the thermal inertia of the light building envelope. Compared with the traditional wallboard, the proposed structure

possesses decreased thickness and promising latent heat capacity with the indoor temperature fluctuation decreased. Li et al. [20] explored the feasibility of integrating form-stable paraffin/nanosilica composites into VIPs, with the expectation that the integration of PCM can improve the thermal mass of VIPs. Their results show that the fabricated PCM-based VIPs possess improved thermal mass and low thermal conductivity (0.02 W/(mK)), showing great potential to benefit the building energy efficiency. Nevertheless, most of those studies mainly focus on the overall thermal performance of VIP and PCM integrated building systems using test cells or a whole room. More research is still needed to explore the thermal interaction between VIP and PCM regarding different design parameters. In addition, the thermal dynamics of building envelopes containing both materials are rarely investigated when they are subjected to different temperature loading conditions, especially the real temperature profiles of U.S. cities during different months.

Therefore, this study aims to investigate the thermal performance of a multilayered frame wall outfitted with both VIPs and PCMs under various loading conditions. The examined multilayer wall system is isolated from a whole room as the major investigation object since the complex interactions between different layers of the wall are the main interest of this study. This wall assembly can find direct application in frame wall construction due to its exceptionally good thermal insulation properties, relatively low thickness, as well as high thermal mass. As a part of a large project, the wall configuration is derived from previous work [21]. A numerical study is developed in this study to comprehensively analyze the instantaneous thermal dynamics of the explored wall configurations. The overall work plan of this study can be classified under three major tasks: (1) comparing the thermal and space-saving performance of VIP with one of the

traditional thermal insulating materials--EPS and (2) assessing the coupling thermal effect of VIP and PCM when they are integrated into the same building envelope.

7.2. Numerically Modeling of VIP-PCM-based Building Wall System

7.2.1. Description of the Multilayer Frame Walls

Heat loss from buildings occurs via external walls, ceilings, floors, windows, and also via air infiltration [22]. To simplify the model, the current study only considers the heat loss through external walls rather than other architectural features such as windows and doors since the external frame wall is the main passageway for heat gain and loss in a building. Moreover, it is more practical to integrate VIP and PCM into the building wall. The original frame wall configuration chosen for this study is a typical North American residential wall as shown in Figure 7.2 [23]. The wall consists of an 89-mm insulating layer sandwiched by a layer of 12.7-mm gypsum wallboard on the wall interior side and a 20.5-mm oriented strand board (OSB) on the exterior side. To evaluate the thermal performance of VIPs and PCMs, the instantaneous heat flux through the wall integrated with and without the VIP-PCM board is compared and analyzed.

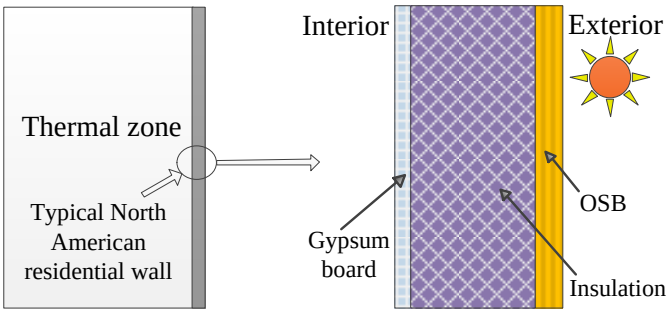

Figure 7.2. Schematic diagram of the original residential wall configuration.

7.2.2. Thermal Behavior of VIPs

Different types of VIPs exist with different core materials and envelopes. The VIP considered in this study consists of fumed silica as core material sealed by a metal foil envelope.

As far as the installation is concerned, the VIPs are hypothesized to be applied within the internal layer of the frame wall. As demonstrated by Fantucci et al. [24], one needs to address the relationship between the ambient temperature and the thermal conductivity evolution for VIP and other organic foam insulation such as polyisocyanurate that operate over the typical temperature range of buildings. Nevertheless, a constant thermal conductivity is assumed for VIPs during a short period in this study considering that when VIPs are applied on the internal layer of the wall, they do not undergo significant temperature variations.

The overall thermal behavior of VIP can be represented with an equivalent thermal conductivity of the panel as shown in Eq. (7.1), which is a function of the core material thermal conductivity and the thermal bridge of the envelope shown below [25],

$$\lambda_{VIP} = \lambda_{eq} = \lambda_c + \lambda_{memb} \tag{7.1}$$

where λ_{VIP} is the global thermal conductivity of VIP ($W \cdot m^{-1}K^{-1}$), λ_{eq} is the equivalent thermal conductivity of VIP ($W \cdot m^{-1}K^{-1}$), λ_c is the core material's thermal conductivity ($W \cdot m^{-1}K^{-1}$), and λ_{memb} is the apparent thermal bridge conductivity ($W \cdot m^{-1}K^{-1}$). The thermal conductivity of the total core material λ_c can be split into several contributions: radiation $[\frac{16}{3}\frac{\sigma n^2 T^3}{E(T)}]$, solid conduction $[\lambda_{cs}^0(T) + \mathrm{B}\tau_w(\phi)]$, and gaseous conduction $[\varepsilon\frac{\lambda_g^0(T)}{1+\frac{\mathrm{CT}}{\phi p_t}}]$. The apparent thermal bridge conductivity of the complex barrier can be written based on the relation between heat flow and the thermal conductivity as shown in Eq. (7.2),

$$\lambda_{memb} = \frac{\mathrm{Pd}}{\mathrm{A}}\psi_{memb} \tag{7.2}$$

Therefore, the global thermal conductivity of the VIP can be rewritten with the following general formula:

$$\lambda_{VIP}(T,\phi,p_t) = \frac{16}{3}\frac{\sigma n^2 T^3}{E(T)} + \lambda_{cs}^0(T) + \mathrm{B}\tau_w(\phi) + \frac{\varepsilon \lambda_g^0(T)}{1+\frac{\mathrm{CT}}{\phi p_t}} + \frac{\mathrm{Pd}}{\mathrm{A}}\psi_{memb} \quad (7.3)$$

where λ_{VIP} is the global thermal conductivity of VIP (W·m-1K-1), σ is the Stefan-Boltzmann's constant which equals to 5.67 ×10^{-8} (W·$m^{-2}K^{-4}$), n is the refractive index, T is the temperature (K), E is the extinction coefficient (m^{-1}), λ_{cs}^0 is the initial solid thermal conductivity (W·$m^{-1}K^{-1}$), B is the influence of water content increase on the thermal conductivity (W·$m^{-1}K^{-1}\%^{-1}$), τ_w is the mass content of water, ϕ is the relative humidity, λ_g^0 is the gaseous thermal conductivity of not confined gas (W·$m^{-1}K^{-1}$), C is the constant depending on gas (J·$K^{-1}m^{-2}$), p_t is the internal total pressure (Pa), P is the panel's perimeter (m), d is the panel's thickness (m), A is the panel's area (m2), and ψ_{memb} is the linear thermal bridge coefficient (W·$m^{-1}K^{-1}$).

7.2.3. PCMs

The PCM selected in this analysis is the pure paraffin blend from Microteck laboratories, Inc. USA, which is available over a wide range of melting temperatures [26]. The heat of fusion of the PCM is 180 kJ/kg. Generally, ideal PCMs melt at a constant temperature, but in reality, they melt over a small range of temperature ($T_m \pm 2$°C) due to impurities. The transition temperature of the PCM is assumed to be 24°C and the transition interval of the PCM between solid and liquid phase is determined by actual material thermal properties as 4 °C in this study. Sari et al. [27] found paraffin has good thermal reliability and chemical stability even after 5000 melt-freeze thermal cycles. Manish K. Rathod and Jyotirmay Banerjee [28] also concluded that paraffin has good thermal and chemical stability after many thermal cycles. Therefore, the thermal property of the PCM is assumed as being constant over years in this study.

7.2.4. Computational Simulation

Computational simulations are conducted by applying both artificial sine function and real temperature profiles of two U.S. cities to the exterior surface of the multilayer wall models. A parametric study consists of four variables including the wall thickness, wall configuration, and loading conditions is carried out to investigate the feasibility of coupling VIP and PCM in the building envelope for thermal management. A computational procedure is utilized since conducting this kind of study by laboratory experiment is very time-consuming, expensive, and impractical. COMSOL Multiphysics® software [29] is used to develop the model, simulate the thermal dynamic behavior of the multilayer wall, and explore the complex interactions between different layers of the wall assembly.

To explore the transient heat transfer through the typical North American residential wall system, a two-dimensional (2D) multi-layered transient conduction model is developed with the COMSOL Multiphysics® software. In this simulation, the transient thermal response of both solid and liquid is involved due to the "phase change" behavior of the PCM. The transient thermal behavior of a solid is governed by the partial differential equation as follows [30]:

$$\frac{\partial}{\partial x}\left(\lambda \frac{\partial T}{\partial x}\right) + \frac{\partial}{\partial y}\left(\lambda \frac{\partial T}{\partial y}\right) = \rho C_P \frac{\partial T}{\partial t}, \tag{7.4}$$

where T is the temperature (K), λ is the thermal conductivity of the material ($W \cdot m^{-1}K^{-1}$), ρ is the density (kg/m^3), C_P is the specific heat (J/kg·K), and t is the time. The thermal and physical properties of the materials used in this study are shown in Table 7.1.

For simplicity, the wall model is established under the following assumptions: (a) All layers of the wall system are assumed to be homogenous and isotropic; (b) The wall is insulated in the vertical direction and the heat transfer is one-dimensional through the wall thickness direction; (c) The thermal expansion of each material is not considered; (d) The thermophysical

properties of the materials are constant during a short test period except the density of PCM in the solid and liquid phase, and (e) For multi-layered wall systems, the contact resistance between different layers is negligible.

Table 7.1. Thermal and physical properties of materials [23, 31].

Materials	**Density (kg/m^3)**	**Specific heat capacity (kJ/ (kg K))**	**Thermal conductivity (W/ m K)**
Gypsum board	800	1.09	0.16
OSB	650	1.21	0.13
PCM	880 (solid)/760 (liquid)	2.0	0.20
VIPs	190	0.8	0.004
EPS	35	1.45	0.045

Since the thermal conductivity is assumed to be constant through each material during a short test period, and the system is isolated in y direction, Eq. (7.4) can be reduced to a 1D heat transfer equation as shown in Eq. (7.5),

$$\frac{\partial^2 T}{\partial x^2} = \frac{\rho C_P}{\lambda}\frac{\partial T}{\partial t}, \tag{7.5}$$

Appropriate exterior and interior boundary conditions are required for the simulation models and showed in Eq. (7.6) and (7.7),

$$T(0, t) = T_i \quad (x = 0) \tag{7.6}$$

$$T(\delta, t) = T_e \quad (x = \delta) \tag{7.7}$$

where δ is the thickness of the frame wall; T_i and T_e are the temperature files applied on the interior and exterior surface of the wall, respectively. For the initial condition, the entire system is assumed to be at room temperature before the heat load is applied as shown in Eq. (7.8),

$$T(x, t = 0) = T_R \tag{7.8}$$

where T_R is the indoor air temperature and assumed to be fixed at 24 °C. The internal heat loads are ignored, and the external heat loads generated from the outside temperature and solar radiation are the only energy source during the test period.

In COMSOL, the dynamics of the phase change process from phase I (solid) to phase II (liquid) in PCM is taken into consideration using the equations below:

$$\rho_{PCM} = \rho_{phase1}\beta + \rho_{phase2}(1-\beta), \tag{7.9a}$$

$$\lambda_{PCM} = \lambda_{phase1}\beta + \lambda_{phase2}(1-\beta), \tag{7.9b}$$

$$C_{p,PCM} = \frac{1}{\rho_{PCM}}\left(\rho_{phase1}C_{p,phase1}\beta + \rho_{phase2}C_{p,phase2}(1-\beta)\right) + L\frac{\partial \alpha_m}{\partial T}, \tag{7.9c}$$

where ρ is the density of the material (k/m^3), λ is the thermal conductivity (W·m^{-1}K^{-1}), β is the volume fraction of PCM at initial phase I (solid), C_p is the specific heat (J·kg^{-1}K^{-1}), L is the latent heat of fusion (J/kg), and α_m represents the mass percentage of PCM that is transferred from phase 1 to phase 2. Given the PCM has an identical thermal conductivity in solid and liquid phases, Eq. (7.9b) can be rewritten as:

$$\lambda_{PCM} = \lambda_{phase1} = \lambda_{phase2}, \tag{7.10a}$$

and α_m is:

$$\alpha_m = \frac{1}{2}\frac{\rho_{phase2}(1-\beta)-\rho_{phase1}\beta}{\rho_{phase2}(1-\beta)+\rho_{phase1}\beta}, \tag{7.10b}$$

7.2.5. Mesh Generation and Grid Check

Figure 7.3 shows the computational domain meshing of the multilayer wall system used for the model validation. A 2D model is chosen for the numerical analysis. For the subdomains and boundaries of the numerical model, triangular elements are used to apply the finite element method. A mesh convergence study is carried out to ensure the accuracy of the finite element results. For the same numerical model, different non-uniform grid systems ranging from “coarse”

to “extremely fine” are checked. By applying the same boundary conditions, the average temperature of the boundary between the interior gypsum board and the insulating layer as marked in red in Figure 7.3(a) is generated as the supervising parameter. Results of three different instants including 24h, 48h, and 96h are captured respectively to ensure the accuracy of the mesh sensitivity study. As shown in Figure 7.3(b), no significant change in supervising temperature is observed for the three tested instants when the meshing changes from “coarse” to “extremely fine”, showing the meshing insensibility of the investigated model. Given the accuracy of “extra fine” meshing can reach 99.8% of that of the “extremely fine” meshing but save 31.8% of the solution time under the same calculating system configuration, “extra fine” meshing is adopted for the numerical simulations of PCM-based wall models in this study.

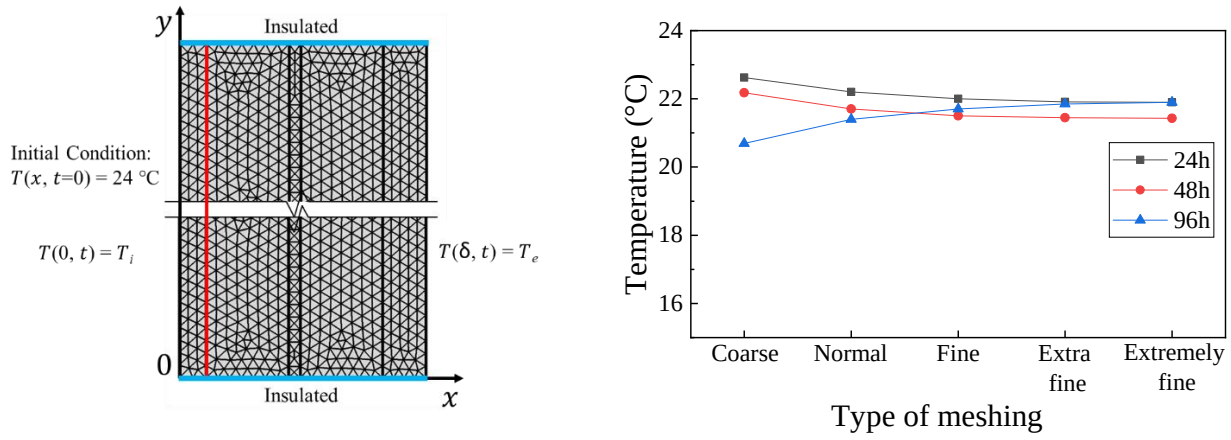

Figure 7.3. COMSOL heat transfer model (a) geometry, mesh, and boundary conditions and (b) mesh sensitivity study.

7.2.6. Temperature Profiles

7.2.6.1. Sinusoidal Function Temperature Profiles

To investigate the thermal performance of the VIP-PCM reinforced wallboard, sinusoidal function temperature profiles as shown in Figure 7.4 are applied on the wall exterior surface respectively as the input loading conditions. Three temperature profiles are applied with

amplitudes of 10°C (T10), 20°C (T20), and 30°C (T30) respectively, centering the same reference temperature of 24°C. These temperature profiles are assumed to be the combined effect of environmental temperature and solar radiation absorbed by the wall exterior surface. A total of one-week test period with seven diurnal periodic test intervals is applied. The temperature profiles with different amplitudes allow it to comprehensively study the effect of the different temperature loading conditions on the thermal behavior of VIPs and PCMs.

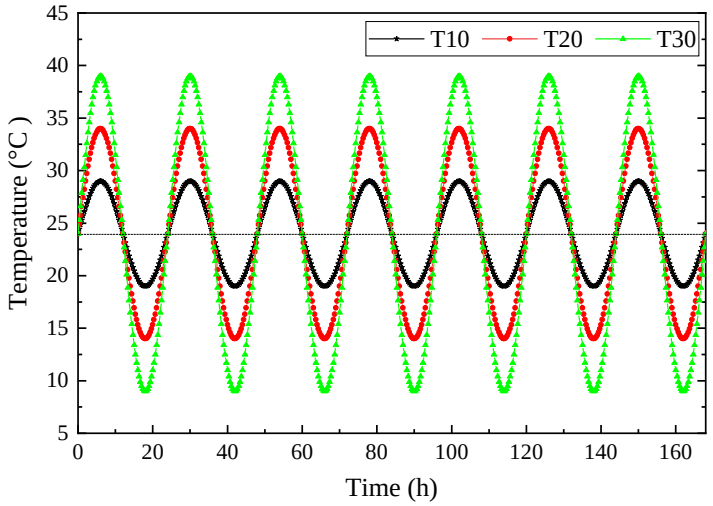

Figure 7.4. Sinusoidal function temperature profiles as input loading conditions.

7.2.6.2. Real Temperature Profiles

In addition to the artificial sine function temperature profiles, real temperature profiles for Austin and Minneapolis are also applied on the wall exterior surface as the thermal loading conditions. The selected cities are distributed in different climate zones of the US, representing cities classified as “hot” and “cold” categories and possessing different peak and lowest temperatures and diurnal temperature variations. According to the classification of the U.S. climate zones by the U.S. Department of Energy, Minneapolis is located in climate zone 6 with an average temperature of below 0°C in January; Austin is located in climate zone 2 with a rather high temperature in both cold and hot seasons. To yield more comprehensive results, the

temperature data of the first week of January and July are used to cover both cold and hot dates in both cities. As a coupling effect of the environment temperature and solar radiation, an equivalent solar-air temperature ($T_{sol-air}$) [32] of the examined cities are used as the wall exterior boundary condition, by which means the wall external surface received the same amount of heat energy in the absence of solar radiation compared with the scenario under the combinational effect of environment temperature and the solar radiation. A clear-sky solar radiation model considering clear-sky direct normal irradiance and diffuse solar irradiances are used to generate $T_{sol-air}$ according to Eq. (7.11):

$$T_{sol-air} = T_e + \frac{\alpha I_t}{h_e}, \tag{7.11}$$

where T_e is the external environment temperature (°C), α is the solar radiation absorption coefficient of the exterior surface, h_e is the heat transfer coefficient of exterior surface (W/m^{2}K), and I_t is the total solar radiation (W/m^2). The hourly external environment temperature and solar radiation of Austin and Minneapolis were obtained from the TMY (typical meteorological year) weather database provided by National Solar Radiation Data Base. Figure 7.5 shows the solar-air temperature of Minneapolis and Austin during the first week of January and July.

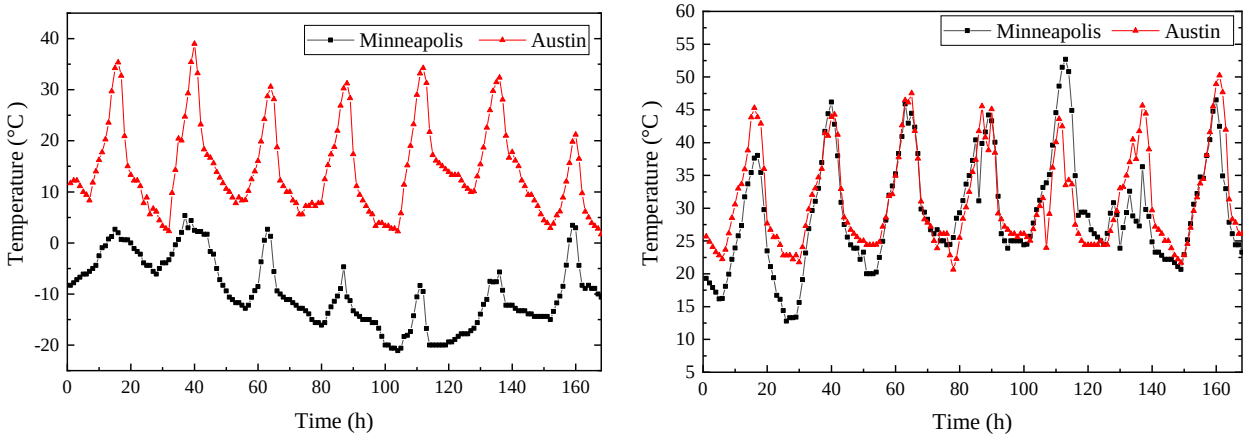

Figure 7.5. Solar-air temperature profiles of Minneapolis and Austin for (a) January and (b) July.

7.3. Validation of the Numerical Model

7.3.1. A Multilayer Wall Building in the Literature

As illustrated in Figure 7.6(a), a cubic box simulator consists of six 1.19m×1.19m multilayer wall panels provided by Jin et al. [23] is utilized to validate the numerical model in this analysis. Figure 7.6(b) shows the wall structure when the PCM layer is located in the center of the insulating layer, which is selected as the representative scenario for the model verification. The wall is subjected to 1D heat transfer in the horizontal direction with both top and bottom sides thermally insulated.

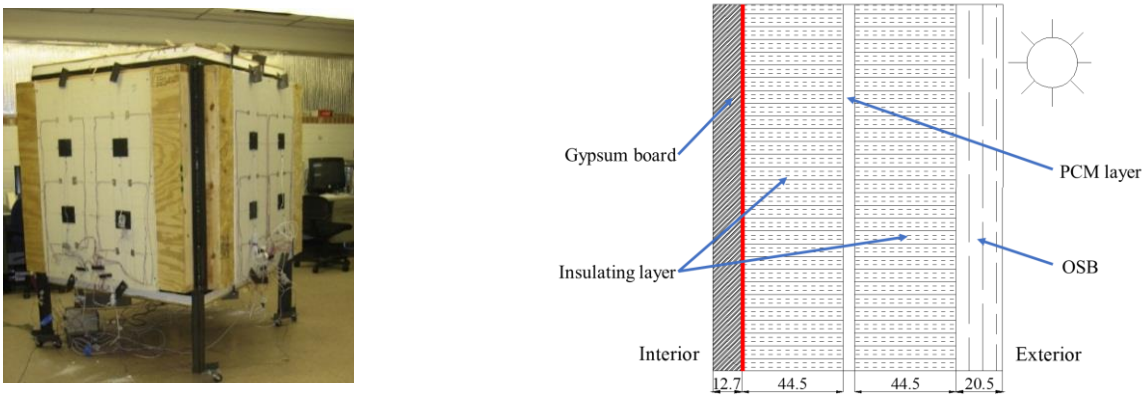

(a) (b)

Figure 7.6. The multilayer wall (a) dynamic wall simulator in the laboratory test [23] and (b) schematic diagram showing the wall assembly.

In this verification analysis, the temperature profiles applied on the exterior surface of the wall model are based on the summer weather conditions in Lawrence, Kansas, USA [23], as shown in Figure 7.7. A test period of 96 hours is adopted in the experiments. The original temperature of the wall structure in COMSOL Multiphysics® software is set to 23 °C to match the experimental setup.

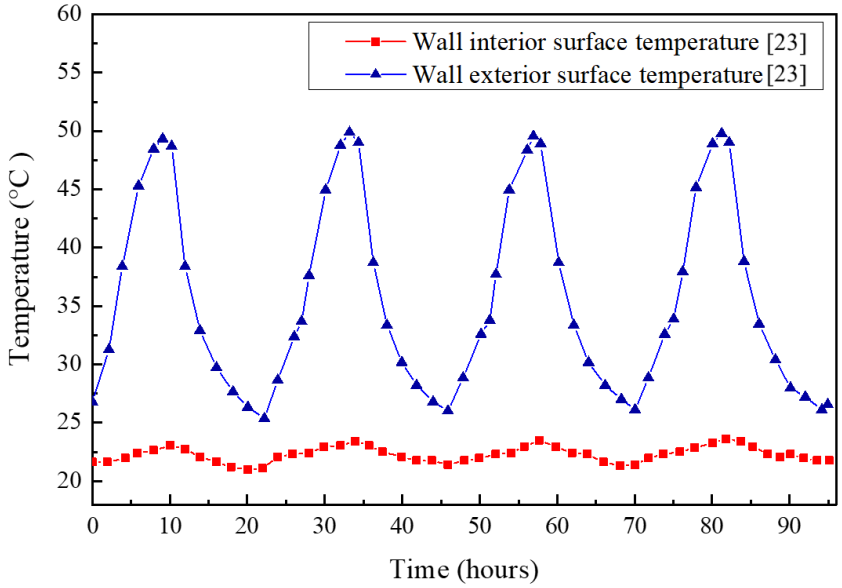

Figure 7.7. The boundary conditions of the multilayer wall.

Table 7.2 shows the thermophysical properties of the materials used in each layer. In the tests, both the transient average temperature at the location marked in red in Figure 7.6 (b) and the heat flux value through the wall are generated to reveal the thermal behavior of the multilayer wall. To validate the accuracy of the numerical model, thermal information at the same location is numerically generated in COMSOL for the corresponding wall structure model possessing the same assembly and materials as the tested model.

Table 7.2. Thermal properties of materials [23].

Materials	**Density (kg/m^3)**	**Specific heat capacity (kJ/(kg K))**	**Heat of fusion (kJ/kg)**	**Melting point (°C)**	**Thermal conductivity (W/m K)**
Gypsum board	800	1.09	/	/	0.16
Insulating layer	12.7	0.84	/	/	0.045
OSB	650	1.21	/	/	0.13
PCM	880 (solid) 760 (liquid)	2.0	179	27	0.20

7.3.2. Model Calibration and Discussion

Figure 7.8(a) shows the temperature comparison results of the proposed numerical model and the tested model [23] under the same loading condition. The maximum temperature deviation between them is 0.52 °C, showing a good agreement between the results generated from the proposed study and the tested results. Figure 7.8(b) shows the heat flux comparison results with a maximum heat flux deviation of 1.31W/m^2. These deviations may be caused by the chain of aspects that the numerical model does not consider, such as the continuum contact resistance between different layers and the anisotropic characteristic of the tested material. Even though a slight difference between the numerical and experimental data exists, it is acceptable based on the assumption made in this analysis. Therefore, the investigated numerical model generated in the COMSOL Multiphysics® software can be used to analyze the thermal behavior of the multilayer wall.

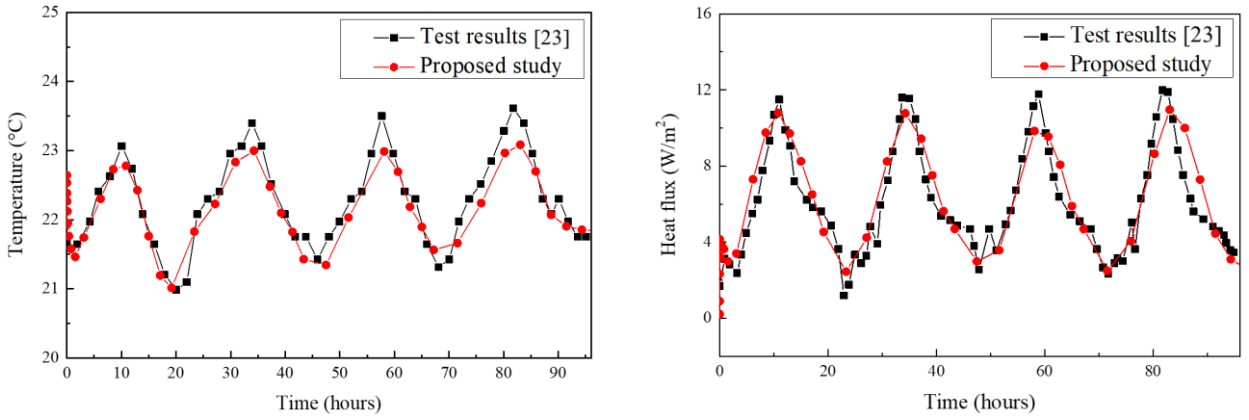

(a) (b)

Figure 7.8. Comparison of test results and proposed study (a) transient temperature result (b) heat flux result.

7.4. Results and Discussion

7.4.1. Comparison of Exterior Wall Thermal Performance with VIP and EPS

7.4.1.1. Insulation Thickness

The frame wall considered is a west wall consists of a 12.7-mm gypsum wallboard, a 5-mm PCM layer, and an insulating layer followed by a 20.5-mm OSB (see Figure 7.9). As one of the most traditional thermal building insulating materials, EPS made from small spheres of polystyrene is selected and compared with the VIP when being integrated into the wall assembly for thermal management.

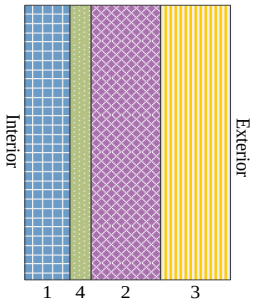

Figure 7.9. Schematic of the wall investigated. 1: gypsum board, 2: insulation layer, 3: OSB, 4: PCM layer.

The U-value is used to characterize thermal transmittance of the wall and is defined as Eq. (7.13) [33]:

$$\frac{1}{U} = \sum_i \frac{e_i}{\lambda_i} \tag{7.12}$$

where U is the thermal transmittance of the wall ($W \cdot m^{-2}K^{-1}$), e_i is the thickness, and λ_i is the thermal conductivity of layer i. Depending on which U-value is targeted for the wall, the thickness of the insulation layer can be varied for different insulating materials with other layers' thicknesses fixed. Note that Eq. (7.13) has neglected the surface thermal resistance of the insulation layer, Eq. (7.14) can be used to include external (R_{se}) and internal (R_{si}) conventional surface thermal resistance to determine the required thickness of VIP and EPS [34],

$$U_{VIP} = U_{EPS} = (R_{se} + s \cdot \lambda^{-1} + R_{si})^{-1} \quad (7.13)$$

where U_{VIP} is thermal transmittance of the wall insulated with VIP ($W \cdot m^{-2}K^{-1}$), U_{EPS} is thermal transmittance of the wall insulated with EPS ($W \cdot m^{-2}K^{-1}$), s is the thickness of the insulating layer, and λ is the thermal conductivity of the insulation material. R_{se} and R_{si} are the conventional external and internal surface resistance. In this study, 0.04 m^2K/W is adopted for R_{se} and 0.13 m^2K/W for R_{si} [34]. The thermal conductivity of VIP and EPS used in this analysis is 0.004 W/mK and 0.045 W/mK, respectively. The thicknesses of VIP and EPS are calculated respectively to achieve the same thermal transmittance of the whole wall.

Table 7.3 summarizes the obtained VIP and EPS thickness when the target *U*-value of the wall is 0.2 W/m^2K. For the scenario that the surface thermal resistance is not considered, to achieve the same thermal transmittance as the wall integrated with an 18.9-mm VIP layer, the equivalent thickness of EPS needed is 213.2 mm. The adoption of VIP saves 77.3% of the total wall thickness compared with the use of EPS. Similarly, a saving rate of 76.8% on the wall thickness is achieved when the surface thermal resistance is considered. One can see that a considerably reduced thickness can be achieved with the utilization of VIP in building envelopes, providing potential savings on the useful space of buildings. The surface thermal resistance shows a small impact (about 5%) on the total wall thickness, hence it is neglected in the following studies.

Table 7.3. Comparison of VIP and EPS thickness.

	VIP thickness (mm)	**EPS thickness (mm)**	**Increasing rate of the wall thickness**
without surface thermal resistance	18.9	213.2	77.3%
with surface thermal resistance	18.3	205.6	76.8%

7.4.1.2. Thermal Dynamic of the Wall with VIP and EPS

To evaluate the thermal insulating performance of VIP and EPS, numerical simulations on different wall configurations are performed using the COMSOL Multiphysics® software. The thermo-physical properties listed in Table 7.1 are utilized and the T30 temperature profiles showed in Figure 7.4 are applied on each wall model as the input loading condition. The instantaneous heat flux through the wall with 18.9-mm VIP is compared to that of the wall incorporating EPS with the equivalent thickness of 213.2 mm. In the context of the research, smaller heat flux oscillation means the wall possesses "better" thermal insulation performance. As shown in Figure 7.10, synchronous heat flux oscillations between the two wall models with different insulating layers can be observed. With 18.9-mm VIP integrated, the heat flux through the wall swings between -0.64 W/m^2 and 0.52 W/m^2 during the 7-day test period. With 213.2-mm EPS integrated into the same location, the heat flux oscillates between -0.56 W/m^2 and 0.36 W/m^2.

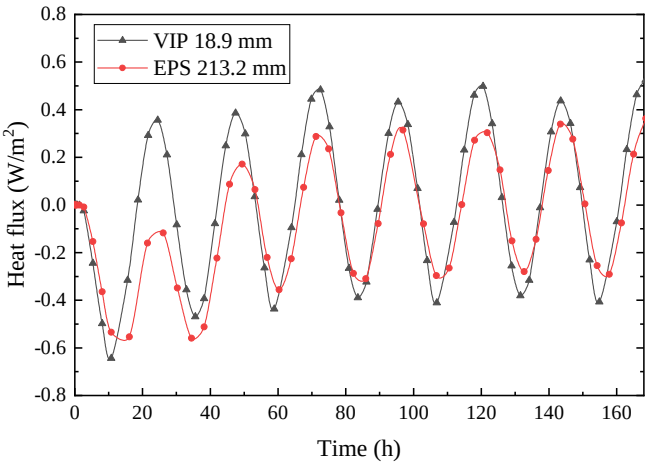

Figure 7.10. Heat flux changes through walls with different insulation layers.

An interesting observation concerns the difference between the heat flux values of the wall integrating VIP and EPS with the same *U*-value. The maximum heat flux swing is smaller when EPS is utilized compared to VIP with the equivalent thickness. To understand this

difference, the thermal dynamics of wall configurations including VIPs with thicknesses ranging from 8.9 to 25.6 mm and EPS with equivalent thicknesses ranging from 100.5 to 288 mm are further explored. The maximum heat flux oscillation results of wall configurations with different insulating materials and different thicknesses are presented in Figure 7.11. One can see that the maximum heat flux oscillation decreases when the thickness of both insulation materials is increasing. This decrease is caused by the better thermal insulation provided by thicker insulating materials when their thermal and physical properties are fixed.

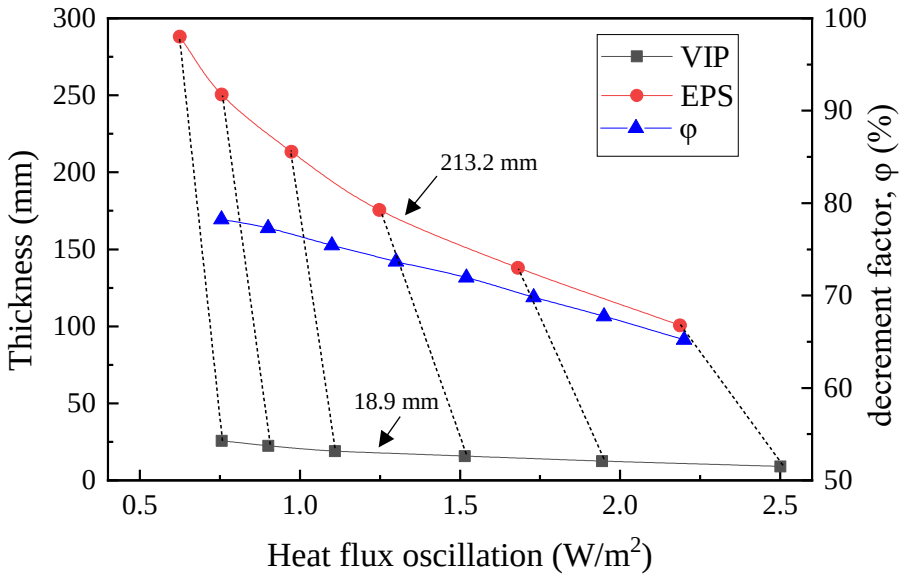

Figure 7.11. Comparison of the thermal performance of walls with VIP and EPS.

By comparing the maximum heat flux oscillation of each VIP and EPS with the equivalent thickness (connected with a dashed line), EPS is found to contribute more to the thermal insulation than the corresponding VIP. For example, the maximum heat flux oscillation of the wall integrated with 213.2-mm EPS is about 0.92 W/m^2. The equivalent thickness of the VIP is 18.9 mm by achieving the same U-value of the wall. Nevertheless, the maximum heat flux oscillation of the wall outfitted with 18.9-mm VIP is 1.16 W/m^2, which is 20.7% higher than the wall with 213.2-mm EPS. The required thickness for VIP is found to be about 19.2 mm to

achieve the same heat flux oscillation with 213.2-mm EPS. Similar results can be reached for cases with the U-value of the wall changed. This discrepancy suggests that VIP and EPS corresponding to the same U-value may result in different thermal dynamics of the wall. For specific, EPS tends to provide more thermal insulation than VIP with the same *U*-value in terms of reducing heat flux through the wall. One can see from Eq. (7.13) that the *U*-value of a building envelope is mainly determined by the wall thickness and thermal conductivity. However, it is not the only parameter influencing the thermal dynamics of the wall. Thermal inertia defined by Eq. (7.14) is another performance index that shows a significant impact on the thermal performance of a wall,

$$\mathrm{I} = \sqrt{k\rho c} \tag{7.14}$$

where I is the thermal inertia of a material, k is the thermal conductivity, ρ is the density, and c is the specific heat capacity. Since the thermal inertia of 213.2-mm EPS is larger than 18.9-mm VIP, it provides relatively more thermal insulation to the building envelope. The diurnal heat flux oscillation of the wall with 213.2-mm EPS is therefore reduced due to this increased thermal inertia. Nevertheless, the thickness needed for EPS is still much larger (about 9 times) than the VIP to achieve the same heat flux oscillation.

In this study, the space-saving effect of VIP regarding the same heat flux oscillation of the wall with EPS is investigated using the decrement factor φ (see Figure 7.11). This factor is the ratio between the thickness that VIP saved and the thickness of EPS to obtain the same heat flux oscillation. Owing to the low thermal conductivity of VIP, the total thickness of the wall is reduced by 65.2% to 77.8% compared to the scenario using EPS as the insulating strategy. The living area of the building can be significantly saved when VIP is adopted. This advantage

translates into the possibility of the building owner obtaining a higher revenue from renting the space or selling the building, resulting in promising economic benefits.

7.4.2. Coupling Effect of VIP and PCM

This section is devoted to the analysis of the coupling effect of VIP and PCM by comparing the instantaneous heat flux through the wall configurations including VIP and PCM with different thicknesses. Both artificial sinusoidal temperature profiles and real temperature profiles of Minneapolis and Austin in January and July are applied on the wall exterior surface as the input loading conditions. In this analysis, a total of 8 cases are designed to address the thermodynamics of building envelopes with different VIP and PCM layers. For the sake of brevity, all cases are consistently labeled in such a way that the first term "P" denotes the thickness of the PCM layer, and the second term "V" denotes the thickness of the VIP layer, unless otherwise stated. For example, P10-V20 in Figure 7.17 represents the wall assembly consists of a 12.7-mm gypsum wallboard, a 10-mm PCM layer, a 20-mm VIP, and a 20.5-mm OSB from the interior to the exterior side of the wall.

7.4.2.1. Sinusoidal Temperature Profiles

7.4.2.1.1 The Influence of the VIP Thickness

Systematic numerical simulations on the instantaneous heat flux through the wall regarding the VIP thickness are carried out to concentrate the knowledge on the thermal performance of VIPs. Figure 7.12 shows the configurations of the wall investigated, with the VIP thickness changing from 5 to 30 mm and the thicknesses of other layers fixed. The thermal conductivity of the VIP is assumed to be constant at 6 $mW \cdot m^{-1}K^{-1}$ during the one-week test period. The scenario that the wall without an insulation layer is not considered in this study. The

sinusoidal temperature profiles (T10, T20, and T30) are applied on the exterior side of each wall as input loading conditions.

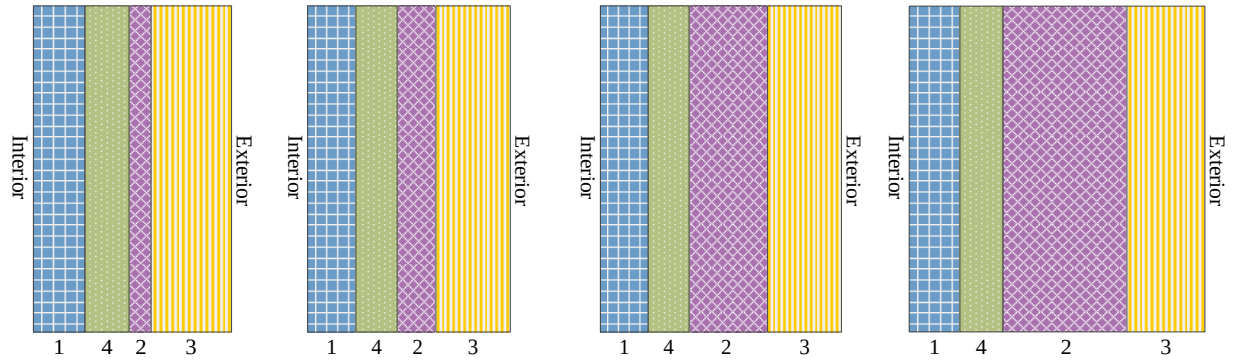

(a) V5-P10 (b) V10-P10 (c) V20-P10 (d) V30-P10

Figure 7.12. Schematic of wall assemblies with various VIP thicknesses.

Figure 7.13 shows the instantaneous heat flux through the wall with different assemblies under sinusoidal temperature profiles with various amplitudes. One can see that the heat flux profiles of all wall models follow the sine-shaped evolution. The maximum heat flux oscillations are in direct proportion to the amplitude of the input loading, and inverse proportion to the VIP thickness. Taking the results for the case of T10 as an example, the heat flux value of model V5-P10 oscillates between -0.56 W/m^2 and 0.4 W/m^2, and the heat flux value of model V10-P10 oscillates between -0.32 W/m2 to 0.22 W/m^2. When the thickness of VIP increases from 5 mm to 10 mm, the maximum heat flux oscillation decreases by 44% due to the increased thermal insulation provided by thicker VIP. Similar conclusions can be reached for cases when the models are subjected to other temperature profiles. For the same input temperature profile, the VIP thickness shows a significant impact on the energy efficiency of the building envelope.

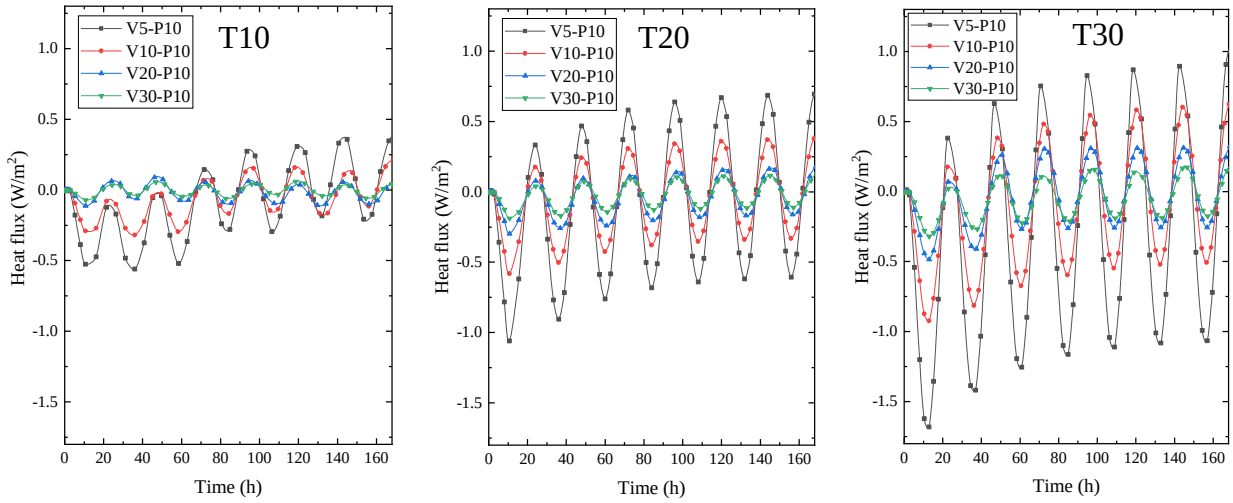

Figure 7.13. Instantaneous heat flux through walls under sinusoidal temperature profiles with different amplitudes.

Figure 7.14 shows the maximum heat flux oscillation results of different walls during the 7-day test period as a function of the VIP thickness and the amplitude of the input temperature profiles. The same tendency can be observed that the resulting heat flux amplitudes are in direct proportion to the amplitude of the input loading, and inverse proportion to the VIP thickness. The slope of the heat flux oscillation decrease is determined by the amplitude difference between each temperature profile and the thickness difference between each wall model. Therefore, thicker VIP should be adopted when being used as the thermal insulation strategy in a location with a larger diurnal temperature difference to decrease the bidirectional heat flux and narrow the indoor temperature fluctuations. This conclusion is consistent with the work by Fantucci et al. [34] that the VIP thickness plays a significant role in enhancing building energy efficiency. It is worth mentioning that, the required thickness of VIP not only depends on the targeted thermal performance of the building envelope but also being driven by the economic issues which can be revealed by the payback period in the practical uses.

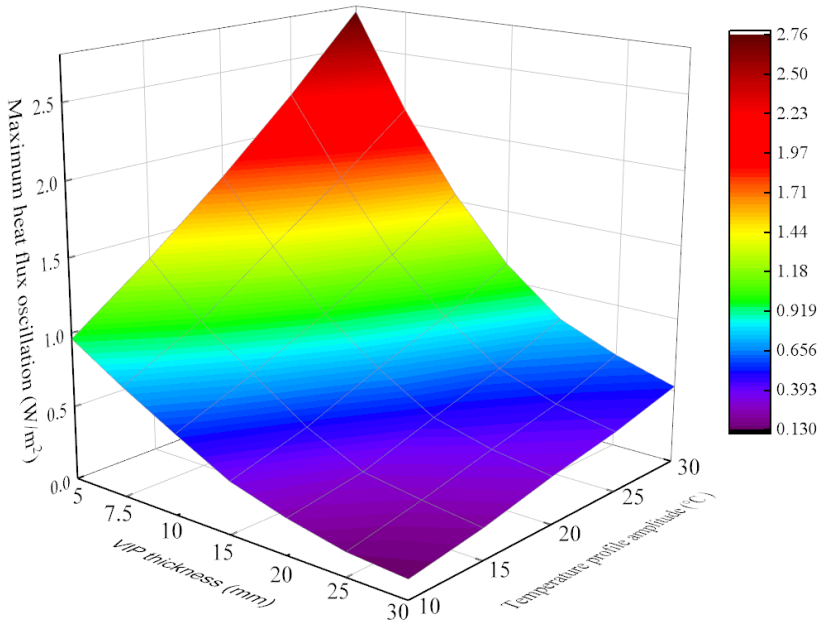

Figure 7.14. Maximum heat flux oscillation of the wall with different VIP thicknesses and subjected to temperature profile with different amplitudes.

3.4.2.1.2 The Influence of the PCM Thickness

To investigate the influence of the PCM thickness on the coupling thermal effect of VIP and PCM, instantaneous heat flux of the wall reinforced with PCM with thicknesses ranging from 0 to 15 mm is generated. Figure 7.15 shows the configuration of the different wall configurations investigated. Only PCM thickness changes and the thicknesses of other layers are fixed. The melting point of the PCM is 24 °C, and the heat of fusion of PCM is 180 kJ/kg. The sinusoidal temperature profiles (T10, T20, and T30) are again applied on the exterior side of each wall as the input loading conditions.

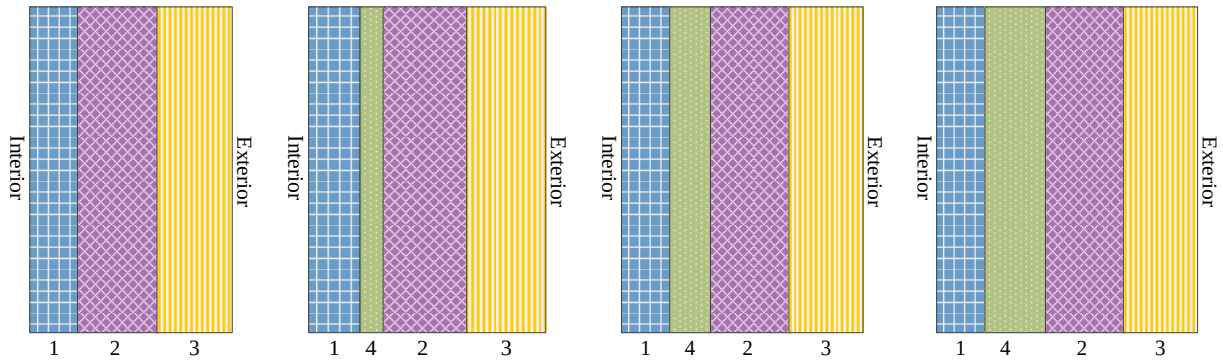

(a) V20-P0 (b) V20-P5 (c) V20-P10 (d) V20-P15

Figure 7.15. Schematic of wall assemblies with various PCM thicknesses.

Figure 7.16 shows the instantaneous heat flux of the walls during the 7-day test period when the PCM thickness changes from 0 to 15mm. One can see that the heat flux profiles of all wall models also follow the sine-shaped evolution. The maximum heat flux oscillations are in direct proportion to the amplitude of the input loading but in inverse proportion to the PCM thickness. In the scenario with T10 as the input loading, the heat flux value of the wall without PCM layer oscillates between -1.17 W/m^2 and 1.08 W/m^2, and this value of the wall with a 5-mm PCM layer decreases to a smaller interval from -0.23 W/m^2 to 0.20 W/m^2. The existence of 5-mm PCM leads to an 81% reduction in the maximum heat flux oscillation. For the scenario with 10-mm PCM, the interval of this value further decreases 29%. As expected, integrating thicker PCM in the building envelope can benefit more on its thermal management by decreasing heat flux oscillation and hence reducing building energy consumption owing to its high latent heat storage capacity and isothermal nature.

On the other hand, the integration of the PCM layer causes a time delay on the peak heat fluxes. Taking the results for the case of T30 as an example, the peak heat flux of the reference wall without PCM appears at 19.5 h during the first day, and the peak heat flux of the wall with 5-mm PCM appears at 23.4 h, leading to a 3.9-h time delay on the peak heat flux for the same

day. The time delay increases with the increasing PCM thickness. The time delay of the peak heat flux shows great potential to reduce the operating costs of the electricity-generating utilities. This is because the HVAC utilities can shift their working load from on-peak to off-peak period due to the time delay effect of PCM. On one hand, the utility companies can run their power plants more efficiently at a lower cost; on the other hand, since the utility companies usually charge higher rates for electricity use during on-peak times, residents and businesses may save on their electricity bills by consuming the electricity for HVAC system during off-peak hours.

One can address that thicker VIP and PCM are capable of reducing more heat flux through the wall, but only PCM can give rise to the time delay for the peak heat fluxes. This is caused by the difference in working principles between VIP and PCM. VIP relies on its extremely low thermal conductivity and provides high thermal resistance to the heat flux through the building envelope, effectively blocking the inward heat or cold. PCM with a large energy storage capacity can significantly increase the thermal mass of the building envelope. It absorbs and stores energy surpluses from solar energy or the internal heat gains and releases the energy to the environment at a later time when needed, which successfully delays the thermal wave and smooths the indoor air temperature swings. The integration of PCM in building envelopes turns out to be one of the most effective ways to diminish building heating and cooling loads [35].

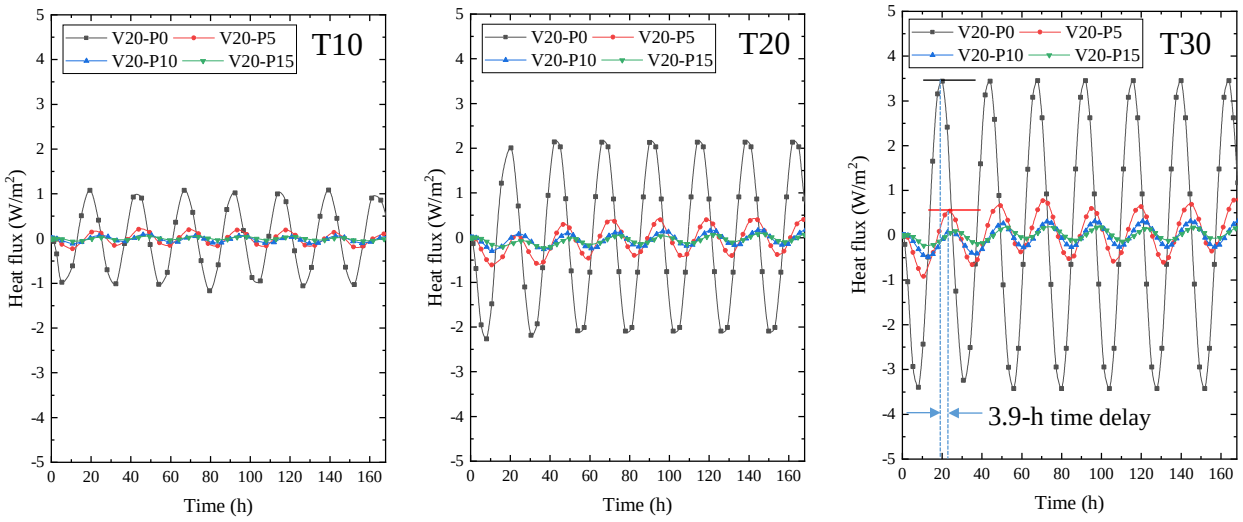

Figure 7.16. Instantaneous heat flux through walls under sinusoidal temperature profiles with different amplitudes.

Table 7.4 summarizes the daily maximum heat flux oscillation of each model and their time delay status caused by the PCM. One can observe that the maximum heat flux oscillation of each day keeps decreasing when the PCM thickness increases from 0 to 15 mm for all three loading conditions. This is because on one hand more PCM can partially lower the thermal transmittance (*U*-value) of the wall, and the more important reason is that thicker PCM can absorb and store more latent heat without a sharp temperature increase, and the heat flux through the wall is therefore decreased due to the smaller temperature gradients. As expected, the inverse relationship between the maximum heat flux oscillation and PCM thickness is consistent for loading conditions with different amplitude, suggesting that this trend is not influenced by the input loading conditions. The decrease in the heat flux oscillation as a result of PCM thickness increasing can translate to a size reduction in space cooling/heating equipment.

The daily time delay results for different wall configurations indicate that the integration of PCM leads to a considerable time delay of the peak heat flux. Compared with that of the reference wall, the average time delay on the peak heat flux of the wall with 15-mm PCM can

reach as much as 6.97 h. This result agrees with the one presented by Lee et al. [36], in which the maximum peak heat flux time delays 6.3 h when 20-mm PCM with a latent heat storage capacity of 149.9 J/g is integrated.

Table 7.4. Maximum heat flux oscillation and time delay of each model under various temperature profiles.

		T1				T2				T3			
PCM thickness (mm)		0	5	10	15	0	5	10	15	0	5	10	15
Thickness decrement ratio (%)		0	9.4	18.8	28.2	0	9.4	18.8	28.2	0	9.4	18.8	28.2
Maximum heat flux oscillation (W/m^2)	Day1	2.06	0.37	0.17	0.08	4.27	0.61	0.38	0.21	6.84	1.45	0.56	0.33
	Day2	1.94	0.36	0.15	0.07	4.33	0.87	0.35	0.22	6.68	1.31	0.67	0.37
	Day3	2.10	0.35	0.13	0.08	4.22	0.82	0.35	0.20	6.88	1.14	0.57	0.24
	Day4	2.19	0.36	0.15	0.08	4.22	0.80	0.34	0.17	6.88	1.12	0.57	0.30
	Day5	1.94	0.35	0.08	0.08	4.22	0.80	0.33	0.20	6.88	1.22	0.52	0.28
	Day6	2.14	0.29	0.16	0.07	4.22	0.80	0.33	0.19	6.88	1.29	0.57	0.30
	Day7	1.93	0.35	0.17	0.08	4.22	0.81	0.34	0.21	6.88	1.28	0.58	0.34
Time delay (h)	Day1	0	0.87	4.56	5.68	0	1.08	3.68	4.96	0	3.94	2.52	6.55
	Day2	0	2.72	4.82	8.13	0	4.49	6.54	7.65	0	5.17	6.56	8.83
	Day3	0	2.38	5.50	7.04	0	6.41	6.50	8.74	0	2.55	4.58	7.97
	Day4	0	1.04	1.88	5.81	0	5.51	6.48	5.52	0	3.04	4.58	7.90
	Day5	0	4.11	7.05	8.95	0	4.65	6.48	7.84	0	3.98	4.58	5.67
	Day6	0	2.83	3.50	7.70	0	6.38	6.48	6.41	0	5.23	4.58	6.07
	Day7	0	2.96	4.56	6.78	0	5.42	6.50	5.67	0	4.56	5.21	6.58

For each input loading amplitude, the time delay intensity is in direct proportion with the PCM thickness since more PCM can absorb and store a larger amount of the inward heat and thus delay the energy saturated duration. According to the study of Zhang et al. [37], there exists

an upper limit of the PCM thickness in the practical applications, above which the PCM cannot undergo complete diurnal melting and solidifying cycle. Therefore, one should consider the input loading conditions to guarantee the full use of PCM's latent heat storage capacity when selecting optimal PCM thickness for a certain building.

7.4.2.2. Real Temperature Profiles

The real temperature profiles of two representative cities including Austin and Minneapolis are also applied to the model to evaluate the coupling effect of VIP and PCM on the thermal performance of wallboards. Temperature profiles of both January and July of the two selected cities are used as the input loading conditions in this analysis. This section deals with the comparisons of the wall thermal performance when the thickness of the VIP and PCM layer is changed, respectively.

7.4.2.2.1 The Influence of the VIP Thickness

Figure 7.17 shows the instantaneous heat flux through the wall with different VIP thicknesses ranging from 5 to 30 mm. One can observe that the VIP thickness plays a considerable role in the heat flux evolution of the wall subjected to four different temperature profiles. The heat flux oscillation is in inverse proportion with the VIP thickness, which is consistent with the conclusion drawn with the sinusoidal temperature profile. Building energy efficiency can benefit from increasing the VIP thickness for both cold and hot months, covering cold and hot regions.

By comparing the heat flux evolution shown in Figure 7.17(a) to (d), a larger heat flux amplitude can be observed in the case of Minneapolis-January. As shown in Figure 7.17(c), the heat flux amplitude of the wall with 5-mm VIP is 34.8 W/m^2. This number reduces to 7.9 W/m^2 when 30-mm VIP is outfitted. A reduction rate of 77% is achieved by increasing the VIP

thickness from 5 to 30 mm, which is much larger than that of the other three cases with smaller input loading intensities. Compared with being used in mild weather, VIP plays a more essential role for the building subjected to harsh weather like that of January in Minneapolis (see Figure 7.5) by blocking the inward cold and hence reducing the temperature gradient between the interior and exterior side of the wall. More energy requested by heating/cooling equipment can be saved with thicker VIP integrated under such extreme weather.

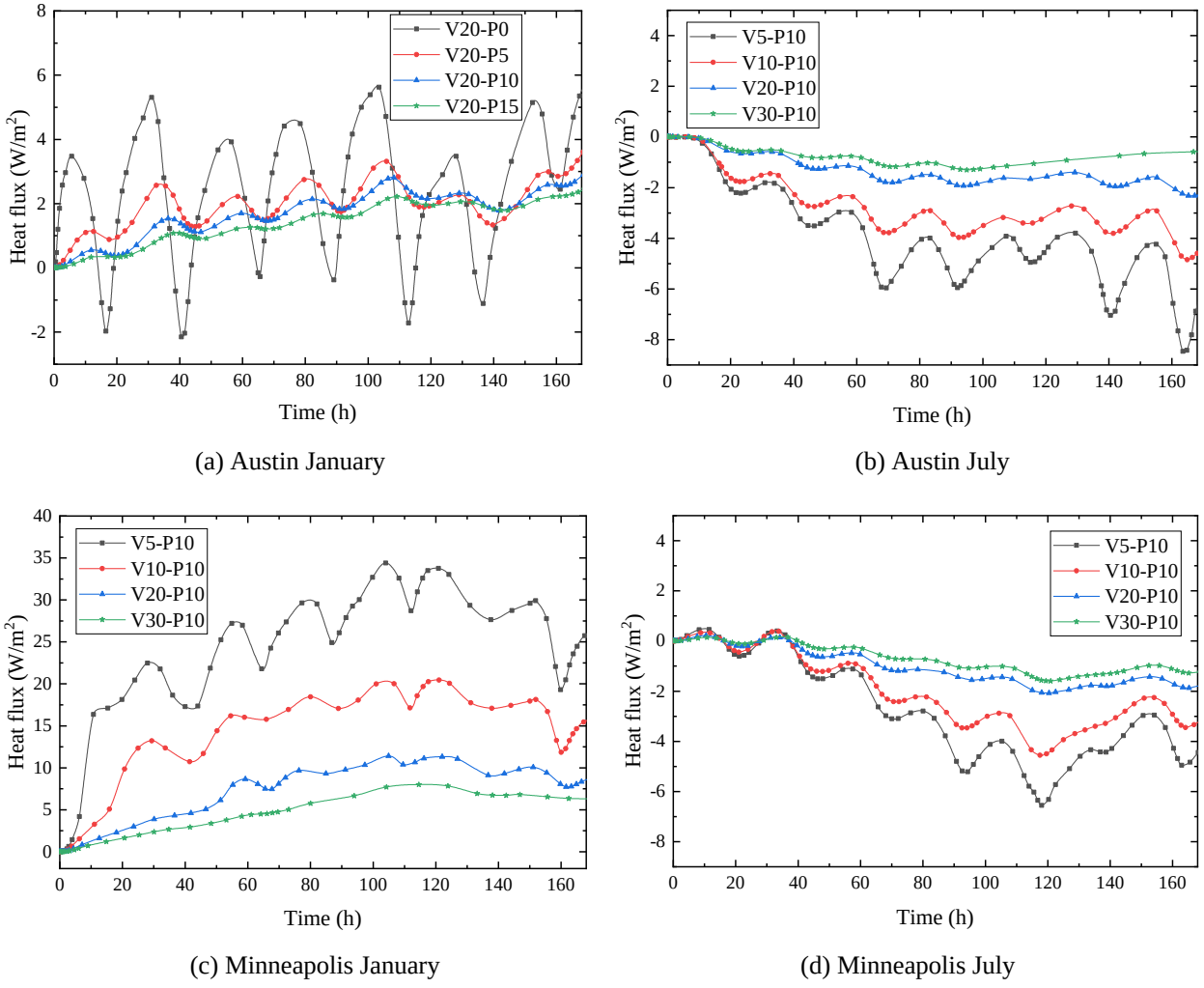

(a) Austin January

(b) Austin July

(c) Minneapolis January

(d) Minneapolis July

Figure 7.17. Instantaneous heat flux through walls under real temperature profiles of Austin and Minneapolis with various VIP thicknesses.

7.4.2.2.2 The Influence of the PCM Thickness

Figure 7.18 shows the instantaneous heat flux through the wall with different PCM thicknesses ranging from 0 to 15 mm. The same conclusion can be achieved that the maximum heat flux oscillation of the investigated models is in inverse proportion with PCM thickness. In the case of Austin-January showed in Figure 7.18(a), the heat flux value through the reference wallboard without PCM is varying between a minimum of -2.1 W/m^2 and a maximum of 5.7 W/m^2, resulting in a maximum heat flux oscillation of 7.8 W/m^2 during the one-week test period. This maximum oscillation is reduced to 3.6 W/m^2, 2.9 W/m^2, and 2.4 W/m^2 with PCM thicknesses of 5 mm, 10 mm, and 15 mm, respectively. The corresponding reduction rate is 36.8%, 49.1%, and 57.9%, respectively. One can address that the PCM thickness plays a considerable role in reducing the heat flux oscillation under the investigated thermal loading condition.

Another observation concerns the impact of PCM thickness on changing the heat flux amplitudes under various input loading conditions. The impact of the PCM thickness on reducing heat flux oscillation becomes smaller for the other three loading conditions shown in Figure 7.18(b)–(d). This is because the melting point of the PCM used in this analysis is 24 °C, which is centering the temperature profile of January in Austin (see Figure 7.5(a)). In such a scenario, the heat capacity of PCM can be made full use of by undergoing diurnal melting and solidifying process. The other three temperature profiles including Austin July, Minneapolis July, and Minneapolis January either run beyond or below the melting point of the PCM during most of the investigated period, significantly decreasing the utilization rate of PCM the latent heat. The small reduction in the maximum heat flux oscillation in those scenarios mostly result from PCM's sensible heat, which is much smaller than its latent heat capacity. Therefore, the selection

of the PCM melting point for a certain building should base on the input thermal loading conditions. This conclusion agrees with that from previous research [25]. The study of Zhang et al. [37] also holds the similar opinion that the optimal melting temperature of PCM used in different buildings should be varied according to their geographic positions and weather conditions. For specific, they found the optimal PCM melting temperature used in their investigated buildings located in Beijing and Shanghai are 20 and 25 °C, respectively.

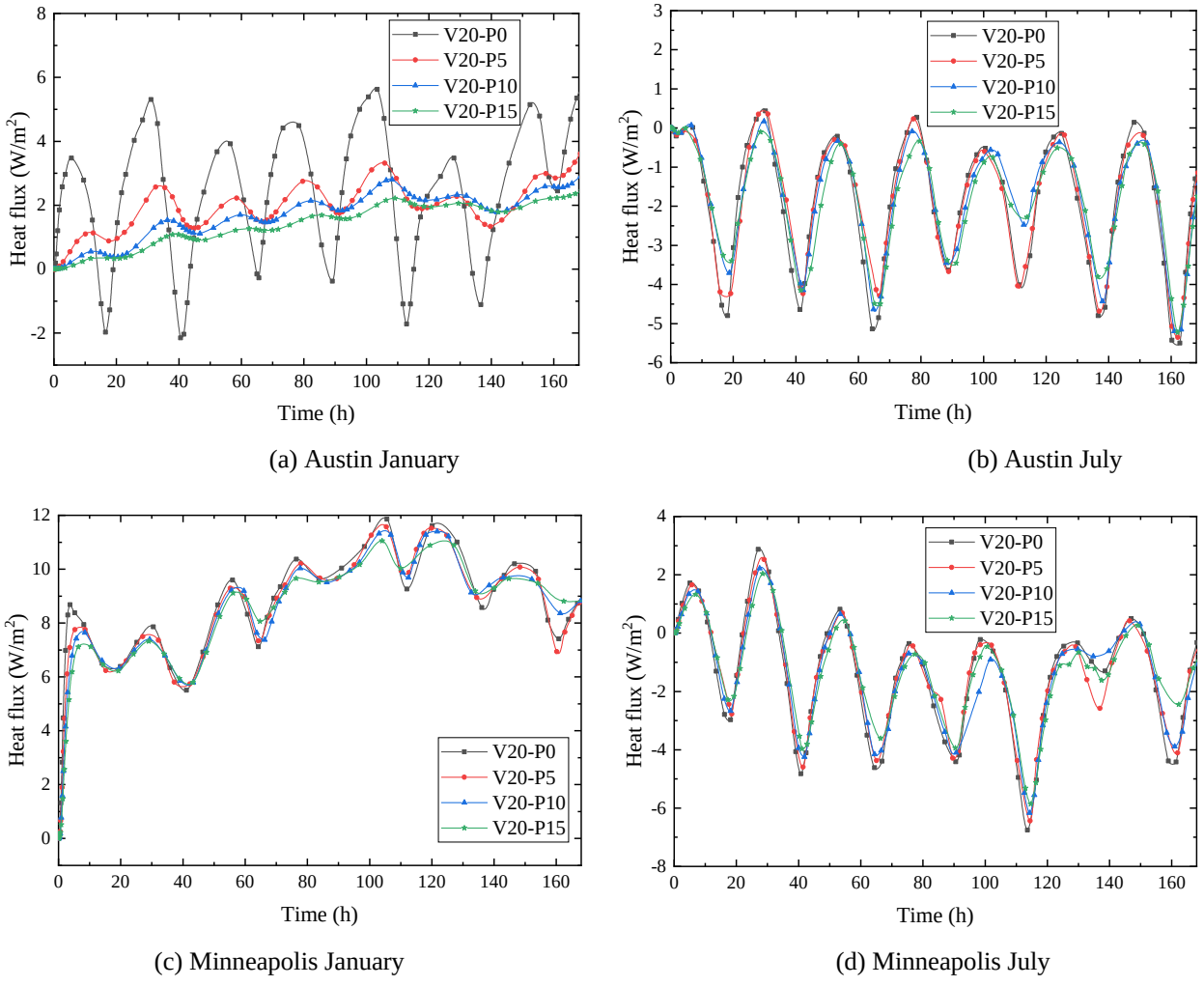

(a) Austin January

(b) Austin July

(c) Minneapolis January

(d) Minneapolis July

Figure 7.18. Instantaneous heat flux through walls under real temperature profiles of Austin and Minneapolis with various PCM thicknesses.

7.5. Summary

A numerical analysis is carried out in this study to assess the feasibility of using VIP to improve building energy efficiency and investigate the thermal dynamics of the wallboards outfitted with VIP and PCM layers. Both artificial sinusoidal and the real temperature profiles are used as the input loading conditions to comprehensively exploring the thermal behavior of the investigated wall configurations. This is one of the rare studies comparing the thermal insulating performance of VIP and EPS basing on the thermal dynamics of building envelope and coupling VIP with the super low thermal transmittance and PCM with large latent heat storage capacity for the sake of improving building energy efficiency. The aging effect of VIP and EPS is considered in the comparison of their long-term thermal performance when being utilized in buildings. A few specific conclusions drawn from the analysis are listed below:

The VIP with extremely low thermal conductivity allows the building envelope to achieve the same thermal performance with more living space saved compared with the traditional insulating material. To achieve the same targeted U-value (0.2 W/m^2K) of the wall investigated, the thickness needed for VIP with thermal conductivity of 0.004 W/mK is 18.9 mm, saving 77.3% of the total wall thickness compared with EPS with thermal conductivity of 0.045 W/mK.

The maximum heat flux oscillation is in direct proportion to the amplitude of the input loading, and inverse proportion to the VIP thickness. Taking the results for the case of T10 as an example, the heat flux value of model V5-P10 oscillates between -0.56 W/m^2 and 0.4 W/m^2 during the test period and the heat flux value of model V10-P10 oscillates between -0.32 W/m^2 to 0.22 W/m^2. When the thickness of VIP increases from 5 mm to 10 mm, the maximum heat flux oscillation decreases by 44% due to the increased thermal insulation provided by thicker

VIP. Therefore, VIP thickness shows a significant impact on the energy efficiency of the building envelope.

The maximum heat flux oscillations are in direct proportion to the amplitude of the input loading, and inverse proportion to the PCM thickness. For specific, the heat flux value through the reference wallboard without PCM is varying between a minimum of -2.1 W/m^2 and a maximum of 5.7 W/m^2, resulting in a maximum heat flux oscillation of 7.8 W/m^2 during the first week of January in Austin. This maximum oscillation is reduced to 3.6 W/m^2, 2.9 W/m^2, and 2.4 W/m^2 with PCM thicknesses of 5 mm, 10 mm, and 15 mm, respectively. The corresponding reduction rate is 36.8%, 49.1%, and 57.9%, respectively. One can address that the PCM thickness plays a considerable role in reducing the heat flux oscillation under the investigated thermal loading condition.

Coupling VIP with extremely low thermal conductivity and PCMs with a large amount of latent heat in the building envelope is a promising strategy to enhance its thermal performance due to the increased thermal insulation and thermal inertia. The integration of the PCM layer causes a time delay on the peak heat fluxes. Compared with that of the reference wall, the average time delay on the peak heat flux of the wall with 15-mm PCM can reach as much as 6.97 h under the investigated sinusoidal loading conditions. The time delay intensity is found in direct proportion with the PCM thickness since more PCM can absorb and store a larger amount of the inward heat and thus delay the energy saturated duration. This time delay of the peak heat flux shows great potential to reduce the operating costs of the electricity-generating utilities by using the HVAC system during off-peak hours. Besides, the selection of the optimal PCM melting point for a certain building should base on the input thermal loading conditions.

7.6. References

[1] K. Du, J. Calautit, Z. Wang, Y. Wu, H. Liu, A review of the applications of phase change materials in cooling, heating and power generation in different temperature ranges, Applied Energy 220 (2018) 242-273.

[2] Iea.org, Buildings -- A source of enormous untapped efficiency potential. Accessed on August 14, 2019. https://www.iea.org/topics/buildings.

[3] Eia.gov, How much energy is consumed in U.S. buildings? Accessed on April 06, 2019. https://www.eia.gov/tools/faqs/faq.php?id=86&t=1.

[4] Eia.gov, More than half of energy use in homes is for heating and air conditioning. Accessed on August 14, 2019. https://www.eia.gov/energyexplained/use-of-energy/homes.php.

[5] B.P. Jelle, Traditional, state-of-the-art and future thermal building insulation materials and solutions – Properties, requirements and possibilities, Energy and Buildings 43(10) (2011) 2549-2563.

[6] T. Nussbaumer, K.G. Wakili, C. Tanner, Experimental and numerical investigation of the thermal performance of a protected vacuum-insulation system applied to a concrete wall, Applied Energy 83(8) (2006) 841-855.

[7] P. Johansson, C.-E. Hagentoft, A. Sasic Kalagasidis, Retrofitting of a listed brick and wood building using vacuum insulation panels on the exterior of the facade: Measurements and simulations, Energy and Buildings 73 (2014) 92-104.

[8] M. Zwerger, H. Klein, Integration of VIP's into external wall insulation systems. In Proceedings of the 7th International Vacuum Insulation Symposium (2005) 173-179.

[9] H. Akeiber, P. Nejat, M.Z.A. Majid, M.A. Wahid, F. Jomehzadeh, I. Zeynali Famileh, J.K. Calautit, B.R. Hughes, S.A. Zaki, A review on phase change material (PCM) for sustainable passive cooling in building envelopes, Renewable and Sustainable Energy Reviews 60 (2016) 1470-1497.

[10] R. Baetens, B.P. Jelle, A. Gustavsen, Phase change materials for building applications: A state-of-the-art review, Energy and Buildings 42(9) (2010) 1361-1368.

[11] N. Soares, J.J. Costa, A.R. Gaspar, P. Santos, Review of passive PCM latent heat thermal energy storage systems towards buildings' energy efficiency, Energy and Buildings 59 (2013) 82-103.

[12] F. Kuznik, D. David, K. Johannes, J.-J. Roux, A review on phase change materials integrated in building walls, Renewable and Sustainable Energy Reviews 15(1) (2011) 379-391.

[13] M. Li, Z. Lin, F. Yan, Graphite-Enabled Phase Change Material Composites for Enhanced Thermal Management of Concrete Pavement, Tranpotation Rearch Board (2017) No. 17-03915.

[14] M. Song, F. Niu, N. Mao, Y. Hu, S. Deng, Review on building energy performance improvement using phase change materials, Energy and Buildings 158 (2018) 776-793.

[15] Numerical thermal characterization and performance metrics of building envelopes containing phase change materials for energy-efficient buildings

[16] L.F. Cabeza, C. Castellón, M. Nogués, M. Medrano, R. Leppers, O. Zubillaga, Use of microencapsulated PCM in concrete walls for energy savings, Energy and Buildings 39(2) (2007) 113-119.

[17] N.P. Sharifi, A.A.N. Shaikh, A.R. Sakulich, Application of phase change materials in gypsum boards to meet building energy conservation goals, Energy and Buildings 138 (2017) 455-467.

[18] I.D. Mandilaras, D.A. Kontogeorgos, M.A. Founti, A hybrid methodology for the determination of the effective heat capacity of PCM enhanced building components, Renewable Energy 76 (2015) 790-804.

[19] M. Ahmad, A. Bontemps, H. Sallée, D. Quenard, Thermal testing and numerical simulation of a prototype cell using light wallboards coupling vacuum isolation panels and phase change material, Energy and Buildings 38(6) (2006) 673-681.

[20] X. Li, H. Chen, H. Li, L. Liu, Z. Lu, T. Zhang, W.H. Duan, Integration of form-stable paraffin/nanosilica phase change material composites into vacuum insulation panels for thermal energy storage, Applied Energy 159 (2015) 601-609.

[21] M. Li, Q. Cao, H. Pan, X. Wang, Z. Lin, Effect of melting point on thermodynamics of thin PCM reinforced residential frame walls in different climate zones, Appl. Therm. Eng. 188 (2021) 116615.

[22] Ö.A. Dombaycı, The environmental impact of optimum insulation thickness for external walls of buildings, Building and Environment 42(11) (2007) 3855-3859.

[23] X. Jin, M.A. Medina, X. Zhang, Numerical analysis for the optimal location of a thin PCM layer in frame walls, Applied Thermal Engineering 103 (2016) 1057-1063.

[24] S. Fantucci, A. Lorenzati, A. Capozzoli, M. Perino, Analysis of the temperature dependence of the thermal conductivity in Vacuum Insulation Panels, Energy and Buildings 183 (2019) 64-74.

[25] A. Batard, T. Duforestel, L. Flandin, B. Yrieix, Modelling of long-term hygro-thermal behaviour of vacuum insulation panels, Energy and Buildings 173 (2018) 252-267.

[26] P. Bose V.A. Amirtham, A review on thermal conductivity enhancement of paraffinwax as latent heat energy storage material, Renewable and Sustainable Energy Reviews 65 (2016) 81-100.

[27] Sari, A., Eroglu, R., Bicer, A. and Karaipekli, A., 2011. Synthesis and thermal energy storage properties of erythritol tetrastearate and erythritol tetrapalmitate. Chemical engineering & technology, 34(1), pp.87-92.

[28] Rathod, M.K. and Banerjee, J., 2013. Thermal stability of phase change materials used in latent heat energy storage systems: A review. Renewable and sustainable energy reviews, 18, pp.246-258.

[29] COMSOL – Multiphysics Modeling and Simulation Software. Multiphysics Modeling and Simulation Software; 2021. <http://www.comsol.com>.

[30] T.L. Bergman, F.P. Incropera, A.S. Lavine, D.P. DeWitt, Introduction to heat transfer, John Wiley & Sons 2011.

[31] A. Batard, T. Duforestel, L. Flandin, B. Yrieix, Prediction method of the long-term thermal performance of Vacuum Insulation Panels installed in building thermal insulation applications, Energy and Buildings 178 (2018) 1-10.

[32] B.M. Marino, N. Muñoz, L.P. Thomas, Calculation of the external surface temperature of a multi-layer wall considering solar radiation effects, Energy Build. 174 (2018) 452-463.

[33] F. Kuznik J. Virgone, Experimental assessment of a phase change material for wall building use, Applied Energy 86(10) (2009) 2038-2046.

[34] S. Fantucci, S. Garbaccio, A. Lorenzati, M. Perino, Thermo-economic analysis of building energy retrofits using VIP - Vacuum Insulation Panels, Energy and Buildings 196 (2019) 269-279.

[35] L. Zhu, R. Hurt, D. Correia, R. Boehm, Detailed energy saving performance analyses on thermal mass walls demonstrated in a zero energy house, Energy and Buildings 41(3) (2009) 303-310.

[36] K.O. Lee, M.A. Medina, E. Raith, X. Sun, Assessing the integration of a thin phase change material (PCM) layer in a residential building wall for heat transfer reduction and management, Applied Energy 137 (2015) 699-706.

[37] Y.P. Zhang, K.P. Lin, R. Yang, H.F. Di, Y. Jiang, Preparation, thermal performance and application of shape-stabilized PCM in energy efficient buildings, Energy and Buildings 38(10) (2006) 1262-1269.

8. CONCLUSIONS AND FUTURE WORK

This dissertation presents both experimental and numerical studies on the application of PCM in building envelopes for energy-saving. In this chapter, the experimental work of investigating the heat transfer behavior of paraffin/EG composite and the numerical work of exploring the thermal performance of building exterior walls containing PCM is summarized. The focus of this work is to develop a systematic and comprehensive holistic framework to gain a deep understanding of the working mechanism of PCM and address how to select proper PCMs for buildings and maximize the activation of their latent heat to effectively improve building energy efficiency under different loading conditions. The research findings and proposed methods developed in this work provide insight into the applications of PCM in buildings.

8.1. Conclusions

A novel form-stabilized PCM composite was prepared from paraffin and EG and its overall property was experimentally investigated. When preparing the paraffin/ EG composite, different exfoliating conditions concerning the expanding time and temperature. Among them, heating the expandable graphite in the muffle furnace at 850 ℃ for 14 seconds resulted in completely expanded EG with the maximum sorption capacity for paraffin (90.8 wt.%). The FTIR analysis demonstrated that many functional groups were produced during the exfoliation process of NEG caused by the oxidation intercalation during high-temperature exfoliation. In addition, the prepared EG has a wide pore size distribution that consisted of mesopores and macropores. Both the functional groups and the porous structure produced may contribute to the absorbing capacity of paraffin. SEM images showed that the porous structure of EG was filled with paraffin uniformly due to absorption, making it a promising supporting media for paraffin to keep its form-stability and meanwhile enhance its thermal conductivity. The DSC results

showed that the total latent heat of the pure paraffin is 180.5 J/g, and that of the composite PCM with 90 wt.% and 85 wt.% is 161.8 J/g and 152.3 J/g, respectively. Therefore, the total latent heat of PCM is in direct proportion to the paraffin content in the composite. The solid-liquid phase change temperatures of the paraffin/EG composites were found slightly less than that of the pure paraffin due to the increased heat transfer rate by EG.

To investigate the thermal behavior of PCM and the potential of applying PCM in buildings, thermal storage and heat transfer test with 2×2×2 inches specimen and laboratory-scale prototypes were conducted. It showed that the paraffin/EG composite possessed favorable thermal energy storage ability to be used for enhancing building energy efficiency. EG can significantly enhance the heat transfer rate of paraffin, but the EG content increase affected the composite's overall heat storage capacity negatively. The thermal performance test of prototypes indicated that the integration of PCM in the test cell walls led to the improvement of the cell's thermal performance in two ways. On one hand, the maximum temperature fluctuation of the test cell reinforced by PCM was reduced by 2.37 ℃ compared to the reference test cell without PCM. On the other hand, the maximum "indoor" temperature of the test cell integrated with PCM was delayed about 0.67 hours. Both improvements proved the high potential of applying the proposed PCM composite in building envelopes to enhance building energy efficiency.

The impact of critical design parameters including the location, thickness, latent heat, melting point, and thermal conductivity of PCM on the thermal performance of a multilayer wall is explored using COMSOL Multiphysics® software. Results revealed that each design variable exhibited high variation in attributes to building energy savings in terms of reduction of peak temperature and temperature swings. Among the variables, the selection of the proper melting point for a PCM was identified as the most crucial parameter for determining building energy

efficiency. If a proper melting point is used, the latent heat and PCM layer thickness also plays a role in building thermal management. A reduction of the maximum instantaneous temperature reached up to 30% when a 15-mm thick PCM layer is integrated into a conventional 185-mm thick wall, as compared to the reference wall without PCM. Findings also demonstrated that the placement of the PCM near the interior wall surface could achieve higher efficiency due to the thermal block function of the insulating layer outside.

The relationship between the optimal PCM melting point and critical design parameters including PCM layer location, thickness, and the loading conditions associated with different climate zones and months was also developed. The results reveal that selecting proper PCM melting point according to those design parameters reduces the indoor peak temperature and temperature oscillation, and thus diminishes the energy consumption by the HVAC system to regulate the indoor temperature. It was found that the selection of the PCM melting point for a certain building envelope is highly dependent on the input thermal loading conditions. The optimal PCM melting point is in direct proportion to the input loading conditions, suggesting that a higher PCM melting point is needed for a building envelope subjected to higher input temperature. Specifically, for the buildings located in cities with a hot climate like the summer of Las Vegas, the optimal PCM melting point ranges from 26 °C to 30 °C to “cool down” the indoor air; for the buildings located in cities with a moderate climate like the summer of Fargo, the optimal PCM melting point is about 24 °C to improve the indoor thermal comfort; for the buildings located in cities with a relatively cold climate like the summer of Seattle, the optimal PCM melting point is about 20 °C to 24 °C to “warm-up” the indoor air. The selection principle for the optimal PCM melting point is making sure the diurnal service effectiveness of the PCM through a maximized converting between solid and liquid under a certain loading condition.

Results also show that PCM with a melting point within the occupant thermal comfort zone (22 °C to 28 °C) can increase indoor thermal comfort duration more effectively for the "moderate" climate loading conditions. The findings are expected to assist engineers in better utilization of the PCM-based building envelope in different climate regions.

A new wall configuration containing PCM with hybrid melting points is developed to enhance the service efficiency of PCM. It was found PCM with hybrid melting points provides more flexibility in the use of its latent heat capacity. Compared to the reference wall without PCM, the integration of a 10-mm PCM with a melting point of 24 °C and latent heat capacity of 180 J/g leads to a 6.4% of reduction in the maximum indoor temperature and 34.2% increase in the minimum indoor temperature. When the PCM with hybrid melting points (16 °C, 24 °C, and 32 °C) is integrated, the corresponding decrement and increment factors increase to 18.5% and 51.9% respectively. The integration of PCM with multiple melting points can benefit more in the indoor thermal comfort than using PCM with a single melting under the investigated loading condition. When the ambient temperature changes within a relatively large interval covering cold, mild, and hot loading conditions, the melting point of PCM can be optimized accordingly to shape the thermal demand and thus save the building energy for the long term. In this way, the proposed PCM-based wall can adapt to the input loading conditions in different seasons and months, and its latent heat can remain active for a longer period of the year. Moreover, the impact of latent heat capacity of the PCM on the thermal performance of the investigated domain was also investigated. Doubling the latent heat capacity of the PCM leads to a 20.9% reduction in the maximum indoor temperature fluctuation and a 3-hour peak temperature shift. The duration of indoor thermal comfort is also increased by about 17.6%.

In order to further improve the building energy efficiency, this study also evaluated the feasibility of an energy-saving building wall by coupling VIP with PCM as a compact unit. The results reveal that the combined utilization of VIP and PCM in the same building envelope can reduce the heat flux oscillation through the wall more effectively and thereby leading to a tremendous reduction in energy consumption. The maximum heat flux oscillation through the wall was found in direct proportion to the amplitude of the input loading, and in inverse proportion to the VIP and PCM thickness. In addition to decreasing the heat flux oscillation through the wall, the integration of the PCM layer also causes a time delay on the peak heat fluxes, showing great potential to shift the electricity load from peak to off-peak hours. In addition, the VIP with extremely low thermal conductivity allows the building envelope to achieve the same thermal performance with more living space saved compared with the traditional insulating material. To achieve the same targeted *U*-value (0.2 W/m^2K) of the wall investigated, the thickness needed for VIP with thermal conductivity of 0.004 W/mK is 18.9 mm, saving 77.3% of the total wall thickness compared with EPS with thermal conductivity of 0.045 W/mK.

8.2. Future Work

PCMs have proven their great potential as a thermal management strategy being able to enhance building energy efficiency. From the results drawn from this research, the following recommendations can be drawn for further research:

1. In Chapter 6, a numerical study has been conducted to investigate the potential thermal comfort benefits of integrating PCM with more than one melting point into an external wall of the residential building. It was found PCM with hybrid melting points provides more flexibility in the use of its latent heat capacity and thus shows great potential for being used to improve

building energy efficiency. The conclusions are drawn based on the numerical simulation so far. Future experimental research concerning the thermal performance of the proposed wall assembly is encouraged to provide more comprehensive insights. Furthermore, the experiment can be conducted in the outdoor environment to evaluate the long-term effect of real loading conditions on the thermodynamics of the proposed wall configuration.

2. Due to the limitation of coverage, the thesis only studied a representative hybrid melting temperature scenario in Chapter 6, which is the combination of 16 °C, 24 °C, and 32 °C. Also, an equal amount of each PCM is applied. Upon this, the application of PCM with hybrid melting points in buildings deserves extensive studies on more melting temperature hybrid forms and combination proportions to adapt to different loading conditions.

3. The investigation on the developed wall configuration coupling VIP and PCM in Chapter 7 was also limited to the numerical simulation up to this point. In this respect, an experiment study needs to be conducted to further verify the thermal performance of the proposed coupling strategy.

4. Due to the service feature of buildings, the degradation of the thermal performance of VIP and PCM is a non-negligible topic from a long-term perspective. Especially for VIP, air and water vapor diffusion into the VIPs could degrade their thermal conductivity from 4 mW/(mK) initially to about 8 mW/(mK) within 25 years. Upon this, more investigations should be conducted to demonstrate the influences of material degradation over time on the long-term thermal performance of the proposed wall assembly containing VIP and PCM.